UNIVERSITY OF HAWAII

# PLANETARY SCIENCES

HAWAII INSTITUTE OF GEOPHYSICS



2525 CORREA ROAD
HONOLULU, HAWAII 96822

(NASA-CR-164072) THE COMPOSITION OF THE MARTIAN DARK REGIONS: OBSERVATIONS AND ANALYSIS Ph.D. Thesis (Hawaii Univ.) 302 p HC A14/MF A01 CSCL 03B

N81-20999

Unclas
G3/91 19527

# THE COMPOSITION
# OF THE
# MARTIAN DARK REGIONS:
# OBSERVATIONS AND ANALYSIS

by

ROBERT BENNETT SINGER

# THE COMPOSITION OF THE MARTIAN DARK REGIONS:
# OBSERVATIONS AND ANALYSIS

by

ROBERT BENNETT SINGER

A.B, (Geological Sciences), Harvard College (1973)

SUBMITTED IN PARTIAL FULFILLMENT
OF THE REQUIREMENTS FOR THE
DEGREE OF

DOCTOR OF PHILOSOPHY

at the

MASSACHUSETTS INSTITUTE OF TECHNOLOGY

JANUARY, 1980

Signature of Author.................................................
Department of Earth and Planetary
Sciences, January 24, 1980

Certified by.................................................
Thesis Supervisor

Accept~~d by.................................................
Chairman, Departmental Committee
on Graduate Students

# THE COMPOSITION OF THE MARTIAN DARK REGIONS: OBSERVATIONS AND ANALYSIS

by

ROBERT BENNETT SINGER

Submitted to the
Department of Earth and Planetary Science on
January 24, 1980 in partial fulfillment of the
requirements for the degree of Ph.D.

## ABSTRACT

The dark regions on Mars contain the surface materials most likely to resemble unmodified crustal rock, but their compositions have yet to be determined directly. New near-infrared (0.65-2.50μm) telescopic spectrophotometry for dark regions is presented here and interpreted using laboratory studies of iron-bearing mineral mixtures and terrestrial oxidized and unoxidized basalts. Upon closer inspection (by spacecraft) the telescopic dark regions have been found to consist of large scale intermixtures of bright soil (aeolian dust) and dark materials. Reflectance studies indicate that areal coverage of spectroscopically observed dark regions by bright materials does not exceed 40%, and is probably more generally 20 to 30% maximum. The dark materials themselves consist of an intimate physical association of very fine-grained ferric-oxide-bearing material with relatively high near-infrared reflectance and darker, relatively unoxidized rocks or rock fragments. While these two components could exist finely intermixed in a soil, a number of lines of evidence indicate that the usual occurrence is probably a thin coating (20 to 30 micrometers thick) of oxidized material physically bound to the rock surfaces. These coating thicknesses are greater than previously thought and should serve to inhibit further gas-solid weathering. With this type of coating geometry the spectral properties of dark materials are largely independent of grain size, from sand (∿1/2mm) to large outcrops. The oxidized coatings seem likely to be derived by alteration of the underlying rocks, although deposition of genetically unrelated dust is not ruled out. The coated rocks are dark and generally clinopyroxene bearing. The shallow band depths and low overall reflectances indicate that opaque minerals such as magnetite are

probably abundant. Regional variations in band positions indicate differing clinopyroxene compositions, mainly augites with varying calcium and iron content. Pigeonite or orthopyroxene may be present but cannot be unambiguously detected in existing data. Low-iron orthopyroxene is particularly difficult to detect because of interference from ferric-oxide absorptions. Contrary to previous interpretations of other data no spectral indication of olivine or basaltic glass is found. Re-examination of previously interpreted data, in the light of recent studies of mineral-mixture spectra and dark region spectral behavior beyond 1.1 μm, also shows no unambiguous evidence for olivine or glass. Spectral study of terrestrial basalts implies that possibly 5% or at most 10% modal olivine could be present in observed martian dark materials without being apparent in existing reflectance spectra. Ultramafic (high-olivine) lavas such as suggested for Mars by a number of researchers are not consistent with these interpretations. Mafic igneous rock types, similar to many terrestrial basalts, seem likely to predominate in observed dark regions. Since earlier data does indicate compositional variability, obtaining high quality near-infrared observations for additional dark regions around the planet is an important task for the future.

Thesis supervisor: Thomas B. McCord, Professor of Planetary Geology

## ACKNOWLEDGEMENTS

Throughout my professional career I will be indebted to my advisor, Dr. Thomas B. McCord, for the training I have received to conduct science productively in the real world. Tom provided a balance between guidance and freedom, coupled with excellent facilities and opportunities. My interest in Mars was initiated by a project suggested by Tom, and then allowed to grow freely. One of the advantages of being a student under Tom has been the opportunity to interact with his many colleagues. In this context I have benefited greatly from working with Dr. John B. Adams. John provided valuable suggestions as well as a free exchange of data and laboratory samples throughout my thesis work. I am also grateful to him for introducing me to the many geologic similarities between Mars and Hawaii. To Dr. Roger G. Burns I owe my theoretical introduction to mineral spectra and my practical introduction to laboratory spectroscopy, which grew into the development of a new instrument. Roger served as my primary contact at M.I.T. while I worked on my thesis *in absentia*, and on many occasions helped with bureaucratic as well as scientific matters. Dr. Robert L. Huguenin has also provided valuable discussion and help, including the use of his laboratory at the University of Massachusetts. One of the liabilities of moving away from Boston was the loss of regular contact with Bob. Dr. Michael J. Gaffey has been a frequent and well-appreciated source of information concerning both geological and astronomical questions. In addition I have learned much from him concerning science-related matters such as the writing of papers and proposals. Frequent interaction with Roger N. Clark, Dr. B. Ray Hawke, and Lucy A. McFadden has been valuable to me. I also appreciate discussions and cooperation with Drs. Carle M. Pieters, Larry A. Soderblom, Stanley Zisk, Jim W. Head, Dale P. Cruikshank, John Sinton, and Michael Garcia. On the Planetary Sciences staff, my thanks go to Karl Hinck, Duncan Chesley, and Rodney Okano for computer-related support, to Jeff Bosel and Mark Rognstad for help with instrumentation, to Pam Owensby and D'Na MacLasky for help with data processing, and last but certainly not least to Zeny Cocson and Sam Ostrowski for keeping things running in spite of people like me. At M.I.T. Debbie Gillette has been of great help with administrative matters.

My wife Arleen deserves special thanks. It would be pointless to speculate on how my graduate career might have progressed without her love, support, and perseverance. This thesis is dedicated to her, with love and appreciation.

TABLE OF CONTENTS

# PREFACE

I began my graduate studies in the Department of Earth and Planetary Sciences in 1975. During my residency at M.I.T. I did research with Prof's. Roger G. Burns and Thomas B. McCord. In the spring of 1977 I passed my general examination and left to continue research in absentia with Tom McCord at the University of Hawaii. The move was of course disruptive and isolated me from the M.I.T. faculty. Overall, however, I feel that it was worthwhile to have spent time at both locations. The resources available through the Institute for Astronomy and the Hawaii Institute for Geophysics are very good, both in terms of faculty and research staff and in terms of facilities, including Mauna Kea Observatory. In addition, that part of my training as a planetary scientist which has come from firsthand exposure to the many aspects of Hawaiian volcanism is not insubstantial.

My initial interest when I arrived at M.I.T. was in terrestrial remote sensing. While working for Roger Burns I received my basic training in the theoretical and laboratory measurement aspects of reflectance spectroscopy. After I began work for Tom McCord (still at M.I.T.) I gained experience with reflectance spectroscopy as a tool for remote determination of planetary surface composition. Throughout this period my general knowledge of planetary science (in contrast to my classical geology undergraduate training) increased.

Sometime after arriving at the University of Hawaii Tom McCord suggested that I take on a project involving multispectral imaging from Viking. This was my introduction to Mars. While little of this work is included in this thesis I am still involved with an outgrowth of the original project. My interest in Mars grew concurrently with the design and construction of a spectrogoniometer system for our laboratory, largely conducted by myself and described in Chapter IV. Tom McCord and John Adams (University of Washington) jointly suggested that the composition of the martian dark regions was a topic in need of both telescopic and laboratory study, and that I might consider this for my thesis. I am indebted to Tom and John for the original suggestion and for many follow-up discussions. As my work progressed I became increasingly involved with basalts and their alteration products. I can foresee coming full-circle, back to using remote sensing as a tool for investigating planetary science problems on Earth.

This thesis was prepared in the form of six papers also intended for publication. Two have been published already (Chapters I and III) and three others have been submitted as of this writing (Chapters IV, V, and VI). I chose this format (before the papers were written) as an efficient way to conduct and report various free-standing segments of a scientific research program. A disadvantage of this thesis format is that some introductory and descriptive material is of necessity repeated. Chapter I is a review paper and serves as an introduction to Mars science from reflectance spectroscopy. The reader may wish to only skim the introductory material in subsequent chapters, although each paper does have a somewhat different emphasis.

# CHAPTER I

## Mars Surface Composition From Reflectance Spectroscopy: A Summary

This paper has been published in J. Geophys. Res., 84, 8415-8426, 1979. Authors: R.B. Singer, T.B. McCord, R.N. Clark, J.B. Adams, and R.L. Huguenin.

## ABSTRACT

Visible and near-infrared (0.3 - 2.6 μm) reflectance spectra of the martian surface have been obtained primarily from earth-based telescopic observations, and multispectral images have been obtained both from spacecraft and earth-based observations. Observations in this wavelength region have confirmed the bimodal albedo distribution of surface materials, first observed visually. All spectra of Mars are characterized by strong $Fe^{3+}$ absorptions from the near-UV to about 0.75 μm. Darker regions show this effect to a lesser degree, and are interpreted to be less oxidized materials. In addition, dark areas have $Fe^{2+}$ absorptions near 1.0 μm, attributed primarily to olivines and pyroxenes. There is evidence at infrared wavelengths for highly dessicated mineral hydrates and for $H_2O$-ice and/or adsorbed $H_2O$. Observations of the north polar cap show a strong $H_2O$-ice spectral signature but no spectral evidence for $CO_2$-ice, while only $CO_2$-ice has been identified in spectra of the south polar cap. While the brightest materials on Mars are widespread and correlate with aeolian dust, darker materials show greater mineralogic variability and are thought to be closer in petrology and physical location to their parent rock. At present the best model for the dark materials is somewhat oxidized basaltic or ultramafic

rock, regionally variable in composition and details of oxidation. The bright materials appear to be finer-grained assemblages of primarily highly oxygen-sharing dessicated mineral hydrate, some ferric oxides, and other less major constituents, including a small amount of relatively unaltered mafic material. The bright materials seem likely to be primary and/or secondary alteration products of the basaltic or ultramafic dark materials.

## INTRODUCTION

To understand the current state and the geologic evolution of Mars it is necessary to characterize surface materials in terms of composition and mineralogy and to define the distribution of these materials around the planet. Remote sensing techniques will continue to be necessary to derive this information on regional and global scales, even if an Apollo- or Luna-type sampling program is carried out (Head et al., 1978).

The primary compositional remote sensing techniques so far applied to Mars are visible and near-infrared reflectance spectroscopy and multispectral mapping (emission spectra of dust clouds have yielded some important compositional information about airborne dust). Multispectral mapping has been done on a global scale from Viking images (Soderblom et al., 1978) and on a very detailed scale at the Viking landing sites (e.g., Evans and Adams, 1979; Guinness et al., 1980; Strickland, 1979). Low spectral resolution reflectance spectra have been generated from Viking lander images for some materials surrounding the spacecraft (Huck et al., 1977). Most of the reflectance spectra and some of the multispectral images have been obtained using earth-based telescopes. Earth-based observations will be the primary source of new data, at least until the Galileo spacecraft passes Mars in 1984 en route to Jupiter, and perhaps until the next Mars mission, hopefully by the late 1980's. Other remote sensing techniques, such as X-ray spectroscopy and X-ray fluorescence, are dependent on future spacecraft missions.

It is the purpose of this paper to discuss available reflectance spectra (primarily telescopic) and multispectral maps, including some new data, and their interpretations. Ongoing analysis and laboratory studies will be reviewed as well as prospects for the future.

# OBSERVATIONS

## Earth-Based Observations

McCord and Adams (1969) reviewed available reflectance data prior to that date. The bulk of the measurements were integral disk and in the spectral range from 0.3 to 1.2 μm. Agreement among the data sets is good, and the basic shape of the reflectance curve is well defined.

During the 1969 apparition ($L_s$ = 162° - 163°), McCord and Westphal (1971) observed seven regions on the surface, approximately 200 km in diameter: five from 0.3 to 1.1 μm (24 filters) and two from 0.3 to 2.5 μm (52 filters). At the same time, Binder and Jones (1972) observed a much larger number of 300- to 500-km-diameter areas from 0.6 to 2.3 μm, but with only 10 filters. Binder and Jones were able to develop good statistics on the Martian albedo distribution, but the spectral resolution is too low for much compositional analysis. In addition, the spectral slopes in the infrared do not agree with more recent observations; this may be due to the standard star calibration problems Binder and Jones described.

During the 1973 apparition ($L_s$ = 301° - 302°), McCord <u>et al</u>. (1977a) observed 26 areas on the surface of Mars, using 25 filters covering the wavelength region from 0.3 to 1.1 μm. Near-simultaneous multispectral images were taken through 20 filters in the same spectral region (McCord et al., 1977b) using a silicon diode vidicon system. These observations occurred during a dust storm originating in Solis Lacus and include some spectra and spectral images of optically thick dust clouds. In 1976, McCord et al. (1978) obtained the first high-precision, 1½% spectral resolution data from 0.6 to 2.6 μm for the integral disk of Mars ($L_s$ = 58°), using a circularly variable filter (CVF) and an indium antimonide detector. During the 1978 apparition ($L_s$ = 48° - 50°), an improved version of this instrument was used to obtain spectra of 11 regions, 1000-2000 km in diameter, from 0.6 to 2.5 μm (McCord et al., 1980). The relatively large size of these areas was due in part to the unfavorable apparition. With further improvements in instrumentation and increasingly favorable oppositions much smaller regions can be observed in the future.

Figure 1 is a map of area locations for data taken by McCord et al. in 1969, 1973, and 1978. Locations of dust cloud spectra, or spectra of areas partially obscured by dust clouds, are not shown on this map. An additional spectrum, 78-11, was taken of the north polar cap.

Spacecraft Observations

Spectral reflectance observations from spacecraft consist mainly of multispectral images from Viking orbiters and landers. Soderblom et al. (1978) have prepared three-color photometric maps for a large portion of the planet between latitudes 30°N and 60°S from VO II approach images ($L_s$ = 105°). These have good spatial resolution (10-20 km) but limited spectral coverage and resolution (three broad bands: 0.45 ± 0.03 μm, 0.53 ± 0.05 μm, and 0.59 ± 0.05 μm). Soderblom and others are preparing additional multispectral maps using Viking orbital images of selected regions and at higher spatial resolution (L.A. Soderblom, personal communication). Viking lander cameras are capable of taking images in six spectral bandpasses from 0.4 to 1.0 μm. Huck et al. (1977) developed a technique for transforming these six brightness values into an estimate of spectral reflectance. These data are being used successfully for determining color differences and properties of the surface at the two landing sites (Evans and Adams, 1979; Strickland, 1979). As with orbital data, repeat coverage is available throughout a martian year, permitting monitoring of variations in surface optical properties (Guinness et al., 1979).

The Viking infrared thermal mapper (IRTM) includes the visible and near infrared in one of its six bandpasses. Kieffer et al. (1977) used this instrument to generate a global map of bolometric normal albedo from latitudes 30°N to 30°S for $L_s$ = 124° - 129°. A histogram presented with the map demonstrates a distinct bimodal albedo distribution. Farmer et al. (1977) combined the continuum bandpasses in the Mars atmospheric water detector (MAWD) to generate a narrow bandpass global map of surface brightness at 1.4 μm for VO I and VO II. Combined coverage extends from latitudes 65°N to 50°S. Both these maps and the IRTM albedo map agree rather well with earth-based observations of bright and dark markings.

Mariner 9 carried an ultraviolet spectrometer (UVS) and a thermal infrared interferometric spectrometer (IRIS). UVS observations were almost entirely dominated by light scattered from atmospheric dust particles (Barth et al., 1972). The IRIS produced emission spectra from 5 to 50 μm of dust clouds and many areas on the surface (Hanel et al., 1972). Mariner 6 and 7 each carried an infrared spectrometer (IRS) covering the spectral region from 1.9 to 14.4 μm. The instrument and some results are described by Pimentel et al., (1974).

Comparison of Viking and Earth-based Observations

The agreement between Viking orbiter and lander multispectral observations and earth-based reflectance spectroscopy is generally good. A comparison of Viking

Orbiter II and earth-based reflectance data for a few regions on Mars is shown in Figure 2 (Singer and McCord, 1980). All spectra have been scaled to a value of 1.0 at 0.56 μm. These and other VO II approach data have a tendency to be slightly less 'red' than corresponding earth-based observations, that is, the slope from 0.45 to 0.59 μm is lower. The Viking images were taken during a martian season ($L_s = 105°$) characterized by white condensates (presumably water ice) at certain locations (Smith and Smith, 1972). Soderblom et al. (1978) demarcated areas where they felt that clouds and frost significantly obscured the surface; it is possible that smaller amounts of condensate over much of the rest of the planet could account for the observed differences in spectrum slope.

Comparison between Viking lander and earth-based observations are less straightforward because telescopic spectra do not yet exist for the exact landing sites and because the lander cameras view the surface on a much more detailed scale. Soil color at both lander sites agrees closely with telescopic reflectance data for bright regions, and spectral reflectance estimates from 0.4 to 1.0 μm are very similar to telescopic spectra (Huck et al., 1977). More detailed studies of spectral comparisons are currently being performed.

## SPECTRAL REFLECTANCE PROPERTIES OF MARTIAN SURFACE MATERIALS

To a visual observer, Mars shows a generally bimodal albedo distribution: bright and dark, with some areas of intermediate albedo. This has been confirmed as a general relationship in the visible and near-infrared by earth-based telescopic observations (e.g. Binder and Jones, 1972) and spacecraft observations (e.g. Farmer et al., 1977; Kieffer et al., 1977). Measurements of bright area to dark area albedo ratios vary from a low of about 1.8 to a high near 3.0 (McCord and Westphal, 1971; Binder and Jones, 1972). Superimposed on these overall albedo differences are more subtle but very important spectral variations.

A composite average spectrum of several typical bright areas is shown at the top of Figure 3, scaled to unity at 1.02 μm (McCord et al., 1977a, 1980). Bright area spectra are characterized by strong $Fe^{3+}$ absorptions from the UV to 0.75 μm with a slope change at about 0.6 μm and a weaker $Fe^{3+}$ absorption near 0.87 μm. These features are attributed to a ferric oxide content of about 6-8 wt. % (Huguenin et al., 1977). From the band minimum near 0.87 μm to about 1.3 μm the spectrum slopes upwards. Between 1.4 and 1.7 μm there is a broad absorption which has been interpreted as $H_2O$ in a hydrate or ice (McCord et al., 1978, 1980). Superimposed on this are sharper Mars atmospheric $CO_2$ absorptions, most noticeably at 1.45 and 1.62 μm. From 1.8 to 2.2 μm the spectrum is dominated by a deep Mars atmospheric $CO_2$ absorption. Removal of a model $CO_2$ atmosphere (McCord et al., 1978) yields a fairly flat spectrum from 1.7 to 2.5 μm, with the possibility of an additional $H_2O$ absorption near 1.9 μm (McCord et al., 1980)

Dark area spectra are substantially different from bright area spectra. The bottom of Figure 3 shows a composite spectrum of visible and infrared data in Iapygia (69-6 and 78-10), also scaled to unity at 1.02 μm (McCord and Westphal, 1971; McCord et al., 1980). The slope from UV to red is reduced compared with that for bright region spectra; the absorption near 0.87 μm is also weaker. These two features indicate a lower $Fe^{3+}$ content (Adams and McCord, 1969; Huguenin et al., 1977; McCord et al., 1977a). In addition, dark area spectra show $Fe^{2+}$ absorptions around 1.0 μm. These vary with location on the planet and are thought to represent differences in mafic mineralogy, mostly pyroxenes and olivines (Adams and McCord, 1969; Huguenin et al., 1977; McCord et al., 1977a; Singer, 1980b). In contrast to the bright area spectra, dark area spectra have a distinctive peak near 0.75 μm and slope fairly uniformly downwards from 1.1 to 2.5 μm (after martian atmospheric $CO_2$ effects are removed) (McCord et al., 1980).

Reflectance spectra from 0.3 to 1.1 μm of dust clouds are very similar to the spectra of the brightest regions on Mars, which appear fairly uniform. This correlates with other evidence that the source for the brightest surface material is rather homogeneous aeolian dust (McCord et al., 1977a). As discussed above, dark area spectra show less uniformity and indicate less oxidized (weathered) material, so they may represent compositionally varied materials closer in optical properties, petrology, and physical location to their parent rocks.

Based on the likelihood that many spectroscopically observed dark areas have partial coverage by streaks and splotches of bright material, Singer and McCord (1979) have applied a simple additive or checkerboard model to investigate the effects of bright spectrum contamination of dark region observations. In this two-component model the observed spectrum is the average, weighted for relative areal coverage, of the spectra of bright and dark surface types. It was assumed that the bright streaks have the same spectral characteristics as observed bright regions and dust clouds and that the observed dark area spectra are actually mixtures of bright and dark spectral components. The spectral influence of varying amounts of bright material is then algebraically removed (subtracted) from observed dark region spectra.

This model is appropriate only where the characteristic size of bright and dark patches is much greater than the mean optical path length in those materials. This assumption is felt to be valid for much of the martian surface.

The results of an analysis for a dark area spectrum using an additive model as described above is shown in Figure 4. Spectral coverage is essentially complete from 0.3 to 2.5 μm and represents a composite of two data sets (McCord and Westphal, 1971; McCord et al., 1980). A model Mars atmosphere (Kieffer, 1968) was used to remove martian $CO_2$ absorptions in the infrared. The top curve, labelled 'Bright,' is the average of a number of typical bright region spectra. The next lower curve, labelled 'Dark.' is the observed spectrum for the telescopic dark region Iapygia. The curves below this show the results of the analysis described above for removal of the influence of 10%, 20%, 30%, and 40% areal coverage by bright material. With removal of increasing amounts of the bright material spectrum the 'dark material' spectra show reduced UV absorption and less indication of an absorption near 0.87 μm. This is consistent with a lower $Fe^{3+}$ content in the dark material. In addition, the $Fe^{2+}$ absorption near 1 μm becomes more apparent, and the peak reflectance shifts slightly toward shorter wavelengths. Removal of bright material effects corresponding to greater than about 40% areal coverage results in an unrealistically low albedo dark material spectrum; this places an approximate upper limit for coverage for dark regions by bright material. A 20%-30% contamination by bright material seems to be a reasonable estimate for a 'typical' dark region; better estimates for specific regions could be obtained using high-resolution Viking images processed to maintain albedo information.

There is some telescopic evidence for spectral variation of high albedo areas with location and/or time. Huguenin et al., (1977) have attributed some of the spectral difference between bright regions and airborne dust to changes in the degree of hydration of the dust, which they suggest becomes dessicated, possibly by UV radiation, after it has been exposed. The bright areas observed in 1969 (McCord and Westphal, 1971) such as 69-1 in Arabia have similarities to those observed in 1973 (McCord et al., 1977a) such as 73-1 and 73-2, but the 69-1 spectrum has a slightly less intense absorption in the blue UV, and the weak $Fe^{3+}$ band near 0.87 μm is not apparent. Instead, a weak band is present near 0.95 μm, a wavelength more characteristic of $Fe^{2+}$ mineralogy. The interpretation is that Arabia, at least in 1969, showed an incomplete masking of a ferrosilicate surface component by a bright surface component having a considerably higher ferric oxide content (Huguenin *et al.*, 1977).

# COMPOSITIONAL INTERPRETATION OF SPECTRAL OBSERVATIONS

## Ferric Oxide

Because of the visual red color and the polarization properties of Mars, ferric oxides have long been considered likely candidates for surface materials (e.g. Wildt, 1934; Dollfus, 1957; Sharonov, 1961; Draper _et al._, 1964; Sagan _et al._, 1965; Binder and Cruikshank, 1966; Younkin, 1966). At wavelengths greater than about 1 μm, however, all Mars spectra, especially for dark regions, deviate substantially from the spectra of pure iron oxides. Huguenin _et al._ (1977) have interpreted bright region spectra to indicate soils with about 6-8 wt. % ferric oxide. The major absorption edge which dominates the visible spectrum arises from a pair of $O^{2-} \rightarrow Fe^{3+}$ charge transfer bands centered near 0.34 and 0.40 μm. Slope changes near 0.6 μm are due to $Fe^{3+}$ interelectronic transitions. Another absorption band occurs centered at 0.84-0.89 μm, depending on the type of ferric oxide, and is also due to an interelectronic transition in $Fe^{3+}$. The details of ferric oxide absorptions depend on the crystal structure and the degree of hydroxylation. It is felt that telescopic spectra are consistent with dessicated goethite as the dominant ferric oxide species (Anderson and Huguenin, 1977).

Because the three Viking orbiter bandpasses fall on intense $Fe^{3+}$ absorptions, multispectral maps generated from these data primarily show differences in ferric oxide mineralogy and content. Soderblom et al. (1978) have identified a number of regional units of uniform color. The highest albedo surface unit (excluding condensates) is rather 'red' and correlates with aeolian dust. (For Viking orbiter observations the term 'red' is used to mean a high reflectance in the 0.59-μm bandpass relative to the 0.45-μm bandpass. This definition is usually, but not always, in concurrence with colors perceived by the eye.) A somewhat less red and less bright soil unit is observed to be stratigraphically lower, a relationship also observed at the Viking Lander I site. Significant color differences are also seen by Viking orbiter in the dark regions; in fact, both the reddest and least red geologic units observed are low in albedo.

A photostimulated oxidation mechanism has been demonstrated for magnetite, olivine, and basaltic glass which could occur at realistic rates in the present martian environment (Huguenin, 1973a, b, 1974). This permits extensive weathering of $Fe^{2+}$ bearing minerals to ferric oxides, other transition metal oxides, hydrated clay minerals, and carbonates. Hydrothermal alteration of mafic or ultramafic materials, associated with volcanic activity, could also be a source for ferric oxides and clay minerals. Palagonitization, caused by volcanic eruption in the presence of water-ice, has been suggested as an alteration mechanism to produce iron-rich clays on Mars (Toulmin et al., 1977; Soderblom and Wenner, 1978).

Mafic and Ultramafic Materials

Adams and McCord (1969) successfully modeled both bright and dark area spectra from 0.4 to 1.1 μm using an olivine basalt with different degrees of oxidation (Figure 5). An acid solution was used to induce oxidation of the basalt; analysis showed that magnetite was the only mineral phase affected but that the weathering product, limonite, precipitated as a partial coating over other mineral grains. This laboratory modeling reproduces well the characteristics of spectra than available but does not address the spectrum beyond 1.1 μm nor does it fully explain some details seen in more recent spectroscopy of Mars. Updated laboratory modeling (Singer, 1980a) has concluded that a thin $Fe^{3+}$ rich layer coating a dark substrate can properly reproduce the characteristic shape of dark region spectra from 0.3 to 2.6 μm without fully masking infrared absorptions in the substrate. In the visible, $Fe^{3+}$ absorptions dominate the spectrum and account for the rise in reflectance to the spectrum peak near 0.75 μm. The long-wavelength side of this peak is defined by the 0.84- to 0.89-μm ferric oxide band and by the continuing decrease in infrared reflectance as the thin ferric-oxide layer becomes increasingly transparent to longer wavelengths. At some wavelength the spectrum will theoretically converge with that of the dark substrate. Diagnostic $Fe^{2+}$ absorptions near 1 μm in such mafic minerals as pyroxenes and olivines are reduced in spectral contrast and somewhat modified but do persist in the spectrum. These conclusions are taken as confirmation and extension of the work by Adams and McCord (1969) and Huguenin (1973a).

Telescopic spectra of martian dark areas that were measured during the 1969 and 1973 (McCord and Westphal, 1971; McCord _et al._, 1977a) and spectra derived from 1973 telescopic multispectral images (McCord _et al._, 1977b) have been interpreted by Huguenin _et al._ (1977, 1978). Each spectrum showed a different composite of absorption bands in the 0.7- to 1.1-μm wavelength region. (A study by Singer and McCord [1979] has shown that the variation seen in these absorptions can not merely be due to variable mixing of bright dust and a single dark material.) While a few of the constituent band positions could be determined directly from the spectra, most band positions were derived by additional data processing. The principal technique used was relative reflectance spectroscopy: all spectra were divided by the spectrum of a standard area, which emphasizes relative differences in absorptions. Recognizing the relatively large uncertainties in the band positions derived by this ratio technique and noting the restricted wavelength range and resolution, tentative mineral identifications were made according to the interpretation scheme outlined by Adams (1975).

Most of the interpretations by Huguenin et al. (1977, 1978) were for dark areas within the Margaritifer S. and Coprates quadrangles (longitudes 0°-90° and latitudes 0°-30°S). The spectra were used for deriving the average mineralogies of dark areas within the quadrangles, and spectrophotometric images used in an attempt to define the spatial extent of the mineralogic units. Nine dark area units were defined, but the average mineralogies for only six of the units were characterized due to band masking by contaminant dust. The spectra showed features that were attributed to mixtures of orthopyroxene (or pigeonite) + clinopyroxenes + olivine (or glass). The relative strengths of the features attributed to these minerals varied from unit to unit, and this was interpreted to indicate possible variations in their relative proportions. Most of the units were interpreted to be olivine-rich, and one of the units in central Erythraeum M. was proposed to contain a titaniferous clinopyroxene based on apparent absorption features at 0.6-0.77 μm (attributed to $Fe^{2+} \rightarrow$

$Ti^{2+}$ charge transfer in augite-diopside) and 0.96-1.00 μm (attributed to an $Fe^{2+}$ interelectronic transition in augite-diopside).

Huguenin <u>et al</u>. (1978) further noted several correlations between their 'petrologic' (mineralogic) units and geologic and albedo units. The lower albedo units, for example, were interpreted to have relatively more clinopyroxene + olivine (or glass) and less orthopyroxene (or pigeonite) than the higher albedo units. One petrologic unit in western Erythraeum M. corresponded closely in location with a cratered plains unit in the Coprates Quandrangle. In addition, chaos and channeled terrain appeared to occur preferentially in the areas characterized by low orthopyroxene/clinopyroxene + olivine (or glass) ratios.

Other dark area interpretations were proposed by Huguenin <u>et al</u>. (1977). The spectrum of an area in Mare Acidalium, for example, showed a unique complex of absorption features between 0.7 and 1.1 μm that is very similar to the spectra of iron-rich calcic pyroxenes discussed by Adams (1975). The higher spectral resolution data now available (McCord et al., 1980) and obtained in the future will allow more positive identification of mineralogy and mineralogic variations (e.g. Singer, 1980b).

Interpretations of reflectance spectra for dark regions on Mars indicate a basaltic or ultramafic source rock. This is consistent with independent proposals by Maderazzo and Huguenin (1977) and McGetchin and Smyth (1978) that martian crustal rocks may be derived from iron-rich ultramafic primary lavas.

Water

Water was first discovered on Mars by Sinton (1967), who observed the strong absorption near 3 μm. This band was further defined by Beer et al. (1971) and Houck et al. (1973). Pimentel et al. (1974) found evidence for at least small amounts of water in or on the surface using the Mariner 6 and 7 IRS instruments in the 3-μm region. An analysis of an integral disc spectrum of Mars by McCord et al. (1978) also shows absorptions in the 1.4- to 2.0-μm region that were attributed to water in the form of ice plus a highly dessicated mineral hydrate. New data and analysis (McCord et al., 1980) have shown additional evidence for a mineral hydrate and/or solid $H_2O$.

All martian IR spectra observed so far show a drop in reflectance from 1.3 to 1.4 μm, independent of Mars atmospheric $CO_2$ absorptions. This effect is greater for bright areas than for dark areas. In order to understand the reason for this drop, Clark (1980) and McCord et al. (1980) approximated the reflectance of Mars with spectra typical of basalts and their oxidation products. The light areas were modeled with a spectrum consistent with heavy oxidation, and the dark areas with a spectrum typical of thin oxidized layer over basaltic material (as discussed above). These spectra were scaled in the same manner as the telescopic spectra and nave a smooth reflectance beyond 1.1 μm. To these spectra, an ice spectrum was algebraically added in small amounts to match the apparent 1.4-μm drop observed in the martian spectra. The ratio of the martian spectra to the simulated spectra shows absorption features which correlate with the expected martian atmospheric $CO_2$ bands (Figure 6a and 6b). The simulations fit the bright area spectra better than the dark spectra and indicate that the relative band intensities are weaker and different for dark areas than bright areas. The results show that the water is present in the martian surface in different forms (e.g., frost or ice sheets on the surface, ice mixed in the regolith, or bound). Clark (1980) has shown that bound water bands which typically occur at 1.4 and 1.9 μm do not shift appreciably ($\lesssim$100 Å) with temperatures from 300° to 150°K and that bound water can be spectrally distinguished from free ice. The simulation of martian spectra described above shows that free water ice is the primary cause of the 1.3- to 1.4-μm drop in reflectance and that there is more water in the bright areas than in the dark areas. The physical details of this ice/regolith combination have yet to be determined and may be difficult to determine with the existing data. There is some evidence for bound water in the martian surface at 1.4 and 1.9 μm, but these are difficult regions to observe from the earth because of uncertainties in telluric water removal and the strong 2-μm martian $CO_2$ atmospheric absorption.

A spectrum of the north polar cap of Mars (McCord et al., 1980), taken in the northern spring ($L_s = 50°$) with extent of the cap to about 60°N, shows very strong water-ice bands. Clark and McCord (1980) have successfully modeled this spectrum by assuming that 60% of the light is reflected by water ice and 40% of the light is reflected by grey material (same reflectance at all wavelengths) (Figure 7). The actual amount of water present is difficult to determine because of the variation in grain size and/or hydration state. There is good evidence that there was not polar hood or clouds present at the time of this observation (James et al., 1979, also personal communication, 1978). A spectrum of the south polar cap taken by Larson and Fink (1972) with a fourier spectrometer (1.2-2.8 μm) shows 11 narrow absorptions, which they identified as solid $CO_2$. No water could be identified in this spectrum, at least in part because of discontinuities in the spectral coverage caused by telluric $H_2O$.

Composition of Martian Dust

Most of the compositional information currently available for martian dust comes from analysis of Mariner 9 IRIS observations of dust suspended in the atmosphere. While this is not reflectance data, a short discussion is included here for completeness. Hanel et al. (1972) concluded from infrared features that the primary constituent of the dust has an $SiO_2$ content of 55-65%, consistent with a rather acidic rock or mineral composition. It was argued by Hunt et al. (1973) that certain other infrared features expected for acidic materials are not present. From comparisons of the IRIS data to infrared transmittance of terrestrial materials, they concluded that a montmorillonite-type clay provided the best match to the reststrahlen band near 9 μm. Aronson and Emslie (1975) have shown that there are several other minerals which could also produce the 9-μm feature, including some feldspars and micas. Like montmorillonite, these minerals are strongly Si-O bond sharing. Toon et al. (1977) concluded that the 9 μm feature could not be accounted for by pure montmorillonite. They suggest that the observed feature is dominated by acidic or intermediate igneous silicates and/or clays, but could also include a significant component of lower $SiO_2$ material such as basalt. Additional results are that limonite, carbonates, nitrates, and carbon suboxide are excluded as major (greater than 5 or 10%) constituents of the airborne dust (Hunt et al., 1973; Toon et al., 1977).

Earth-based reflectance spectra of optically thick dust clouds have been shown to be very similar to spectra of uniform bright regions on the surface (McCord et al., 1977a). This material has been interpreted as 6-8 wt. % ferric oxide, with the remaining bulk largely composed of an $Fe^{2+}$-poor dessicated mineral hydrate, possibly a clay mineral (Huguenin et al., 1977). Huguenin et al. (1977) also suggested that the airborne dust might be less dessicated than apparently similar materials on the surface. Newer infrared reflectance spectra of bright surface materials on Mars (McCord et al., 1978, 1980) are consistent with the presence of dessicated mineral hydrates and are actively under study. At this point, however, a positive mineral identification is not possible for this rather spectrally neutral (in the visible and near-infrared) strongly oxygen-sharing component of the dust.

## PROSPECTS FOR THE FUTURE

Earth-based spectrophotometric observations of Mars will continue to be important as a major and perhaps the only source of new compositional information through the next decade. Oppositions, approximately every 26 months, will become increasingly favorable through 1988 as the angular size of Mars as seen from the earth increases. If appropriate instrumentation is available, worthwhile observations can be made with the space telescope. Interpretation of existing data is of course a continuing process. Several groups are involved in laboratory studies aimed at better understanding the materials and processes on Mars. Results of these programs are helpful in planning future observations, both from the earth and from spacecraft.

We strongly emphasize the need for high spectral resolution mapping of a significant fraction of the martian surface in the visible and near-infrared from a spacecraft. The first opportunity for data of this type is when the Galileo Near Infrared Mapping Spectrometer (NIMS) flies by en route to Jupiter. Up to one third of the martian surface could be mapped with high spectral quality at spatial resolution better than that possible from the earth. Full coverage at far better resolution would be possible as part of an orbital science package on the next Mars mission, hopefully by the late 1980's. This type of global study is necessary to expand on and place in context results from local exploration or sample return.

## ACKNOWLEDGEMENTS

This work was supported by NASA grants NSG 7312 and NSG 7590. We are grateful to Laurence A. Soderblom for his helpful review. Contribution number 233 of the Planetary Sciences Laboratory.

## REFERENCES

Adams, J. B., Interpretation of visible and near-infrared diffuse reflectance spectra of pyroxenes and other rock forming minerals, in Infrared and Raman Spectroscopy of Lunar and Terrestrial Minerals, edited by C. Karr, Jr., pp. 91-116, Academic, 1975.

Adams, J. B., and T. B. McCord, Mars: Interpretation of spectral reflectivity of light and dark regions, J. Geophys. Res., 74, 4851-4856, 1969.

Anderson, K. L., and R. L. Huguenin, Photodehydration of martian dust (abstract), Bull. Amer. Astron. Soc., 9, 449, 1977.

Aronson, J. R., and A. G. Emslie, Composition of the martian dust as derived by infrared spectroscopy from Mariner 9, J. Geophys. Res., 80, 4925-4931, 1975.

Barth, C. A., C. W. Hord, A. I. Steward, A. L. Lane, Mariner 9 ultraviolet spectrometer experiment: Initial results, Science, 175, 309-312, 1972.

Beer, R., R. H. Norton, J. V. Martonchik, Astronomical infrared spectroscopy with a Connes-type interferometer: II, Mars, 2500-3500 $cm^{-1}$, Icarus, 15, 1-10, 1971.

Binder, A. B., and D. P. Cruikshank, Lithological and Mineralogical investigation of the surface of Mars, Icarus, 5, 521-525, 1966.

Binder, A. B., and J. C. Jones, Spectrophotometric studies of the photometric function, composition, and distribution of the surface materials of Mars, J. Geophys. Res., 77, 3005-3019, 1972.

Clark, R. N., The spectral reflectance of water-mineral mixtures at low temperatures, submitted to J. Geophys. Res., 1980.

Clark, R. N., Mars: Water-ice features in near infrared spectra of small areas (abstract), Proc. Amer. Astron. Soc., 10, 567, 1978.

Clark, R. N., and T. B. McCord, Mars Residual North Polar Cap: Earth-based spectroscopic confirmation of water ice as a major constituent and Evidence for hydrated minerals, submitted to J. Geophys. Res., 1980.

Dollfus, A., Propriétés photométrique des contrées désertique sur la planéte Mars, Comptes Rendus, 244, 162-164, 1957.

Draper, A. L., J. A. Adamcik, and E. K. Gibson, Comparison of the spectra of Mars and a geothite-hematite mixture in the 1 to 2 micron region, Icarus, 3, 63-65, 1964.

Evans, D. L., and J. B. Adams, Comparison of Viking lander multispectral images and laboratory reflectance spectra of terrestrial samples, Proc. Lunar Planet. Sci. Conf. 10th, 1829-1834, 1979.

Farmer, C. B., D. W. Davies, and A. L. Holland, Mars: Water vapor observations from the Viking Orbiters, J. Geophys. Res., 82, 4225-4248, 1977.

Guinness, E. A., R. E. Arvidson, D. C. Gehret, and L. K. Bolef, Color changes at the Viking landing sites over the course of a Mars year, J. Geophys. Res., 84, 8355-8364, 1979.

Hanel, R., B. Conrath, W. Hovis, V. Kunde, P. Lowman, W. Maguire, J. Pearl, J. Pirraglia, C. Probhadara, B. Schlachman, G. Levin, P. Straat, and T. Burke, Investigation of the martian environment by infrared spectroscopy on Mariner 9, Icarus, 17, 423-442, 1972.

Head, J. W., J. B. Adams, T. B. McCord, C. Pieters, and S. Zisk, Regional stratigraphy and geologic history of Mare Crisium, in Proceedings of the Conference on Luna 24 entitled Mare Crisium: The View from Luna 24, edited by R. B. Merrill and J. J. Papike, pp. 43-74, Pergamon, New York, 1978.

Houck, J. R., J. B. Pollack, C. Sagan, D. Schaack, and J. A. Decker, Jr., High altitude infrared spectroscopic evidence for bound water on Mars, Icarus, 18, 470-480, 1973.

Huck, F. O., D. J. Jobson, S. K. Park, S. D. Wall, R. E. Arvidson, W. R. Patterson, and W. D. Benton, Spectrophotometric and color estimates of the Viking lander sites, J. Geophys. Res., 82, 4401-4411, 1977.

Huguenin, R. L., Photostimulated oxidation of magnetite, I. Kinetics and alteration phase identification, J. Geophys. Res., 78, 8481-8493, 1973a.

Huguenin, R. L. Photostimulated oxidation of magnetite, 2, Mechanism, J. Geophys. Res., 78, 8495-8506, 1973b.

Huguenin, R. L., The formation of geothite and hydrated clay minerals on Mars, J. Geophys. Res., 79, 3895-3905, 1974.

Huguenin, R. L., J. B. Adams, and T. B. McCord, Mars: Surface mineralogy from reflectance spectra, in Lunar Science VIII, pp. 478-480, Lunar Science Institute, Houston, 1977.

Huguenin, R. L., J. W. Head, T. R. McGetchin, Mars: Petrologic units in the Margaritifer Sinus and Coprates Quadrangle, Reports of Planetary Geology Program, 1977-1978, NASA Tech. Memo. 79729, 1978.

Hunt, G. R., L. M. Logan, and J. W. Salisbury, Mars: Components of infrared spectra and composition of the dust cloud, Icarus, 18, 459-469, 1973.

James, P. B., G. Briggs, J. Barnes, A. Sprick, Seasonal recession of Mars' south polar cap as seen by Viking, J. Geophys. Res., 84, 2889-2922, 1979.

Kieffer, H. H., Near infrared spectral reflectance of simulated Martian frosts, Ph.D. thesis, Calif. Inst. of Technol., Pasadena, 1968.

Kieffer, H. H., T. Z. Martin, A. R. Peterfreund, and B. M. Jakosky, Thermal and albedo mapping of Mars during the Viking primary mission, J. Geophys. Res., 82, 4249-4291, 1977.

Larson, H. P., and U. Fink, Identification of carbon dioxide frost on the Martian polar caps, Astrophys. J., 171, L91-95, 1972.

Madarazzo, M., and R.L. Huguenin, Petrologic implications of Viking XRF analysis based on reflection spectra and the photochemical weathering model (abstract), Bull. Amer. Astron. Soc., 9, 527-528, 1977.

McCord, T. B., and J. B. Adams, Spectral reflectivity of Mars, Science, 163, 1058-1060, 1969.

McCord, T. B., and J. A. Westphal, Mars: Narrowband Photometry, from 0.3 to 2.5 microns, of surface regions during the 1969 apparition, Astrophys. J., 168, 141-153, 1971.

McCord, T. B., R. L. Huguenin, D. Mink, and C. Pieters, Spectral reflectance of Martian areas during the 1973 opposition: Photo-electric filter photometry 0.33-1.10μm, Icarus, 31, 25-39, 1977a.

McCord, T. B., R. L. Huguenin, and G. L. Johnson, Photometric imaging of Mars during the 1973 opposition, Icarus, 31, 293-314, 1977b.

McCord, T. B., R. Clark, and R. L. Huguenin, Mars: Near-infrared spectral reflectance and compositional implications, J. Geophys. Res., 83, 5433-5441, 1978.

McCord, T. B., R. N. Clark, R. B. Singer, and R. L. Huguenin, Mars: Near-infrared reflectance spectra of surface regions and compositional implication, submitted to J. Geophys. Res., 1980. Thesis Ch. II

McGetchin, T. R., and J. R. Smyth, The mantle of Mars: Some possible geological implications of its high density, Icarus, 34, 512-536, 1978.

Pimentel, G. C., P. B. Forney, and K. C. Herr, Evidence about hydrate and solid water in the Martian surface from the 1969 Mariner infrared spectrometer, J. Geophys. Res., 79, 1623-1634, 1974.

Sagan, C., J. P. Phaneuf, and M. Ihnat, Total reflection spectrophotometry and thermogravimetric analysis of simulated Martian surface materials, Icarus, 4, 43-61, 1965.

Sharonov, V. V., A lithological interpretation of the photometric and colorimetric studies of Mars, Soviet Astron.-AJ, 5, 199-202, 1961.

Singer, R. B., The composition of the Martian dark regions: I. Visible and near-infrared spectral reflectance of analog materials and interpretation of telescopically observed spectral shape, submitted to J. Geophys Res., 1980a. Thesis Ch. V

Singer, R. B., The composition of the Martian dark regions: II. Analysis of telescopically observed absorptions in near-infrared spectrophotometry, submitted to J. Geophys. Res., 1980b. Thesis Ch. VI

Singer, R. B., and T. B. McCord, Mars: Large scale mixing of bright and dark surface materials and implications for analysis of spectral reflectance, Proc. Lunar Planet. Sci. Conf. 10th, 1835-1848, 1979. Thesis Ch.III

Singer, R. B., and T. B. McCord, Mars surface color units from Viking Orbiter and groundbased telescope data: A comparison, to be submitted to J. Geophys. Res., 1980.

Sinton, W. M., On the composition of Martian surface material, Icarus, 6, 222-228, 1967.

Smith, S. Q., and B. A. Smith, Diurnal and seasonal behavior of discrete white clouds on Mars, Icarus, 16, 509-521, 1972.

Soderblom, L. A., and D. B. Wenner, Possible fossil $H_2O$ liquid-ice interfaces in the Martian crust, Icarus, 34, 622-637, 1978.

Soderblom, L. A., K. Edwards, E. M. Eliason, E. M. Sanchez, and M. P. Charette, Global color variations on the Martian surface, Icarus, 34, 446-464, 1978.

Strickland, E. L., III, Soil stratigraphy and rock coatings observed in color enhanced Viking Lander Images, In Lunar and Planetary Science X, pp. 1192-1194, Lunar and Planetary Institute, Houston, 1979.

Toon, O. B., J. B. Pollack, and C. Sagan, Physical properties of the particles composing the Martian dust storm of 1971-1972, Icarus, 30, 663-696, 1977.

Toulmin, P., III, A. K. Baird, B. C. Clark, K. Kiel, H. J. Rose, Jr., R. P. Christian, P. H. Evans, and W. C. Kelliher, Geochemical and mineralogical interpretation of the Viking onorganic chemical results, J. Geophys. Res., 82, 4625-4634, 1977.

Wildt, R., Ozon and Sauerstoff in den Planeten-Atmosphären, Veröffentlich Univ.-Sternwarte Göttingen, 38, 1934.

Younkin, R. L., A search for limonite near-infrared spectral features on Mars, Astrophys. J., 144, 808-818, 1966.

## FIGURE CAPTIONS

Figure 1. Locations on Mars for spectrophotometric observations by McCord and others. The first two digits represent the year of observation (e.g., 69-1 was observed in 1969). Observations made in 1969 are described by McCord and Westphal (1971); 1973 observations are described by McCord et al. (1977a); 1978 observations are described by McCord et al. (1980). Locations of observations for which the surface was partially or wholly obscured by atmospheric dust are not shown. (Base map: USGS topographic map of Mars I-961, 1976.)

Figure 2. Comparison of Viking orbiter and ground-based spectrophotometry for identical areas on Mars (see Figure 1 for locations). All data are scaled to unity at a wavelength of 0.56 μm. Vertical bars on Viking data points do not represent observational errors; rather they show the 1σ variation of spectral reflectance characteristics within each region of ground-based observation. Horizontal bars on Viking data points show the half amplitude band widths (from Singer and McCord, 1980).

Figure 3. Representative bright and dark region reflectance spectra, scaled to unity at 1.02 μm. The bright region spectrum (top) is composed of an average

of the brightest areas observed in 1973 (visible) and 1978 (infrared). The dark region spectrum (bottom) is a composite of data from two nearby locations in Iapygia: 69-6 (visible) and 78-10 (infrared).

Figure 4. Demonstration of the effects of bright material contamination in observed dark regions. Details of the analysis are described in text. Curves labelled 'observed bright' and 'observed dark' are observational data for bright and dark regions, respectively, with a model $CO_2$ atmosphere removed. The curve labelled '-10% brt' is the dark material spectrum resulting from the assumption of 10% areal coverage of the observed dark region by bright material, and similarly through '-40% brt.' Notice that an assumption of more than 40% coverage by bright material would yield an unrealistically low reflectance for the dark material (from Singer and McCord, 1979).

Figure 5. Comparison of observed Mars bright and dark region spectra with laboratory spectra of weathered basalt. A single olivine basalt, oxidized in the laboratory, provided the best match for both bright and dark regions in this spectral range; the bright region spectrum requires a higher degree of oxidation and a finer grain size than the dark region spectrum (from Adams and McCord, 1969).

Figure 6a. The average of the brightest region spectra from McCord et al. (1980) is shown (top) compared with an additive model (simulation) of a spectrum characteristic of a combination of oxidized basalt and water ice. The ratio of the bright area to the simulation (residual) is shown (bottom) and compared with a standard martian $CO_2$ transmittance spectrum (Kieffer, 1968; McCord et al., 1978).

Figure 6b. Same analysis as in Figure 6a but compared with a model (simulation) based on an $H_2O$-ice spectrum and a spectrum characteristic of photo-oxidized magnetite, where the oxidation layer is about 1 μm thick (Huguenin, 1973a) (from McCord et al., 1980).

Figure 7. The martian north polar cap spectrum compared with an additive simulation of ice and a grey material (top). The ratio of the polar cap spectrum to the simulation is then comapred with the expected $CO_2$ martian transmittance (bottom). (From Clark and McCord, 1980).

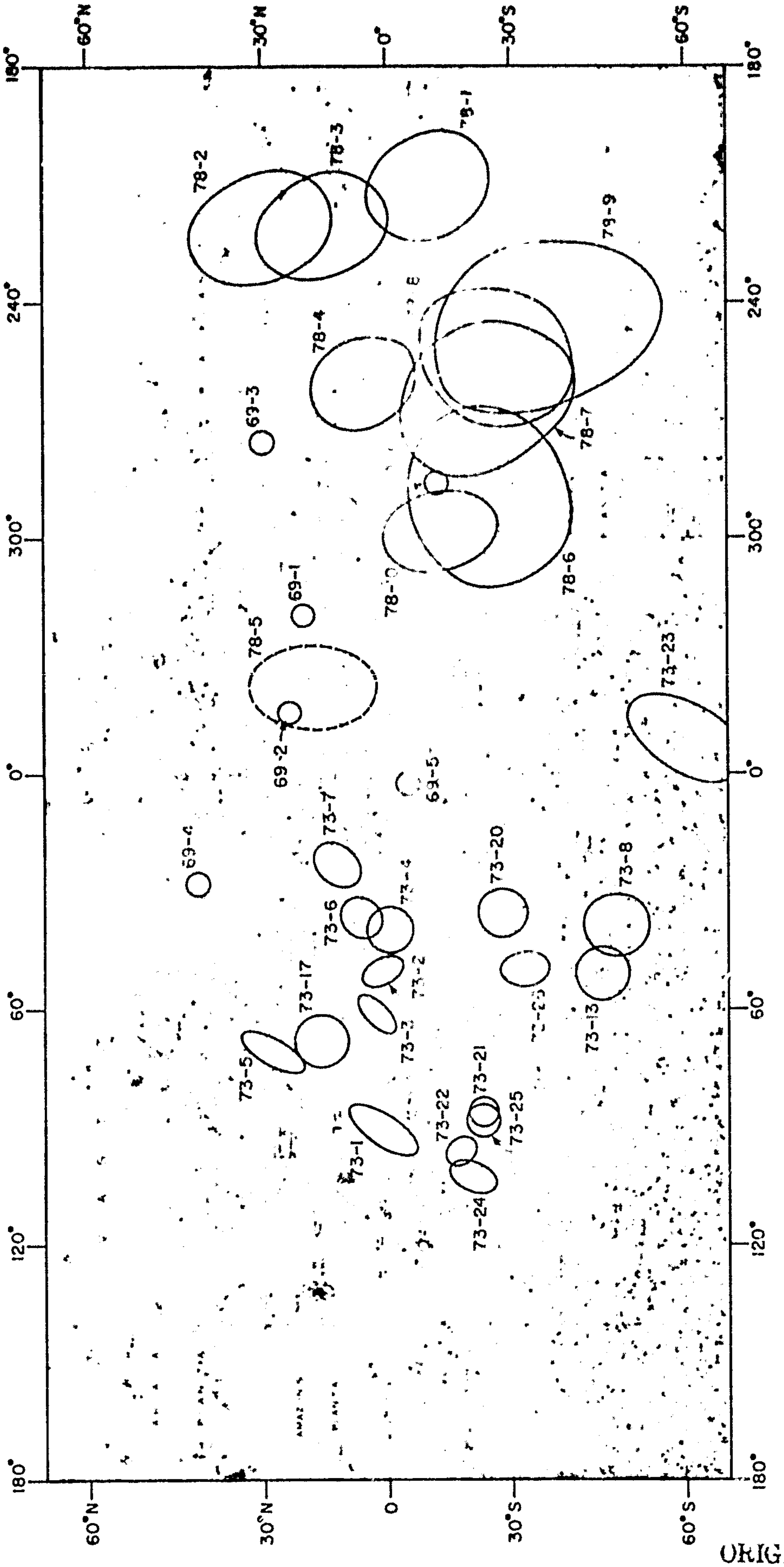
180°
240°
300°
0°
60°
120°
180°
60°N
30°N
0°
30°S
60°S
78-1
78-2
78-3
78-4
78-5
78-6
78-7
79-9
69-1
69-2
69-3
69-4
69-5
73-1
73-2
73-4
73-5
73-6
73-7
73-8
73-13
73-17
73-20
73-21
73-22
73-23
73-24
73-25

Figure 1

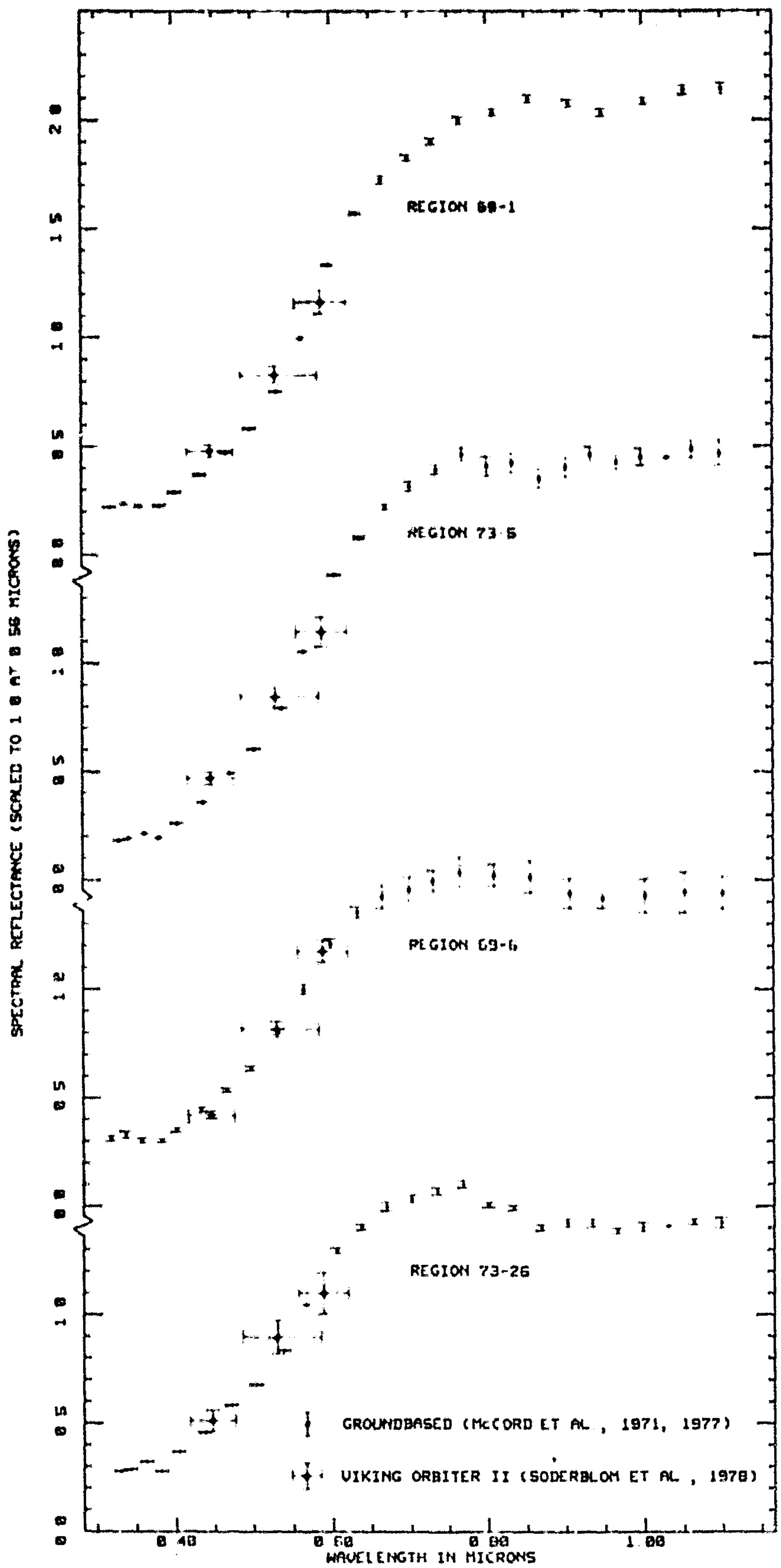
REGION 68-1
REGION 73-6
REGION 69-6
REGION 73-26
GROUNDBASED (McCORD ET AL., 1971, 1977)
VIKING ORBITER II (SODERBLOM ET AL., 1978)
SPECTRAL REFLECTANCE (SCALED TO 1.0 AT 0.56 MICRONS)
WAVELENGTH IN MICRONS
0.40
0.60
0.80
1.00

Figure 2

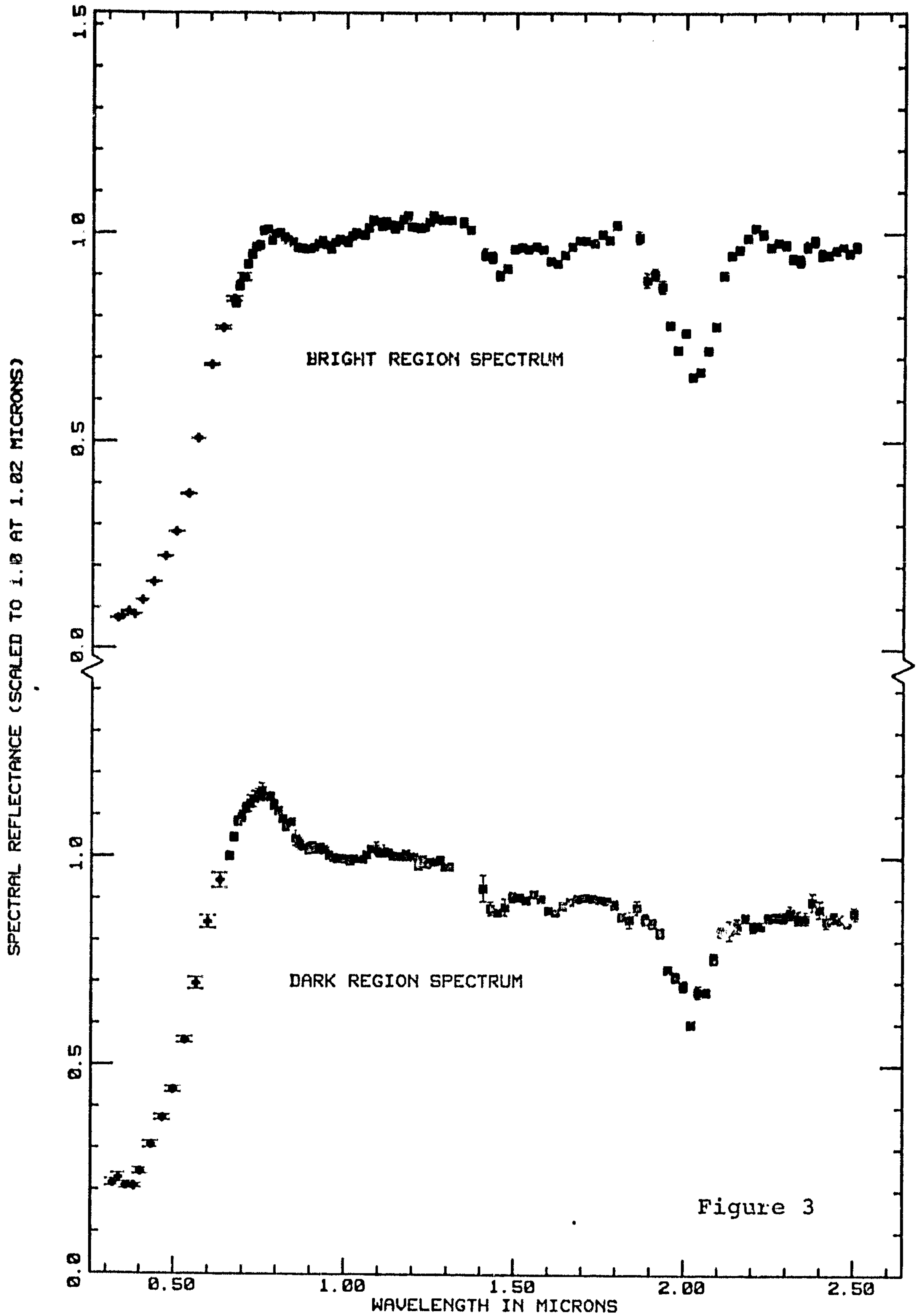
SPECTRAL REFLECTANCE (SCALED TO 1.0 AT 1.02 MICRONS)
WAVELENGTH IN MICRONS
BRIGHT REGION SPECTRUM
DARK REGION SPECTRUM
0.0
0.5
1.0
1.5
0.50
1.00
1.50
2.00
2.50

Figure 3

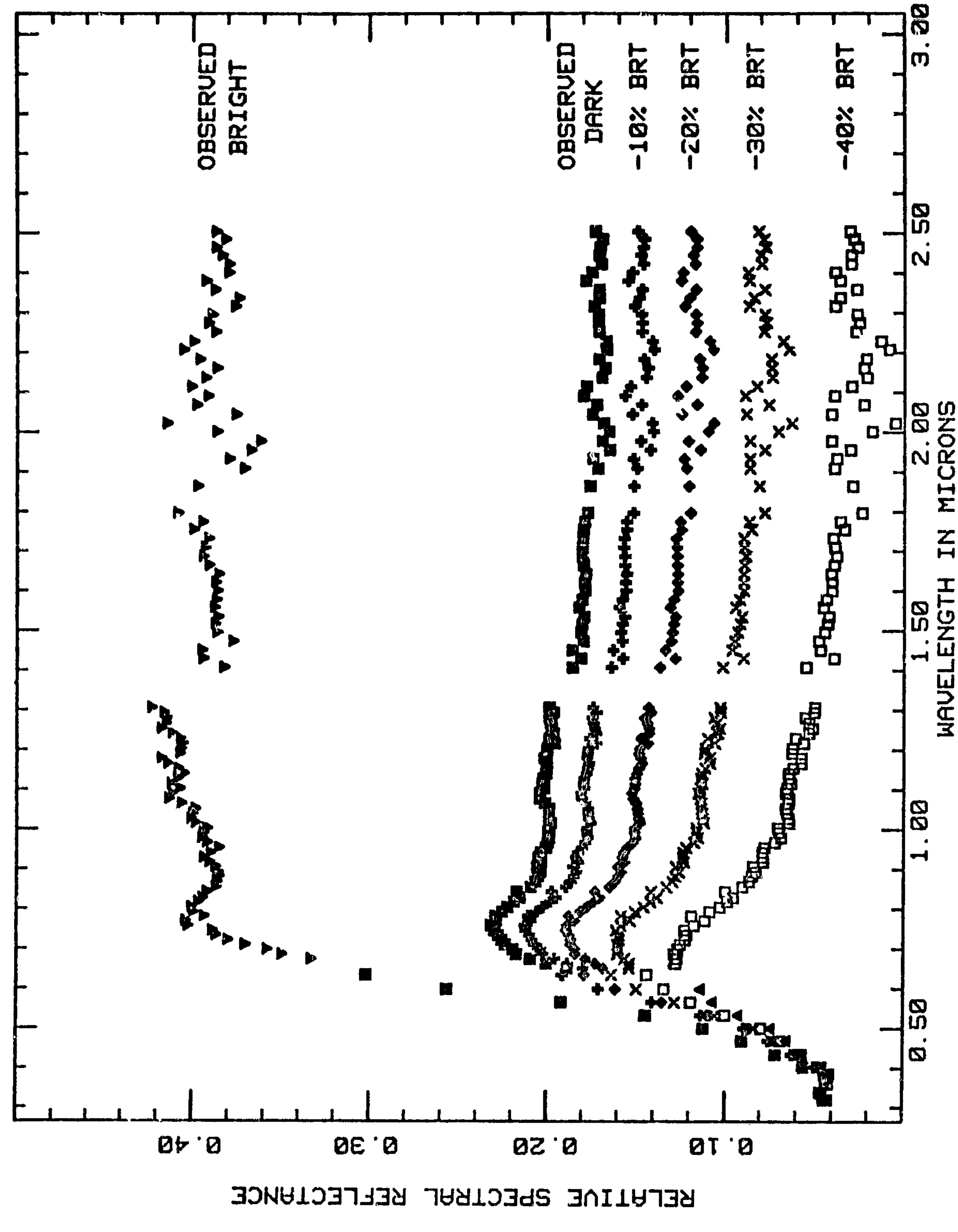
OBSERVED BRIGHT
OBSERVED DARK
-10% BRT
-20% BRT
-30% BRT
-40% BRT
0.50
1.00
1.50
2.00
2.50
3.00
WAVELENGTH IN MICRONS
0.10
0.20
0.30
0.40
RELATIVE SPECTRAL REFLECTANCE

Figure 4

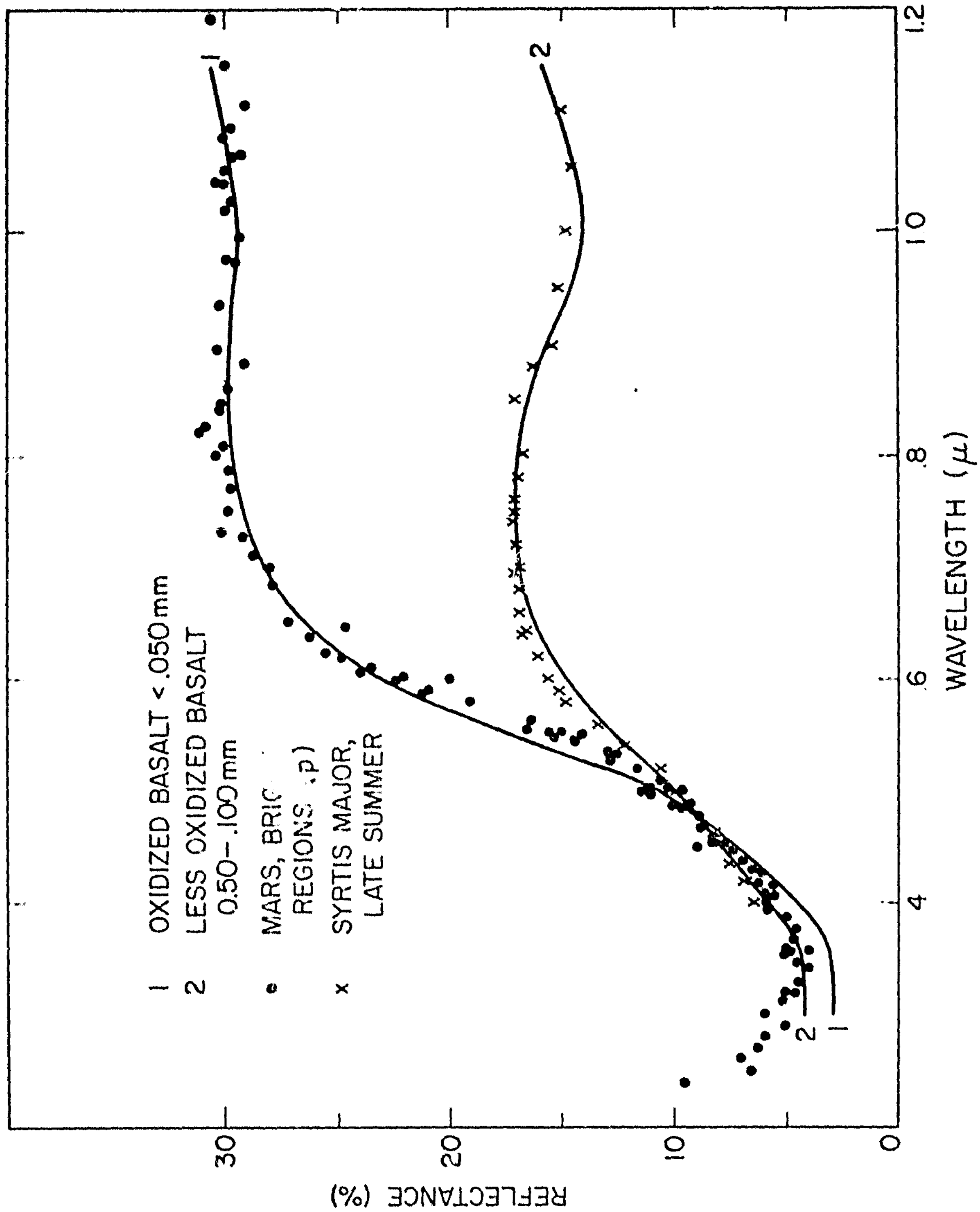

1 OXIDIZED BASALT < .050 mm
2 LESS OXIDIZED BASALT
0.50–.100 mm
● MARS, BRIG
REGIONS .p)
× SYRTIS MAJOR,
LATE SUMMER
WAVELENGTH (μ)
REFLECTANCE (%)
.4
.6
.8
1.0
1.2
0
10
20
30


Figure 5

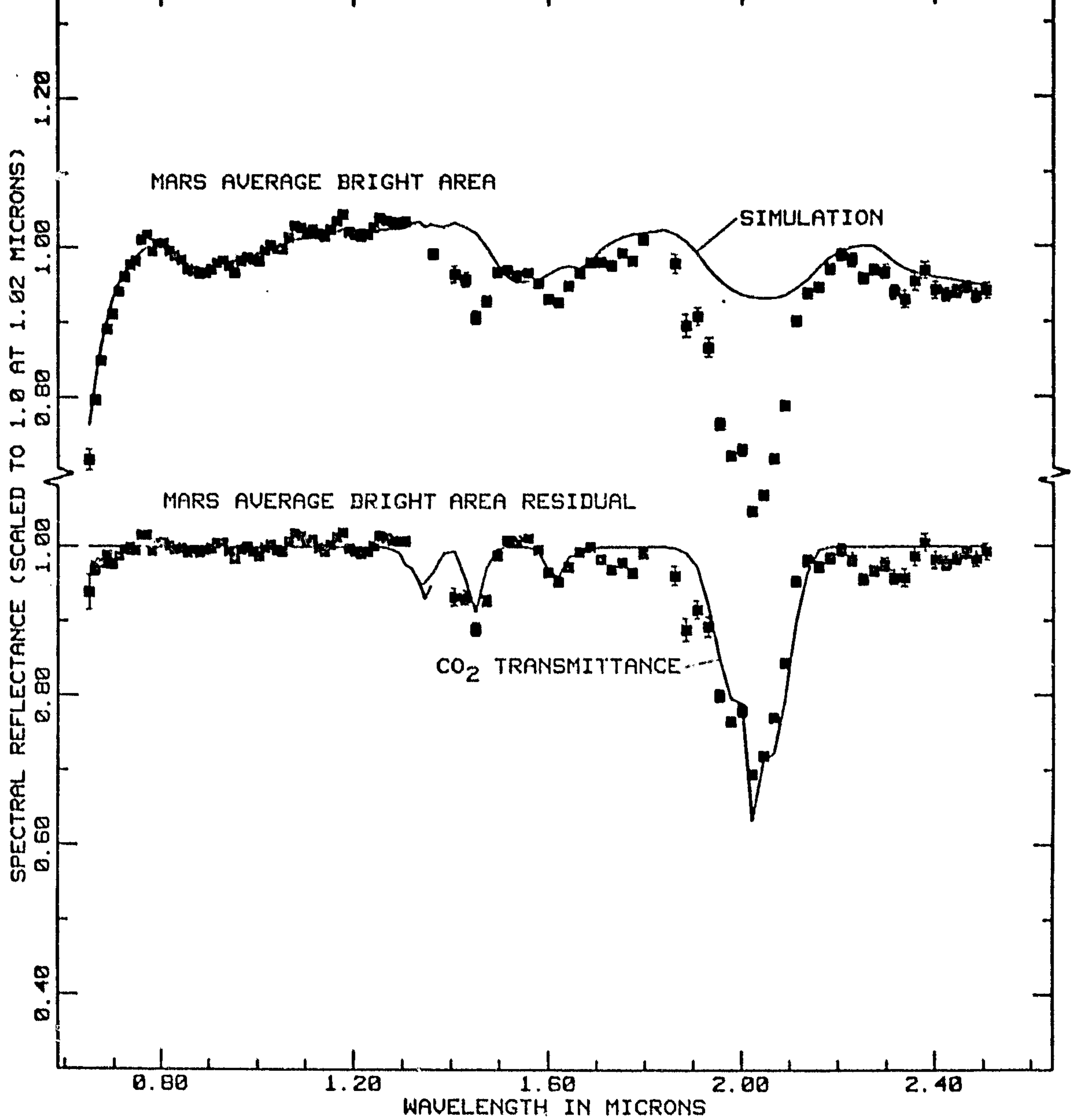
MARS AVERAGE BRIGHT AREA
SIMULATION
MARS AVERAGE BRIGHT AREA RESIDUAL
$CO_2$ TRANSMITTANCE
SPECTRAL REFLECTANCE (SCALED TO 1.0 AT 1.02 MICRONS)
1.20
1.00
0.80
1.00
0.80
0.60
0.40
0.80
1.20
1.60
2.00
2.40
WAVELENGTH IN MICRONS

Figure 6a

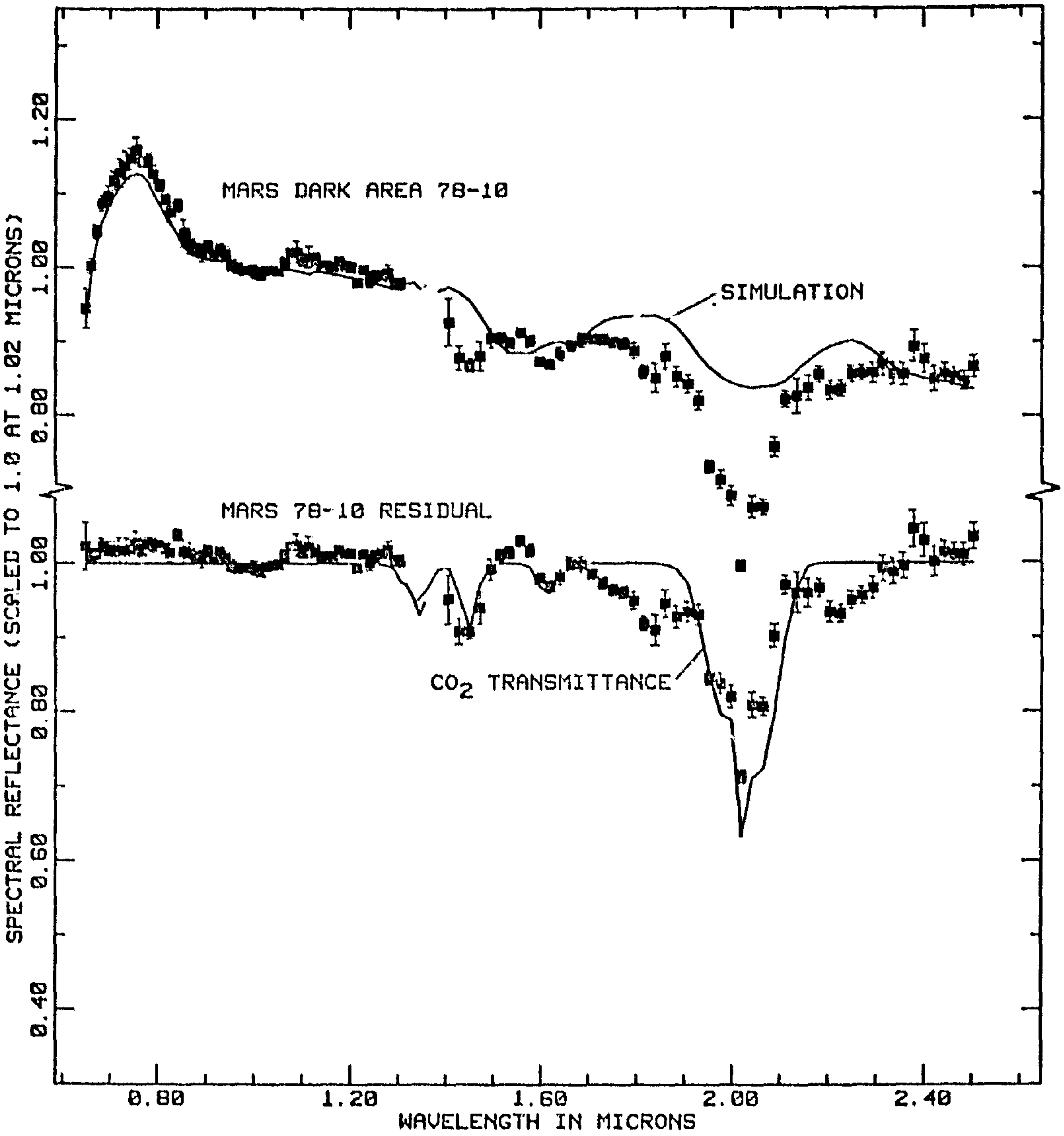
MARS DARK AREA 78-10
SIMULATION
MARS 78-10 RESIDUAL
$CO_2$ TRANSMITTANCE
SPECTRAL REFLECTANCE (SCALED TO 1.0 AT 1.02 MICRONS)
1.20
1.00
0.80
1.00
0.80
0.60
0.40
0.80
1.20
1.60
2.00
2.40
WAVELENGTH IN MICRONS

Figure 6b

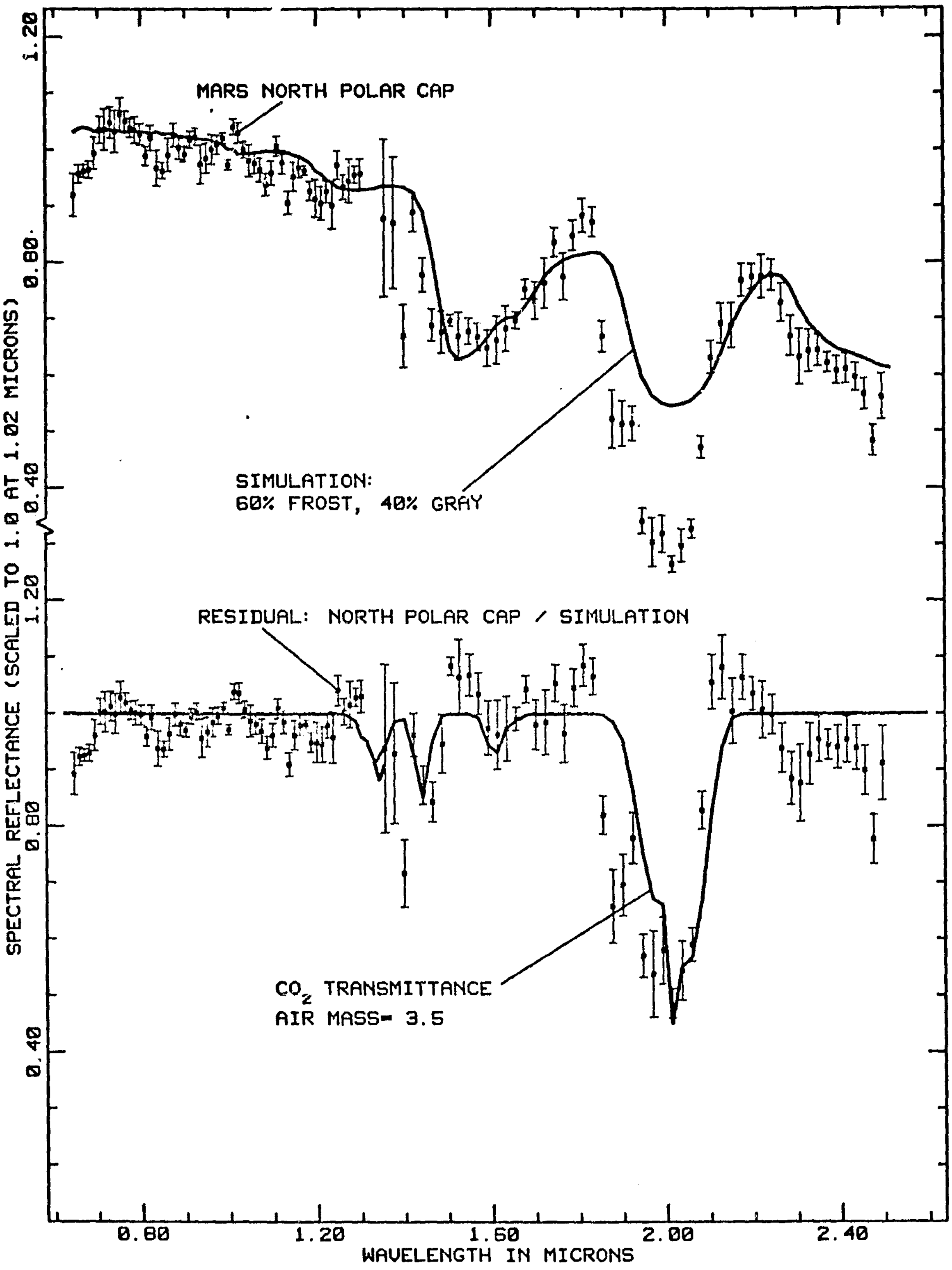
SPECTRAL REFLECTANCE (SCALED TO 1.0 AT 1.02 MICRONS)
1.20
0.80
0.40
1.20
0.80
0.40
MARS NORTH POLAR CAP
SIMULATION:
60% FROST, 40% GRAY
RESIDUAL: NORTH POLAR CAP / SIMULATION
CO2 TRANSMITTANCE
AIR MASS= 3.5
0.80
1.20
1.60
2.00
2.40
WAVELENGTH IN MICRONS

Figure 7

# CHAPTER II

## MARS: Near-Infrared Spectral Reflectance of Surface Regions and Compositional Implications

This paper is by T.B. McCord, R.N. Clark, and R.B. Singer. It will be submitted to J.Geophys.Res. in 1980 in revised form.

## ABSTRACT

Reflectance spectra (0.65 - 2.50 μm) are presented for 11 martian areas. The spectral resolution is ∼1½% and the spatial resolution is 1000 - 2000 km. These are the first high quality spectrophotometric data at these wavelengths for regions on the surface. Spectral features previously observed are confirmed and better defined, and a number of important spectral properties are characterized for the first time. The spectra show water-ice absorptions in the 1.5 and 2 μm regions, which if due to surface frost would imply the presence of 1 to 2 $mg/cm^2$ $H_2O$. However, other studies have shown that the presence of a frost on the surface is unlikely. Water-ice may exist in the pore structure of clay minerals if the clay structure is saturated. The dark region spectra indicate about four times less water ice than seen in bright regions. Since some bright material is present in dark regions there may be no water ice associated with the dark materials themselves. The presence of weak 2.3-μm absorption bands in many of the spectra imply the presence of hydroxylated magnesium-rich minerals such as amphiboles (anthophyllite) and sheet silicates (serpentine, talc, and magnesian smectites). The apparent absence of a 2.2-μm absorption implies that montmorillonite may not be a major component of the martian regolith. Many of the spectra also show

apparent absorptions at 1.9 μm, in the wing of the 2.0-μm martian atmospheric $CO_2$ absorption, which are due to bound water, strengthening the previous conclusions. Observed dark regions have previously not well determined near-infrared spectral shapes characteristic of thin semi-transparent alteration coatings overlying dark unaltered rock. Previously observed ferrous- and ferric-iron absorptions in the 1-μm region are better defined by these new data. Clinopyroxene (augite) is definitely present but olivine is not spectrally apparent.

## INTRODUCTION

In order to define and characterize surface geologic units on Mars, one needs both morphological and compositional information. Although the recent spacecraft missions to Mars have provided a wealth of data on the type of surface features present, limited compositional and mineralogical information was returned, and most of that information was obtained only in the immediate vicinities of the two Viking landers. The reflectance spectrum of minerals, rocks and soils often contain electronic and molecular absorptions which are diagnostic of surface mineralogy. A review of this technique for geochemical remote sensing as applied to Mars is provided by Singer, et al. (1979). The Viking orbiters provided 3-color images, some of which have been processed into multispectral maps showing the extent of compositionally different surface color units (Soderblom, et al., 1978; Strickland, 1979; McCord et al., 1980b). The visible spectral region is dominated by strong ferric-oxide absorptions and most other mineralogic information is masked. Reflectance spectra covering a broader spectral region, particularly at near-infrared wavelengths, are required to further investigate the mineralogy and petrology of the martian surface.

The ideal source for this type of data would be a visible and near-infrared spectral mapper in orbit around Mars; this experiment is unfortunately not likely to be flown for a number of years to come. The Galileo mission to Jupiter provides an excellent opportunity to obtain this type of data on its swingby of Mars, but the passage will be rapid and data will not be available until 1982 at the earliest. It is clear that earthbased telescopic reflectance spectroscopy will be an important source of compositional information for many years to come.

We report here on new, near-infrared reflectance spectra (0.65 to 2.50 μm) for regions on the martian surface observed in 1978. The high photometric quality of these data combined with increased near-infrared spectral coverage compared to previous regional observations provide new information about the spectral behavior and therefore the composition and physical nature of martian surface materials.

## OBSERVATIONS AND DATA REDUCTION

The spectral reflectance (0.65 to 2.50 μm) of 11 regions on Mars, 1000-2000 km in diameter, were obtained during the 1978 apparition using the University of Hawaii 2.2m telescope located on Mauna Kea, Hawaii. A cooled (to 77 K) CVF (circular variable filter) spectrometer with an InSb detector was used to measure alternatively Mars and the standard star Beta Geminorum. The instrument and the method are described in detail by McCord _et al_. (1978, 1980a).

The CVF scans the spectrum from 0.65 μm to 2.50 μm every 10 seconds with 1½% spectral resolution. Successive scans were co-added and then written onto magnetic tape after 10 scans (100 seconds) which we call a run. The spectrum is divided into 120 data points (separate spectral channels). A mirrored chopper rotating a 24 Hz was used to chop between the object and sky. The sky signal was subtracted from the object signal by the digital data system. Two chop cycles make up one data channel. The aperture consists of a cooled mirror (at 77 K) mounted 45° to the optical axis at the cassegrain focus with the aperture hole in the center. Thus the location of the aperture appears as a black spot in the field of view. A beam splitter in the viewing optics allows photographs of the aperture location and the field of view to be taken while data is being obtained.

The aperture location during each observation was determined from the photographs using an orthographic- to mercator- projection computer program; areas of multiple observations of a region were combined to obtain the composite locations displayed in Figure 1.

The reflectance of each Martian area was determined using the star Beta Geminorum as a standard flux source and performing an extinction analysis as described by McCord and Clark (1979). The Beta Geminorum/Sun spectrum was measured on previous observing runs using the Apollo 16 lunar landing site and returned samples as intermediate standards (McCord _et al._, 1978, 1980a).

## RESULTS

The reflectance spectra of 11 regions on Mars are shown in Figures 2 and 3. The spectra have been scaled to unity at a wavelength of 1.02 μm. The error bars represent ± 1 standard deviation of the mean of several independent measurements of the same region. Bright region results are shown in Figure 2, arranged with spectra most characteristic of bright regions at the top grading into spectra showing some intermediate characteristics at the bottom. Figure 3 shows spectral results for five dark regions and for the north polar region.

The locations of the bright and dark areas observed during the 1978 apparition, as well as those previously observed by this group (McCord and Westphal, 1971; McCord et al., 1977) are shown in Figure 1. The larger size of the 1978 regions is due to poor observing conditions and the relatively small angular size of Mars (12.6 arcsec.) at the time of these observations. Nevertheless these new near-infrared data substantially increase our knowledge of the martian surface. The dates, times, earth air mass range, integration time, and martian central meridian for each observation are given in Table 1.

A comparison of representative martian spectra types is given in Figure 4. Included is an average of the highest quality bright region spectra, the spectrum for area 78-5, which has predominantly bright region characteristics but with some indication of intermediate to dark material, and the spectrum for area 78-10, which is the highest quality dark region spectrum.

These observations were made during a period ($L_s$=48-50°) of nearly maximum transparency of the martian atmosphere as measured directly by the Viking landers (afternoon visible optical depth ≃0.4, Pollack *et al.*, 1979). Observational problems caused by the Earth's atmosphere are responsible for much of the variation in data quality. Bright region spectra 78-1B and 78-2 show rather sharp but repeatable features near 0.75 μm, 0.93 μm, and from 2.2 to 2.5 μm. A careful study of these and other data obtained on the same nights has shown that these features are probably instrumental in origin and do not represent martian phenomena.

# ANALYSIS AND INTERPRETATION

## General Spectral Characteristics

Bright region spectra are characterized from the visible to 0.75 μm by the wing of intense $Fe^{3+}$ charge-transfer absorptions centered in the U.V., and by a weaker, asymmetric $Fe^{3+}$ crystal-field absorption near 0.87 μm. These features have been attributed to a ferric-oxide content of about 6 to 8 wt. % (Huguenin et al., 1977). From the band minimum near 0.87 μm to about 1.3 μm the spectrum slopes upwards. Between 1.4 and 1.7 μm there is a broad absorption which has been interpreted as $H_2O$ ice from previous integral disc observations (McCord et al., 1978). Superimposed on this are narrower Mars atmospheric $CO_2$ absorptions, at 1.34, 1.45, and 1.62 μm. From 1.8 to 2.2 μm the spectrum is dominated by a deep, partially resolved triplet absorption also caused by martian atmospheric $CO_2$.

In contrast to bright region spectra, dark region spectra have a more distinctive peak near 0.75 μm and slope fairly uniformly downwards to 2.5 μm. This infrared spectral shape was not previously well defined and has important implications for compositional analysis, as discussed below. The martian $CO_2$ absorptions are of course the same as those discussed for bright regions. Dark region spectra show $Fe^{2+}$ crystal-field absorptions near 1 μm as well as the $Fe^{3+}$

band near 0.87 μm described for bright regions.

Dark regions observed in 1978 had approximately one-half the reflectance at 1 μm as bright regions. This value is consistent with previous observations of regional reflectance differences made by McCord and Westphal (1971) and Binder and Jones (1972). Typical bright and dark region spectra from 0.3 to 2.5 μm are shown scaled to approximate normal reflectance in Figure 5. The spectra are composites of infrared data presented here and visible data from McCord and Westphal (1971) and McCord _et al_. (1977). Spectral effects of a model martian $CO_2$ atmosphere have been removed (Kieffer, 1968; McCord _et al_., 1978). This $CO_2$ correction is approximate, neglecting variations in surface topography.

Spectrum 78-5 is for Arabia, which although considered a classic bright region shows characteristics in some ways intermediate between bright and dark regions. The near-infrared absorption minimum occurs at longer wavelengths than for other bright regions and the slope is much flatter from 1.0 to 1.3 μm, although not negative as it is for dark region spectra. The implication here is that Arabia has a moderate amount of exposed dark material, or at least an excess ferrosilicate soil component compared to some other bright regions. Similar properties were noted by Huguenin _et al_. (1977) in 1969 observations of this area (McCord and Westphal, 1971). If these characteristics have in fact survived through nearly ten years of global dust cyclying, a surface composed of dark boulders scattered on a background of bright soil seems plausible. Such a situation is observed at both Viking lander sites, for which no detailed spectra have yet been obtained.

The spectrum of the martian north polar cap region is shown in Figure 3. The spectrum appears similar to the dark region spectrum 78-10 shortward of 1.3 μm. Longward of 1.3 μm is a relatively strong water ice absorption extending from 1.4 to 1.8 μm. Centered at 2.0 μm is the strong $CO_2$ (atmospheric) absorption and the 2-μm ice band. Beyond 2.2 μm the reflectance decreases as seen in spectra of water frost. This spectrum is analyzed in detail in Clark and McCord (1980a).

## Dark Region Composition

The earliest positive determination that dark regions on Mars consist largely of mafic igneous rocks was provided by Adams and McCord (1969) who successfully modeled a dark region spectrum from 0.3 to 1.1 μm using basalt grains with artificially induced surface oxidation. Huguenin (1973a, b,1974) proposed that UV-photostimulated oxidation on Mars would produce surface alteration layers about 1 micrometer thick on basaltic rocks. He interpreted previously obtained spectrophotometry from 0.3 to 1.1 μm (McCord and Westphal, 1971; McCord et al., 1977) to indicate such a thin oxidized layer (Huguenin, 1976).

The near-infrared dark region spectra presented here provide new information about dark region spectral shape. The negative slope from about 1.1 μm to 2.5 μm had not been previously determined, and is atypical of unweathered or homogeneously oxidized rocks and minerals. Singer (1980a) has shown that this distinctive shape is in fact indicative of a brighter, oxidized layer overlying a dark unoxidized iron-bearing substrate, such as basaltic or ultramafic rock, in agreement with the earlier work described above. Analogy to naturally occuring alteration layers on terrestrial basalts indicates that the coatings on martian rocks (or rock fragments) are thicker than originally suggested by Huguenin (1973a, 1976), probably being about twenty to thirty micrometers in thickness. (Singer, 1980a).

Absorptions near 1 μm, observed in nearly all previous dark region spectra, are defined significanlty better in the new data, particularly for region 78-10. Adams (1968) was the first to suggest that these might be caused by $Fe^{2+}$ in ferromagnesian minerals such as pyroxenes and olivines. Huguenin et al. (1977, 1978) have provided detailed interpretations of the dark region spectra obtained in 1969 (McCord and Westphal, 1971) and 1973 (McCord et al., 1977). Spectrum 78-10 shows a compound structure near 1 μm, with a band centered near 0.88 μm and one near 0.99 μm. Detailed analysis by Singer (1980b) has shown that the 0.88 μm band is most likely caused by $Fe^{3+}$ crystal-field transitions in the oxidized coating, with the possibility of some contribution from $Fe^{2+}$ crystal-field absorptions in orthopyroxene or low-calcium pigeonite in the underlying rocks. The 0.99-μm band is firmly interpreted as indicating an augite clinopyroxene as a major component of these dark region rocks. Olivine, interpreted by Huguenin et al. (1977, 1978) to be abundant in most previously observed dark regions, was found to not be a major constituent in dark regions observed in 1978. A detailed discussion about olivine determination and the petrologic significance of olivine on Mars is given by Singer (1980b).

## Spectral Evidence for Water

The spectra in Figures 2 and 3 all show a drop in reflectance from 1.3 to 1.4 μm. McCord et al. (1978) interpreted integral disc spectra with features similar to those seen here to be due to water ice plus a highly desiccated mineral hydrate. In order to investigate this possibility further the martian spectra were modeled using an ice spectrum and spectra typical of oxidized basalt. Figure 6 show the spectra used in the simulation. The simulated spectrum for the bright area is typical of alteration products of mafic igneous rocks. The simulated spectrum for the dark area is typical of spectra of a thin (a few to over 10 micrometers thick) layer of alteration product overlying unweathered basalt (c.f. Adams and McCord, 1969; Singer, 1980a).

The ice spectrum is typical of a medium grained frost with grain sizes around 200 micrometers (see Clark, 1980a) and is scaled to a value of 0.18 at 1.02 μm. This scaling gave the best fit in the simulation below. The reflectance of an optically thick, medium grained frost is above 0.9 at 1.02 μm. If the simulated bright spectrum and the ice spectrum are added, then rescaled to 1.0 at 1.02 μm, the result can be compared to the Mars average bright area spectrum as seen in Figure 7a (top). The resultant simulation shows a reasonable match to the Mars spectrum. Dividing the bright area spectrum by the simulated spectrum gives the residual spectrum shown in Figure 7a (bottom). This residual spectrum agrees very well with the martian atmospheric $CO_2$ transmittance spectrum (described previously).

A similar analysis for the dark area spectrum 78-10 is shown in Figure 7b (top). The fit is not as good as that obtained for the bright area although some of the apparent drop beyond 1.4 μm may still be explained by water ice. If the water ice absorption features were only about half as deep as those in Figure 7B, the fit would be better. Also, since the dark areas have a reflectance about half that of bright areas, the amount of water contributing to the dark area 78-10 spectrum is less. Thus the amount of water ice present is at least four times less in the dark areas.

The water ice spectrum fit to the bright area in Figure 7a indicates that an optically thick patch of medium grained frost covers approximately 5% of the area measured if the ice and bright material are in large scale patches. If the frost were evenly distributed on the surface, approximately 1 to 2 mg/cm$^2$ would be present based on laboratory studies by Clark (1980b). If the water ice is mixed with the other minerals in the surface, the amount of water in the top few millimeters would be about 5-10 wt. % (see Clark, 1980b). This amount of ice is difficult to explain based on current models (e.g. Clark, 1978; Farmer and Doms, 1979) unless the amount of bound water in the regolith is saturated.

The residual spectrum in Figure 7a shows apparent absorptions around 2.3 μm and at 1.9 μm in the wing of the 2.0-μm martian atmospheric $CO_2$ band. These absorptions are indicative of bound water, the 1.9 μm absorption due to the $\nu_1 + \nu_2$ and $\nu_3 + \nu_2$ overtones and that at 2.3 μm due to an overtone of an Mg-OH bending mode and the OH stretch (e.g. Hunt and Salisbury, 1970; Hunt et al., 1971). Clark (1980b) has shown that bound water absorptions do not shift in wavelength appreciably ($\lesssim$100 Å) in the temperature range 290K to 150K. Clark (1980a, b) also showed that the bound water absorptions are distinguishable from pure water frost or ice. Anderson et al. (1967) showed the amount of water bound to montmorillonite decreases as the temperature is decreased below 273K. As the temperature decreases, bound water is forced out of clay structures and forms micro-crystals of ice in the pore structure. This would tend to occur during the martian night. As the temperature rises the next day, the ice will sublime if the $H_2O$ vapor pressure in the atmosphere is too low. However, the ice crystals are within the clay mineral grains and as the temperature rises the clay minerals will tend to reabsorb the water. Thus an increase in vapor pressure may never be seen above the surface. Further study is needed to test this hypothesis.

The dark area simulation shows that there is about four times less water ice apparent than in the bright area simulation. The dark area observed was over 1000 km in diameter and some bright area material is almost certainly present in patches. Singer and McCord (1979) investigated the affects of streaks and splotches of spectrally isolated bright material on the spectral reflectance of dark regions. Their results show that the drop in reflectance from 1.3 to 1.4 μm and the other signatures of water ice are decreased when the contribution of bright material to the spectrum is removed. Although a unique solution cannot be obtained, the water ice signature appears to be absent in spectra of "pure" dark materials.

The 2.3 μm Absorption

Nearly every spectrum in Figures 2 and 3 shows the presence of a 2.3-μm absorption feature. Because of the subtlety of these features a detailed examination was conducted of observations of Saturn's rings, the Gallilean satellites, and the Moon taken with the same instrument and two different calibration routes (Clark and McCord, 1980b,c; McCord et al., 1980a). No similar bands were found in other data, even those taken the same nights; therefore it is quite certain that these absorptions are characteristic of Mars. The presence and center wavelengths of these features can be determined well from these data, but the band depths, or even the relative depths, are much less certain.

A single absorption at this location (~2.3 μm) indicates an Mg-OH bond; often a weaker band of similar origin appears near 2.4 μm (Hunt and Salisbury, 1970). An absorption near 2.4 μm is possibly also present in some of these spectra, but the depth is approaching the noise limit of the data. Absorptions near 2.2 μm, characteristic of Al-OH bonds, may also be weakly present but are much less certain than the bands near 2.3 μm. One reason for this might be masking of any 2.2-μm features by the wing of the strong atmospheric $CO_2$ absorption. Weak absorptions just longward of 2.3 and 2.4 μm, and perhaps a very weak absorption just longward of 2.2 μm, are apparent in a spectrum of the integral martian disk obtained in 1976 by McCord et al. (1978). Carbonates are apparently not detected in any of the near-infrared data since a stronger 2.55 μm absorption would be expected to accompany one near 2.35 μm (Hunt and Salisbury, 1971).

In addition to providing evidence for hydroxylated minerals on Mars, a 2.3 μm band has interesting petrologic implications. Mg content greater than Al content in an unweathered igneous rock is characteristic of a mafic to ultramafic composition, generally with abundant olivine. Relative enrichments of Mg are also seen in certain pyroxenites, relatively uncommon terrestrial ultramafic rocks consisting primarily of pyroxenes (Nockhold et al., 1978). These observations correlate with the Viking XRF analysis team conclusions.

that the measured soil chemistry is most consistent with the weathering products of mafic igneous rock (Toulmin et al., 1977); more recently a pyroxenite parent composition has been considered (B.C. Clark, personal communication, 1979). Very mafic to ultramafic average compositions for martian lavas have also been suggested by Maderazzo and Huguenin (1977) and McGetchin and Smyth (1978).

Mg-OH features would most probably be characteristic of alteration products of mafic igenous rocks rather than the rocks themselves. Possible Mg-rich minerals which might form by such alteration are anthophyllite (ferromagnesian amphibole) and a variety of trioctohedral sheet silicates such as serpentine, talc, and magnesian smectities (saponite, hectorite). The apparent absence (or at least extreme weakness) of any 2.2 μm Al-OH absorptions would seem to argue against montmorillonite as a major component martian soils.

## ACKNOWLEDGEMENTS

Much of this work was carried out at the University of Hawaii's Mauna Kea Observatory and Institute for Astronomy. This research was supported by the NASA grants NGS 7323 and 7590.

## REFERENCES

Adams, J.B., Lunar and martian surfaces: Petrologic significance of absorption bands in the near-infrared, Science 159, 1453-1455, 1968.

Adams, J.B., and T.B. McCord, Mars: Interpretation of spectral reflectivity of light and dark regions, J. Geophys. Res. 74, 4851-4856, 1969.

Anderson, D.M., Gaffney, E.S., and Low, P.F., Frost phenomena on Mars, Science 155, 319-322, 1967.

Binder, A.B., and J.C. Jones, Spectrophotometric studies of the photometric function, composition and distribution of the surface materials of Mars, J. Geophys. Res. 77, 3005-3019, 1972.

Clark, B.C., Implications of abundant hygroscopic minerals in the Martian regolith, Icarus 34, 645-655, 1978.

Clark, R.N., Water frost and ice: The near-infrared spectral reflectance 0.65-2.5μm , J. Geophys. Res., submitted 1980a.

Clark, R.N., The spectral reflectance of water-mineral mixtures at low temperatures, J. Geophys. Res., submitted 1980b.

Clark, R.N., and T.B. McCord, Mars residual north polar cap: Earth-based spectroscopic confirmation of water ice as a major constituent and evidence for hydrated minerals, J. Geophys. Res., submitted 1980a.

Clark, R.N., and T.B. McCord, The Galilean satellites: Near-infrared spectral reflectance measurements (0.65-2.5μm) and a 0.325-5 μm summary, Icarus, in press 1980b.

Clark, R.N., and T.B. McCord, The rings of Saturn: New near-infrared reflectance measurements and a 0.326-4.08 μm summary, Icarus, submitted 1980c.

Farmer, C.B., and P.E. Doms, Global seasonal variation of water vapor on Mars and the implications for permafrost, J. Geophys. Res. 84, 2881-2888, 1979.

Huguenin, R.L., Photostimulated oxidation of magnetite. 1. Kinetics and alteration phase identification, J. Geophys. Res. 78, 8481-8493, 1973a.

Huguenin, R.L., Photostimulated oxidation of magnetite. 2. Mechanism, J. Geophys. Res. 78, 8495-8506, 1973b.

Huguenin, R.L., The formation of goethite and hydrated clay minerals on Mars, J. Geophys. Res. 79, 3895-3905, 1974.

Huguenin, R.L., Mars: Chemical weathering as a massive volatile sink, Icarus 28, 203-212, 1976.

Huguenin, R.L., J.B. Adams, and T.B. McCord, Mars: Surface mineralogy from reflectance spectra, in Lunar Science VIII, 478-480, Lunar Science Institute, Houston, 1977.

Huguenin, R.L., J.W. Head, and T.R. McGetchin, Mars: Petrologic units in the Margaritifer Sinus and Coprates

Quadrangle, Reports of Planetary Geology Program, 1977-1973, NASA Tech. Memo 79729, 1978.

Hunt, G.R., Spectral signatures of particulate minerals in the visible and near infrared, Geophys. 74, 501-513, 1977.

Hunt, G.R., and J.W. Salisbury, Visible and near-infrared spectra of minerals and rocks: I. Silicate minerals, Mod. Geol. 1, 283-300, 1970.

Hunt, G.R., and J.W. Salisbury, Visible and near-infrared spectra of minerals and rocks: II. Carbonates, Mod. Geol. 2, 23-30, 1971.

Hunt, G.R., J.W. Salisbury, and C.J. Lenhoff, Visible and near-infrared spectra of minerals and rocks: III. Oxides and Hydroxides, Mod. Geol. 2, 195-205, 1971.

Kieffer, H.H., Near infrared spectral reflectance of simulated Martian frosts, Ph.D. Dissertation, Calif. Inst. of Technol., Pasadena, 1968.

Madarazzo, M., and R.L. Huguenin, Petrologic implications of Viking XRF analysis based on reflection spectra and the photochemical weathering model, (abstract) Bull. Am. Astron. Soc. 9, 5270528, 1977.

McCord, T.B., and J.A. Westphal, Mars: Narrow-band photometry, from 0.3 to 2.5 microns of surface regions during the 1969 apparition, Astrophys. J. 168, 141-153, 1971.

McCord, T.B., R.L. Huguenin, D. Mink, and C. Pieters, Spectral reflectance of Martian areas during the 1973 opposition: Photoelectric filter photometry 0.33-1.10 μm, Icarus 31, 25-39, 1977.

McCord, T.B., R.N. Clark, and R.L. Huguenin, Mars: Near-infrared spectral reflectance and compositional implication, J. Geophys. Res. 83, 5433-5441, 1978.

McCord, T.B., and R.N. Clark, Atmospheric extinction 0.65-2.50 μm above Mauna Kea, Pub. Astron. Soc. Pac. 91, 571-576, 1979.

McCord, T.B., R.N. Clark, L.A. McFadden, C.M. Pieters, P.D. Owensby, and J.B. Adams, Moon: Near-infrared spectral reflectance, A first good look, J. Geophys. Res. to be submitted, 1980a.

McCord, T.B., Singer R.B., Adams, J.B., Hawke, B.R. Head, J.W. III, Huguenin, R.L. Pieters, C.M., Zisk, S., and Mouginis-Mark, P.,Definition and characterization of Mars surface units. to be submitted to J. Geophys. Res., 1980b.

McGetchin, T.R., and J.R. Smyth, The Mantle of Mars: Some possible geological implications of its high density, Icarus 34, 512-536, 1978.

Nockolds, S.R., R.W.O'B Knox, and G.A. Chinner, Petrology for Students, Cambridge University Press, 1978.

Pollack, J.B., D.S. Colburn, C.M. Flaser, R. Kahn, C.E. Carlston, and D. Pidek, Properties and effects of dust particles suspended in the Martian atmosphere, J. Geophys. Res. 84, 2929-2946, 1979.

Singer, R.B., The Composition of the Martian dark regions: I. Visible and near-infrared spectral reflectance of analog materials and interpretation of telescopically observed spectral shape, submitted to J. Geophys. Res., 1980a. Thesis Ch. V

Singer, R.B., The composition of the Martian dark regions: II.Analys s of telescopically observed absorptions in near-infrared spectrophotometry, submitted to J. Geophys. Res., 1980b. Thesis Ch.VI

Singer, R.B., T.B. McCord, R.N. Clark, J.B. Adams, and R.L. Huguenin, Mars surface composition from reflectance spectroscopy: A summary, J. Geophys, Res., 84, 8415-8426, 1979. Thesis Ch. I

Soderblom, L.A., K. Edwards, E.M. Eliason, E.M. Sanchez, and M.P. Charette, Global color variations on the Martian surface, Icarus 34, 446-464, 1978.

Strickland, E.L. III, Martian albedo/color units: Viking lander 1 stratigraphy vs. Orbiter color observations, (abstract) Bull. Am. Astron. Soc. 11, 574, 1979.

Toulmin, P. III, A.K. Baird, B.C. Clark, K, Keil, H.J. Rose, Jr., R.P. Christian, P.H. Evans, and W.C. Kelliher, Geochemical and mineralogical interpretation of the Viking inorganic chemical results, J. Geophys. Res. 82, 4625-4634, 1977.

## TABLE CAPTIONS

The martian observational parameters for the spectra in Figures 2 and 3 are tabulated. The times are the beginning times of the first and last runs (100 seconds per run). The air mass values are also the values at the beginning of the first and last run. The last column, $CM_0$, is the central meridian longitude in degrees of the Martian sub-earth point at the mid-point of the observation. The spectrum 78-10 in Figure 3 is the average of data from two nights (February 14 and 16). The martian north pole was tilted toward the earth 9$^\circ$.25 and toward the sun 18$^\circ$.70. The planetocentric longitude of the sun, $L_s$, was 49° (spring in the northern hemisphere.

TABLE I

Mars Observational Parameters

| UT Date Feb. 1978 | Area | Time (UT) | Earth Air Mass Range | Runs | Total Integration Time Sec. | $CM_0$ |
|---|---|---|---|---|---|---|
| 20 | 78 - 1A | 05:55 - 06:05 | 1.17 - 1.14 | 6 | 600 | 205 |
| 21 | 78 - 1B | 06:41 - 07:00 | 1.07 - 1.04 | 11 | 1100 | 208 |
| 21 | 78 - 2 | 08:01 - 08:18 | 1.00 - 1.01 | 9 | 900 | 227 |
| 20 | 78 - 3 | 07:20 - 07:31 | 1.02 - 1.02 | 6 | 600 | 226 |
| 16 | 78 - 4 | 08:57 - 09:04 | 1.01 - 1.02 | 4 | 400 | 285 |
| 14 | 78 - 5 | 07:19 - 07:24 | 1.05 - 1.05 | 2 | 200 | 278 |
| 20 | 78 - 6 | 10:52 - 11:06 | 1.27 - 1.33 | 6 | 600 | 278 |
| 20 | 78 - 7 | 10:05 - 10:23 | 1.12 - 1.17 | 8 | 800 | 267 |
| 21 | 78 - 8 | 08:21 - 08:33 | 1.01 - 1.01 | 7 | 700 | 232 |
| 20 | 78 - 9 | 07:47 - 08:00 | 1.01 - 1.00 | 7 | 700 | 233 |
| 14 | 78 - 10 | 07:26 - 07:28 | 1.05 - 1.04 | 2 | 200 | 280 |
| 16 | 78 - 10 | 10:09 - 10:14 | 1.09 - 1.10 | 4 | 400 | 302 |
| 20 | 78 - 11 | 06:11 - 06:22 | 1.13 - 1.10 | 6 | 600 | 209 |

## FIGURE CAPTIONS

Figure 1: Locations on Mars for spectrophotometric observations by McCord and others. The first two digits represent the year of observation (e.g. 69-1 was observed in 1969). The 1969 observations (0.3 to 1.1 μm ) are described by McCord and Westphal (1971); the 1973 observations (0.3 to 1.1 μm) are described by McCord *et al.* (1977); The 1978 observations (0.65 to 2.50 μm) are presented in this paper. The locations of observations for which the surface was partially or wholly obscured by atmospheric dust are not shown. (Base map: USGS Topographic Map of Mars I-961, 1976.)

Figure 2: The reflectance spectra of bright regions obtained in this study are plotted here scaled to a value of 1.0 at 1.02 μm. The error bars represent ± standard deviation of the mean of several independent observations.

Figure 3: The reflectance spectra of the dark regions and the north polar region obtained in this study are plotted here scaled to 1.0 to 1.02 μm. The error bars represent ±1 standard deviation of the mean of several independent observations.

Figure 4: The reflectance spectra of three characteristic martian surface types are compared: (top) the average of three bright region spectra (78-1A, 3, and 4) from Figure 2, (middle) an intermediate type spectrum (78-5), and (bottom) a dark region spectrum (78-10).

Figure 5: Composite reflectance spectra from 0.33 to 2.50 μm are shown for typical bright and dark region spectra scaled approximately to normal reflectance. A model atmospheric $CO_2$ spectrum has been removed so that these spectra are more representative of surface material. The visible data are from McCord and Westphal (1971) and McCord *et al.* (1977).

Figure 6: The reflectance spectrum representing the continuum or the bright (top) and dark (middle) regions are shown. These spectra were chosen as described in the text. The top spectrum is approximately that of a heavily oxidized basalt and the middle spectrum that of a thin layer of oxidation layer on basalt. The bottom spectrum is that of $H_2O$ ice (Clark, 1980a). These spectra are used in producing those shown in Figure 7.

Figure 7: The reflectance spectrum of the average bright area shown in Figure 4 (top) is shown

here (a) with an over-plot of a combination of the bright area continuum and the $H_2O$ ice spectrum shown in Figure 6. Beneath is shown the residual spectrum created by dividing the two spectra shown at top. Plotted on the residual spectrum is the transmission spectrum of $CO_2$ for the path length of the Mars atmosphere as described in the text. Most of all of the features in the residual spectrum are accounted for by the $CO_2$ absorptions. In part (b) of this figure a similar sequence to part (a) is shown, but for the dark area spectrum 78-10. The simulation, which represents about half the water ice in the part (a) simulation does not fit as well as for bright area spectra and indicates even less water ice is present in the dark region.

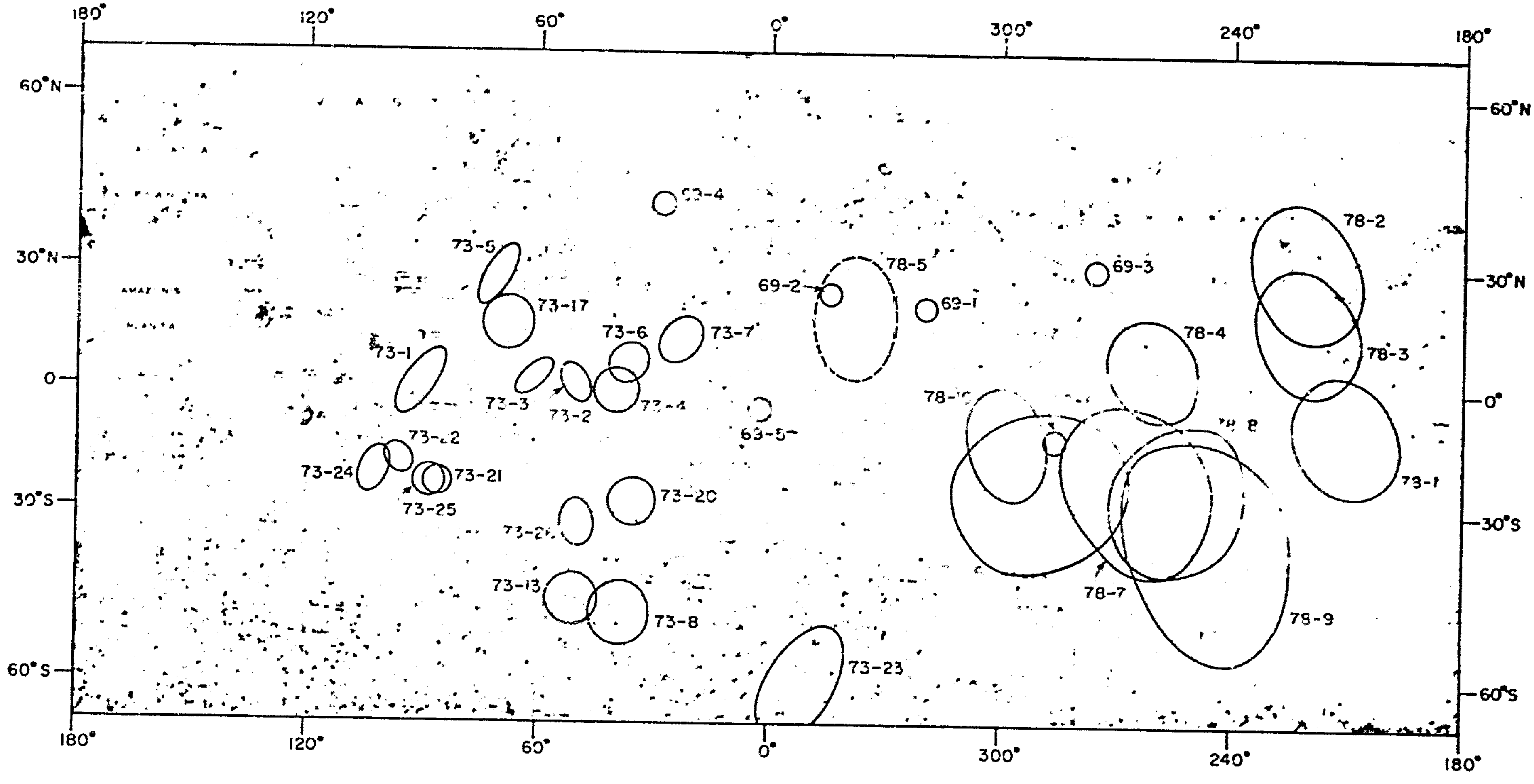
180°
120°
60°
0°
300°
240°
60°N
30°N
0
30°S
60°S
0°
73-1
73-2
73-3
73-5
73-6
73-7
73-8
73-13
73-17
73-20
73-21
73-23
73-24
73-25
69-1
69-2
69-3
78-2
78-3
78-4
78-5
78-7
78-9

Figure 1

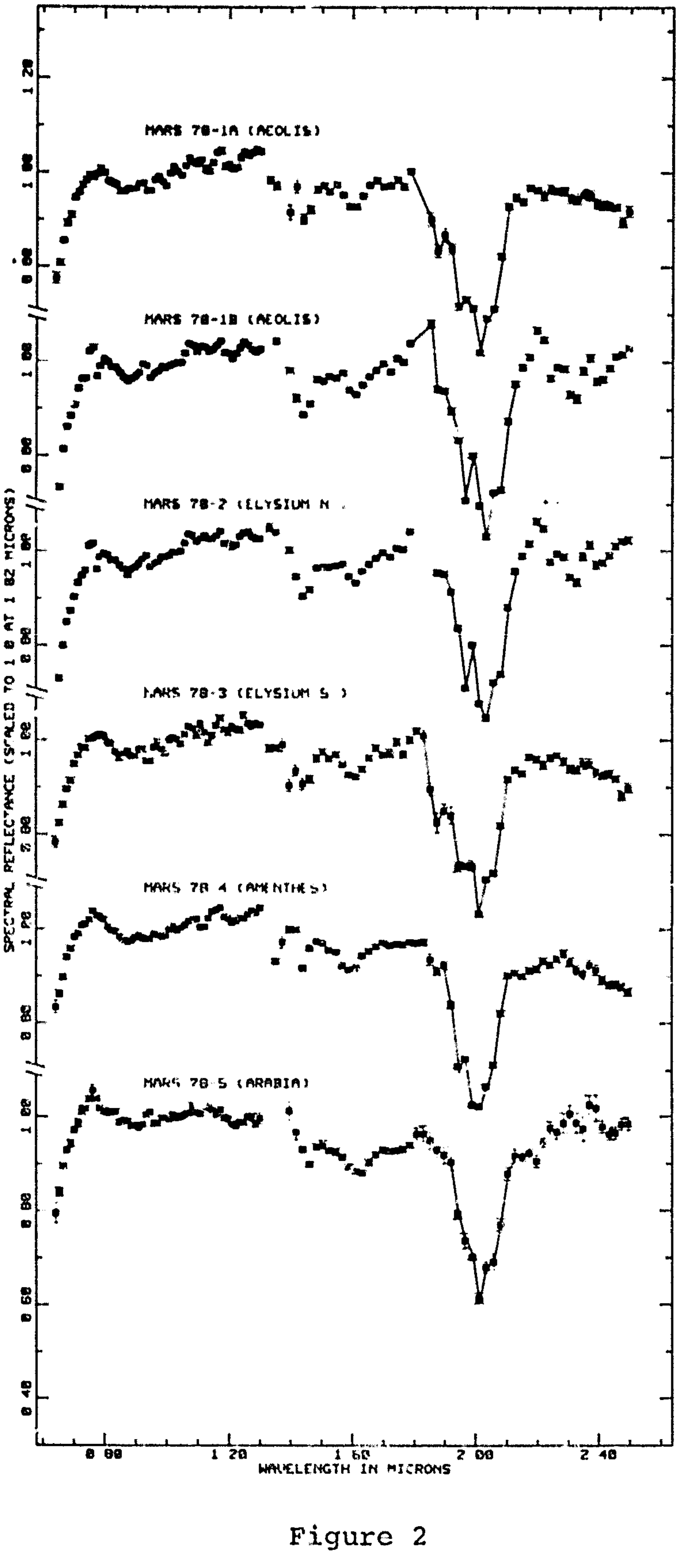
MARS 78-1A (AEOLIS)
MARS 78-1B (AEOLIS)
MARS 78-2 (ELYSIUM N.)
MARS 78-3 (ELYSIUM S.)
MARS 78-4 (AMENTHES)
MARS 78-5 (ARABIA)
SPECTRAL REFLECTANCE (SCALED TO 1.0 AT 1.02 MICRONS)
WAVELENGTH IN MICRONS

Figure 2

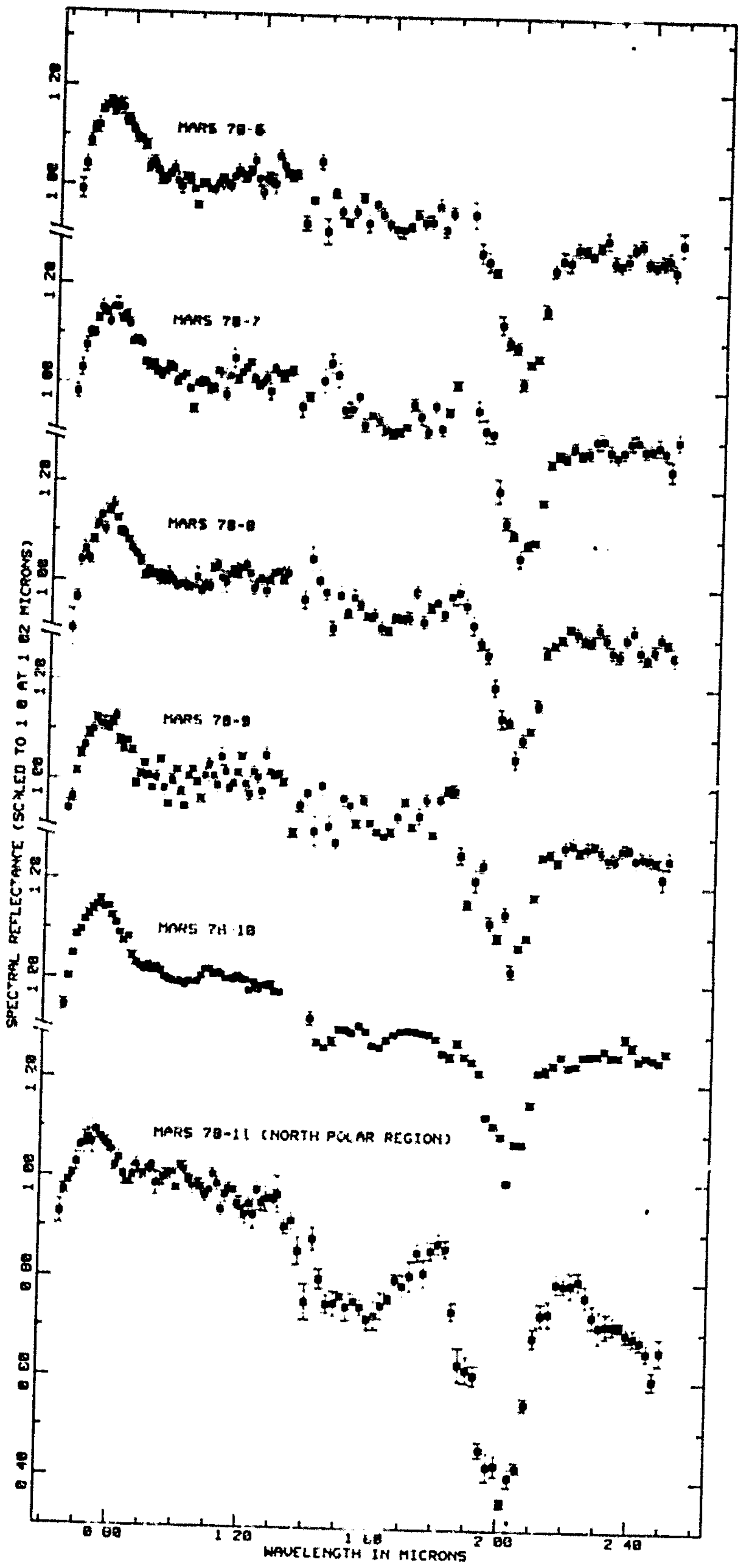
MARS 78-6
MARS 78-7
MARS 78-8
MARS 78-9
MARS 78-10
MARS 78-11 (NORTH POLAR REGION)
SPECTRAL REFLECTANCE (SCALED TO 1.0 AT 1.02 MICRONS)
1.20
1.00
0.80
0.60
0.40
0.80
1.20
1.60
2.00
2.40
WAVELENGTH IN MICRONS

Figure 3

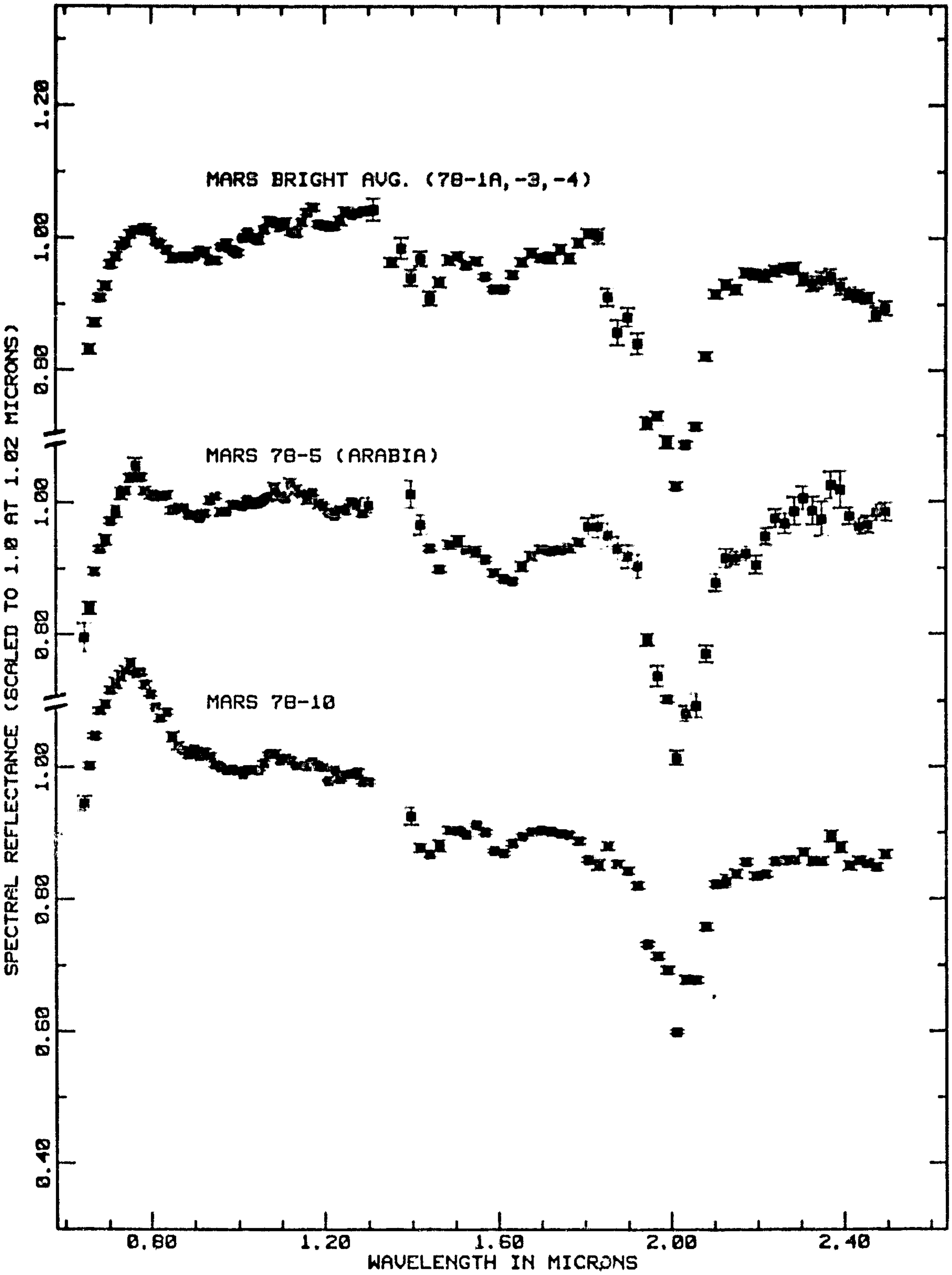
MARS BRIGHT AVG. (78-1A,-3,-4)
MARS 78-5 (ARABIA)
MARS 78-10
SPECTRAL REFLECTANCE (SCALED TO 1.0 AT 1.02 MICRONS)
WAVELENGTH IN MICRONS
1.20
1.00
0.80
0.60
0.40
0.80
1.20
1.60
2.00
2.40

Figure 4

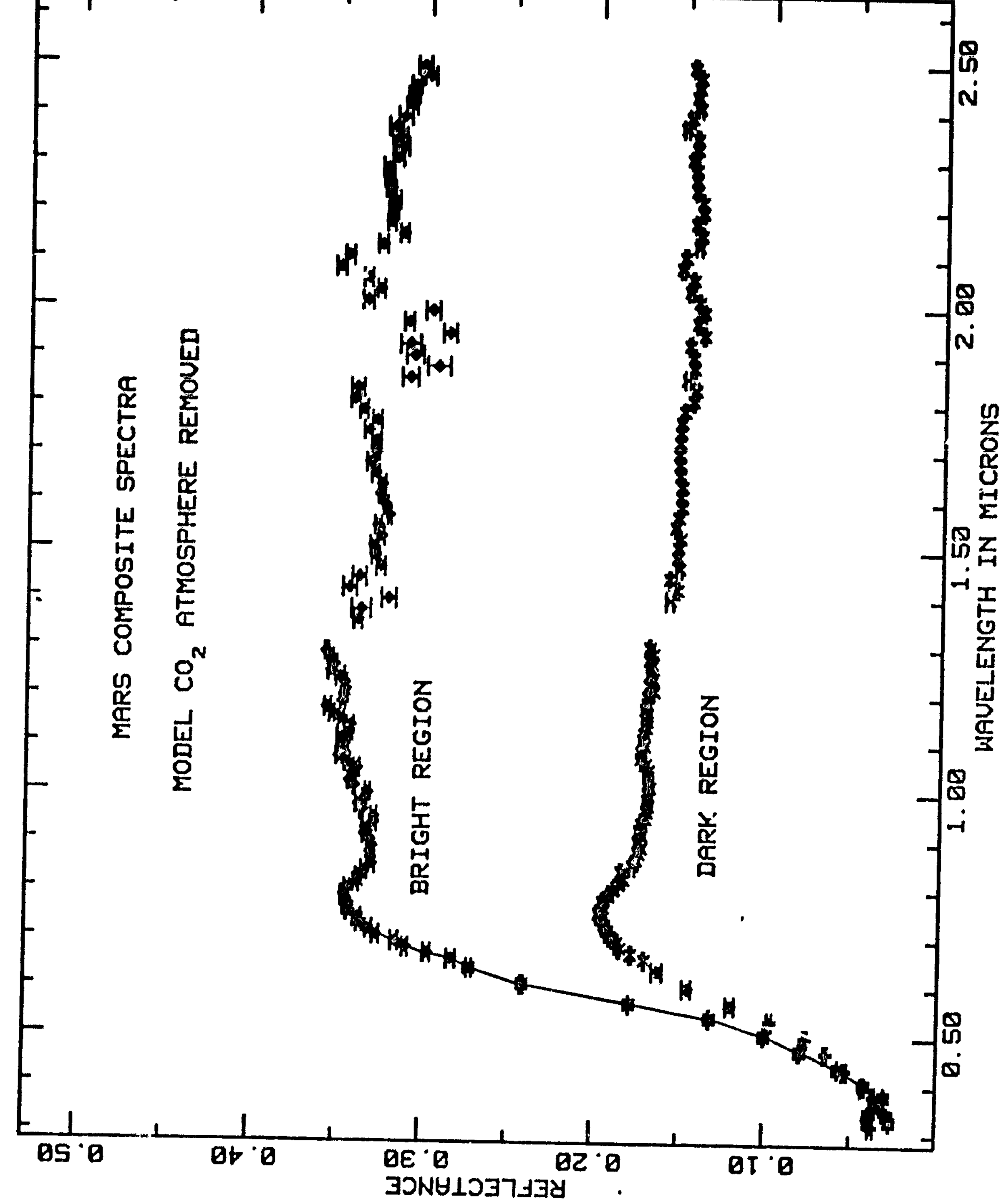
MARS COMPOSITE SPECTRA
MODEL $CO_2$ ATMOSPHERE REMOVED
BRIGHT REGION
DARK REGION
REFLECTANCE
0.10
0.20
0.30
0.40
0.50
WAVELENGTH IN MICRONS
0.50
1.00
1.50
2.00
2.50

Figure 5

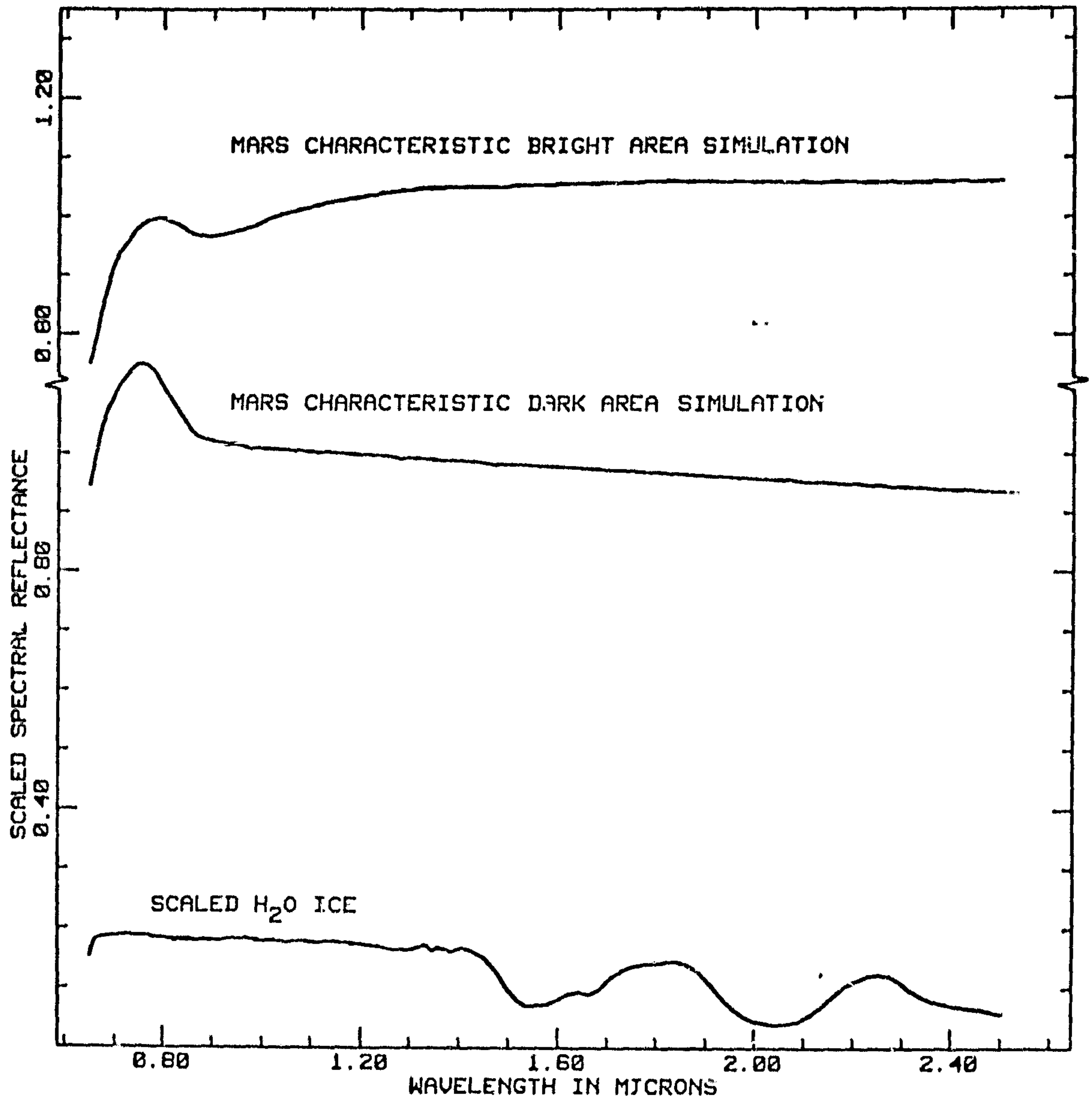
MARS CHARACTERISTIC BRIGHT AREA SIMULATION
MARS CHARACTERISTIC DARK AREA SIMULATION
SCALED $H_2O$ ICE
SCALED SPECTRAL REFLECTANCE
1.20
0.80
0.80
0.40
0.80
1.20
1.60
2.00
2.40
WAVELENGTH IN MICRONS

Figure 6

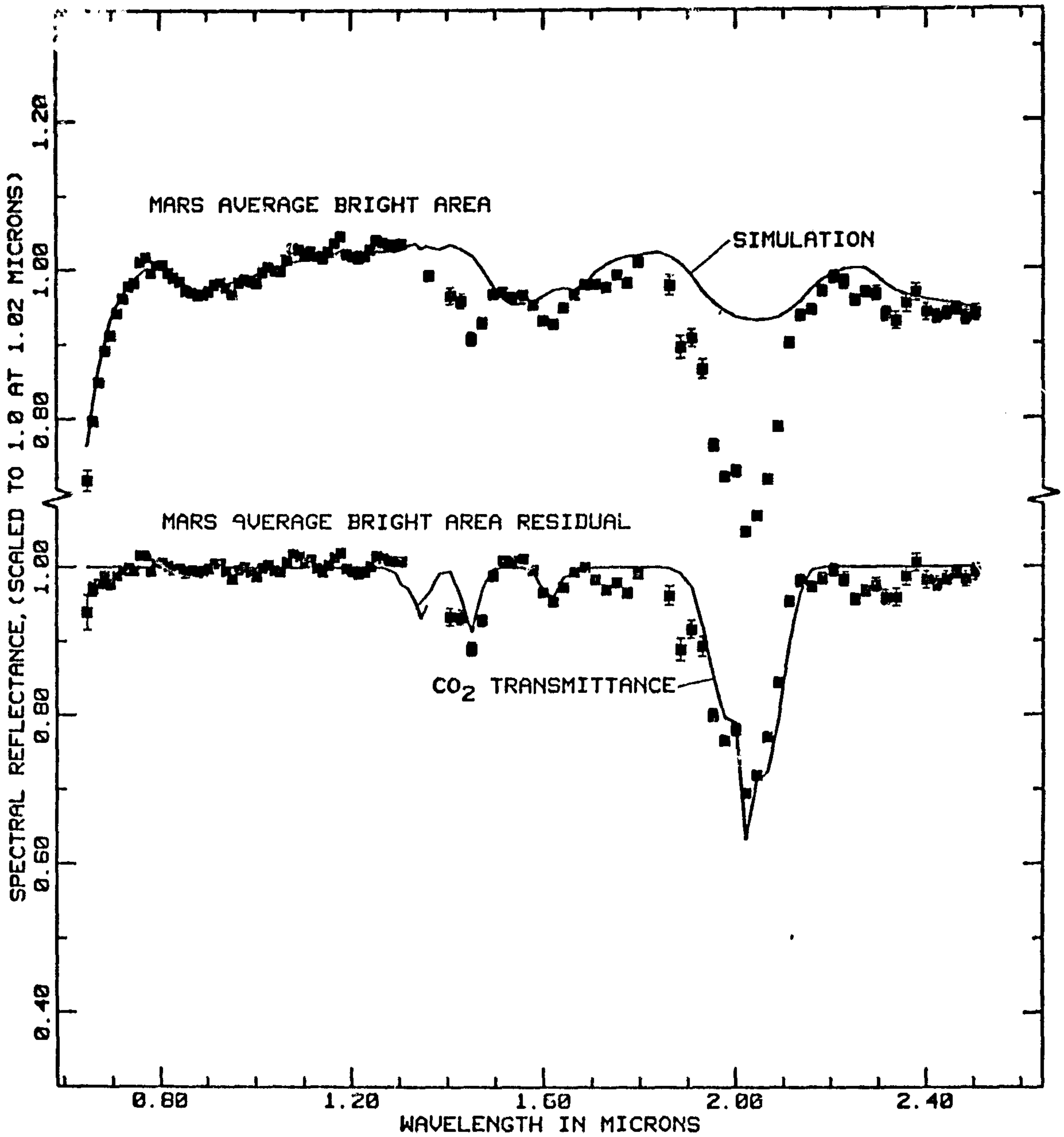

MARS AVERAGE BRIGHT AREA
SIMULATION
MARS AVERAGE BRIGHT AREA RESIDUAL
CO2 TRANSMITTANCE
SPECTRAL REFLECTANCE, (SCALED TO 1.0 AT 1.02 MICRONS)
1.20
1.00
0.80
0.60
0.40
0.80
1.20
1.60
2.00
2.40
WAVELENGTH IN MICRONS


Figure 7a

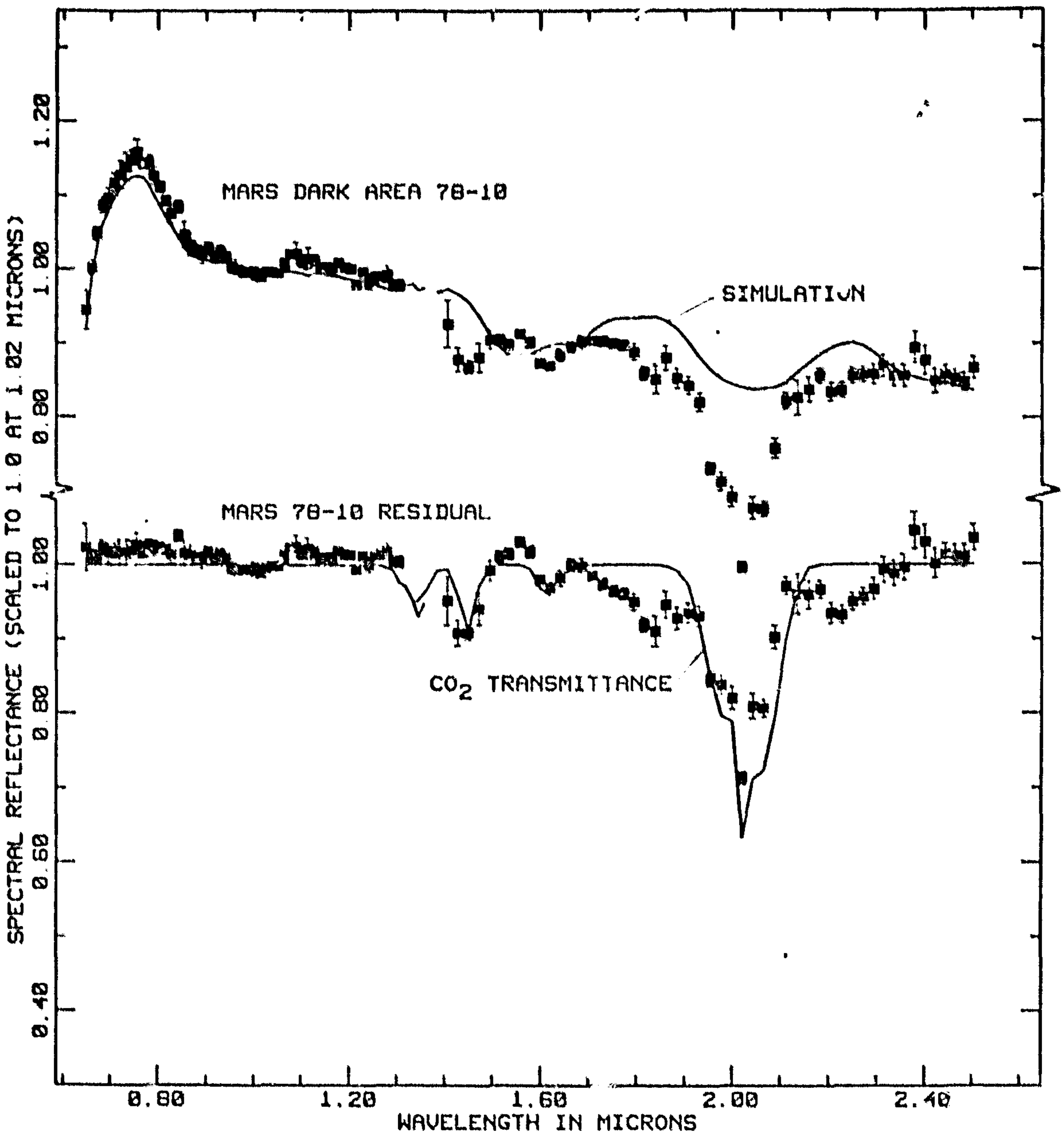

MARS DARK AREA 78-10
SIMULATI∪N
MARS 78-10 RESIDUAL
CO2 TRANSMITTANCE
SPECTRAL REFLECTANCE (SCALED TO 1.0 AT 1.02 MICRONS)
1.20
1.00
0.80
1.00
0.80
0.60
0.40
0.80
1.20
1.60
2.00
2.40
WAVELENGTH IN MICRONS


Figure 7b

# CHAPTER III

## MARS: Large Scale Mixing of Bright and Dark Surface Materials and Implications for Analysis of Spectral Reflectance

This paper has been published in Proc. Lunar Planet. Sci. Conf. 10th, 1835-1848, 1979. Authors: R.B. Singer and T.B. McCord.

## ABSTRACT

Earthbased observations of the spectral reflectance of Mars have a spatial resolution of 300 km or larger. Spacecraft observations have shown that many of the telescopic dark regions on the planet have substantial mixing of bright and dark materials. It is therefore probable that at least some spectral observations include significant contributions from multiple surface components. A model was developed to describe spectral reflectance from a two-component surface with large scale (greater than centimeter size) mixing. This model involves significant simplifications but is felt to be adequate for present purposes. Using this model the influence of differing degrees of bright material (aeolian dust) coverage in observed dark regions was removed. With increasing bright spectrum removal the reflectivity of the inferred dark material decreases, particularly in the infrared. $Fe^{3+}$ spectral features are reduced in magnitude but not eliminated. The broad absorption near 1 μm, attributed to $Fe^{2+}$ in mafic minerals such as pyroxenes and olivines, is progressively enhanced. Within the constraints of this analysis an upper limit of about 40% is placed on physical coverage of observed dark regions by bright dust. The two-component reflectance model was also used to investigate spectral differences observed among dark regions. We conclude that in most cases the observed

spectral variety cannot be fully explained by differential coverage of dark regions by discrete patches or streaks of bright dust. This is taken as confirmation of previous conclusions that there is a compositional variety of dark materials on Mars.

## INTRODUCTION

Spacecraft observations of Mars have shown that many of the telescopic low and intermediate albedo regions are covered with discrete streaks and splotches of bright and dark materials on a scale of tens of kilometers down to the limit of resolution (e.g. Sagan et al., 1972, 1973; Veverka et al., 1977; Greeley et al., 1978). The Viking landers provide a much more detailed look at two particular locations on the martian surface. They show a variety of surface types (rocks, dust, and soils); the overall impression is still one of separation of surface components on a scale of meters to centimeters, rather than a more homogeneous mixing. (Binder et al., 1977; Mutch et al., 1977; Guinness et al., 1979; Strickland, 1979). This apparent tendency towards discrete distribution is consistent with the observed and implied grain size distribution and aeolian sorting of martian surface materials (Mutch et al., 1976, Chapter 7).

Earthbased reflectance spectra of Mars (e.g. McCord and Westphal, 1971; McCord et al., 1977, 1980) integrate light over regions 300 km or greater in diameter. It therefore seems likely that at least some of these observations show significant spectral contributions from multiple types of surface materials. This paper describes some analyses designed to investigate this possibility and the implications for interpretation of martian spectra.

To a visual observer Mars shows a generally bimodal albedo distribution: bright and dark, with some areas of intermediate or mixed albedo. Groundbased and spacecraft observations have confirmed this as a general relationship from the visible into the infrared (e.g. Binder and Jones, 1972; Farmer *et al.*, 1977; Kieffer *et al.*, 1977; Soderblom *et al.*, 1978) but some important spectral variation has been demonstrated. Measurements of bright area to dark area albedo ratios near 1 μm vary from a low of about 1.8 to a high of about 3.0 (McCord and Westphal, 1971; Binder and Jones, 1972).

A map showing locations on Mars for which groundbased reflectance spectra have been measured (McCord and Westphal, 1971; McCord *et al.*, 1977, 1980) is given in Figure 1. All spectrum and location numbers used in this paper refer to this map. For 1969 observations $L_s$ = 162-163°, for 1973 observations $L_s$ = 301-302°, and for 1978 observations $L_s$ = 48-50°.

A composite spectrum typical of bright areas is shown at the top of Figure 2, scaled to unity at 1.02 μm. The visible portion is an average of 73-1, -2, and -3 while the infrared is an average of 78-1, -2, and -3. Bright area spectra are characterized by the edge of a steep $Fe^{3+}$ charge transfer absorption band from the UV to 0.75 μm with a slope change at about 0.6 μm, and a weaker $Fe^{3+}$ interelectronic absorption near 0.86 µm. These features are attributed to a ferric oxide content of about 5 to 8% (Huguenin et al., 1977). From the band minimum near 0.86 µm to about 1.3 µm the spectrum slopes upwards slightly. Between 1.4 and 1.7 µm there is an absorption which has been interpreted as $H_2O$ in a hydrate or ice (McCord et al., 1978, 1980). From 1.8 to 2.2 µm the spectrum is dominated by a deep Mars atmospheric $CO_2$ absorption. Removal of a model $CO_2$ atmosphere (McCord et al., 1978) yields a fairly flat spectrum from 1.7 to 2.5 µm, with the possibility of an additional $H_2O$ absorption near 1.9 µm (McCord et al., 1980).

Dark area spectra are substantially different from bright area spectra. A composite spectrum of visible (69-6) and infrared (78-10) data from the region Iapygia is shown at the bottom of Figure 2, also scaled to unity at 1.02 µm. The slope from UV to red is reduced compared to that for bright region spectra; the absorption near 0.86 µm is also weaker, and it is superimposed on a sharp decrease in reflectance from the peak near 0.75 µm. These two features indicate a lower $Fe^{3+}$ content (Adams and McCord, 1969; Huguenin et al., 1977; McCord et al., 1977). In addition, dark area spectra show $Fe^{2+}$ absorptions centered near 1.0 µm. These vary with location on the planet and are thought to represent differences in the compositions and relative abundances of the mafic minerals, primarily pyroxenes and olivines (Adams and McCord, 1979; Huguenin et al., 1977; McCord et al., 1977). In sharp contrast to the bright area spectra, dark area spectra slope fairly uniformly downwards from 1.1 to 2.5 μm (after Martian atmospheric $CO_2$ effects are removed) (McCord et al., 1980).

Reflectance spectra from 0.3 to 1.1 μm of dust clouds are very similar to the spectra of the brightest regions on Mars, which appear uniform. These observations correlate with other evidence that the source for the brightest surface material is rather homogeneous aeolian dust (McCord et al., 1977). As discussed above dark area spectra show less uniformity and indicate less oxidized (weathered) material, so they may represent a variety of materials closer in composition to unmodified surface rock.

## REMOVAL OF EFFECTS OF BRIGHT MATERIAL FROM DARK REGION OBSERVATIONS

Since there is evidence that some of the spectral observations of dark regions on Mars may include light reflected from bright dust on the surface, a two-component model for reflectance from the surface has been developed and used to investigate the removal of contributions by bright dust from martian spectral observations. Two major simplifying assumptions have been made. First, we deal with the bulk spectral reflectivity of each component, as would be measured when remotely observing just this material. Second, we assume that the distribution of the two surface components is completely discrete, as discussed above. With more intimate mixing a significant proportion of observed photons will have passed through grains of both types, and spectral mixing models must increase in complexity.

A schematic representation of this model for an area in the field of view of a spectrometer is shown in Figure 3. Light reflected from only dark material or bright material has the spectral characteristics of that bulk material. If there is physical relief, such as a boulder or an outcrop, light reflected from bright material can also reflect off dark material, or vice versa, before reaching the instrument. In this case the spectral properties of the two materials combine in a multiplicative fashion. The relative importance of multiple reflection is heavily dependent on geometry. Based on various distributions of one-meter boulders with a reflectance of 15 to 20% on a flat surface with a reflectance of 30 to 40%, we have estimated that an upper limit of 5 to 10% of the total observed flux is likely to be contributed from multiple reflections. As shown in the enlargement, light entering the surface very near a boundary can be scattered by grains of both materials before reaching the instrument. In this case the resultant spectrum would also be some multiplicative combination of bright and dark spectral characteristics. This effect can only be significant within about one mean optical path length of the boundary; a few millimeters would seem to be a reasonable upper limit, based on terrestrial analogs for martian surface materials. If the minimum dimensions of surface streaks and splotches are a few centimeters or larger, which we assume here, this contribution from the boundaries is negligibly small compared to the total observed flux.

The model can be written as the following equations:

$$R_{OBS,\lambda} = (X_B\ R_{B,\lambda}) + (X_D\ R_{D,\lambda}) + (X_{BD}\ R_{B,\lambda}\ R_{D,\lambda}) \quad (1)$$

and

$$X_B + X_D + X_{BD} = 1 \quad (2)$$

where

$\lambda$ = wavelength

$R_{OBS}$ = observed reflectivity

$R_B$ = reflectivity of bright material

$R_D$ = reflectivity of dark material

$X_B$ = weighting factor for bright material term

$X_D$ = weighting factor for dark material term

$X_{BD}$ = weighting factor for first order multiplicative term

Negative values for the weighting factors would be physically meaningless and are not allowed. Higher-order multiplicative terms have been neglected. The justification is twofold. First, as discussed above, we feel that the apparent physical distribution of materials on Mars and the current level of knowledge about these materials do not warrant the complication of additional terms. Second, given the measured reflectivities of bright materials (<40%) and dark materials (<20%), higher-order multiplicative terms quickly decrease in relative importance.

If the first-order multiplicative term is neglected also ($X_{BD} = 0$), which we feel is probably a valid approximation for parts of Mars, then what is left is a simple additive or "checkerboard" model of spectral combination. In this case $X_B$ represents the relative areal coverage in the field of view by bright material, and $X_D$ represents the relative coverage by dark material.

By taking an observed dark region spectrum for $R_{OBS,\lambda}$ an observed bright spectrum (assumed to be aeolian dust deposits) for $R_{B,\lambda}$, and choosing values for $X_B$, $X_D$, and $X_{BD}$, equation (1) can be solved for $R_{D,\lambda}$, the dark material spectrum. Thus we can investigate what the spectral characteristics of the dark material would be for various amounts of contamination of the observed region by bright dust.

Because the available spectra are not reduced to albedo or absolute reflectance it was necessary to determine a reasonable scaling for the observed bright area spectra relative to the observed dark area spectra. A literature search (Adams and McCord, 1969; McCord and Westphal, 1971; Binder and Jones, 1972) and examination of unscaled telescopic data showed a range of bright area to dark area reflectance ratios of about 1.8 to 3.0 at 1 μm, with a strong tendency for values near 2.0. Therefore, all analysis were performed with a bright to dark spectrum ratio of 2.0 at 1 μm, with an investigation of the possible errors caused by such an assumption.

The results of such an analysis are shown in Figure 4. In this case $X_{BD}$ was chosen to be zero. Spectral coverage is essentially complete from 0.3 to 2.5 μm and represents a composite of visible data (McCord and Westphal, 1971) and infrared data (McCord et al., 1979). A model $CO_2$ atmosphere has been removed from the infrared data (McCord et al., 1980). The top curve, labeled "Observed Bright", represents the brightest region spectra observed and is used as $R_{B,\lambda}$ (69-1 visible, average of 78-1, -2, and -3 infrared). The next lower curve, labeled "Observed Dark", is a spectrum for part of the telescopic dark region Iapygia and is used as $R_{OBS,\lambda}$ (69-6 visible, 78-10 infrared). The curve below that, labeled "-10% Brt" is the dark material spectrum which results when equations (1) and (2) are solved for $R_{D,\lambda}$ with $X_B = 0.1$ and $X_D = 0.9$ (10% areal coverage by bright material, 90% areal coverage by dark material). Similarly, the remaining curves represent the dark material spectra derived by removing the influence of 20%, 30%, and 40% coverage of the observed dark region by bright dust. With the removal of increasing amounts of bright material spectrum the dark material spectra show reduced UV to visible absorption and less indication of an absorption near 0.86 μm. This is consistent with a lower $Fe^{3+}$ content in the dark material. The $Fe^{2+}$ absorption near 1 μm becomes more apparent, although superimposed on a steeper spectral falloff towards longer wavelengths. The peak of the spectrum shifts to slightly shorter wavelengths with increased bright removal.

It can be seen that the removal of more than about 40% bright material influence leads to an unreasonably low reflectance for the deduced dark material in the infrared. This places an upper limit of about 40% on coverage of this dark region by bright dust. The primary dependence of this value on the model is in the choice of observed bright spectrum ($R_{B,\lambda}$) to observed dark spectrum ($R_{OBS,\lambda}$) scaling (discussed above). A value of 2.0 (at 1 μm) yields an upper limit of about 40%; a value of 2.5 yields an upper limit of about 33%; and a value of 3.0 yields an upper limit of about 25%. There is also a minor change in shape of the deduced dark material spectrum with varying observed bright to observed dark spectrum scaling, mostly along the UV-visible slope. This is because scaling is multiplicative, while the analysis is subtractive. For our present purposes the magnitude of this effect is not significant.

This analysis involves a number of simplifications. The surface of Mars is not a two-component system (see the next section) and there must certainly be situations where higher-order multiple scattering cannot be ignored. With these qualifications it is not certain that any of the deduced dark material spectra represent actual single petrologic units. The probability of contamination of observed dark regions by bright dust is quite high, however; we feel that some of these deduced dark material spectra are likely to be a closer approximation to physical reality than direct observations, and should be considered when performing spectral analyses and laboratory simulations.

## ANALYSIS OF SPECTRAL UNIQUENESS
## OF LOW ALBEDO REGIONS

As noted above the brightest regions observed on Mars have very similar spectral characteristics, while lower albedo areas demonstrate greater spectral diversity. We investigated these differences by removing the effects of potential coverage of the observed lower albedo regions by bright material. The goal was to better understand actual variability among dark materials on Mars.

This technique is based on the model described above [equations (1) and (2)]. An "intermediate" spectrum is assumed to be produced by some mixture, as permitted by the model, of a "bright endmember" (aeolian dust) and a "dark endmember". Differing amounts of bright endmember spectrum are removed from the intermediate spectrum while other free parameters are varied until the optimum fit is obtained between the modified intermediate spectrum and the dark endmember spectrum. The quality of this fit is a measure of similarity, within the limitations of this analysis, between the dark material in the intermediate region and the dark material in the dark endmember region. A poor fit demonstrates that the intermediate spectrum cannot be produced by large scale mixing between the dark endmember and the bright endmember (aeolian dust). We feel confident in this negative conclusion because this technique is most likely to err by producing an artificially favorable match. Because the absolute reflectances of the observed regions have not been determined, this parameter is allowed to vary in the analysis and there is no direct justification for the scaling relationship which yields the optimum fit. A good fit demonstrates the possibility that the primary differences between intermediate and dark endmember regions is the amount of coverage by bright dust. Because of the limitations discussed above, a good fit does not prove that the dark material is identical in the intermediate and dark endmember regions. As will be shown below, however, in a few cases the similarity is striking.

An interactive computer program was developed to perform this analysis. The user chooses three spectra, one each to serve as bright endmember, dark endmember, and intermediate. A value for the multiplicative weighting factor, $X_{BD}$, is also entered. The program then increments the scaling of the intermediate spectrum between bright and dark endmember spectra and uses equations (1) and (2) for varying degrees of bright spectrum removal from the intermediate spectrum. For every scaling increment equations (1) and (2) are solved for each wavelength channel in the spectra separately, yielding the value of $X_B$ (bright removal) which results in a perfect fit (solves the equations) for that channel. The mean value ($\overline{X}_B$) and standard deviation ($\sigma$) of $X_B$ are then calculated from the individual values for each channel. (The value of $X_D$ is not independent of the value of $X_B$.) $\sigma$ is used as an indication of quality of fit between the two spectra. For each set of input parameters the program automatically finds the scaling which yields the minimum value of $\sigma$, and displays these two numbers as well as $\overline{X}_B$ and $\overline{X}_D$.

Some results from this analysis are shown in Table 1. This is a matrix of eight Mars spectra (McCord et al., 1977) fitted to each other as described above. 73-17 is classified as an intermediate albedo region. The remaining seven represent observations of different dark regions. An average of 73-1, 73-2, and 73-3, the brightest areas observed, was used as the bright endmember in all calculations. This bright average was scaled to have twice the reflectance at 1 μm as 73-26, the darkest region observed. For each combination two parameters for the optimum fit are tabulated: $\sigma$ and $\overline{X}_B$. Where a spectrum is fitted to itself, both parameters are equal to zero, indicating a perfect fit with no modification of the intermediate spectrum. A crossed-out box indicates that the best fit was obtained with a negative value of $\overline{X}_B$, which is not physically meaningful. This is generally an indication that the spectrum used as the dark endmember is more like the bright endmember than is the intermediate spectrum. The spectra were numbered by McCord et al. (1977) in order of decreasing bright characteristics; inspection of Table 1 shows general agreement with this ordering, with a few exceptions.

Calculations for tnese data were performed in the infrared only, from 0.67 to 1.10 μm. The emphasis of this work was to examine similarities or differences among mafic surface components, which are best characterized by $Fe^{2+}$ crystal field absorptions near 1 μm. Attempts to match the entire spectrum from 0.3 to 1.1 μm using the method described above produced subjectively poorer fits, particularly in the region of greatest interest, the near-infrared. A contributing factor might be variations in atmospheric opacity, which are not dealt with in this model and become increasingly significant at shorter wavelengths.

It is interesting to note that in all but one case the optimum value for the multiplicative coefficient, $X_{BD}$, was zero. This means that the best matches were obtained with just an additive, or "checkerboard" model.

Spectra for a few of these results are shown in Figure 5 matched to 73-26, the region with the darkest characteristics observed in 1973. The top curve shows the best match obtained: that of 73-24 to 73-26. Here $\sigma = 0.009$, and $\overline{X}_B = 0.084$, indicating that the effect of 8.4% bright material coverage was removed from 73-24 to make it best resemble 73-26. The agreement between the two curves is excellent from 0.33 to 1.10 μm. The implication is that the dark materials at both locations are very similar, but that region 73-24 has slightly more coverage by bright dust.

The next lower curve shows 73-17, originally classified as an intermediate albedo region, best matched to 73-26. Here $\sigma = 0.012$, and $\overline{X}_B = 0.326$, indicating the removal of 32.6% bright influence. In the infrared the overall agreement is good, with some potentially significant differences in detail, primarily between 0.7 and 0.9 μm. Thus there is a possibility of dark material in the 73-17 region similar but not identical to that seen at 73-26. From the red to the near UV, however, the curves diverge. This could be due to a relatively higher degree of oxidation of the dark materials at 73-17.

The third curve from the top shows the best fit to 73-26 obtained for the dark area 73-23, with $\sigma = 0.031$. The general shape of the curves is similar. In the infrared, however, there are extensive differences larger than the formal errors and involving more than one data point. In remotely analyzing the occurrence and composition of minerals with reflectance spectroscopy, it is these types of variations which have proven very significant (see Pieters, 1978, for a summary of variation in spectral details seen in lunar basalts). The conclusion here is that the dark materials in 73-23 are mineralogically different than those in 73-26.

It is not unreasonable that spectra of dark regions on Mars have similar overall shapes even if they differ in spectral details. There is strong evidence for mafix composition of the dark materials (Adams and McCord, 1979; Toulmin et al., 1977; Smyth et al., 1978) oxidized at the time of implacement (e.g. palagonitization, Soderblom and Wenner, 1978) and/or subsequently (e.g. photostimulated oxidation, Huguenin, 1973a, b). $Fe^{3+}$ characteristics dominate the spectrum in the UV and visible and continue to influence it into the near infrared. Much of the shape of the spectrum, then, is controlled by the degree and nature of the oxidation. The infrared spectral features which contain information about mafic mineralogy are more subtle by comparison.

An example of an exceedingly poor fit is shown at the bottom of Figure 5. This is the best match possible (with this model) of 73-20 to 73-26. Here $\sigma = 0.040$ and the differences between the two curves are not subtle. Inspection of Table 1 shows that 73-20 cannot be made to match any of the spectra well. It would appear that the dark material(s) in 73-20 are substantially different from those in other observed dark regions.

The quality of fit parameter, $\sigma$, has two components: a component due to observational uncertainty and a component due to true differences in spectral reflectivity. Since the best fit obtained in this analysis was $\sigma = 0.009$, the random (observational) component is estimated to be on the average somewhat less than this value. Based on visual inspection of a number of spectral fits, including those presented in Figure 5, we have chosen a value of $\sigma \approx 0.015$, above which we feel that a good match has not been attained in the infrared portions of these spectra. This choice was somewhat arbitrary, and $\sigma$ should be used only as a relative guide to the quality of the fit. More detailed analysis would require the inspection of each set of fitted spectra individually.

We conclude from this analysis that the spectral variety observed among the telescopic dark regions of Mars cannot be fully explained by differential coverage of these regions by patches or streaks of bright dust. In approximately 20% of the cases analyzed this mechanism appears to be sufficient, but is not proven to be so. From the remaining cases it seems highly probable that there are true spectral variations. This is taken as confirmation of previous conclusions that there is a compositional variety of dark materials on Mars. (Huguenin et al., 1977; McCord et al., 1977; Soderblom et al., 1978).

It is almost certain that still greater variation could be detected and analyzed with higher spatial and spectral resolution. Much of the variation among lunar basalts, for comparison, occurs on a scale of tens of kilometers and is lost in observations made with a much larger field of view. Observations of Mars with greater spectral resolution would allow compositional interpretation to be carried out in more detail and with greater certainty. The best way to meet both these requirements is with a spacecraft-borne mapping spectrometer.

## ACKNOWLEDGEMENTS

We are grateful to Michael J. Gaffey, John B. Adams, and Roger N. Clark for helpful discussions and suggestions, and to Ray Arvidson for a careful review. We also wish to thank Duncan M. Chesley for guidance in software development. This work was performed at the University of Hawaii Institute for Astronomy. This research was supported by NASA grant NSG No. 7590. Contribution 238 of the Planetary Sciences Laboratory.

## REFERENCES

Adams, J. B. and McCord, T. B., Mars: Interpretation of spectral reflectivity of light and dark regions. J. Geophys. Res. 74, 4851-4856, 1969.

Binder, A. B. and Jones, J. C., Spectrophotometric studies of the photometric function, composition, and distribution of the surface materials of Mars. J. Geophys. Res. 77, 3005-3019, 1972.

Binder, A. B., Arvidson, R. E., Guinness, E. A., Jones, K. L., Morris, E. C., Mutch, T. A., Pieri, D. C. and Sagan, C., The geology of the Viking Lander 1 site. J. Geophys. Res. 82, 4439-4451, 1977.

Farmer, C. B., Davies, D. W. and Holland, A. L., Mars: Water vapor observations from the Viking Orbiters. J. Geophys. Res. 82, 4225-4248, 1977.

Greeley, R., Papson, R. and Veverka, J., Crater streaks in the Chryse Planitia region of Mars: Early Viking results. Icarus 34, 556-567, 1978.

Guinness, E. A., Arvidson, R. E., Gehret, D. C. and Bolef, L. K., Color changes at the Viking Landing sites over the course of a Mars year. J. Geophys. Res., in press, December 1979.

Huguenin, R. L., Photostimulated oxidation of magnetite. 1. Kinetics and alteration phase identification. J. Geophys. Res. 78, 8481-8493, 1973a.

Huguenin, R. L., Photostimulated oxidation of magnetite. 2. Mechanism. J. Geophys. Res. 78, 8495-8506, 1973b.

Huguenin, R. L., Adams, J. B. and McCord, T. B., Mars: Surface mineralogy from reflectance spectra. In Lunar Science VIII, p. 478-480, 1977. The Lunar Science Institute, Houston.

Kieffer, H. H., Martin, T. Z., Peterfreund, A. R. and Jakosky, B. M., Thermal and albedo mapping of Mars during the Viking primary mission. J. Geophys. Res. 82, 4249-4291, 1977.

McCord, T. B., Clark, R. and Huguenin, R. L., Mars: Near-infrared spectral reflectance and compositional implications. J. Geophys. Res. 83, 5433-5441, 1978.

McCord, T. B., Clark, R. N., Singer, R. B. and Huguenin, R. L., Mars: Near-infrared reflectance spectra of surface regions and compositional implications. To be submitted to J. Geophys. Res., 1980. Thesis Ch. II

McCord, T. B., Huguenin, R. L., Mink, D. and Pieters, C., Spectral reflectance of Martian areas during the 1973 opposition: Photoelectric filter photometry 0.33-1.10 μm. Icarus 31, 25-39, 1977.

McCord, T. B. and Westphal, J. A., Mars: Narrowband photometry, from 0.3 to 2.5 microns, of surface regions during the 1969 apparition. Astrophys. J. 168, 141-153, 1971.

Mutch, T. A., Arvidson, R. E., Head, J. W., III, Jones, K. L. and Saunders, R. S., The Geology of Mars, Princeton Univ. Press, Princeton, New Jersey.

Mutch, T. A., Arvidson, R. E., Binder, A. B., Guinness, E. A. and Morris, E. C., The geology of the Viking Lander 2 site. J. Geophys. Res. 82, 4452-4467, 1977.

Pieters, C. M., Mare basalt types on the front side of the moon A summary of spectral reflectance data. Proc. Lunar Planet. Sci. Conf. 9th, p. 2825-2849, 1978.

Sagan, C., Veverka, J., Fox, P., Dubisch, R., Lederberg, J., Levinthal, E., Quam, L., Rucker, R., Pollack, J. B. and Smith, B. A., Variable features on Mars: Preliminary Mariner 9 television results. Icarus 17, 346-372, 1972.

Sagan, C., Veverka, J., Fox, P., Dubisch, R., French, R., Gierrasch, P., Quam, L., Lederberg, J., Levinthal, E., Tucker, R., Eross, B. and Pollack, J. B., Variable features on Mars, 2, Mariner 9 global results. J. Geophys. Res. 78, 4163-4196, 1973.

Smyth, J. R., Huguenin, R. and McGetchin, T. R., Composition of Martian primary lavas - convergence of Model results (abstract). In Lunar and Planetary Science IX, p. 1077-1079, 1978. Lunar and Planetary Institute, Houston.

Soderblom, L. A., Edwards, K., Eliason, E. M., Sanchez, E. M. and Charette, M. P., Global color variations on the Martian surface. Icarus 34, 446-464, 1978.

Soderblom, L. A. and Wenner, D. B., Possible fossil $H_2O$ liquid-ice interfaces in the Martian crust. Icarus 34, 622-637, 1978.

Strickland, E. L., III, Soil stratigraphy and rock coatings observed in color enhanced Viking lander images (abstract). In Lunar and Planetary Science X, p. 1192-1194, 1979. Lunar and Planetary Institute, Houston.

Toulmin, P., III, Baird, A. K., Clark, B. C., Keil, K., Rose, H. J., Jr., Christian, R. P., Evans, P. H. and Kelliher, W. C., Geochemical and mineralogical interpretation of the Viking inorganic chemical results. J. Geophys. Res. 82, 4625-4634, 1977.

Veverka, J., Thomas, P. and Greeley, R., A study of variable features on Mars during the Viking primary mission. J. Geophys. Res. 82, 4167-4187, 1977.

TABLE CAPTION

Table 1. Numerical results of spectrum fitting analysis described in text. "Bright Endmember" used for all calculations was an average of spectra 73-1, 73-2, and 73-3. Unless otherwise noted, the multiplicative coefficient, $X_{BD}$, equals zero.

**TABLE 1**

| SPECTRUM USED AS "INTERMEDIATE" | | SPECTRUM USED AS "DARK ENDMEMBER" | | | | | | | |
|---|---|---|---|---|---|---|---|---|---|
| | | 73-17 | 73-20 | 73-21 | 73-22 | 73-23 | 73-24 | 73-25 | 73-26 |
| 73-17 | $\sigma$ | 0.000 | | 0.025 | 0.013 | 0.025 | 0.011 | 0.018 | 0.012 |
| | $\overline{X}_B$ | 0.000 | | 0.232 | 0.012 | 0.272 | 0.242 | 0.197 | 0.326 |
| 73-20 | $\sigma$ | 0.090 | 0.000 | 0.056 | 0.027 | 0.039 | 0.032 | 0.035 | 0.040 |
| | $\overline{X}_B$ | 0.245 | 0.000 | 0.414 | 0.130 | 0.426 | 0.377 | 0.339 | 0.527 |
| 73-21 | $\sigma$ | | | 0.000 | 0.018 | 0.029 | 0.020 | 0.022 | 0.022 |
| | $\overline{X}_B$ | | | 0.000 | 0.151 | 0.080 | 0.063 | 0.003* | 0.152 |
| 73-22 | $\sigma$ | 0.041 | | 0.024 | 0.000 | 0.019 | 0.012 | 0.020 | 0.017 |
| | $\overline{X}_B$ | 0.016 | | 0.215 | 0.000 | 0.259 | 0.239 | 0.185 | 0.324 |
| 73-23 | $\sigma$ | | | | | 0.000 | | | 0.031 |
| | $\overline{X}_B$ | | | | | 0.000 | | | 0.076 |
| 73-24 | $\sigma$ | | | | | 0.022 | 0.000 | | 0.009 |
| | $\overline{X}_B$ | | | | | 0.005 | 0.000 | | 0.084 |
| 73-25 | $\sigma$ | | | 0.032 | | 0.019 | 0.012 | 0.000 | 0.019 |
| | $\overline{X}_B$ | | | 0.010 | | 0.078 | 0.066 | 0.000 | 0.157 |
| 73-26 | $\sigma$ | | | | | | | | 0.000 |
| | $\overline{X}_B$ | | | | | | | | 0.000 |

*$X_{BD}$ = 0.002

# FIGURE CAPTIONS

Figure 1: Locations on Mars for spectrophotometric observations by McCord and others. The first two digits represent the year of observation (e.g. 69-1 was observed in 1969). 1969 observations (0.3 to 1.1 μm) are described by McCord and Westphal (1971); 1973 observations (0.3 to 1.1 μm) are described by McCord et al. (1977); 1978 observations (0.7 to 2.5 μm) are described by McCord et al. (1980). Locations of observations for which the surface was partially or wholly obscured by atmospheric dust are not shown. (Base map: USGS Topographic Map of Mars I-961, 1976.)

Figure 2: Representative bright and dark region reflectance spectra, scaled to unity at 1.02 μm. The bright region spectrum is composed of an average of brightest areas observed in 1973 (visible) and 1978 (infrared). The dark region spectrum is a composite of data from two nearby locations in Iapygia: 69-6 (visible) and 78-10 (infrared).

Figure 3: Schematic representation of a model for spectral reflectance from the martian surface, with two surface components with large scale mixing only. Light reflected from just

bright material (B) or dark material (D) has the spectral distribution characteristic of the bulk reflectivity of that material. Light reflected from both surface types before observation has a spectral distribution determined by a multiplicative combination of bright and dark reflectivities. See text for full discussion of this model.

Figure 4: Removal of the effects of bright material contamination in observed dark regions. Details of the analysis are described in text. Curves labelled "observed Bright" and "Observed Dark" are observational data, for bright and dark regions, respectively, with a model $CO_2$ atmosphere removed. Curve labelled "-10% Brt" is the dark material spectrum resulting from the assumption of 10% areal coverage of the observed dark region by bright material, and similarly through "-40% Brt". Notice that an assumption of more than 40% coverage by bright material would yield an unrealistically low reflectance for the dark material.

Figure 5: Four examples of best fits to 73-26. Matching was performed by procedure described in text, using only the infrared portion of the spectra. $\sigma$ is a measure of

the error in fit, $\overline{X}_B$ represents the fraction of aeolian dust spectrum removed. Error bars represent ±1 standard deviation of the final results. Error bars for ±1 standard deviation of the mean would be smaller.

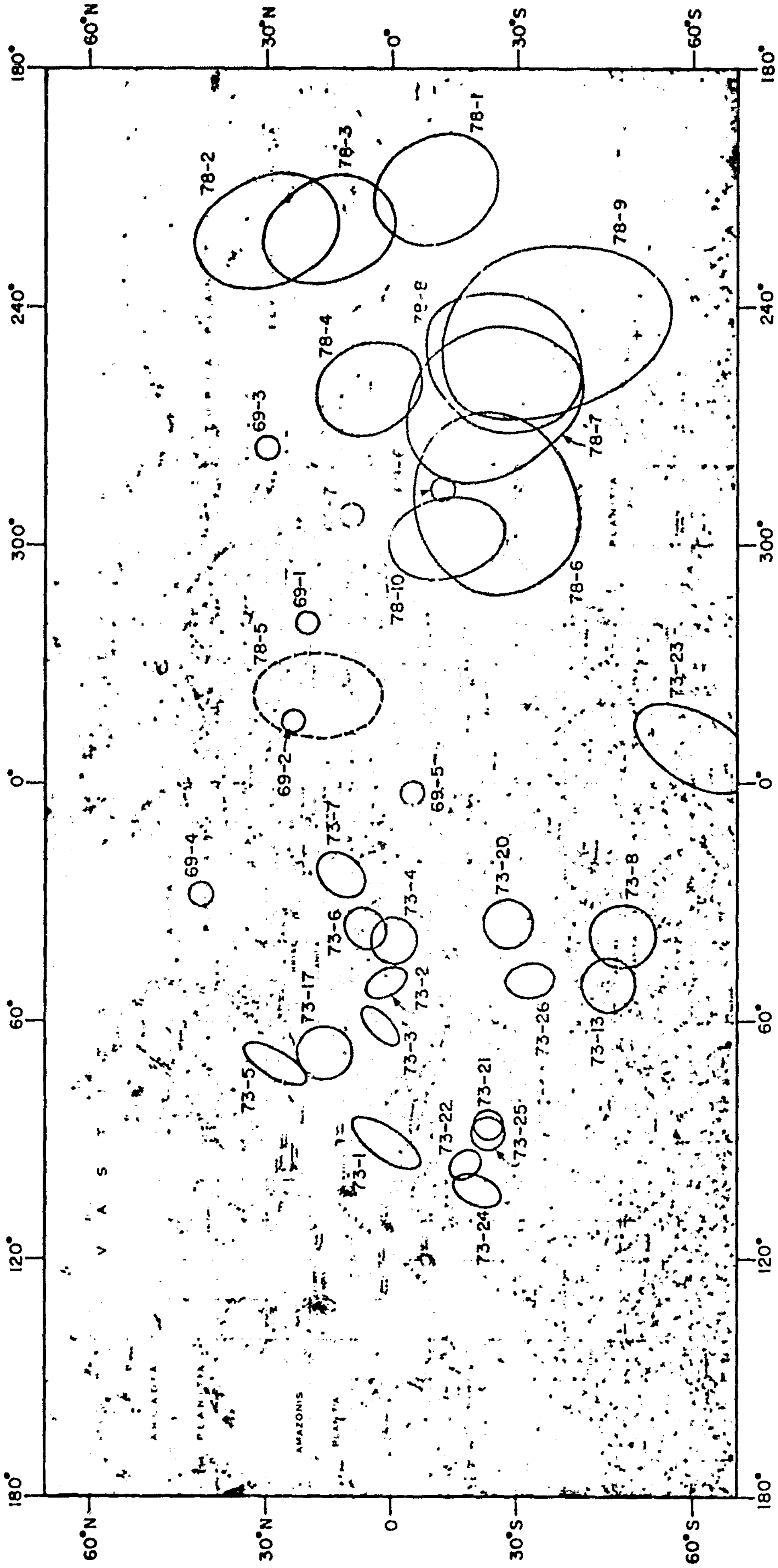
180°
240°
300°
0°
60°
120°
180°
60°N
30°N
0°
30°S
60°S
78-1
78-2
78-3
78-4
78-5
78-6
78-7
78-9
78-10
69-1
69-2
69-3
69-4
69-5
73-1
73-2
73-3
73-4
73-5
73-6
73-7
73-8
73-13
73-17
73-20
73-21
73-22
73-23
73-24
73-25
73-26
AMAZONIS
PLANITIA

Figure 1

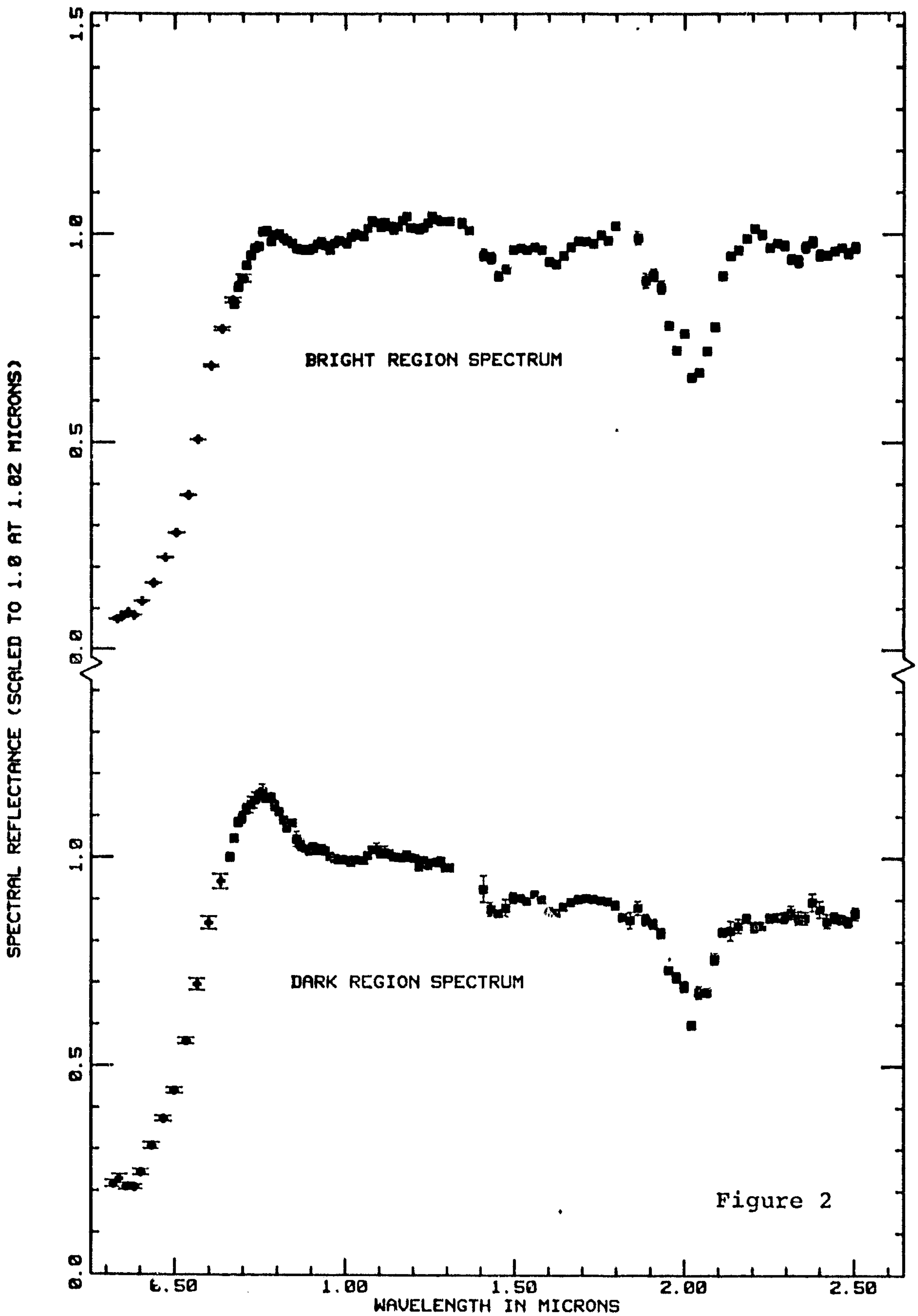

SPECTRAL REFLECTANCE (SCALED TO 1.0 AT 1.02 MICRONS)
BRIGHT REGION SPECTRUM
DARK REGION SPECTRUM
WAVELENGTH IN MICRONS


Figure 2

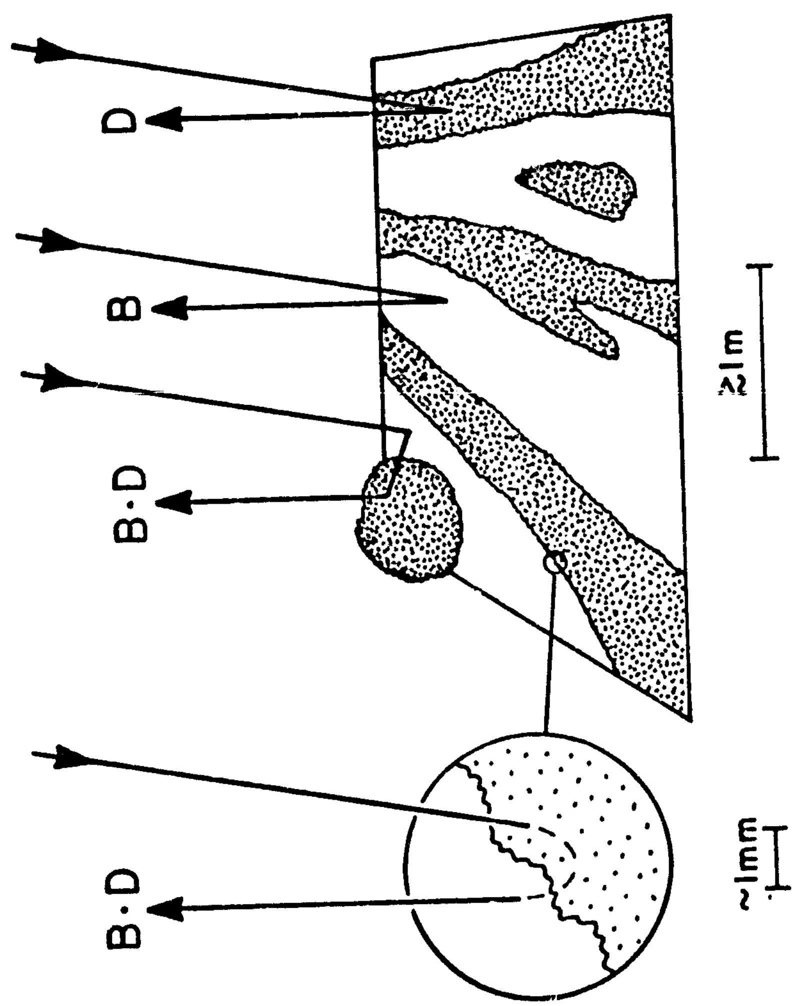


Figure 3

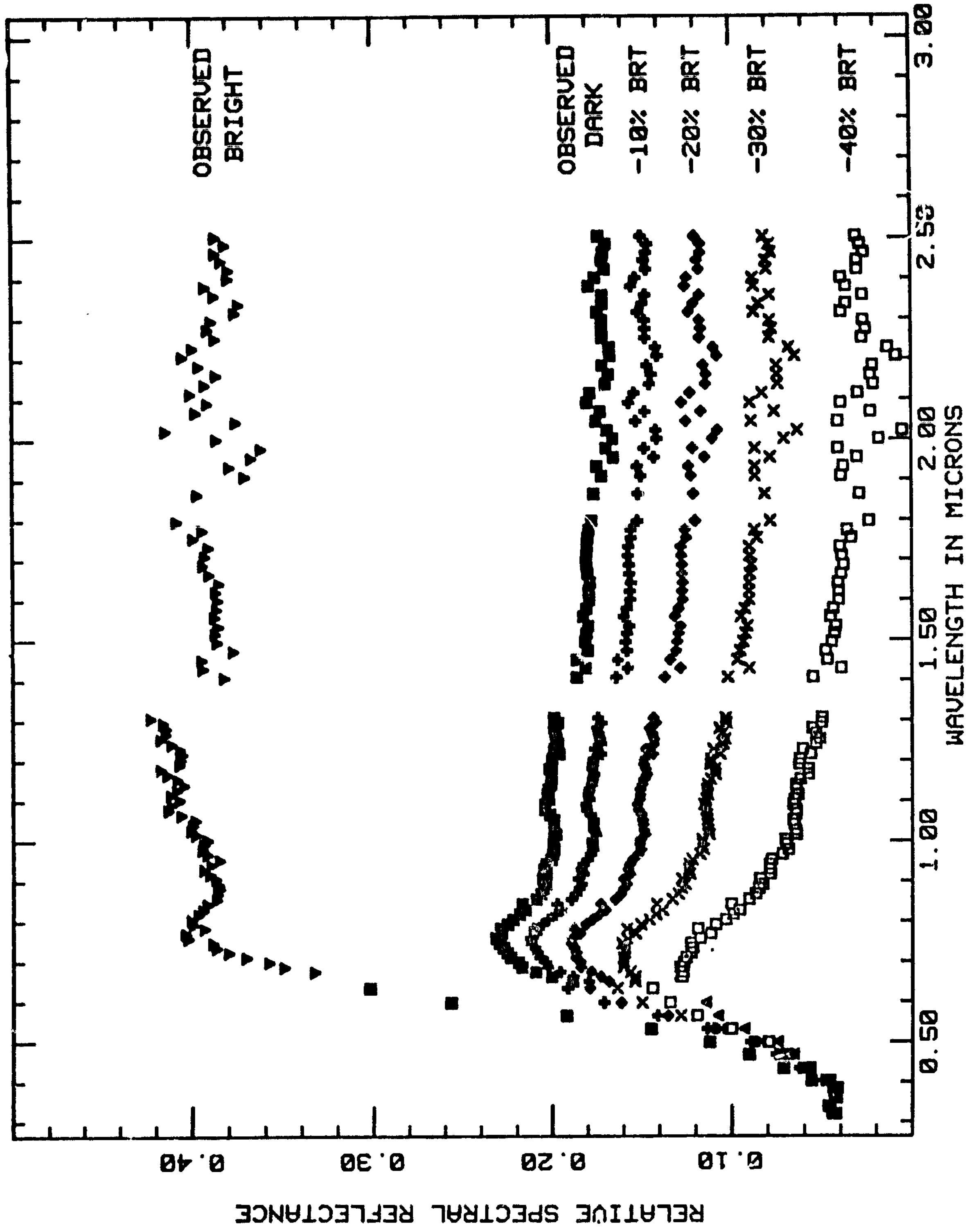
OBSERVED
BRIGHT
OBSERVED
DARK
-10% BRT
-20% BRT
-30% BRT
-40% BRT
0.50
1.00
1.50
2.00
2.50
3.00
WAVELENGTH IN MICRONS
0.10
0.20
0.30
0.40
RELATIVE SPECTRAL REFLECTANCE

Figure 4

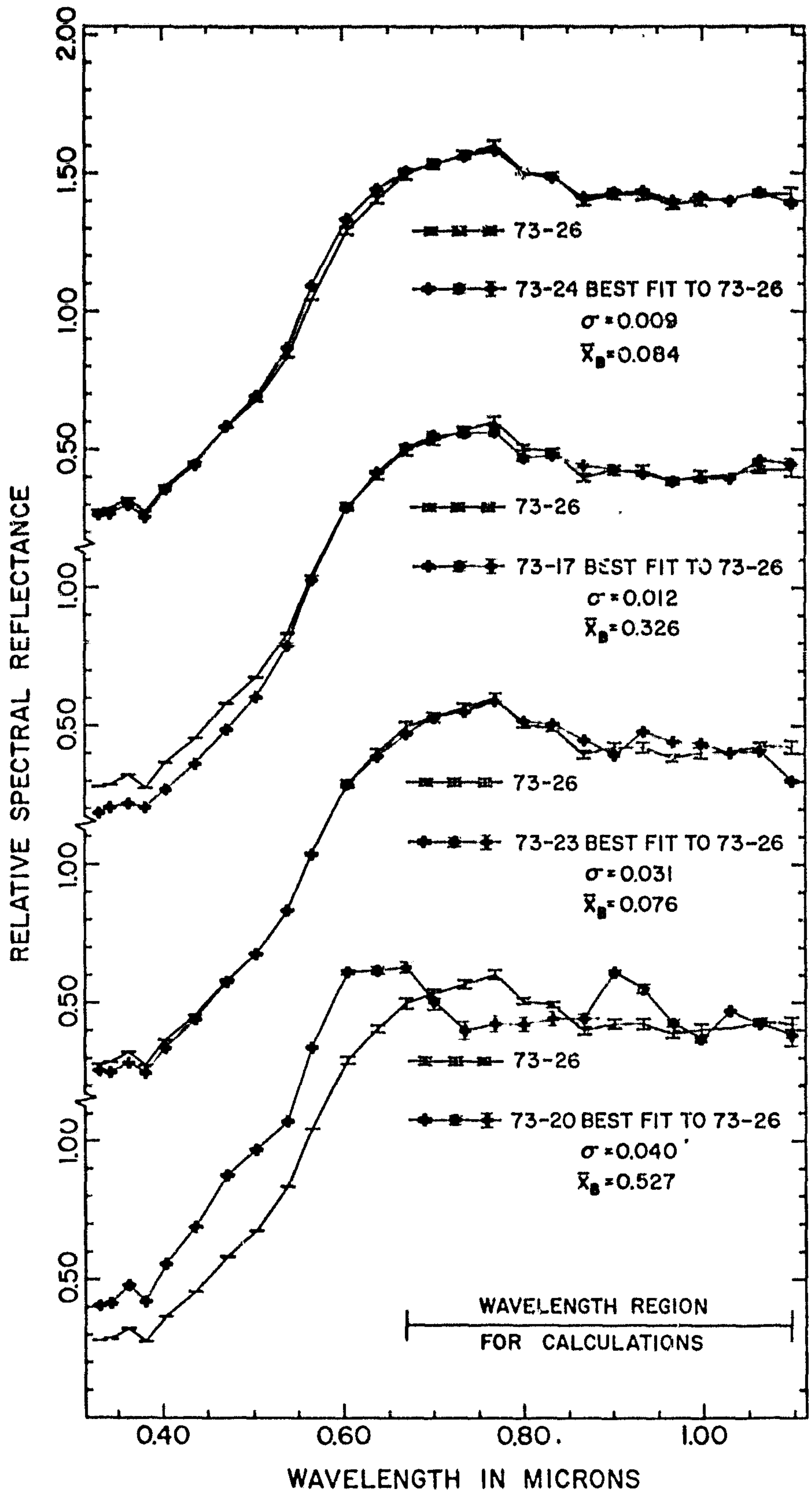
2.00
1.50
1.00
0.50
1.00
0.50
1.00
0.50
1.00
0.50
RELATIVE SPECTRAL REFLECTANCE
73-26
73-24 BEST FIT TO 73-26
σ = 0.009
X̄B = 0.084
73-26
73-17 BEST FIT TO 73-26
σ = 0.012
X̄B = 0.326
73-26
73-23 BEST FIT TO 73-26
σ = 0.031
X̄B = 0.076
73-26
73-20 BEST FIT TO 73-26
σ = 0.040
X̄B = 0.527
WAVELENGTH REGION
FOR CALCULATIONS
0.40
0.60
0.80
1.00
WAVELENGTH IN MICRONS

Figure 5

# CHAPTER IV

## Near-Infrared Spectral Reflectance of Mineral Mixtures: Systematic Combinations of Pyroxenes, Olivine, and Iron Oxides

This paper has been submitted to J.Geophys.Res., 1980.

Author: R.B. Singer.

## ABSTRACT

Near-infrared spectral reflectance has been measured for two-component mixtures of ferro-magnesian and iron-oxide minerals at ambient temperatures. Results are presented for systematic variations in weight percent of each component. Minerals and combinations were chosen for application to the study of the dark materials on Mars but the results are equally useful for interpretating spectral reflectance of potentially oxidized mafic and ultramafic assemblages elsewhere in the solar system, including on Earth. Olivine spectral features are greatly reduced in intensity by admixture of other phases but remain recognizable on a subtle level, even for low olivine contents. Clinopyroxene and orthopyroxene mixtures show spectrally resolved "2-μm" pyroxene absorptions but unresolved composite absorptions near 1 μm. The addition of limonite greatly modifies pyroxene and olivine reflectance but does not fully eliminate distinctive spectral characteristics. Orthopyroxene and limonite (goethite) spectral signatures in a mixture can be difficult to differentiate in the 1-μm region and additional evidence is desirable for a unique interpretation. All composite mineral absorptions observed in this study are either weaker than or intermediate in strength to the endmember absorptions, and have

bandwidths greater than or equal to those for the endmembers.

# INTRODUCTION

Analysis of near-infrared absorptions in reflectance spectra is a powerful tool for remote mineralogic determination (e.g. Adams, 1975; McCord et al., 1980b). Much laboratory work has been performed to understand the spectral behavior of minerals and rocks and to calibrate systematic changes in spectral reflectance with compositional variation (Burns, 1970; Burns et al., 1972; Hunt and Salisbury, 1970a, 1971; Hunt et al., 1971, 1973a, b, 1974a, b; Adams, 1974, 1975; McCord et al., 1980b). Fewer studies have been performed to investigate the ways in which individual components combine spectrally to produce rock and soil reflectance characteristics. As discussed by McCord et al. (1980b) intimate mixtures of several mineral components produce a reflectance spectrum that is considerably more complicated than a simple additive combination of individual spectral characteristics. Laboratory studies of combinations of ferric oxides and basalts were conducted by Adams and McCord (1969) to help interpret reflectance spectra of Mars. Investigations of lunar analog mixtures (pyroxene, plagioclase, and an opaque) have been published by Pieters (1973) and Nash and Conel (1974). Examples of laboratory mineral combinations involving two pyroxenes and a pyroxene and olivine have been presented by Adams

(1974, 1975). Some discussion of qualitative and quantitative analysis of spectra for mineral mixtures is also provided by Adams (1974, 1975), Gaffey (1976), and Gaffey and McFadden (1977).

The use of reflectance spectroscopy for remote compositional analysis of Mars, Earth, the moon, and asteroids has reached a level of data quality and sophistication of technique which requires additional knowledge of the ways in which mineral spectral signatures combine. For non-lunar-like objects there is the additional complication of possible $Fe_3O_3$ content, a major consideration for Mars and Earth. The laboratory studies presented here were specifically designed to aid interpretation of reflectance spectra for dark regions of Mars. These results are nevertheless generally applicable to remote sensing of potentially oxidized mafic and ultramafic assemblages elsewhere in the solar system, including on Earth. Application of these results to spectral interpretation of the dark regions on Mars can be found in a separate publication (Singer, 1980b).

# PROCEDURE

## Instrumentation

Laboratory data were obtained with the Hawaii Institute of Geophysics/Planetary Sciences spectrogoniometer, largely designed and assembled by the author. This device can be used for bidirectional reflectance measurements of virtually any material with independently adjustable incidence and emission geometry (±85° from normal). Samples are oriented horizontally and a wide variety of sample holders, including environment chambers, may be used. All optics are reflecting and arranged to minimize instrumental polarization. The collimated light source consists of an f/8 off-axis parabolic mirror illuminated by a 250W, 3400K quartz-halogen bulb in an integrating enclosure. The aperture of this bulb enclosure is located at the focal point of the mirror and may be varied in diameter to produce collimations of 1.75° to about 0.25°. The integrating enclosure, coated with a diffuse white reflector, dramatically increases the useful flux and provides excellent uniformity of illumination across the 5 cm diameter maximum sample size.

A variety of instruments may be mounted, two at a time, for use at the focal plane (photometers or multispectral imaging devices). This allows use of state-of-the-art astronomical instrumentation, providing high sensitivity and a direct means of comparison to telescopic observations. Field of view, and therefore size of the spot measured on the sample, is selected by choice of aperture in each instrument. The optical path may be switched rather quickly between the two mounted instruments to provide increased spectral range or any other combination of near-simultaneous observations.

The laboratory reflectance data presented in this paper were obtained with the instrument and under the observing conditions described below. Near-infrared coverage (0.7 and 2.6 μm) was provided by a cooled circularly variable filter (CVF) spectrometer with an InSb detector, all operating at liquid nitrogen temperature (77K). This is the same instrument used telescopically for Mars observations in 1978 (McCord et al., 1980a), with a resolution ($\frac{\Delta\lambda}{\lambda}$) of about 1.5%. An earlier version of this instrument, using an uncooled CVF, is described in detail by McCord et al. (1978). All laboratory measurements were made with an incidence angle (I) of 10° and an emission or viewing angle (E) of 0° (measured from normal), giving a phase angle (α) of 10°. Collimation of the light source was 1.7°, and the viewed beam was collimated to 1.1°. Light was measured from a spot on each sample about 6mm diameter.

Reproducibility of laboratory data has proved to be excellent: routinely a fraction of one percent at each spectral channel for the Halon standard over a period of many hours. Each spectrum consists of a number of separate observations of the sample which are averaged to improve signal-to-noise and then divided by an average of reflectance standard observations taken near-contemporaneously. All data processing is carried out in digital form using an interactive computer system (Clark, 1980) and formal errors are calculated for each operation. Data are presented here with ±1 standard deviation of the mean error bars.

Reflectance standard

Halon powder was used as a diffuse reflectance standard, gently packed with a roughened tool to a density of 0.8 gm/cc in a cavity 1.5cm deep and 3.0cm in diameter. Manufactured by Allied Chemical Corporation, Halon consists of 50-micrometer sized beads of fluorocarbon plastic which, in thicknesses greater than 0.6cm, has an absolute reflectance $\geq$0.99 from the near-UV to 1.2 μm and $\geq$0.98 from 1.2 μm to 2.0 μm. At wavelengths between 2.0 and 2.5 μm there is more variation in the absolute reflectance, although at all wavelengths it is greater than 0.96. Halon was chosen over MgO as a standard because a) Halon has a greater reflectance than MgO over this spectral range, b) Halon is easier to handle and prepare, giving more reproducible results, and c) Halon does not absorb water or suffer UV radiation damage, as does MgO. Documentation of the reflectance properties of Halon were obtained from Venable *et al*. (1976).

Because of the potential mineralogical significance of subtle features in the 2 μm region, laboratory spectra presented here were corrected for the slightly imperfect reflectance of Halon. The correction was developed from the absolute reflectance measured for compacted Halon by the National Bureau of Standards (Venable *et al*., 1976). The final results are felt to be within a few percent of absolute bidirectional reflectance.

## Sample preparation

Individual samples were chosen to represent characteristic spectral properties of mineral classes prominent in mafic to ultramafic assemblages. Crystalline samples were examined for obvious impurities, crushed with a hardened steel mortar and pestle, and then ground further with an alumina mortar and pestle. Particle size fractions were obtained by wet sieving with methanol. Relative proportions in mixtures represent weight percent. After thorough physical mixing in a vial samples and mixtures were poured into cylindrical cavities in horizontally oriented sample holders and gently tapped to produce a level surface. No other form of compaction or surface preparation was employed. Particle size was not used as a variable in these studies.

## SAMPLE DESCRIPTIONS

### Olivine OLV01, 45-90 micrometer grain size

This sample was prepared from unaltered transparent green crystals sorted from green beach sand found near South Point on the island of Hawaii. This olivine has a chemical composition of $Fo_{85}$; a full chemical analysis is given in Table 1. In reflectance this specimen demonstrates well the olivine three-component $Fe^{2+}$ crystal field absorption centered just longward of 1 μm (Figure 1). The weaker side bands appear as shoulders on the strong central absorption. Individual band components, in order of decreasing strength, are centered at 1.06 μm, 1.33 μm, and 0.86 μm (determined by non-linear least-square fitting of three gaussian bands). Assignments of these components to specific crystallographic sites and electronic transitions is provided by Burns (1970). With increasingly fayalitic composition all three absorptions shift to slightly longer wavelengths and increase in depth, with a larger proportional increase of the shoulders (Burns, 1970; Hunt and Salisbury, 1970a; Adams, 1975). The net effect is a broadening of the total absorption envelope, especially on the long-wavelength side (due to enhancement of the 1.3-μm band).

Orthopyroxene PYX02, 45-90 micrometer grain size

This sample is from a massive rock labeled "enstatite" from Bamble, Norway (Wards's Natural Science Establishment). There is a small amount of white fibrous contaminant, suspected to be anthophyllite or chrysotile. Chemical analysis (Table 1) shows this sample to be a hypersthene, $En_{86}$. The spectrum shown in Figure 1 demonstrates two major bands centered at about 0.92 and 1.87 μm, characteristic of a hypersthene (Adams, 1974). These are crystal-field absorptions caused by $Fe^{2+}$ in a preferentially occupied rather distorted octahedral site (Burns, 1970). With increasing iron content both absorptions move to slightly longer center wavelengths (Burns, 1970; Adams, 1974, 1975).

The narrow, weak absorptions seen for PYX02 near 1.4 and 2.3 μm are respectively vibrational overtone and combination bands of OH in the incompletely removed hydroxylated contaminant (Hunt and Salisbury, 1970a).

Clinopyroxene PYX07, 45-90 micrometer grain size

This sample was separated from a granular peridotite found as the core of a volcanic bomb on the upper slopes of Mauna Kea. Chemical analysis (Table 1) shows this mineral to be a diopside or diopsidic augite ($Wo_{41}En_{51}Fs_{8}$) with some aluminum, titanium, and ferric iron. The spectrum shown in Figure 1 displays two prominent $Fe^{2+}$ crystal field absorptions, at about

1.03 and 2.31 μm. These band center positions and the general shape of the spectrum yield an estimate of composition very close to that calculated from the chemical analysis (Adams, 1974, 1975). Clinopyroxenes have cation sites analogous to orthopyroxenes, but $Ca^{2+}$ preferentially fills the more distorted M2 sites, increasing the occupancy of the somewhat less distorted M1 sites by $Fe^{2+}$. These changes and the modified crystal structure account for the occurrence of clinopyroxene absorptions at longer wavelengths than for orthopyroxene, and cause a different dependence of band location on composition (Burns et al., 1972; Adams, 1975). For this sample the band near 2 μm is shallower compared to the 1-μm band than for the orthopyroxene PYX02. This appears to be a characteristic of clinopyroxenes in general (M. Gaffey, personal communication, 1979; Adams, 1975). The downturn from 0.85 to 0.66 might represent an absorption caused by a small amount of $Cr^{3+}$ (∿1% $Cr_2O_3$) located in M1 sites (Adams, 1975). The break in spectral slope at 1.2 μm and the near linearity from there to 1.55 μm probably indicates that a small amount of olivine was included with the hand-picked pyroxene grains. This will be discussed further in the next section.

Limonite FOX02, very fine powder

This sample is a very fine-grained brownish-yellow limonite, variety yellow ocher, from Cartersville, Georgia (Ward's Natural Science Establishment). Particle size is much smaller than a 38 micrometer sieve. Limonite is a loosely used term for hydrated ferric oxides showing no obvious evidence of crystallinity. Most materials identified as limonite are actually very fine-grained goethite, $FeO \cdot OH$, frequently containing additional water and silicate impurities. The term yellow ocher implies fine clay as a contaminant (Hurlbut, 1959), which is consistent with the chemical analysis (Table 1). The spectrum of this sample in the visible and near-infrared is described elsewhere in detail (Singer, 1980a). Of interest here is the asymmetric absorption centered near 0.9 μm, shown in Figure 1. This band is caused by an $Fe^{3+}$ interelectronic transition forbidden by ionic crystal-field theory. As explained by Huguenin (1975; McCord et al., 1980b) however, ferric oxides are not strictly ionic because of the intense $O^{2-}$-$Fe^{3+}$ charge transfers which show strong absorption centered in the near-UV. The asymmetry of the 0.9-μm band is also attributed to its location on the wing of the charge transfer absorptions. Less hyrdroxylated ferric oxides have an analogous band centered at wavelengths as short as 0.85 μm (Huguenin et al., 1977; McCord et al., 1980b).

Magnetite MAG01, <45 micrometer grain size

This sample was ground from a massive block of magnetite from Marmora, Ontario (Ward's Natural Science Establishment). The chemical analysis is given in Table 1, and the spectrum is shown at the bottom of Figure 1. The magnetite was prepared to a finer grain size than the ferrosilicate samples because that is the usual situation for opaques in terrestrial basalts, meteorites, and lunar basalts. The reflectance is quite low with a very shallow, broad absorption centered near 1 μm and a slight positive slope overall. The continuum optical absorption of magnetite is due to high rate $Fe^{2+}$-$Fe^{3+}$ charge transfers as is discussed in detail by Huguenin (1973).

## RESULTS AND DISCUSSION

### Two-component mixtures of pyroxenes and olivine

1) Olivine and clinopyroxene, Figure 2.

The maximum band depth or contrast in the spectral reflectance of powders occurs when the grain size is about one optical depth (Adams and Filice, 1967; McCord et al., 1980b). Here the more opaque clinopyroxene is closer to that condition that is the olivine, and therefore the spectra of mixtures are dominated by pyroxene characteristics. Because the 1-μm band minima for these two minerals are close there is little change in the locations of the mixture band minima (Figure 5a). The shape and width of the total absorption envelope, however, change dramatically as the olivine side bands are masked by increasing pyroxene content. With pyroxene contents of 50% or greater the curve looks similar to that of pure pyroxene. The location of the pyroxene reflectance minimum at 2.3 μm remains unaltered by even large amounts of olivine.

Observation of more subtle changes can identify the presence of olivine in rather small amounts. Adams (1974) suggested that the shift caused by olivine in the apparent position of the pyroxene 1-μm band, in conjunction with the unchanged 2-μm band location, will cause the spectrum of a mixture to deviate from the well defined 1-μm vs. 2-μm band plot for pure pyroxenes. This method is not effective for calcic clinopyroxenes, such as the one used in this study, which have band center locations close to those for olivines. A very diagnostic feature for olivine is the persistent visibility of the 1.3-μm band even for small quantities of the mineral. This appears as a depression or shoulder on the pyroxene spectrum between about 1.15 and 1.55 μm. The spectra of olivine, clinopyroxene, and the 50-50 mixture are shown overlaid in Figure 3. The spectrum of the mixture agrees very closely with that of the clinopyroxene at wavelengths shorter than about 1.1 μm, and fairly closely at wavelengths greater than about 1.5 μm. In the middle region, however, centered on 1.3 μm, the mixture is spectrally much more similar to olivine. Another diagnostic characteristic is that increased olivine content raises the reflectance of the mixture for wavelengths longer than about 1.5 μm. This makes the 2-μm band appear weaker and gives a line connecting the pyroxene band minima an increased positive slope (Figure 5b). Because many variables can affect spectrum slope this is not by itself an unambiguous indication of olivine content. It is useful, however, in conjunction with other indications. As an example plagioclase mixed with pyroxene gives rise to a shoulder centered near 1.25 μm which might be mistaken for olivine. Plagioclase, however, does not affect the overall slope of the mixture spectrum and leaves the pyroxene bands with more nearly equal depths (c.f. Adams (1974), Figure 11, examples 2 and 3).

From the last two criteria it appears that this clinopyroxene sample is itself contaminated by a small amount of olivine, indicated primarily by the break in slope at 1.2 μm and the flatness of the spectrum from there to 1.5 μm. It is estimated that at most a few percent olivine could have passed the separation procedure, indicating the great persistence of the 1.3-μm absorption. Olivines with more fayalitic compositions have enhanced 1.3 μm absorption and are expected to be even more readily detectable.

2) Olivine and orthopyroxene, Figure 4.

This combination of minerals exhibits much of the same behavior described for olivine and clinopyroxene. A significant modification is caused by the difference in band minima positions for the olivine (1.06 μm) and the orthopyroxene (0.92 μm). As discussed by Adams (1974), the minimum for the composite band of a mixture such as these occurs at an intermediate wavelength. However, as shown in Figure 5a, the band minimum position for these mixtures is not a linear function of composition. Because the orthopyroxene has a more nearly optimum grain-size to optical-depth ratio it tends to dominate the mixture spectra. With quantities of olivine up to 50% the minimum of the 1-μm band occurs at virtually the same wavelength as for pure orthopyroxene, and the 1-μm and 2-μm band positions fall on the trend for pure pyroxenes (Adams, 1974). This band location criterion, then, does not appear to be a sensitive test for olivine content less than or equal to pyroxene content.

The shape of the orthopyroxene absorption near 1 μm is more radically altered by olivine than was the clinopyroxene. The center and 1.3-μm olivine absorptions broaden the long wavelength side of the orthopyroxene band, giving the composite band a marked asymmetry. As with clinopyroxene, the olivine 1.3-μm band causes a shoulder of reduced reflectance. With increasing olivine content the point of maximum reflectance between 1 and 2 μm shifts to longer wavelengths. This effect is more dramatic for the orthopyroxene than for the clinopyroxene because the clinopyroxene reflectance maximum occurs at a wavelength where olivine is not strongly absorbing. As with the clinopyroxene, increased olivine content with this orthopyroxene diminishes the depth of the 2-μm band with respect to the 1-μm band (Figure 5b). The trends for this orthopyroxene and clinopyroxene are very similar, with slightly lower slopes for the orthopyroxene over most of the mixing range.

3) Clinopyroxene and orthopyroxene, Figure 6.

Examination of Figure 6 shows that these samples have similar optical-depth to grain-size ratios, with the orthopyroxene being slighty dominant. The 1-μm absorptions are not resolved for these mixtures, but rather show broadening and asymmetry, particularly noticeable for 25% and 50% orthopyroxene content. The wavelengths of the minimum reflectance points for these bands vary non-linearly with composition between the two endmember positions. The 2-μm absorptions are resolved, shown most clearly in the same mixtures which best show asymmetry in the shorter wavelength band. Terrestrial basalts with two pyroxenes (such as an augite and a pigeonite) frequently display this double structure in the 2-μm region even if the band near 1 μm resembles that for a single pyroxene. Composite absorptions are either intermediate in strength to or less intense than absorptions for either individual component. In the multiple-pyroxene case (Figure 6) reduction of band contrast in the 2-μm region due to only partial absorption overlap causes an overall increase in spectral slope similar to that observed for olivine-pyroxene mixtures. The most generally applicable indication of two pyroxenes is a very broad, double structure in the region around 2 μm. The most useful indication of olivine content in a pyroxene bearing assemblage is a broadening of the long wavelength side of the 1-μm band and a shoulder or shallow depression centered near 1.3 μm.

Two-component mixtures of limonite with pyroxenes and olivine

This series of measurements was performed to investigate the ways in which ferric oxide masks or complicates $Fe^{2+}$ crystal-field absorptions in ferromagnesian minerals. The limonite sample used is very fine grained (typical of many natural ferric oxide occurrences) and tends to form a coating on the larger pyroxene and olivine grains. For this reason the limonite has a greater spectral effect in a mixture than might be expected from its weight percent, and a maximum of 50% limonite content was used for these measurements. Other aspects of the spectral effects of ferric-oxide coatings and mixtures, and spectra of limonite-magnetite mixtures, are discussed in detail by Singer (1980a).

1) Olivine and limonite, Figure 7.

As little as 5% limonite significantly alters the olivine spectrum but leaves the three-band structure near 1 μm recognizable. With 25% limonite the 0.9-μm $Fe^{3+}$ band in limonite and the central olivine band are of equal strength, producing a very flat-bottomed composite absorption which is quite distinct from that seen for pure limonite. There is also a clear depression around 1.3 μm caused by the long wavelength olivine band. With 50% limonite the spectrum shape looks very similar to that for pure limonite. Careful inspection shows a broadening and slight shift to longer wavelengths of the band near 0.9 μm, and a flattening of the characteristic ferric-oxide reflectance turnover which normally occurs near 1.25 μm. As seen in the previous section, a depression or shoulder near 1.3 μm is one of the most persistent indications of olivine in a mineral mixture. It is of major importance to remote sensing of Mars and Earth that weathering (oxidation) does not automatically negate our ability to spectrally identify ferromagnesian minerals in rocks and soils.

2) Clinopyroxene and limonite, Figure 8.

The most noticeable spectral effect of mixing 5% limonite with this clinopyroxene is an asymmetry of the 1-μm band caused by a slight broadening of the short wavelength side. Also, the band at 2.3 μm is somewhat reduced in depth. With 25% limonite content the band near 1 μm has become broader and very asymmetric, but is still dominated by the clinopyroxene component. The spectrum for a limonite content of 50% largely resembles that of pure limonite, except for the persistent broadening of the 1-μm band to longer wavelengths by the pyroxene absorption. The primary remaining evidence for the 2.3-μm pyroxene absorption is a slight convexity of the mixture spectrum, peaking at about 1.8 μm. The lack of this convex shape and the slightly lower reflectance around 1.3 μm are the only features which distinguish 50% olivine + 50% limonite from 50% clinopyroxene + 50% limonite.

3) Orthopyroxene and limonite, Figure 9.

This case is of particular interest because the minerals have band minima almost overlapping: 0.92 μm for the orthopyroxene and 0.90 μm for the limonite. Inspection of this figure shows that the pyroxene spectral character is very persistent, showing a quite recognizable 2-μm band even with 50% limonite. This is largely because the orthopyroxene, unlike the clinopyroxene, has both sides of this band fully occurring within this spectral region. For wavelengths shorter than about 1.3 μm there is a marked increase in spectral slope with increasing limonite content, caused by the wings of intense $O^{2-}$-$Fe^{3+}$ charge transfer absorptions which are centered in the near-UV (Huguenin, 1975; Huguenin et al., 1977).

The composite bands near 0.9 μm become shallower monotonically with increased limonite content, but this effect can be caused by other mechanisms as well (see next section). The most diagnostic difference between the 1-μm absorptions of these minerals is the difference in band symmetry. The vertical line drawn through the band minima in Figure 9 bisects the pyroxene absorption quite evenly. The limonite band, in contrast, has a broader, shallower absorption envelope on the long wavelength side of the minimum; this is not just a geometric effect of the band being superimposed on the wing of another absorption. The spectra for mixtures of these minerals vary regularly between the endmembers in degree of band symmetry.

The presence of a broad absorption near 2 μm and a matching absorption near 1 μm (in accordance with the band *vs*. band plot developed by Adams, 1974, 1975) is the most solid spectral determination of a pyroxene. If the absorption near 2 μm is somehow masked, or data is not available at those wavelengths, it becomes difficult to differentiate relative contributions to a band near 0.9 μm from orthopyroxene and ferric oxide. The occurrence of ferric oxide in an unknown assemblage is readily determined by spectral behavior in the visible (e.g. McCord *et al.*, 1980b). However, some ferric-oxide-bearing substances with strong visible absorptions have little or no absorption between 0.85 and 0.90 μm (Singer, 1980a). The source of an absorption near 0.89 - 0.92 μm observed for a ferric-oxide-bearing unknown is therefore not uniquely determined by only the location of the band minima. If data through the 2-μm region is not available or useful, the symmetry of the band in question might be the primary criterion for determining its source.

Two-component mixtures of olivine and magnetite

A series of mixtures of olivine and magnetite were observed spectrally (Figure 10) to determine the effects of an opaque mineral on $Fe^{2+}$ crystal-field absorptions. Olivine was chosen because it has a more complicated band structure than the pyroxenes; the general optical effects of mixture with an opaque phase are expected to be similar for many combinations of minerals. Magnetite is a common opaque accessory mineral in mafic and ultramafic assemblages, usually fine grained. Note that Figure 10 has a continuous reflectance scale and that no scaling or "stacking" has been performed to the data.

It is immediately apparent that a small amount of magnetite is very effective at reducing the reflectance and spectral contrast of the mixture. This is consistent with previous studies of opaque + non-opaque mineral assemblages (Johnson and Fanale, 1973; Pieters, 1973; Nash and Conel, 1974). Fifty percent magnetite content reduces the reflectance of the mixture to less than 0.1 but does not entirely eliminate the olivine absorptions. Figure 11 shows the data for this half-and-half mixture with a greatly expanded vertical scale overlaid on an unscaled spectrum of 100% olivine. Scaling of the mixture spectrum was performed to provide a good subjective fit at the band minimum and near 2.5 μm. The agreement between 0.8 and 1.1 μm is excellent. The well defined concavity caused by the 1.3 μm band and the fairly sharp change in slope observed near 1.7 μm for pure olivine are replaced by a more uniform rise in reflectance into the infrared, a characteristic of magnetite. The modified absorption envelope for the mixture is rather like a check mark; despite the reduction of absorption around 1.3 μm the shape and width are still distinct from that of a pyroxene band. While the spectra of these minerals definitely do not combine in a linear or additive manner, Figure 11 shows that some combination of multiplicative and additive scaling can be used to approximate the qualitative spectral effects around 1 μm of adding an opaque phase to olivine. Other ferromagnesian minerals such as pyroxenes are expected by analogy to show similar spectral variations when mixed with opaque minerals; the distinguishing characteristics are not likely to be altered beyond recognition, given adequate data quality (c.f. Pieters, 1973; Nash and Conel, 1974).

# SUMMARY OF CONCLUSIONS

## Olivine and pyroxenes

Because olivine tends to be more transparent than pyroxene, for a mixture of equal grain sizes the spectral contribution from olivine is disproportionately low. Large olivine contents (about 50% or greater) produce substantial distortion of the composite band near 1 μm from that for pure pyroxene. Certain indications of olivine content are distinctive and persistent though, even for smaller amounts of the mineral. These features are a shallow depression or shoulder centered near 1.3 μm and a reduction in depth of the pyroxene absorption near 2 μm, giving the overall spectrum a greater positive slope. The location of the pyroxene band near 2 μm remains virtually unchanged. The shift in wavelength of the composite band minimum near 1 μm is not an ideal indication of olivine because of the non-linearity of this effect with olivine content and the small difference in position for this feature between olivine and calcium-rich clinopyroxenes.

## Clinopyroxene and orthopyroxene

The pyroxenes used in this study have similar transparencies, with the orthopyroxene showing a slightly greater influence on the half-and-half mixture. The absorptions near 1 μm combine for mixtures to form a single, somewhat broadened, and in some cases asymmetric composite band with a minimum located at wavelengths intermediate between the endmembers. The absorptions near 2 μm have a larger wavelength spread as a function of composition and are resolved into two weaker absorptions for spectra of mixtures (this effect was also observed by Adams (1974)). The increase in overall spectrum slope caused by the reduced depth of the individual 2-μm absorptions in two-pyroxene mixtures is roughly similar to the effect caused by olivine, but can be distinguished by the presence of double band structure.

Limonite and ferromagnesian minerals

An important conclusion from this series of measurements is that characteristic olivine and pyroxene absorptions are suppressed but not eliminated when the minerals are mixed with up to 50% fine-grained ferric oxide. With 50% limonite the central olivine band is still apparent as a broadening of the long wavelength side of the 0.9 μm $Fe^{3+}$ absorption, and reflectance around 1.3 μm is noticeably lowered relative to pure limonite. The clinopyroxene causes a similar effect near 1 μm without the change in shape around 1.3 μm, and in addition retains a trace of the band near 2.3 μm. This band would be more recognizable if the long-wavelength side was defined by spectral observations further into the infrared. The orthopyroxene demonstrates a more persistent band near 2 μm when mixed with limonite but is more ambiguous near 0.9 μm because the two minerals have bands at nearly the same location. If the presence or absence of a 2-μm band is undetermined in observations of an unknown, then the symmetry of the 0.9-μm absorption could be the primary clue as to the responsible mineral(s).

## Olivine and magnetite

The addition of magnetite to olivine causes a drastic reduction in reflectance and spectral contrast compared to a pure olivine spectrum. The olivine characteristics are retained in a modified but recognizable form, however, even for a mixture with 50% magnetite. There is no change in band width or location. Other minerals such as pyroxenes are expected to behave in a similar fashion spectrally when mixed with opaque minerals (Pieters, 1973; Nash and Conel, 1974).

## General

Spectral properties of minerals in an intimate mixture combine in a non-additive, generally unique manner. Features demonstrate a regular but usually non-linear variation as a function of proportion of endmember phases. The locations of unresolved composite band centers fall between those for endmember spectra, while the spectral contrast of composite bands is either intermediate to or less than that for pure endmember absorptions. In no case was a composite band observed to have greater intensity or lesser bandwidth than the bands for either endmember phase.

This work covers only a small number of the possible combinations of different mineral compositions, relative abundances, and grain sizes. Additional studies are necessary to fully quantify the spectral properties of key mineral mixtures, so that those results can be applied to the near-infinite variety of naturally occurring assemblages. The results presented here nevertheless provide important new qualitative and to some extent quantitative information about the ways in which spectral properties combine for mixtures of geologically important minerals. This work has seen immediate application to the interpretation of spectrophotometry of Mars (Singer, 1980b) and is expected to be important for spectral studies of terrestrial basalts and asteroids in the near future.

## ACKNOWLEDGEMENTS

The author thanks M. Gaffey for providing the olivine and clinopyroxene samples, for helpful discussions, and for reviewing the manuscript. Careful reviews and suggestions were also provided by T. McCord, R. Burns, R. Huguenin, R. Clark, and L. McFadden. P. Owensby provided help with computer processing for figure preparation. Much of this research was conducted at the Institute for Astronomy, University of Hawaii. Funding was provided by NASA grants NSG 7312 and NSG 7590.

# REFERENCES

Adams, J.B., Visible and near infrared diffuse reflectance spectra of pyroxenes as applied to remote sensing of solid objects in the solar system, J. Geophys, Res. 79, 4329-4336, 1974.

Adams, J.B., Interpretation of visible and near-infrared diffuse reflectance spectra of pyroxenes and other rock forming minerals, in Infrared and Raman Spectroscopy of Lunar and Terrestrial Minerals, C. Karr, Jr., ed., Academic Press, 91-116, 1975.

Adams, J.B., and A.L. Filice, Spectral reflectance 0.4 to 2.0 microns of silicate rock powders, J. Geophys. Res. 72, 5705-5715, 1967.

Adams, J.B., and T.B. McCord, Mars: Interpretation of spectral reflectivity of light and dark regions, J. Geophys. Res. 74, 4851-4856, 1969.

Burns, R.G., Mineralogical applications of crystal-field theory, Cambridge University Press, London, 1970.

Burns, R.G., R.M. Abu-Eid, and F.E. Huggins, Crystal field spectra of lunar pyroxenes, Proc. Lunar Sci. Conf. 3rd 1, 533-543, 1972.

Clark, R.N., A large scale interactive one dimensional array processing system, Pub. Astron. Soc. Pacific, in press, 1980.

Gaffey, M.J., Spectral reflectance characteristics of the meteorite classes, J. Geophys. Res. 81, 905-920, 1976.

Gaffey, M.J., and L.A. McFadden, Quantitative plagioclase/pyroxene abundance from reflectance spectra: A calibration, (abstract) Bull. Am. Astron. Soc. 9, 530, 1977.

Huguenin, R.L., Photostimulated oxidation of magnetite. 1. Kinetics and alteration phase identification, J. Geophys. Res. 78, 8481-8493, 1973.

Huguenin, R.L., Crystal-field and charge-transfer band assignments in iron (III) oxides and oxyhydroxides: Application to Mars, (abstract) Bull. Am. Astron. Soc. 7, 370, 1975.

Huguenin, R.L., J.B. Adams, and T.B. McCord, Mars: Surface mineralogy from reflectance spectra, in Lunar Science VIII, 478-480, Lunar Science Institute, Houston, 1977.

Hunt, G.R., and J.W. Salisbury, Visible and near infrared spectra of minerals and rocks: I. Silicate minerals, Mod. Geol. 1, 283-300, 1970a.

Hunt, G.R., and J.W. Salisbury, Visible and near infrared spectra of minerals and rocks: II. Carbonates, Mod. Geol. 2, 23-30, 1971.

Hunt, G.R., J.W. Salisbury, and C.J. Lenhoff, Visible and near infrared spectra of minerals and rocks: III. Oxides and hydroxides, Mod. Geol. 2, 195-205, 1971.

Hunt, G.R., J.W. Salisbury, and C.J. Lenhoff, Visible and near infrared spectra of minerals and rocks: VI. Additional silicates, Mod. Geol. 4, 85-106, 1973a.

Hunt, G.R., J.W. Salisbury, and C.J. Lenhoff, Visible and near infrared spectra of minerals and rocks: VII. Acidic igeneous rocks, Mod. Geol. 4, 217-224, 1973b.

Hunt, G.R., J.W. Salisbury, and C.J. Lenhoff, Visible and near infrared spectra of minerals and rocks: VIII. Intermediate igneous rocks, Mod. Geol., 1974a.

Hunt, G.R., J.W. Salisbury, and C.J. Lenhoff, Visible and near infrared spectra of minerals and rocks: IX. Basic and ultrabasic igneous rocks, Mod. Geol., 1974b.

Johnson, T.V., and F.P. Fanale, Optical properties of carbonaceous chondrites and their relationship to asteroids, J. Geophys. Res. 78, 8507-8518, 1973.

McCord, T.B., J.B. Adams, and R.L. Huguenin, Reflection spectroscopy: A technique for remotely sensing planetary surface mineralogy, to be submitted to Space Sci. Rev., 1980b.

McCord, T.B., R.N. Clark, and R.L. Huguenin, Mars: Near-infrared spectral reflectance and compositional implications, J. Geophys. Res. 83, 5433-5441, 1978.

McCord, T.B., R.N. Clark, R.B. Singer, and R.L. Huguenin, Mars: Near infrared reflectance spectra of surface regions and compositional implication, to be submitted to J. Geophys. Res., 1980a. Thesis Ch. II

Nash, D.B., and J.E. Conel, Spectral reflectance systematics for mixtures of powdered hypersthene, labradorite, and ilmenite, J. Geophys. Res. 79, 1615-1621, 1974.

Pieters, C., Polarization in a mineral absorption band, in Planets, Stars and Nebulae Studied with Photopolarimetry, T. Gehrels, ed., 405-418, University of Arizona Press, Tucson, 1973.

Singer, R.B., The composition of the martian dark regions: I. Visible and near-infrared spectral reflectance of analog materials and interpretation of telescopically observed spectral shape, submitted to J. Geophys. Res., 1980a. Thesis Ch. V

Singer, R.B., The composition of the martian dark regions: II. Analysis of telescopically observed absorptions in near-infrared spectrophotometry, submitted to J. Geophys. Res., 1980b. Thesis Ch.VI

Venable, W.H., Jr., V.R. Weidner, J.J. Hsia, Information sheet on optical properties of pressed Halon coatings, National Bureau of Standards, Washington, DC. 20234, 1976.

TABLE I

Analysis of Mineral Samples Used in This Study[(1)]

| | Olivine OLV01 | Orthopyroxene PYX02 | Clinopyroxene PYX07 | Limonite FOX02 | Magnetite MAG01 |
|---|---|---|---|---|---|
| $SiO_2$ | 38.90 | 55.30 | 50.10 | 24.40 | 0.12 |
| $TiO_2$ | 0.03 | 0.05 | 0.66 | 0.33 | 0.00 |
| $Al_2O_3$ | 0.46 | 0.12 | 2.71 | 6.41 | 0.84 |
| $Fe_2O_3$ | (as FeO) | (as FeO) | 1.11 | 51.40 | 62.70 |
| FeO | 10.70 | 9.38 | 4.00 | 0.20 | 29.30 |
| MnO | 0.22 | 0.15 | 0.24 | 1.45 | 0.03 |
| MgO | 47.20 | 32.80 | 17.60 | 0.85 | 0.00 |
| CaO | 0.41 | 0.45 | 20.00 | 0.20 | 0.39 |
| $Na_2O$ | 0.00 | 0.00 | 0.19 | 0.00 | 0.00 |
| $K_2O$ | 0.02 | 0.02 | 0.00 | 1.64 | 0.03 |
| $P_2O_5$ | 0.02 | 0.01 | 0.01 | 0.53 | 0.03 |
| L.O.I.[(2)] | 0.77 | 2.00 | 0.69 | 8.92 | -2.77 |
| TOTAL | 98.73 | 100.28 | 97.33 | 96.33 | 90.67 |

[1] Analyses performed by XRA LAB., Ontario, Canada.
FeO by wet chemistry, other oxides by XRF.

[2] Lost on ignition (indicative of volatiles).

## FIGURE CAPTIONS

Figure 1: Bidirectional reflectance spectra of the five mineral samples used in this study. Samples and spectra are described in the text. The reflectance scale of this figure and most others in this paper is discontinuous ("stacked") to avoid overlap of curves. All spectra presented here were obtained with an illumination angle of 10° and an emission angle of 0° (normal). Error bars represent ±1 standard deviation of the mean.

Figure 2: Reflectance spectra of weight-percentage mixtures of olivine and clinopyroxene. Pyroxene dominates the mixture spectra but olivine remains apparent as a depression or shoulder centered near 1.3 μm.

Figure 3: Overlay of spectra for olivine, clinopyroxene, and a half-and-half mixture. The mixture spectrum is dominated by that of pure clinopyroxene except near 1.3 μm, where it more closely resembles the olivine spectrum.

Figure 4: Reflectance spectra of weight-percentage mixtures of olivine and orthopyroxene. As with clinopyroxene, orthopyroxene dominates the mixture spectra. The olivine causes broadening of the pyroxene 1-μm band and is

most persistent as a shoulder centered near 1.3 μm.

Figure 5: a) Plot of wavelength position of reflectance minimum near 1 μm for olivine-pyroxene mixtures. Note small magnitude of change for clinopyroxene series and non-linearity of change for both clinopyroxene and orthopyroxene.

b) Plot of slope between pyroxene band minima as a function of olivine content. The slope is calculated as the difference between 2-μm and 1-μm band minimum reflectances, divided by the wavelength separation between the band minima.

Figure 6: Reflectance spectra of weight-percentage mixtures of clinopyroxene and orthopyroxene. Note that the 2 μm bands are separated enough in wavelength to be resolved, while the 1 μm bands combine to form a single but sometimes asymmetric composite band.

Figure 7: Reflectance spectra of weight-percentage mixtures of olivine and limonite. Despite the strong masking effect of the ferric oxide the olivine spectral signature persists as a broadening of the long wavelength side of the 0.9-μm limonite band, and as a depression centered near 1.3 μm.

Figure 8: Reflectance spectra of weight-percentage mixtures of clinopyroxene and limonite. The clinopyroxene absorption persists strongly near 1 μm, either dominating the limonite 0.9 μm band or broadening it to longer wavelengths. The pyroxene band near 2.3 μm appears somewhat less pronounced, in part because the long wavelength side of this absorption occurs partially beyond the observed range.

Figure 9: Reflectance spectra of weight-percentage mixtures of orthopyroxene and limonite. The 2-μm pyroxene band persists as a very recognizable feature. Because of the near-coincidence of bands shortward of 1 μm for both samples there is little shift of center wavelength. With increased limonite content this composite band becomes broader on the longer wavelength side only and is increasingly superimposed on the steeply sloping ferric-oxide continuum.

Figure 10: Reflectance spectra of weight-percentage mixtures of olivine and magnetite. Note that the reflectance scale is continuous for this figure and somewhat exaggerated compared to other figures. Magnetite severely reduces overall reflectance and spectral contrast

but does not fully eliminate the characteristic olivine spectral shape in amounts up to at least 50%.

Figure 11: Reflectance spectrum of 50% olivine - 50% magnetite mixture, with greatly expanded reflectance scale, overlaid on normal olivine spectrum. In spite of drastic non-linear decrease in reflectance caused by magnetite the characteristic olivine absorption persists and is unambiguously identifiable.

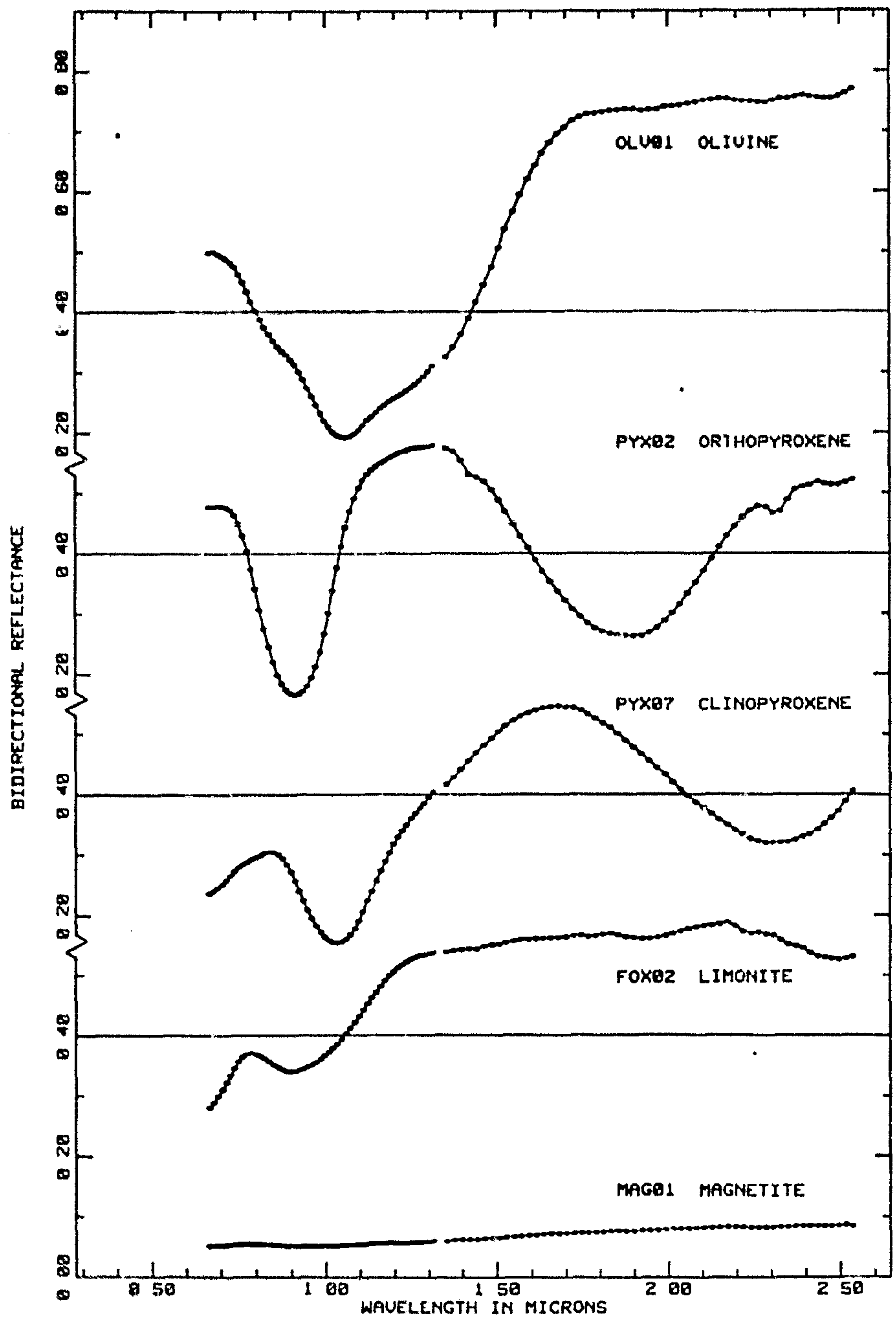
OLV01 OLIVINE
PYX02 ORTHOPYROXENE
PYX07 CLINOPYROXENE
FOX02 LIMONITE
MAG01 MAGNETITE
BIDIRECTIONAL REFLECTANCE
WAVELENGTH IN MICRONS
0 50
1 00
1 50
2 00
2 50
0 00
0 20
0 40
0 60
0 80

Figure 1

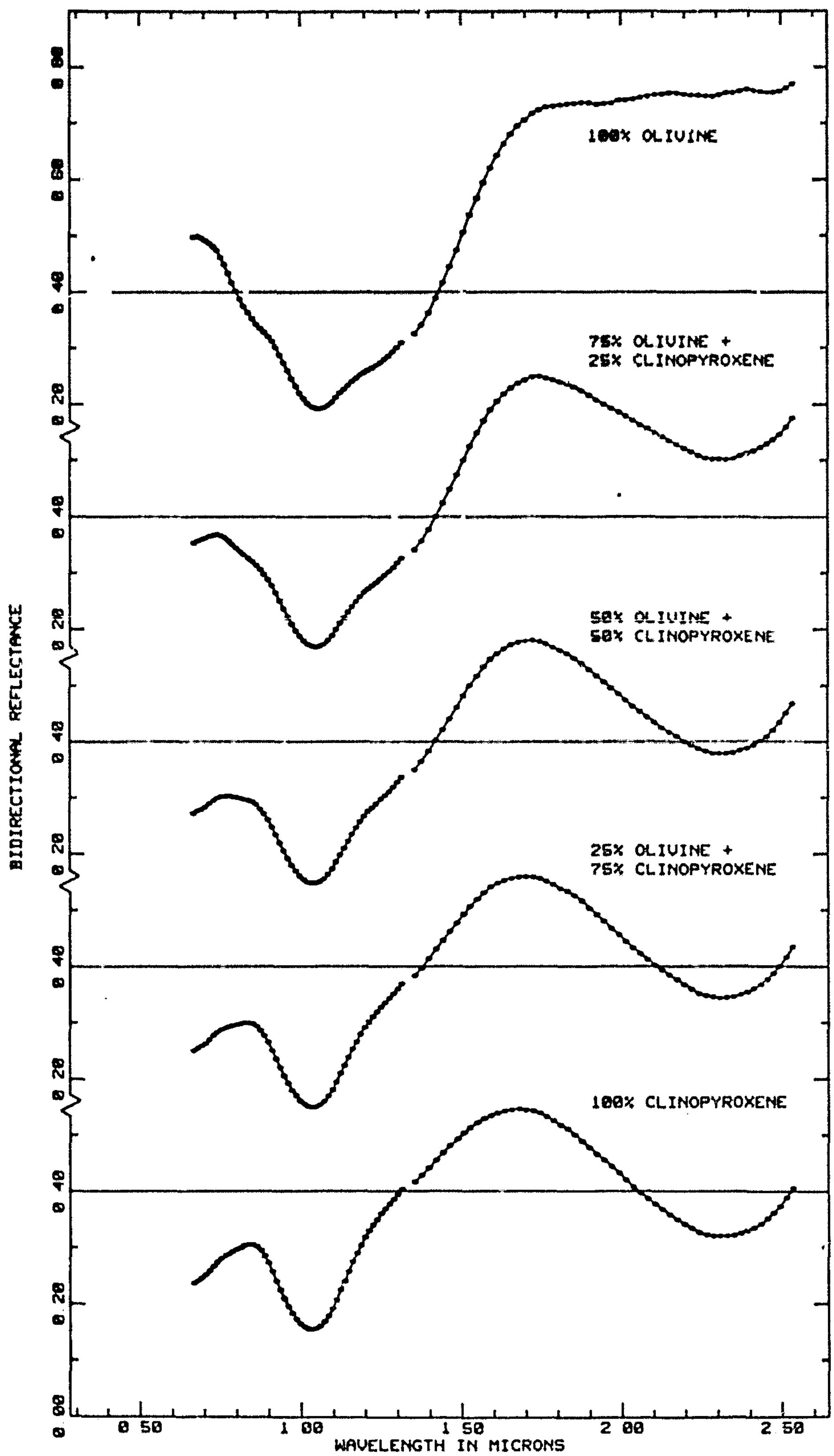
100% OLIVINE
75% OLIVINE +
25% CLINOPYROXENE
50% OLIVINE +
50% CLINOPYROXENE
25% OLIVINE +
75% CLINOPYROXENE
100% CLINOPYROXENE
BIDIRECTIONAL REFLECTANCE
WAVELENGTH IN MICRONS
0.50
1.00
1.50
2.00
2.50
0.00
0.20
0.40
0.60
0.80

Figure 2

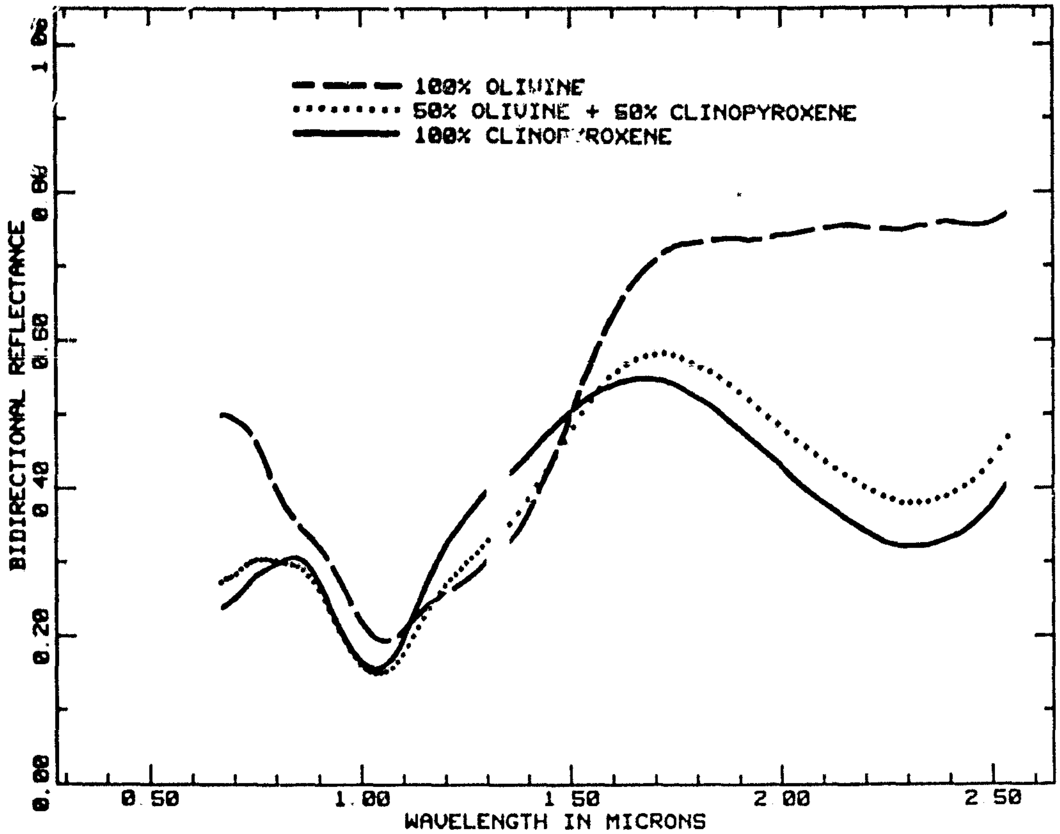

100% OLIVINE
50% OLIVINE + 50% CLINOPYROXENE
100% CLINOPYROXENE
BIDIRECTIONAL REFLECTANCE
0.00
0.20
0.40
0.60
0.80
1.00
0.50
1.00
1.50
2.00
2.50
WAVELENGTH IN MICRONS


Figure 3

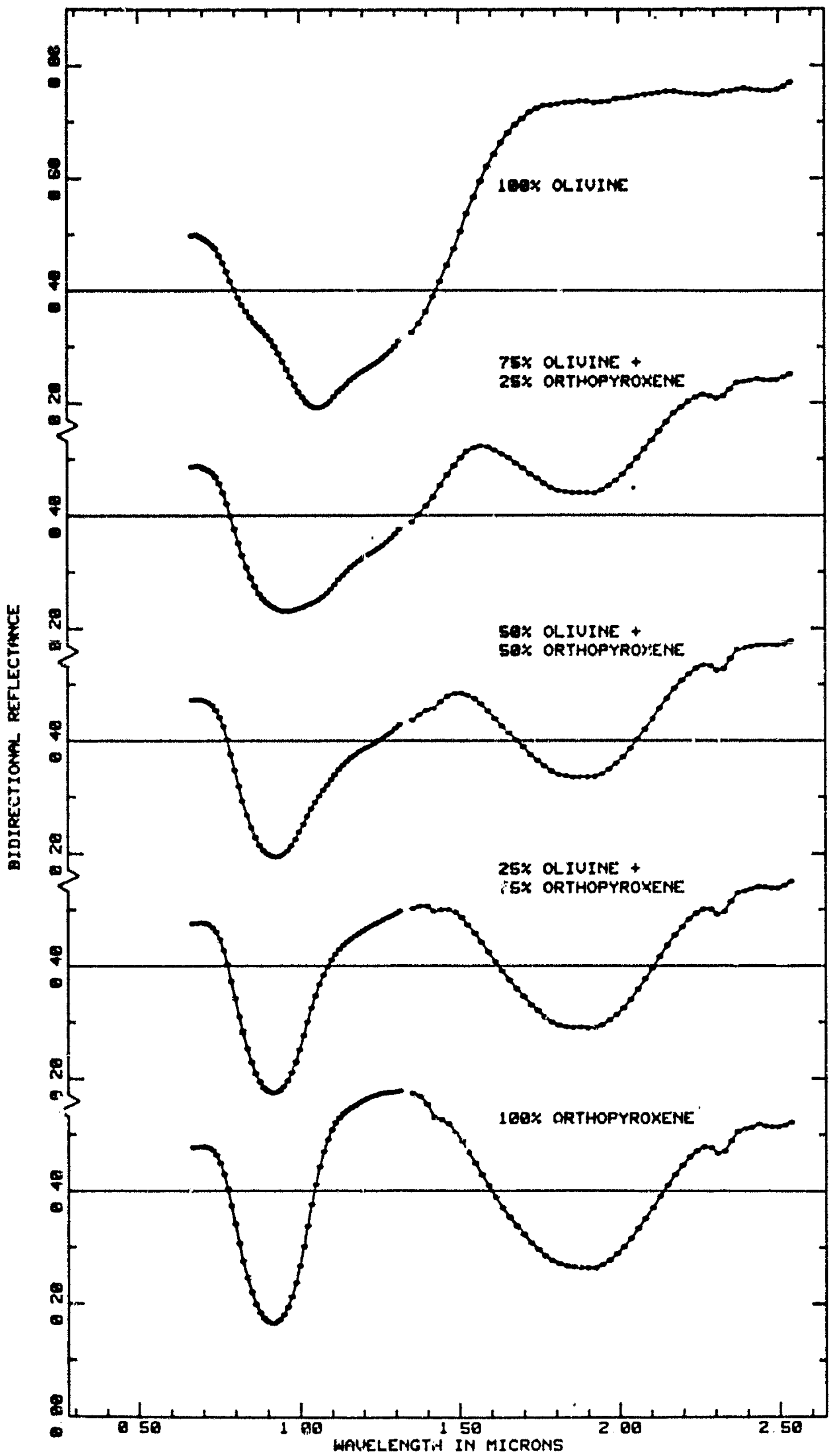
100% OLIVINE
75% OLIVINE +
25% ORTHOPYROXENE
50% OLIVINE +
50% ORTHOPYROXENE
25% OLIVINE +
75% ORTHOPYROXENE
100% ORTHOPYROXENE
BIDIRECTIONAL REFLECTANCE
WAVELENGTH IN MICRONS
0.50
1.00
1.50
2.00
2.50

Figure 4

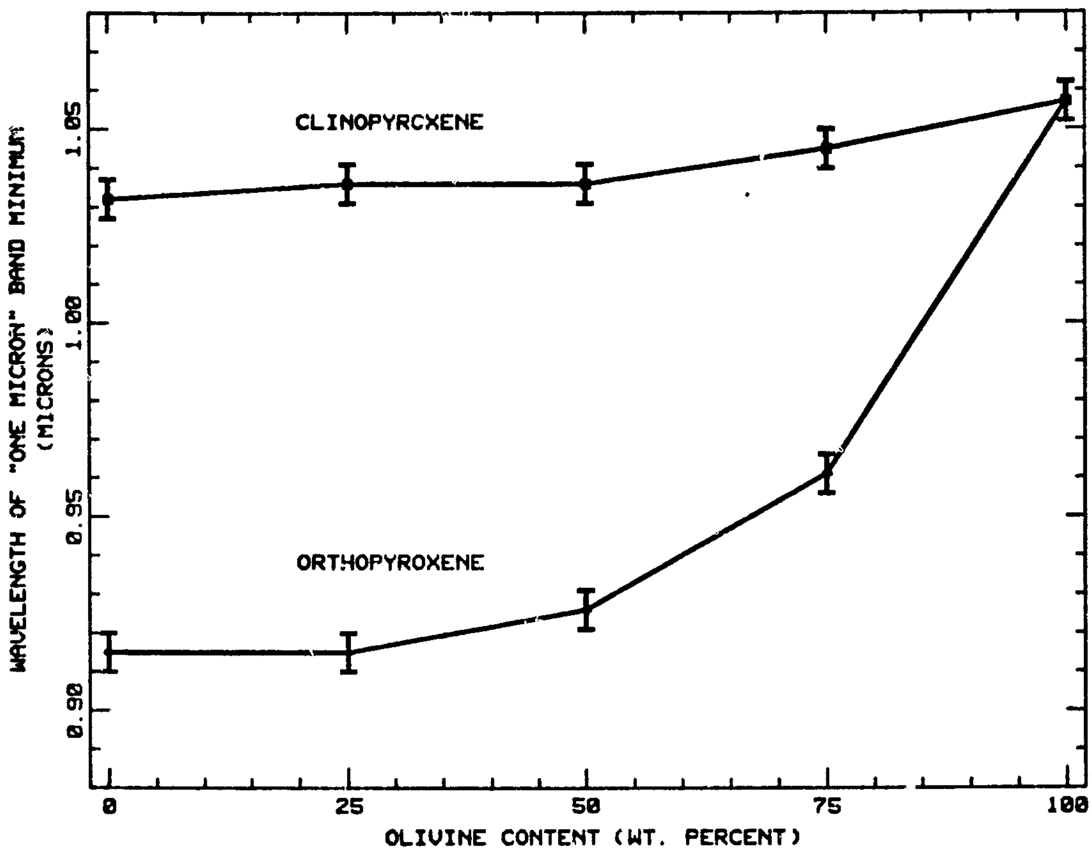
CLINOPYRCXENE
ORTHOPYROXENE
WAVELENGTH OF "ONE MICRON" BAND MINIMUM (MICRONS)
0.90
0.95
1.00
1.05
0
25
50
75
100
OLIVINE CONTENT (WT. PERCENT)

Figure 5a

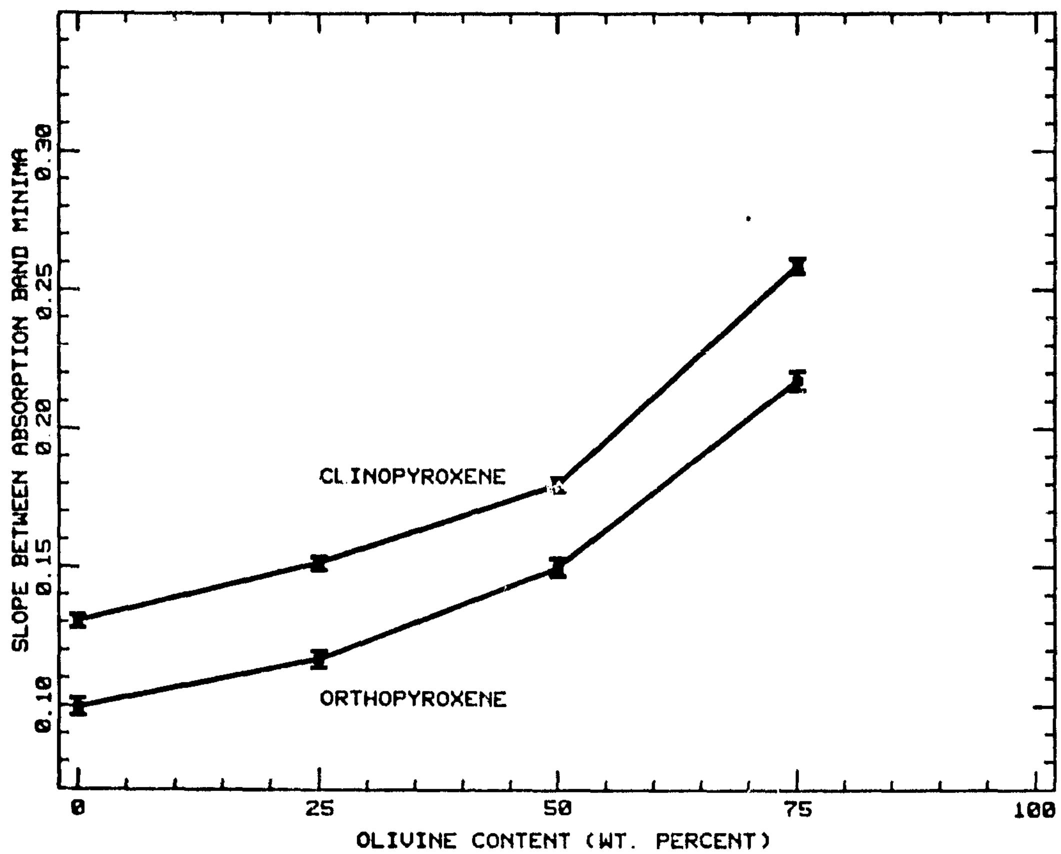
SLOPE BETWEEN ABSORPTION BAND MINIMA
0.10
0.15
0.20
0.25
0.30
CLINOPYROXENE
ORTHOPYROXENE
0
25
50
75
100
OLIVINE CONTENT (WT. PERCENT)

Figure 5b

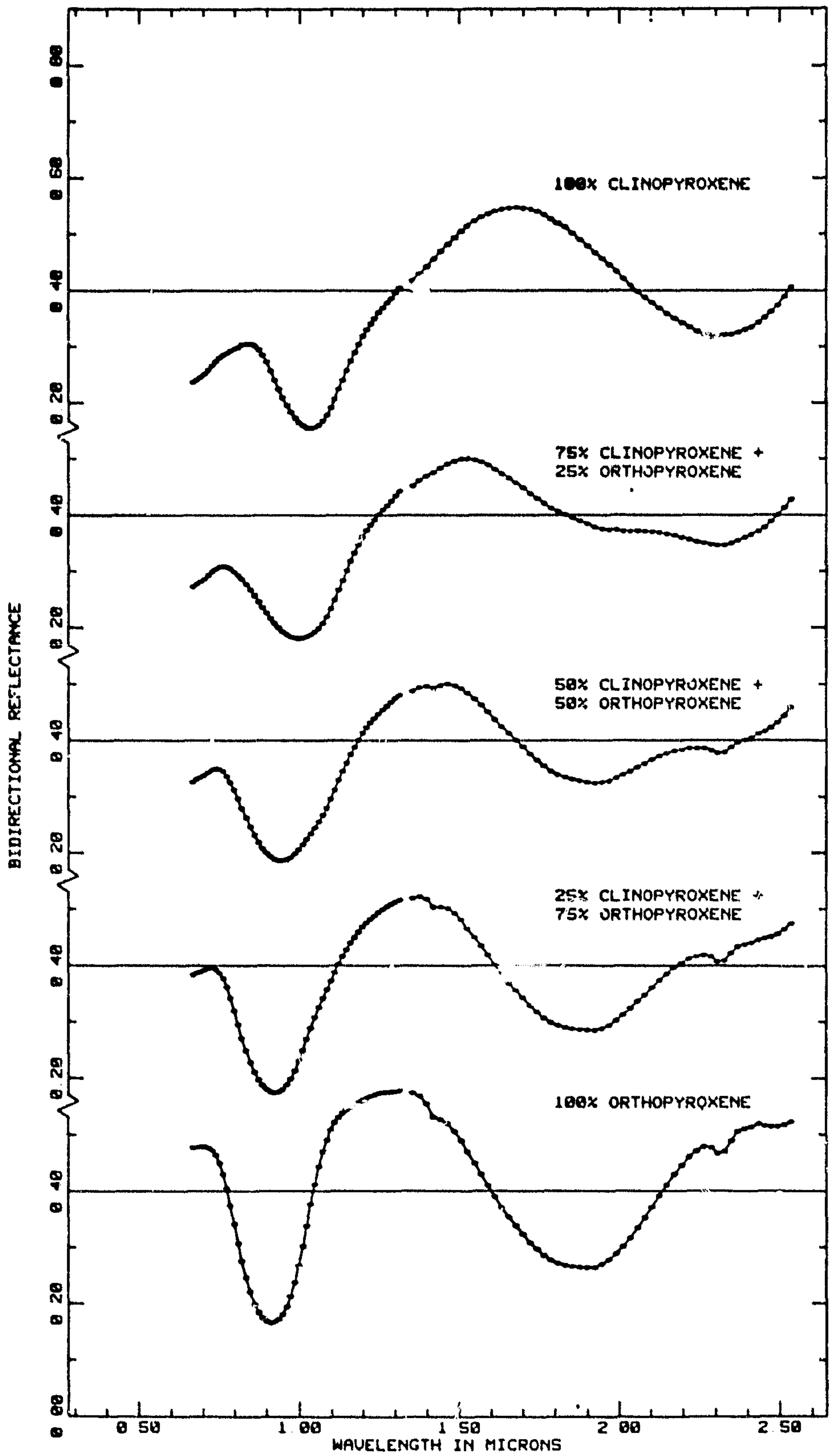
100% CLINOPYROXENE
75% CLINOPYROXENE +
25% ORTHOPYROXENE
50% CLINOPYROXENE +
50% ORTHOPYROXENE
25% CLINOPYROXENE +
75% ORTHOPYROXENE
100% ORTHOPYROXENE
BIDIRECTIONAL REFLECTANCE
0.80
0.60
0.40
0.20
0.00
0.50
1.00
1.50
2.00
2.50
WAVELENGTH IN MICRONS

Figure 6

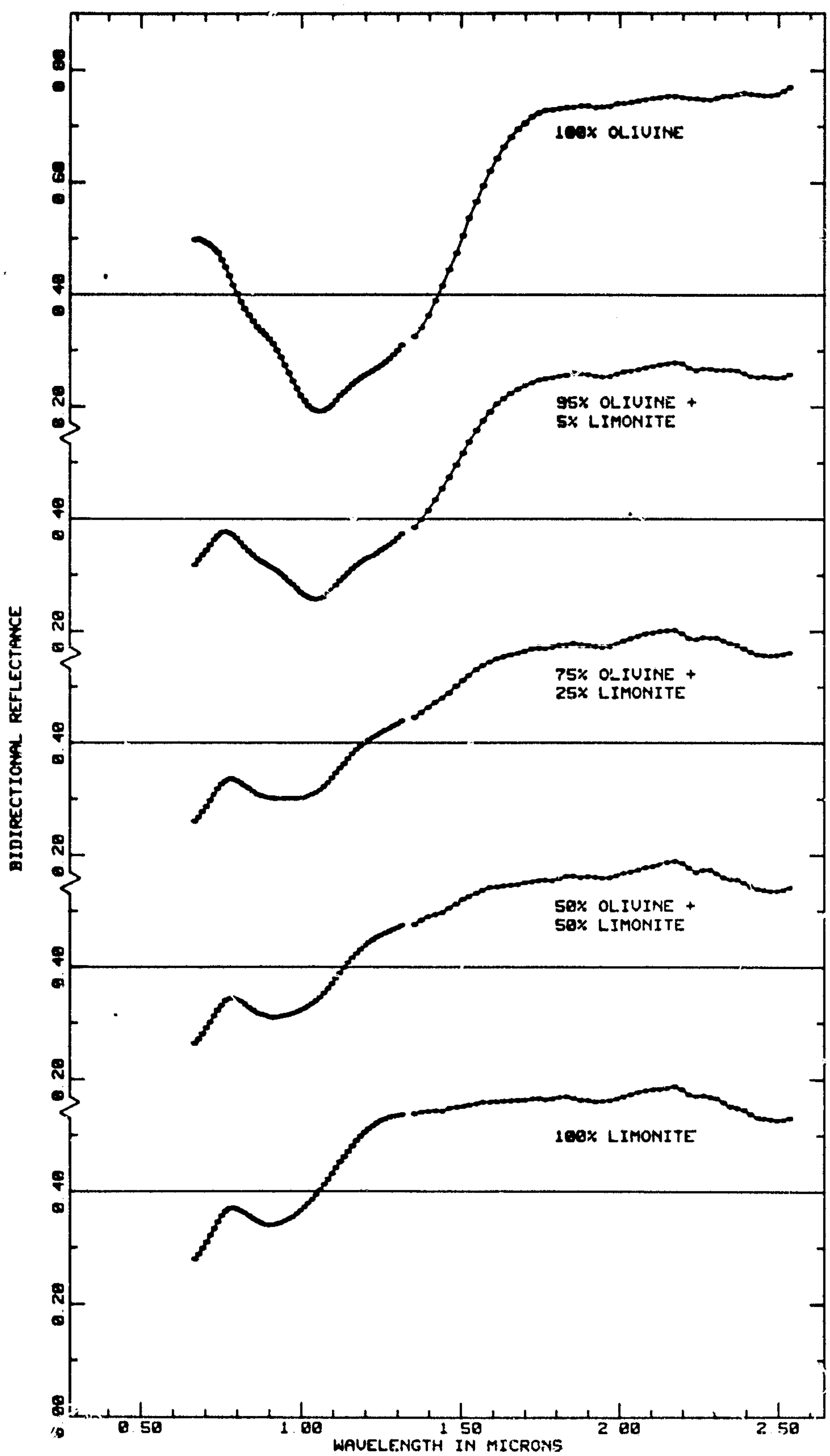
100% OLIVINE
95% OLIVINE +
5% LIMONITE
75% OLIVINE +
25% LIMONITE
50% OLIVINE +
50% LIMONITE
100% LIMONITE
BIDIRECTIONAL REFLECTANCE
WAVELENGTH IN MICRONS
0.50
1.00
1.50
2.00
2.50

Figure 7

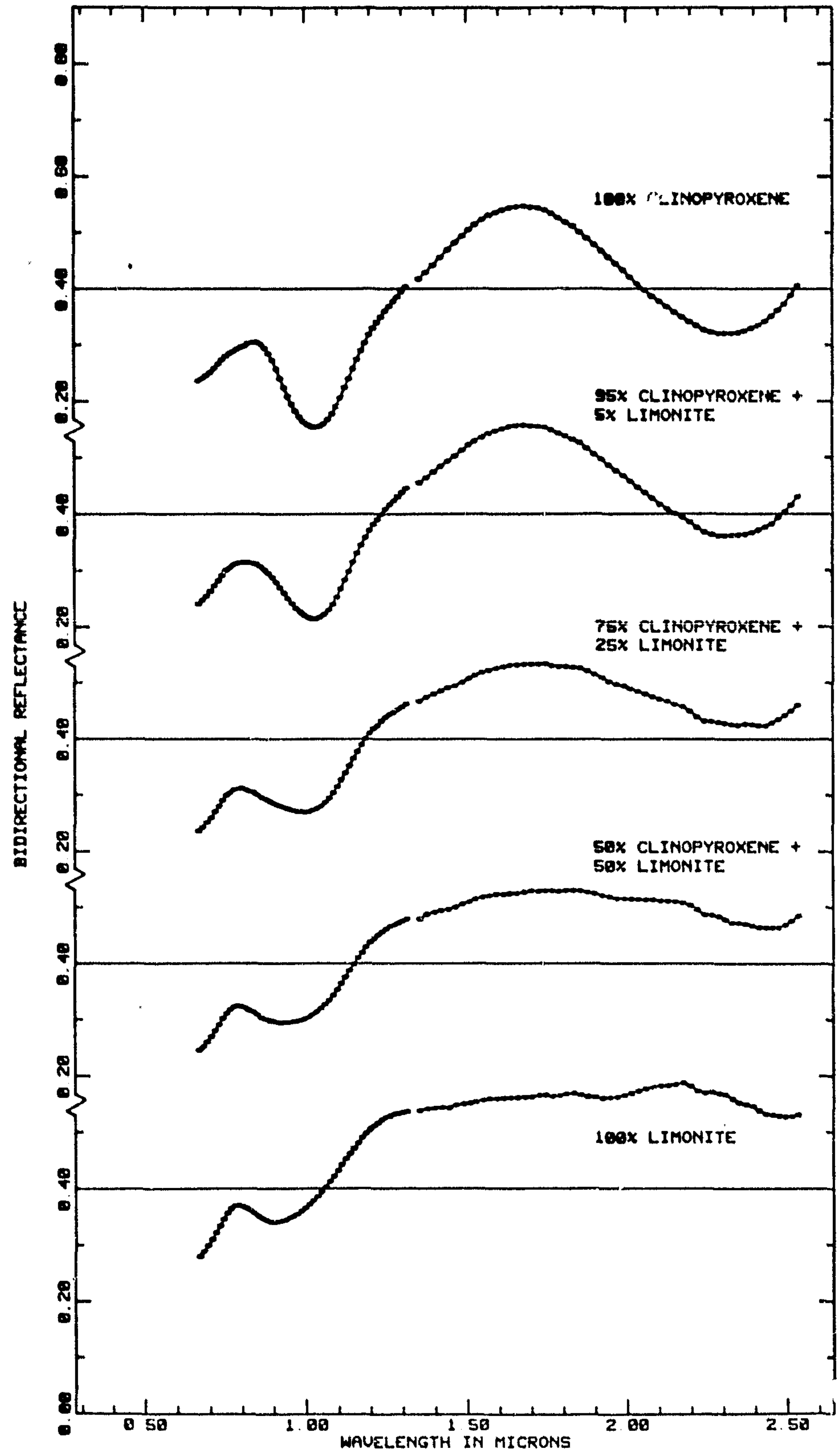
100% CLINOPYROXENE
95% CLINOPYROXENE +
5% LIMONITE
75% CLINOPYROXENE +
25% LIMONITE
50% CLINOPYROXENE +
50% LIMONITE
100% LIMONITE
BIDIRECTIONAL REFLECTANCE
0.00
0.20
0.40
0.60
0.80
0.50
1.00
1.50
2.00
2.50
WAVELENGTH IN MICRONS

Figure 8

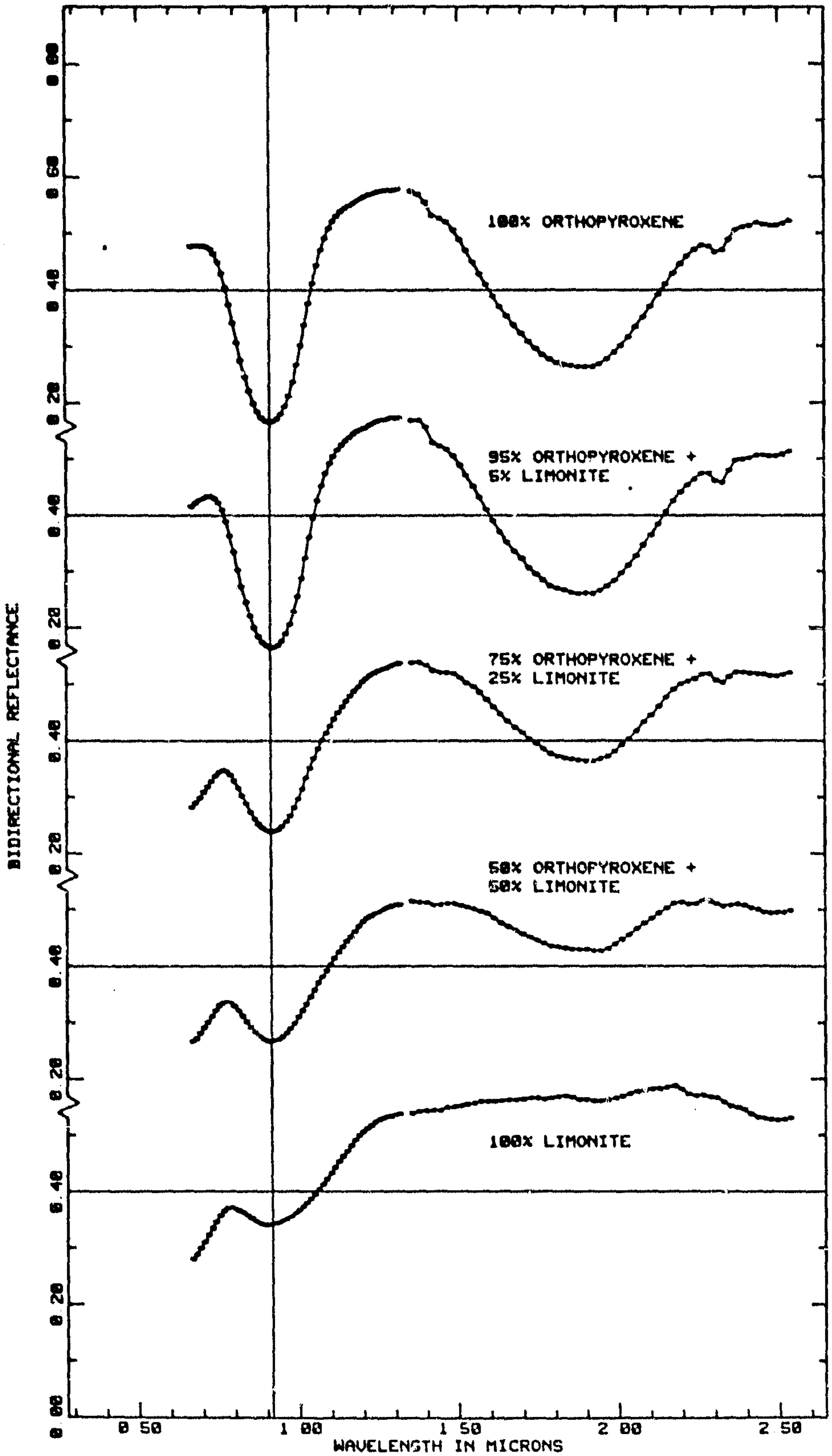
100% ORTHOPYROXENE
95% ORTHOPYROXENE +
5% LIMONITE
75% ORTHOPYROXENE +
25% LIMONITE
50% ORTHOPYROXENE +
50% LIMONITE
100% LIMONITE
BIDIRECTIONAL REFLECTANCE
WAVELENGTH IN MICRONS
0.50
1.00
1.50
2.00
2.50

Figure 9

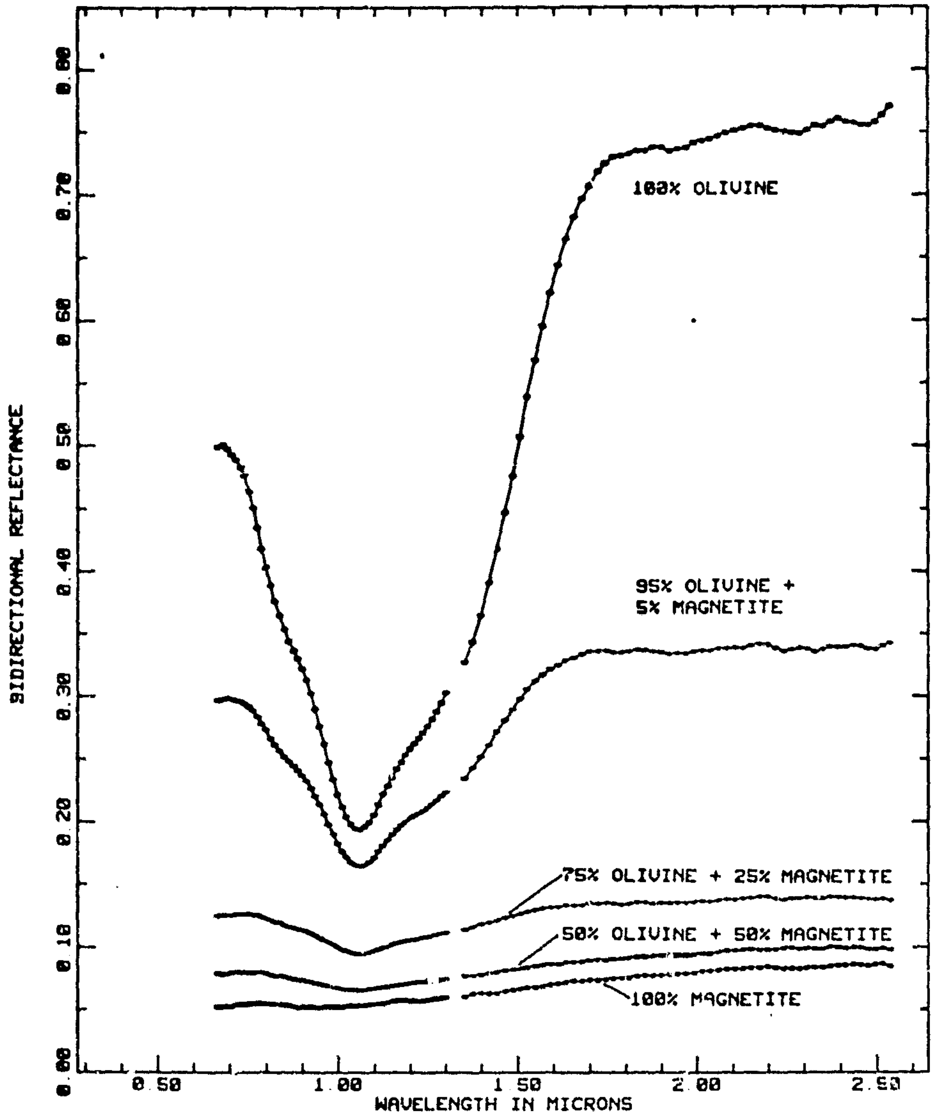
BIDIRECTIONAL REFLECTANCE
0.00
0.10
0.20
0.30
0.40
0.50
0.60
0.70
0.80
0.50
1.00
1.50
2.00
2.50
WAVELENGTH IN MICRONS
100% OLIVINE
95% OLIVINE +
5% MAGNETITE
75% OLIVINE + 25% MAGNETITE
50% OLIVINE + 50% MAGNETITE
100% MAGNETITE

Figure 10

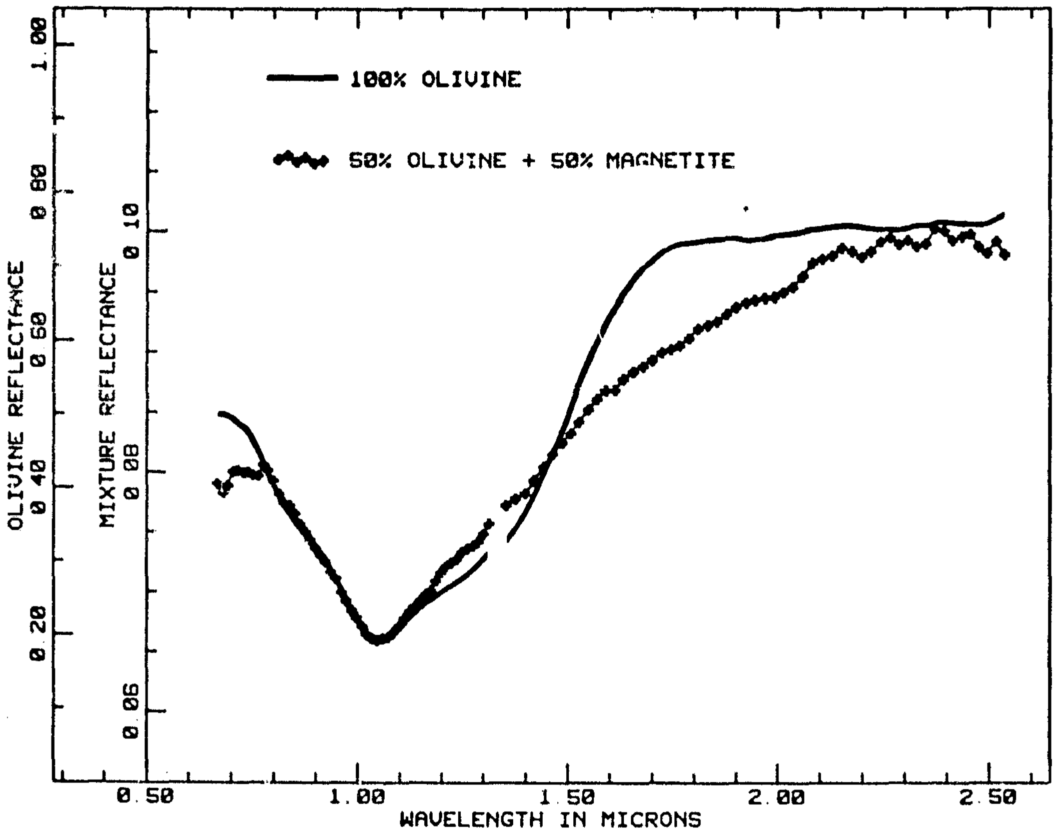
100% OLIVINE
50% OLIVINE + 50% MAGNETITE
OLIVINE REFLECTANCE
MIXTURE REFLECTANCE
1.00
0.80
0.60
0.40
0.20
0.10
0.08
0.06
0.50
1.00
1.50
2.00
2.50
WAVELENGTH IN MICRONS

Figure 11

# CHAPTER V

## The Composition of the Martian Dark Regions, I: Visible and Near-Infrared Spectral Reflectance of Analog Materials and Interpretation of Telescopically Observed Spectral Shape

This paper has been submitted to J. Geophys. Res., 1980. Author: R.B. Singer.

## ABSTRACT

The compositions of dark materials on Mars, more closely related to their parent rocks than the brighter, finer-grained materials, have yet to be directly determined. A number of lines of evidence, including earth-based spectral reflectance, Viking XRF analyses of bright fines, and morphology of volcanic features, point to a basaltic to ultramafic parent composition. Previous interpretations of dark region spectrophotometry from 0.3 to 1.1 μm are consistent with a regionally variable, somewhat oxidized mafic material presently exposed on the surface (Adams and McCord, 1969; Huguenin et al., 1977). Recent high quality infrared telescopic data (0.65 to 2.50 μm) have distinct spectral characteristics not typical of uniformly oxidized materials. New laboratory studies presented here show that the observed visible and near-infrared spectral shape and albedo for martian dark regions is most readily explained by a thin coating of a bright $Fe^{3+}$-bearing material overlying a dark substrate, as previously suggested from less complete spectral information by a number of researchers. The generation this spectral shape depends on the trans-opaque behavior of $Fe^{3+}$-bearing materials. Both coating and substrate contribute importantly to the net spectral reflectance of the combination. Overall spectral shape is sensitive to coating thickness, composition, and

packing. Physical thicknesses of coatings for observed dark regions on Mars are estimated to be as great as 30 micrometers, in contrast to previous estimates of only a few micrometers. The periodic aeolian clearing of global dust from dark regions suggests that the coating is mechanically bound to the substrate, either resistant to abrasion or regenerated. The coating geometry described here is spectrally insensitive to substrate dimensions and is equally effective for particle sizes from sand (dark dunes) to large outcrops. These results are not necessarily in conflict with Viking lander XRF results which constrain bright soil particles to have coatings which are either discontinuous or less than ¼ micrometer thick, since quite different surface materials are being discussed. Spectral data excludes homogeneously oxidized rocks as major surface components in dark regions observed from Earth.

## INTRODUCTION

The very successful Viking program, still in progress, has enormously increased our available information about Mars and provided an entirely new perspective: detailed examination of the surface at two locations. Yet in a key area of investigation, mineralogic identification of surface materials, Viking can provide only limited information. Chemical analyses of bright fine-grained material at both sites are exceedingly valuable but it does not come as a complete surprise that both landers found similar soil chemistries (e.g. B.C. Clark et al., 1977). Both Viking landing sites occur in classic intermediate- to high-albedo regions, interpreted from previous observations to be largely surfaced with fine-grained aeolian materials transported on a global scale (e.g. Sagan et al., 1973; McCord et al., 1977). The dark regions on Mars, felt to contain materials petrologically closer to their parent rock (Adams and McCord, 1969; Huguenin, 1974; Huguenin et al., 1977) have yet to be examined at this close range. It has not been possible to analyze chemically any dark materials, including rocks found at each landing site.

The best source of compositional data for the dark materials on Mars, at least for the next several years, is earthbased visible and near-infrared reflectance spectroscopy. The purpose of the research presented here is to interpret the composition and mode of occurrence of these dark materials from existing data, including new near-infrared spectrophotometry analyzed here for the first time. This paper addresses the significance of the very distinctive spectral shape of observed dark regions. In addition, the bidirectional reflectance spectra presented here of geologic materials and their mixtures should be valuable for future interpretation of spectral reflectance data for many solar system objects including the Earth. A separate paper (Singer, 1980a) deals with interpretating the petrology of martian dark materials from specific absorptions in earth-based spectral observations.

## BACKGROUND

It is beyond the scope of this paper to provide a complete summary of Mars surface composition interpreted from spectral observations; only specific topics and references will be discussed. Comprehensive reviews of Mars spectra and interpretations up to 1969 were published by McCord and Adams (1969) and Salisbury and Hunt (1969). A more recent summary is provided by Singer et al. (1979).

The laboratory model presented by Adams and McCord (1969) gives an excellent match for dark region spectra then available (0.3 to 1.1 μm) using grains of a particular basalt artificially oxidized on the surface with an acid solution. The spectral behavior of dark regions from 1.1 to 2.5 μm, however, was poorly known at that time and could not be modeled. Huguenin (1973a, b) proposed a UV photostimulated oxidation mechanism which can produce surface alteration layers on mafic igneous rocks under present martian conditions. He interpreted Mars dark region spectrophotometry from 0.3 to 1.1 μm (McCord and Westphal, 1971; McCord et al., 1977) as indicating the occurrence of such oxidation layers, estimated to be roughly a few micrometers in thickness (Huguenin, 1976). Earlier suggestions that the martian surface might consist of relatively unoxidized rocks covered with a surface coating or stain of ferric oxide were made by Binder and Cruikshank (1963, 1966). Using thermal infrared observations and experiments, Van Tassel and Salisbury (1964) suggested that the observed properties of the martian surface could be produced by either fine-grained silicates with ferric-oxide impurities or a wider size range of silicates with fine-grained ferric-oxide coatings. Viking lander XRF measurements have been interpreted to constrain ferric-oxide coatings on silicate soil particles to be discontinuous and/or less that ½ micrometer thick (Clark <u>et al</u>., 1976). The Viking inorganic chemistry team concluded that ferric oxides present in the landing site soils exist either as discrete grains or as inclusions in silicates (Toulmin <u>et al</u>., 1977). Warner (1979) observed that rocks near the landers which have been poked or scraped show neither scratch marks nor flakes of weathering coating, and took this to indicate that the observed red color might be due to primary oxidation throughout these rocks.

When the first high quality near-infrared (0.65 to 2.50 μm) spectrophotometry of dark regions was obtained during the 1978 Mars apparition (McCord <u>et al</u>., 1980a) the results were puzzling. Composite spectra from 0.3 to 2.50 for typical bright and dark regions are shown in Figure 1. These curves have been scaled to unity at 1.02 μm; dark regions have an average 1 μm reflectance of about 17 to 18%, while bright regions are about a facter of two more reflective at 1 μm (Binder and Jones, 1972). Both spectra show moderately sharp Mars atmospheric $CO_2$ absorptions at 1.34, 1.45, and 1.62 μm as well as the deep $CO_2$ triplet (not resolved here) located near 2.0 μm (Kieffer, 1968). Dark region spectra are characterized by a marked peak reflectance near 0.75 μm, well known from previous observations. At wavelengths shortward of this peak the spectrum is dominated by $Fe^{3+}$ absorptions of similar origin but lesser intensities than for the bright regions. As wavelength increases from the spectrum peak there is a shallow absorption band complex around 1 μm (discussed in detail by Singer, 1980a) superimposed on a smooth decrease in reflectance out to 2.5 μm (excluding the effects of martian atmospheric $CO_2$). This negative slope throughout the near infrared is a newly observed but well substantiated phenomenon (McCord et al., 1980a) not addressed in any previous interpretations. This spectral behavior is not characteristic of lunar and terrestrial basalts or other rocks and minerals, which generally have positively sloping near-infrared spectra (Hunt and Salisbury, 1970, 1971; Hunt et al., 1971, 1973a b 1974a, b; Adams, 1974, 1975; McCord et al., 1980b). Taken as a whole these visible and near-infrared spectral characteristics place significant constraints on the compositions and physical occurrence of materials in the dark regions.

A few laboratory spectra found in the literature do bear a resemblance to these dark region observations and influenced the planning of the laboratory studies presented here. A spectrum of photostimulated oxidized magnetite published by Huguenin (1973a) was found to have the proper characteristics, i.e. a steep positive visible slope, a peak near 0.75 μm and a negative slope out to 1.7 μm, where it converged with the spectrum of unaltered magnetite. Huguenin stated that this behavior was typical of a ferric-oxide thin film or layer, probably about 1 μm thick, on a magnetite substrate. Johnson and Fanale (1973) presented laboratory spectra of a number of meteorite samples which show steep positive slopes in the visible and less severe negative slopes in the near-infrared, although the reflectances are generally lower than observed for Mars dark regions. They modeled this spectral shape approximately with a mixture of 95% $Fe^{3+}$- or ferric-oxide-bearing montmorillonite and 5% carbon black; no mechanism for the spectral behavior of this mixture was discussed.

A consideration when analyzing earthbased spectrophotometry of regions hundreds of kilometers or larger in size is the homogeneity of the surface. Many dark regions on Mars have been shown by spacecraft imaging to be composed of streaks and splotches of bright and dark material on scales of tens of kilometers down to the limit of resolution (Sagan et al., 1973; Veverka et al., 1977; Greeley et al., 1978). This prompted a study by Singer and McCord (1979) into the likely spectral effects of large scale additive or "checkerboard" mixing of bright and dark surface materials on Mars. With the removal of increasing amounts of bright material influence from dark region observations: a) the UV-visible slope decreases in intensity but always remains significant, b) the near-infrared drop-off in reflectance becomes more pronounced, and c) the spectrum peak, while moving to slightly shorter wavelengths, increases in prominence. These results imply that the distinctive dark region spectral characteristics are inherent to the dark materials themselves on a scale of a few millimeters or smaller (Singer and McCord, 1979).

## LABORATORY INVESTIGATIONS.

The bidirectional laboratory reflectance spectra presented here were obtained with the Hawaii Institute of Geophysics/Planetary Sciences spectrogoniometer. This facility is described by Singer (1980b). All observations were made with an incidence angle (I) of $10^{\circ}$ and an emission or viewing angle (E) of $0^{\circ}$ (normal). Data are presented with a $\pm 1$ standard deviation of the mean error bars except where this would confuse comparison of many overlapping curves. In most cases errors are 0.5% or less. Near-infrared spectral coverage (0.65 to 2.55 µm) was provided by a cooled circularly variable filter (CVF) spectrometer with an InSb detector, all operating at liquid nitrogen temperature (77K). This is the same instrument used telescopically for 1978 Mars observations (McCord et al., 1980a). Near-UV and visible coverage (0.33 to 0.75) was provided by a similiar CVF spectrometer operating at ambient temperature and using as the detector a S-1 phototube cooled with dry ice (195K). Halon powder, discussed by Singer (1980b), was used as the reflectance standard. The absolute reflectance of Halon deviates from perfect by less than 4% throughout the visible and near-infrared; these variations have not been removed from the data presented here. The most noticeable effect of this is a slight artificial rise in apparent reflectance centered near 2.15 μm in the laboratory spectra. Halon was chosen over MgO as a standard because of its higher reflectance and reproducibility.

Homogeneously oxidized materials

The laboratory spectra of four homogeneously oxidized materials are shown in Figure 2. Note that the curves are "stacked": the reflectance scale is discontinuous to prevent overlap.

The top two spectra are ferric oxides shown for comparison purposes. FOX01 is a reagent grade synthetic hematite, Fe2O3 (Alfa Products and has an exceedingly fine particle size (a few micrometers or smaller). FOX02 is a naturally occurring limonite, variety yellow ocher, from Cartersville, GA (Ward's Natural Science Establishment). Mean particle size is greater than the hematite but still much finer than a 38-micrometer sieve. Limonite is a loosely used term for hydroxylated ferric oxides showing no definite evidence of crystallinity. Most materials identified as limonite are actually very fine-grained goethite, $\alpha FeO \cdot OH$. Chemical analysis (Singer, 1980b) has shown that this sample has substantial (~30wt.%) silicate impurities, probably in the form of clay minerals.

Both of these spectra are dominated by an intense absorption edge in the visible caused by

$O^{2-}$ - $Fe^{3+}$ charge - transfer absorptions in the near - UV and by $Fe^{3+}$ crystal - field absorptions in the visible (Huguenin et al., 1975; McCord et al., 1980b; R.G. Burns, personal communication, 1980).

Huguenin (1975) has shown that the intensities of these UV - visible absorptions decrease with increased hydroxylation of the mineral; this is demonstrated by the band saturation from the near - UV to 0.53 μm for the non-hydroxylated hematite, while the reflectance of the hydroxylated limonite starts to rise by 0.40 μm. In familiar terms hematite appears blood red, while limonite and goethite appear yellow to yellow-brown. When compared spectrally to Figure 1 or visually to a properly color balanced Viking lander frame, hydroxylated ferric oxides seem more reasonable for most of the martian surface.

In the context of Mars dark region spectra (Figure 1) these ferric oxide curves are of interest because of their steep slope in the visible and the relative spectral peak near 0.75 μm (defined by an absorption to each side). Spectral details in the visible are, however, quite disparate. Even more significantly, the ferric-oxide spectra continue to rise in reflectance sharply to a break in slope near 1.25 μm and maintain a high reflectance to beyond 2.5 μm, very much different from Mars observations.

Spectra of two homogeneously oxidized mafic materials, in which ferric oxide is a less significant component, are shown at the bottom of Figure 2. BAS05 basalt is from the Keweenawan lava group found in northeastern Minnesota (Basaltic Volcanism project sample KEW-12). This hydrothermally altered, weakly alkaline basalt contains a total of 13.3 wt. % iron oxide, with three times as much $Fe_2O_3$ FeO by weight (Green, 1980). The $Fe^{3+}$ absorptions in the visible are recognizable but distorted. The shallow asymmetric absorption centered near 1 μm is a composite of $Fe^{3+}$ and $Fe^{2+}$ crystal-field absorptions (cf. Singer, 1980b). A major flaw with this sample as a dark material analog is the continued (if gradual) rise in reflectance out to 2.5 μm, rather than the required reflectance decrease. Sample VOL01 has a similar deficiency as a Mars analog. This material is a brick-red glassy tephra, uniformly oxidized and erupted from a cinder cone near the summit of Mauna Kea. It contain 4.7 times as much $Fe_2O_3$ by weight as FeO. This sample is spectrally very similar to red cinders from Sunset Crater, Arizona (C.M. Pieters, personal communication, 1979).

The oxidized basalt and cinder are representative of a class of materials which are geologically reasonable but which cannot explain the spectral shape seen for martian dark materials. It must be concluded that homogeneously oxidized mafic silicates, as proposed by Warner (1979), are not a major surface component in observed dark regions on Mars.

## Additive spectral combinations

Because a single homogeneous geologic material is ruled out on spectral grounds as an important dark region component, multiple-component surfaces must be considered. The simplest such surface would consist of discrete exposures of two materials. If the exposures have dimensions of about a centimeter or greater there will be very little optical interaction and the resultant spectrum will be a simple average of individual spectra, weighted for the relative surface area covered by each component. This is an additive or "checkerboard" combination.

It has already been demonstrated that removing a "checkerboard" component of martian bright material enhances, rather than eliminates, the distinctive spectral shape of the dark materials (Singer and McCord, 1979) Is there any possibility that the dark materials themselves could be composed of smaller scale discrete exposures of some oxidized ($Fe^{3+}$-rich) material and fresh exposures of unoxidized rock?

Such a case has been simulated here and is displayed in Figure 3. For an oxidized material the limonite sample discussed above (FOX02) was used.

A specimen of magnetite ($Fe_3O_4$) (Ward's Natural Science Establishment), ground and passed through a 45 micrometer sieve, was used as the dark unoxidized component. The pure magnetite spectrum (bottom of Figure 3) is relatively featureless with a slight positive slope. It represents the general shape, but not the detail, of many mafic igneous rock spectra. The additive combinations were calculated based on relative areal coverage by the two endmember components. Note that this figure has a continuous reflectance scale; it is not stacked, and the reflectance crossover near 0.45 μm is a real phenomenon. Clearly an additive situation such as this is inadequate to explain the spectral reflectance of the dark materials. The weighted average of two positively sloping spectra will always have an intermediate positive slope. Taken together, these last two sections lead to the conclusion that the dark materials on Mars must consist of physically close ($\lesssim$mean optical path length) associations of multiple components.

Intimate physical mixtures

The spectral properties of a fine intermixture of bright $Fe^{3+}$- rich material and darker unoxidized material were tested with physical mixtures of the limonite and magnetite samples described above. Results are shown in Figure 4, which has the same continuous reflectance scale as Figure 3.

It is immediately apparent that mixtures with 25% and 50% limonite have spectra with the desired peak near 0.75 μm and a decrease in reflectance extending out beyond 2.5 μm. For 5% limonite the spectrum also has a decreased slope relative to pure magnetite, although the slope is still positive. It appears that spectra for all three mixtures would converge on the pure magnetite spectrum if these curves were extrapolated to a wavelength of about 4 μm. While none of these mixtures provides an excellent match for dark region observations they demonstrate a way to produce a sharp reflectance rise in the visible followed by a decrease in reflectance in the infrared, a characteristic not seen for either single component.

The responsible mechanism for this optical behavior is a wavelength dependent transparency for thin particles or layers of ferric oxides. In the visible region the intense absorbance corresponds to a low transmittance, making even a thin layer of ferric oxide optically thick. The reflectance increase with wavelength exhibited by 100% limonite (for example) corresponds to decreasing absorbance and therefore increasing transmittance. Hunt et al., (1971) refer to this as "trans-opaque" behavior. Each particle of a good diffuse reflector, such as MgO or Halon, is quite transparent; many scattering events in a thick layer are required for the highest return of flux (Wendlandt and Hecht, 1966). Operating in parallel with this mechanism is the general increase in radiation penetration depth with increasing wavelength. For the physical mixtures described here the finer-grained limonite can be thought of as forming a coating on the larger magnetite grains. At short wavelengths this coating is optically thick and the resultant reflectance is nearly that of pure limonite. At some longer wavelength, dependent on coating thickness, the coating is transparent enough that net reflectance is equally influenced by the coating and the substrate (magnetite). Beyond this wavelength the substate increasingly dominates the resultant spectrum and the curves appear to converge.

Microscopic examination of these limonite-magnetite mixtures showed that not all magnetite grains were completely coated, particularly for the mixture with only 5% limonite. This implies a subsidiary additive spectral contribution from magnetite; the net reflectance is then determined in a slightly more complicated manner than discussed above. Nevertheless this experiment serves to demonstrate a specific mechanism by which the characteristics of observed Mars dark region spectra can be generated.

The incomplete coverage of magnetite was at least in part due to the cohering of very fine limonite particles into larger grains. This effect is largely caused by physically adsorbed water. After dessication for 48 hours at 100-110$^{o}$C and re-mixing, the limonite exhibited far less clumping and covered the magnetite grains more evenly. This case is probably similar to what might occur in the highly dessicating martian environment.

Trans-opaque behavior such as described above can also account for the spectral behavior of the montmorillonite-carbon black construct of Johnson and Fanale (1973). The spectrum for the physical mixture has a peak in the visible and a negative slope throughout the near-infrared. When the mixture was fused by melting the sample was converted into a homogeneous mass, and the distinct spectral properties of the two-component mixture were destroyed.

Thin oxidized surface coatings

Based on the work of Adams and McCord (1969) and Huguenin (1973a, b, 1976), as well as the results presented above, dark unoxidized rocks with thin $Fe^{3+}$-rich coatings would appear to be excellent candidates for Mars dark materials. A number of naturally occurring samples of this type were collected and examined in the laboratory. Coating thicknesses were measured from hand samples and/or epoxy impregnated thin sections, cut perpendicularly through the coated surface.

Sample BAS10 (Figure 5a) is from a massive, fine-grained, dark gray hawaiite boulder with a heavily oxidized exterior, found on Mauna Kea. Hawaiite is the name given to andesine andesites which predominate during the late stages of Hawaiian volcanoes. These rocks grade into alkalic olivine basalt and are basaltic in appearance; the term hawaiite is used to differentiate them from continental andesites, which are quite dissimilar (MacDonald and Abbott, 1970). The altered zones are medium to light brick red with some areas slightly more yellow. The oxidized material is genetically related to the rock and has a gradational inner boundary; in some locations it penetrates centimeters deep. The reflectance spectrum was taken of a spot where the surface alteration varied from one-half to two millimeters thick. The reflectance rises very steeply in the visible, peaks at about 1.2 μm, and shows a slight average decline out to 2.5 μm. The high value of the peak reflectance (0.37) and its location at a wavelength longer than the well defined 0.87 μm $Fe^{3+}$ band are indicative of a very strong ferric-oxide influence quite unlike Mars. This sample provides an example of an oxidation layer too thick to allow much spectral influence from the dark substrate.

Sample BAS12 (Figure 5b) is a Mauna Kea hawaiite similar to BAS10 but with a much thinner, more uniform oxidation rind. This surface appears dark reddish-brown and is genetically related to the rock, with plagioclase phenocrysts protruding to the surface. The oxidized layer over most of this sample averages 25 micrometers in thicknesses, varying from about 16 to 36 micrometers. In addition there are scattered areas where oxidation penetrates the rock further, generally a few hundred micrometers or less but occassionally as deep as a millimeter.

The peak reflectance of this sample is lower (0.24) and at a slightly shorter wavelength than for the previous case. The 0.87 μm $Fe^{3+}$ band is less prominent, while the infrared drop in reflectance is more pronounced. These spectral characteristics are consistent with the thinner oxidation layer. The coating is optically thin enough to show some transparency as discussed in the previous section but is apparently still too opaque to generate the spectral shape observed for martian dark regions.

Sample BAS09 (Figure 5b) is also a massive rock from Mauna Kea but compared to the previous two samples is somewhat coarser grained, and lighter in color because of much more abundant plagioclase. The coating is slightly redder in appearance than that on BAS12 but is of similar subjective brightness. The alteration layer consists of an irregular heavily oxidized surface layer, generally 10 to 25 micrometers thick, backed up by a zone of less severe oxidation and staining which varies in thickness from about 100 to 200 micrometers. Spectrally BAS09 behaves as though its oxidized layer is more transparent than the previous samples. The peak refectance near 0.77 μm is similar to that for BAS12 but represents a real rather than a local maximum. The near-infrared $Fe^{3+}$ absorption appears broadened and apparently shifted to longer wavelengths. This effect was also seen for the 50% magnetite-50% limonite physical mixture (Figure 4) and can be attributed to the lowering of the long wavelength edge of the band by the increasing influence of the low reflectance substrate. BAS12 is spectrally more like martian dark regions than the previous examples, with visible reflectance smoothly rising to a peak reflectance near 0.77 μm and a more gradual negative slope throughout most of the infrared. Dissimilarities include too low a reflectance in the mid-visible (BAS12 is too "red") and too high a reflectance from about 1 to 2 μm.

Sample BAS11 (Figure 5b), also from Mauna Kea, is somewhat different from the previous rocks. It is of similar dark gray color and fine grain size as BAS10 and BAS12 but is somewhat vesicular and contains abundant plagioclase phenocrysts up to 1mm in length. This rock was found buried about 20cm deep in a layer of yellow-brown heavily weathered tephra and has a thin tightly bonded coating of yellow-brown material. The oxidation process in the tephra seems currently active and involves liquid water (J. Adams, personal communication, 1979). The surface coating appears to be a composite of oxidation products from this rock and from the surrounding tephra. In some cases plagioclase laths penetrate the coating, but many are coated as thickly as the surrounding more mafic groundmass. Some alteration is also present lining vesicles up to a few millimeters from the surface. The mean surface coating thickness is 30 micrometers, with extremes of 15 and 60 micrometers. Spectrally the coated BAS11 shows a smooth rapid rise in reflectance from the UV to a rounded peak near 0.76 μm, and then a more gradual slightly concave decrease in reflectance out to 2.5 μm. There is no indication of $Fe^{3+}$ or $Fe^{2+}$ absorptions in the 1-μm region. Nevertheless this curve is very similar to dark region spectra in overall shape.

The bottom spectrum in Figure 5b is presented for reference rather than for geologic plausability. This is of a thin slightly discontinous oxidation surface on a massive block of magnetite (Ward's Natural Science Establishment). The coating appears slightly pinkish-red on the magnetite and a more intense red when scraped off: it is very hematitic. This oxidation layer is very thin and proved difficult to measure; its thickness is estimated to be a few micrometers or less in places. The spectrum shows strong ferric-oxide features in the visible and very-near-infrared, and a greater degree of transparency out to a 2.5 μm than seen for other samples. The change from negative to positive slope between 1.6 and 1.7 μm is thought to correspond to the convergence of oxidized and unoxidized spectra discussed by Huguenin (1973a).

Despite the variations in rock and coating composition and morphology for the examples in this section, it has clearly been demonstrated that a thin alteration layer overlying a dark unoxidized rock is a successful mechanism for generating the observed visible and near-infrared spectral reflectance for dark materials on Mars. One of these examples in particular deserves further attention. There is an excellent correlation between the coated BAS11 spectrum and the dark material spectrum inferred by the removal of 20% coverage by bright material from the dark region observations shown in Figure 1 (Singer and McCord, 1979). An overlay of both spectra, scaled for best fit, is shown in Figure 6. Multiplicative scaling is necessary because the absolute reflectance of these Mars data has not been determined, and is legitimate because the relative data values (e.g. slope, ratios) remain unchanged. Nevertheless the 1-μm reflectance of coated BAS11 is 18%, strikingly close to the the 17 to 18% average value measured for dark regions by Binder and Jones (1972). The dark material spectrum in Figure 6 has a model $CO_2$ atmosphere spectrally removed. The dips in the BAS11 data near 1.4 and 1.9 μm and the decline in reflectivity beyond 2.1 or 2.2 μm are due to adsorbed $H_2O$ in the coating. The correspondence in the visible, dependent primarily on the spectral properties of the coating, is excellent. The correspondence beyond 1.2 μm, dependent on both the high reflectivity of the coating and low reflectivity of the substrate, is also very good. The primary discrepancy is between 0.8 and 1.2 μm, the important "1 μm" absorption region. For Mars these absorptions are interpreted to be caused by ferromagnesian minerals (Adams, 1968; Huguenin <u>et al</u>., 1977; Singer, 1980a);

such absorptions can be observed, with reduced contrast, through a semi-transparent surface coating. The implications of at least part of the discrepancy seen in Figure 6 are that while the surface coating on BAS11 is spectrally very much like those observed on Mars, the underlying rock is not as mafic as the coated rocks or rock fragments that cover most of surface in martian dark regions.

The yellow-brown material coating BAS11 and the very similar weathered tephra from the same location are of extreme interest. Evans and Adams (1979) have identified this weathered tephra, which they refer to as HI-34, as having spectral characteristics very nearly the same as certain martian surface materials imaged by Viking lander 1 in six visible and near-infrared bandpasses. Of interest in the laboratory spectrum of HI-34 is the absence of a prominent $Fe^{3+}$ band between 0.8 and 0.9 μm. This is also apparent from Figure 5b for coated BAS11. The potential significance of the absence of this band is discussed by Singer (1980a). Studies of this material are continuing, including chemical and mineralogic analyses currently being performed by D. Evans (personal communication, 1979).

## DISCUSSION AND CONCLUSIONS

Observed spectral reflectance from 0.3 to 2.5 μm for dark regions and Mars has been shown to be quite distinctive and is not characteristic of a single homogeneously oxidized material such as suggested by Warner (1979). It has also been shown that discrete exposures of different surface components can not produce the observed spectral shape for the dark materials themselves, although this situation does occur on a larger scale with partial coverage of the classic dark regions by streaks and splotches of bright material (e.g. Singer and McCord, 1979). It is concluded here that the preponderant dark materials on Mars consist of close physical associations of fine-grained $Fe^{3+}$ - bearing materials with high near-infrared reflectance and unoxidized material with lower and more uniform spectral reflectance.

Based on many lines of evidence and much work by others it seems almost certain that the darker unoxidized component is mafic to ultramafic rock, of somewhat variable composition around the planet. The fine-grained oxidized component appears to be of uniform composition from earth-based spectrophotometry; global three-color mapping by Viking Orbiter II, however, has shown certain dark regions which are anomolously red (Soderblom _et al._, 1978; McCord _et al._, 1980c). These redder dark regions have color characteristics unlike any widely distributed surface material on Mars and appear to have a different oxidized component. These areas have yet to be spectroscopically observed and are important targets for future earth-based work. The more common oxidized component of the dark materials is spectrally similar to global dust. If these two materials are in fact the same then the dark materials could be a current or fossil source of global dust, although deposition of genetically unrelated dust is not ruled out by this study.

The results presented here do not by themselves resolve the question as to whether dark materials occur predominantly as soil mixtures or as coated rocks or rock fragments. The persistent recovery of low albedo features from episodes of aeolian inundation, however, along with the observed consistency of the overall spectral shape for dark regions, provides evidence for oxidized coatings bound to substrates of rocky material. The sizes of the coated materials could range from sand (∿ ½ mm) to large outcrops and lava flows without major variation in spectral properties.

Based on the properties of the surface-altered terrestrial rocks discussed in the previous section, dark region spectral observations are interpreted here to indicate alteration coatings on the order of 20 to 30 micrometers average thickness, dependent on the optical properties of the specific coating substance(s), These results are not necessarily in conflict with Viking lander XRF results which constrain any ferric-oxide coatings on silicate particles to be discontinuous or less than ¼ micrometer thick (Clark et al., 1976). Both landers sampled very fine-grained bright soils which may resemble the coatings found in the dark regions, but which are not representative of the composite dark materials discussed here. Huguenin (1976) concluded that an alteration-layer thickness of about 10 micrometers or greater would significantly inhibit cation migration and therefore gas-solid alteration rates of mafic materials. Variation of such factors as coating continuity, porosity, and composition could alter the actual equilibrium thickness attained by such layers on martian rocks. As discussed by Huguenin (1974) aeolian abrasion is likely to be the major process on Mars for removing "surface clogging" alteration rinds. The implication is that aeolian abrasion is presently operating slowly enough in spectrally observed dark regions to allow alteration layers to reach an equilibrium thickness and substantially reduce the rate of further reaction. If damaged or removed such a coating would be regenerated at a higher reaction rate. To have derived the observed global dust inventory by gas-solid surface alteration in the scenario described above might require periods and/or regions characterized by aeolian abrasion greater than than apparently now operating in observed dark regions.

## ACKNOWLEDGEMENTS

The author is grateful to J. Adams for suggesting Mauna Kea as a Mars analog, for other helpful discussions during this research, and for supplying a number of the samples. Thanks go to C. Pieters for initiating my quest for naturally occuring alteration layers. Additional helpful suggestions and reviews of the manuscript were kindly provided by T. McCord, R. Huguenin, R. Burns, D. Cruikshank, R. Hawke, and R. Clark. Much of this research was conducted at the Institute for Astronomy, University of Hawaii.

Funding was provided by NASA grant NSG# 7590.

## REFERENCES

Adams, J.B., Lunar and Martian surfaces: Petrologic significance of absorption bands in the near-infrared, Science, 159, 1453-1455, 1968.

Adams, J.B., Visible and near infrared diffuse reflectance spectra of pyroxenes as applied to remote sensing of solid objects in the solar system, J. Geophys, Res. 79, 4329-4336, 1974.

Adams, J.B., Interpretation of visible and near-infrared diffuse reflectance spectra of pyroxenes and other rock forming minerals, in Infrared and Raman Spectroscopy of Lunar and Terrestrial Minerals, C. Karr, Jr., ed., Academic Press, 91-116, 1975.

Adams, J.B., and T.B. McCord, Mars: Interpretation of spectral reflectivity of light and dark regions, J. Geophys. Res. 74, 4851-4856, 1969.

Binder, A.B., and D.P. Cruikshank, Comparison of the infrared sepctrum of Mars with the spectra of selected terrestial rocks and minerals, Commun. Lunar Planet, Lab. 2, 193-196, 1964.

Binder, A.B., and D.P. Cruikshank, Lithological and mineralogical investigation of the surface of Mars, Icarus, 5, 521-525, 1966.

Binder, A.B., and J.C. Jones, Spectrophotometric studies of the photometric function, composition, and distribution of the surface materials of Mars, J. Geophys. Res., 77, 3005-3019, 1972.

Clark, B.C., III, A.K. Baird, H.J. Rose, Jr., P. Toulmin III, K. Keil, A.J. Castro, W.C. Kelliher, C.D. Rowe and P.H. Evans, Inorganic analysis of Martian surface samples at the Viking landing sites, Science, 194, 1283-1288, 1976.

Clark, B.C., III, A.K. Baird, H.J. Rose, Jr., P. Toulmin III, R.P. Christian, W.C. Kelliher, A.J. Castro, C.D. Rowe, K. Keil, and G.H. Huss, The Viking X ray fluorescence experiment: Analytical methods and early results, J.Geophys.Res., 82, 1977.

Evans, D.L. and J.B. Adams, Comparison of Viking lander multispectral images and laboratory reflectance spectra of terrestrial samples, Proc. Lunar and Planet. Sci. Conf. 10th, 1829-1834, 1979.

Greeley, R., Papson, R. and Veverka, J., Crater streaks in the Chryse Planitia region of Mars: Early Viking results. Icarus 34, 556-567, 1978.

Green, J.C., Pre-Tertiary plateau basalts, in Basaltic volcanism on the terrestrial planets, Lunar and Planetary Science Institute, Houston, TX, in press 1980.

Huguenin, R.L., Photostimulated oxidation of magnetite. 1. Kinetics and alteration phase identification, J. Geophys. Res., 78, 8481-8493, 1973a.

Huguenin, R.L., Photostimulated oxidation of magnetite. 2. Mechanism, J. Geophys. Res., 78, 8495-8506, 1973b.

Huguenin, R.L., The formation of goethite and hydrated clay minerals on Mars, J. Geophys. Res., 79, 3895-3905, 1974.

Huguenin, R.L., Mars: Chemical weathering as a massive volatile sink, Icarus 28, 203-212, 1976.

Huguenin, R.L., Crystal-field and charge-transfer band assignments in iron (III) oxides and oxyhydroxides: Application to Mars, (abstract) Bull. Am. Astron. Soc. 7, 370, 1975.

Huguenin, R.L., J.B. Adams, and T.B. McCord, Mars: Surface mineralogy from reflectance spectra, in Lunar Science VIII, 478-480, Lunar Science Institute, Houston, 1977.

Hunt, G.R., and J.W. Salisbury, Visible and near infrared spectra of minerals and rocks: I. Silicate minerals, Mod. Geol. 1, 283-300, 1970.

Hunt, G.R., and J.W. Salisbury, Visible and near infrared spectra of minerals and rocks: II. Carbonates, Mod. Geol. 2, 23-30, 1971.

Hunt, G.R., J.W. Salisbury, and C.J. Lenhoff, Visible and near infrared spectra of minerals and rocks: III. Oxides and hydroxides, Mod. Geol. 2, 195-205, 1971.

Hunt, G.R., J.W. Salisbury, and C.J. Lenhoff, Visible and near infrared spectra of minerals and rocks: VI. Additional silicates, Mod. Geol, 4, 85-106, 1973a.

Hunt, G.R., J.W. Salisbury, and C.J. Lenhoff, Visible and near infrared spectra of minerals and rocks: VII. Acidic igeneous rocks, Mod. Geol. 4, 217-224, 1973b.

Hunt, G.R., J.W. Salisbury, and C.J. Lenhoff, Visible and near infrared spectra of minerals and rocks: VIII. Intermediate igneous rocks, Mod. Geol., 1973c.

Hunt, G.R., J.W. Salisbury, and C.J. Lenhoff, Visible and near infrared spectra of minerals and rocks: IX. Basic and ultrabasic igneous rocks, Mod. Geol., 1974.

Johnson, T.V., and F.P. Fanale, Optical properties of carbonaceous chondrites and their relationship to asteroids, J. Geophys. Res. 78, 8507-8518, 1973.

Kieffer, H.H., Near infrared spectral reflectance of simulated Martian frosts, Ph.D. Thesis, Cal. Inst. of Tech., 1968.

MacDonald, G.A. and A.T. Abbott, Volcanoes in the Sea, Univ. Press of Hawaii, Honolulu, 1974 .

McCord, T.B. and J.B. Adams, Spectral reflectivity of Mars, Science, 163, 1058-1060, 1969.

McCord, T.B. R.L. Huguenin, D. Mink, and C. Pieters, Spectral reflectance of Martian areas during the 1973 opposition: Photolectric filter photometry 0.33-1.10 μm, Icarus 31, 25-39, 1977.

McCord, T.B., R.N. Clark, R.B. Singer, and R.L. Hugugenin, Mars: Near infrared reflectance spectra of surface regions and compositional implication, to be submitted to J. Geophys. Res., 1980a. Thesis Ch. II

McCord, T.B., J.B. Adams, and R.L. Huguenin, Reflection spectroscopy: A technique for remotely sensing planetary surface mineralogy, to be submitted to Space Sci. Rev., 1980b.

McCord, T.B., R.B. Singer, J.B. Adams, B.R. Hawke, J.W. Head III, R.L. Huguenin, C.M. Pieters, S. Zisk, and P. Mouginis-Mark, Definition and characterization of Mars surface units, Icarus, to be submitted, 1980c.

McCord, T.B., and J.A. Westphal, Mars: Narrowband photometry, from 0.3 to 2.5 microns, of surface regions during the 1969 apparition, Astrophys. J., 168, 141-153, 1971.

Sagan, C., Veverka, J., Fox, P., Dubisch, R., French, R., Gierrasch, P., Quam, L., Lederberg, J., Levinthal, E., Tucker, R., Eross, B. and Pollack, J.B., Variable features on Mars, 2, Mariner 9 global results. J. Geophys. Res. 78, 4163-4196, 1973.

Salisbury, J.W. and G.R. Hunt, Compositional implications of the spectral behavior of the martian surface, Nature 222, 132-136, 1969.

Singer, R.B., The composition of the martian dark regions: II. Analysis of telescopically observed absorptions in near-infrared spectrophotometry, submitted to J. Geophys. Res., 1980a. Thesis Ch. VI

Singer, R.B., Near-infrared spectral reflectance of mineral mixtures: Systematic combinations of pyroxenes, olivine, and iron oxides, submitted to J. Geophys. Res., 1980b. Thesis Ch. IV

Singer, R.B. and T.B. McCord, Mars: Large scale mixing of bright and dark surface materials and implications for analysis of spectral reflectance, Proc. Lunar and Planet. Sci. Conf. 10th, 1835-1848, 1979. Thesis Ch. III

Singer, R.B., T.B. McCord, R.N. Clark, J.B. Adams, and R.L. Huguenin, Mars surface composition from reflectance spectroscopy: A summary, J. Geophys. Res., 84, 8415-8426, 1979. Thesis Ch. I

Soderblom, L.A., K. Edwards, E.M. Eliason, E.M. Sanchez, and M.P. Charette, Global color variations on the Martian surface, Icarus 34, 446-464, 1978.

Toulmin, P., III, A.K. Baird, B.C. Clark, K. Keil, H.J. Rose, Jr., R.P. Christian, P.H. Evans and W.C. Kelliher, Geochemical and mineralogical interpretation of the Viking inorganic chemical results, J. Geophys. Res., 82, 4625-4634, 1977.

Van Tassel, R.A., and J. W. Salisbury, The composition of the martian surface, Icarus 3, 264-269, 1964.

Veverka, J., Thomas, P. and Greeley, R., A study of variable features on Mars during the Viking primary mission. J. Geophys. Res. 82, 4167-4187, 1977.

Warner, J., Oxidation state of martian basalts, (abstract) Second Intern. Coll. on Mars, NASA Conf. Pub. 2072, 86-87, 1979.

Wendlandt, W.W., and H.G. Hecht, Reflectance spectroscopy, Interscience Publishers, N.Y., 1966.

## FIGURE CAPTIONS

Figure 1: Representative bright and dark region reflectance spectra, scaled to unity at 1.02 μm. The bright region spectrum is composed of an average of the brightest areas observed in 1973 (visible, McCord *et al.*, 1977) and 1978 (infrared, McCord *et al.*, 1980a). The dark region spectrum is a composite of data from two nearby locations in Iapygia: 69-6 (visible, McCord and Westphal, 1971) and 78-10 (infrared, McCord *et al.*, 1980a).

Figure 2: Laboratory reflectance spectra of four homogeneously oxidized powders: two ferric oxides and two heavily oxidized volcanic products. Reflectance scale is discontinuous to avoid overlap of curves.

Figure 3: Calculated results for additive or "checkerboard" mixing of limonite and magnetite samples. The reflectance scale here is continuous; the spectral crossover near 0.45 μm is not an artifact of scaling.

Figure 4: Laboratory reflectance spectra for physical mixtures of limonite and

magnetite powders. The reflectance scale is continuous and identical to Figure 3. Note that two of the mixture spectra have negative infrared slopes, a property not seen in either endmember spectrum.

Figure 5: Laboratory reflectance spectra for five naturally occurring alteration layers on dark rocks. They progress in order of increasingly transparent alteration layers from BAS10 to MAG01. The rocks for spectra labeled "basalt" are technically hawaiite, a basaltic andesite characteristic of late stage Hawaiian volcanism.

Figure 6: Laboratory spectrum for coated rock BAS11 (Figure 6) scaled to match a Mars dark region spectrum with the effects of 20% areal contamination by bright material removed (Singer and McCord, 1979). Overall correspondence is excellent, deviating primarily in the "1 μm" absorption region.

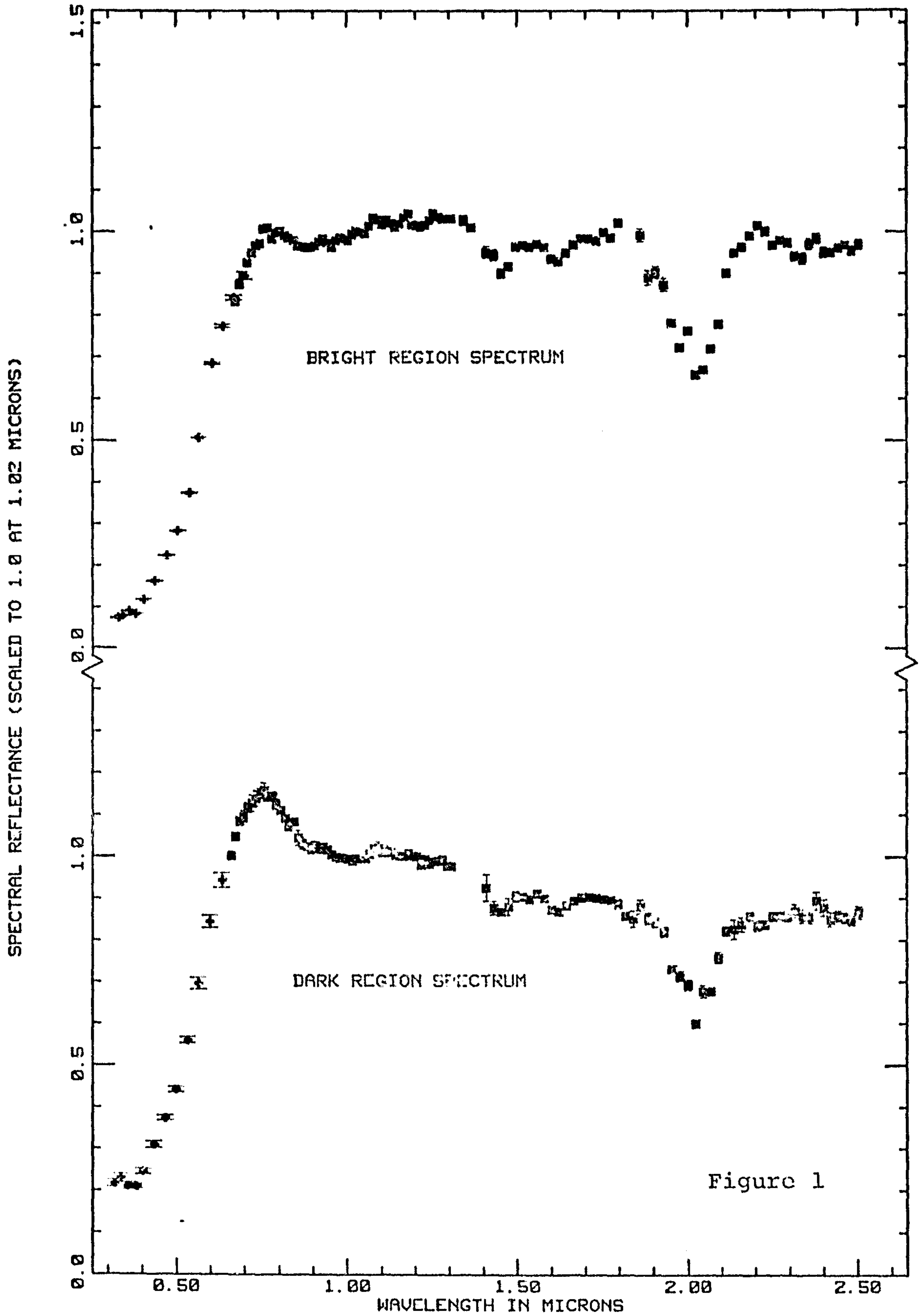
SPECTRAL REFLECTANCE (SCALED TO 1.0 AT 1.02 MICRONS)
WAVELENGTH IN MICRONS
BRIGHT REGION SPECTRUM
DARK REGION SPECTRUM
1.5
1.0
0.5
0.0
1.0
0.5
0.0
0.50
1.00
1.50
2.00
2.50

Figure 1

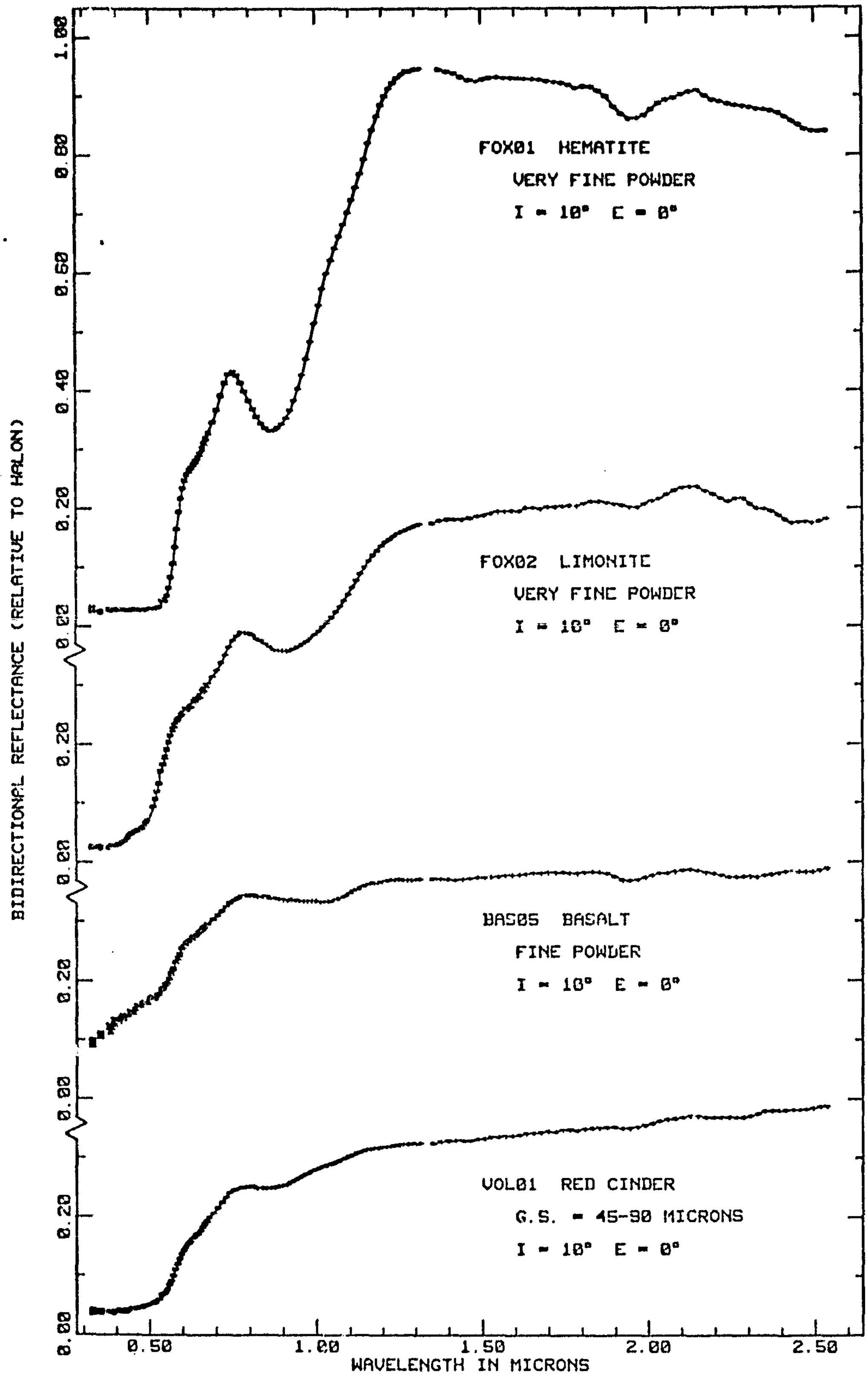

BIDIRECTIONAL REFLECTANCE (RELATIVE TO HALON)
WAVELENGTH IN MICRONS
FOX01 HEMATITE
VERY FINE POWDER
I = 10° E = 0°
FOX02 LIMONITE
VERY FINE POWDER
I = 10° E = 0°
BAS05 BASALT
FINE POWDER
I = 10° E = 0°
VOL01 RED CINDER
G.S. = 45-90 MICRONS
I = 10° E = 0°


Figure 2

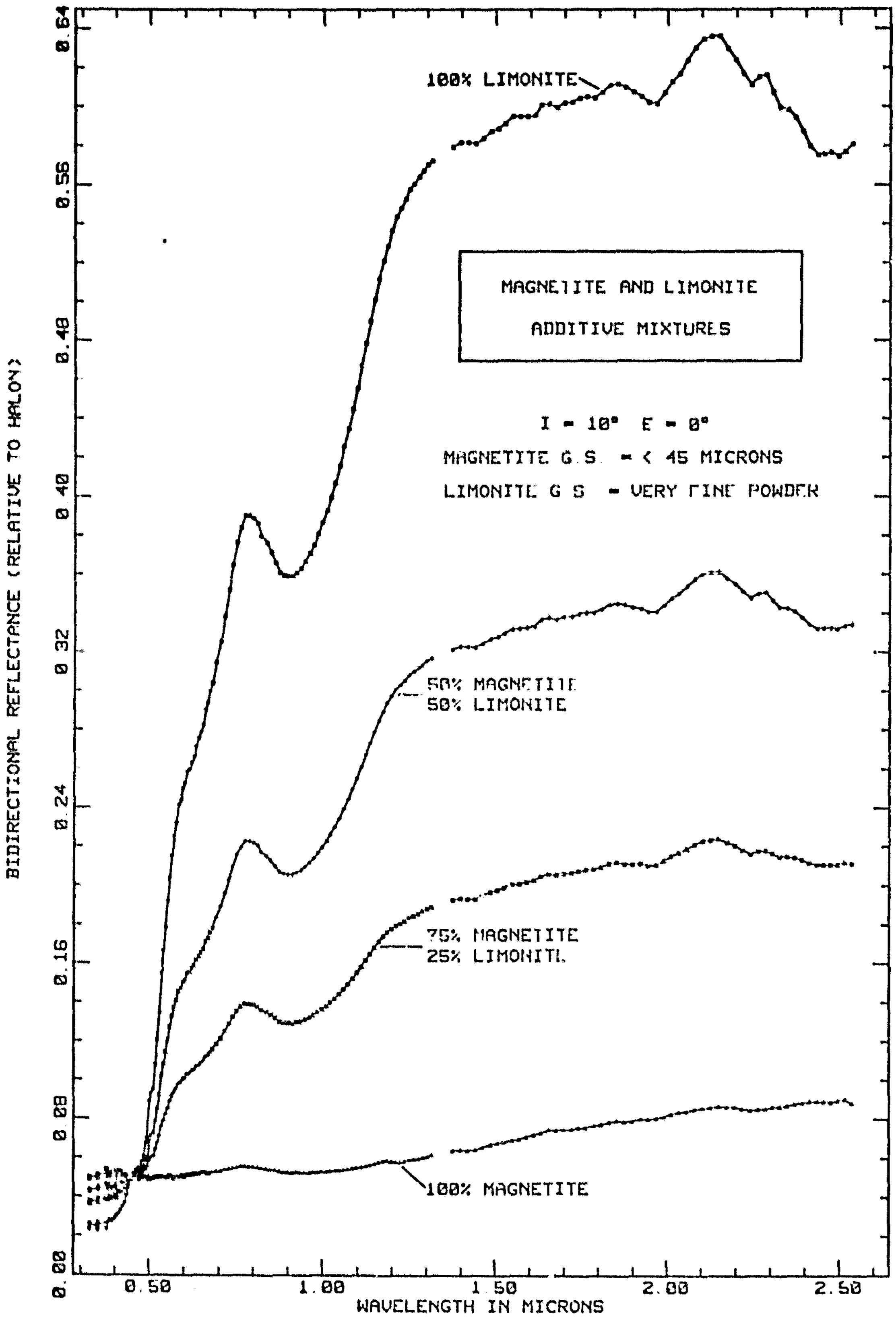
100% LIMONITE
MAGNETITE AND LIMONITE
ADDITIVE MIXTURES
I = 10° E = 0°
MAGNETITE G.S. = < 45 MICRONS
LIMONITE G.S. = VERY FINE POWDER
50% MAGNETITE
50% LIMONITE
75% MAGNETITE
25% LIMONITE
100% MAGNETITE
BIDIRECTIONAL REFLECTANCE (RELATIVE TO HALON)
0.00
0.08
0.16
0.24
0.32
0.40
0.48
0.56
0.64
0.50
1.00
1.50
2.00
2.50
WAVELENGTH IN MICRONS

Figure 3

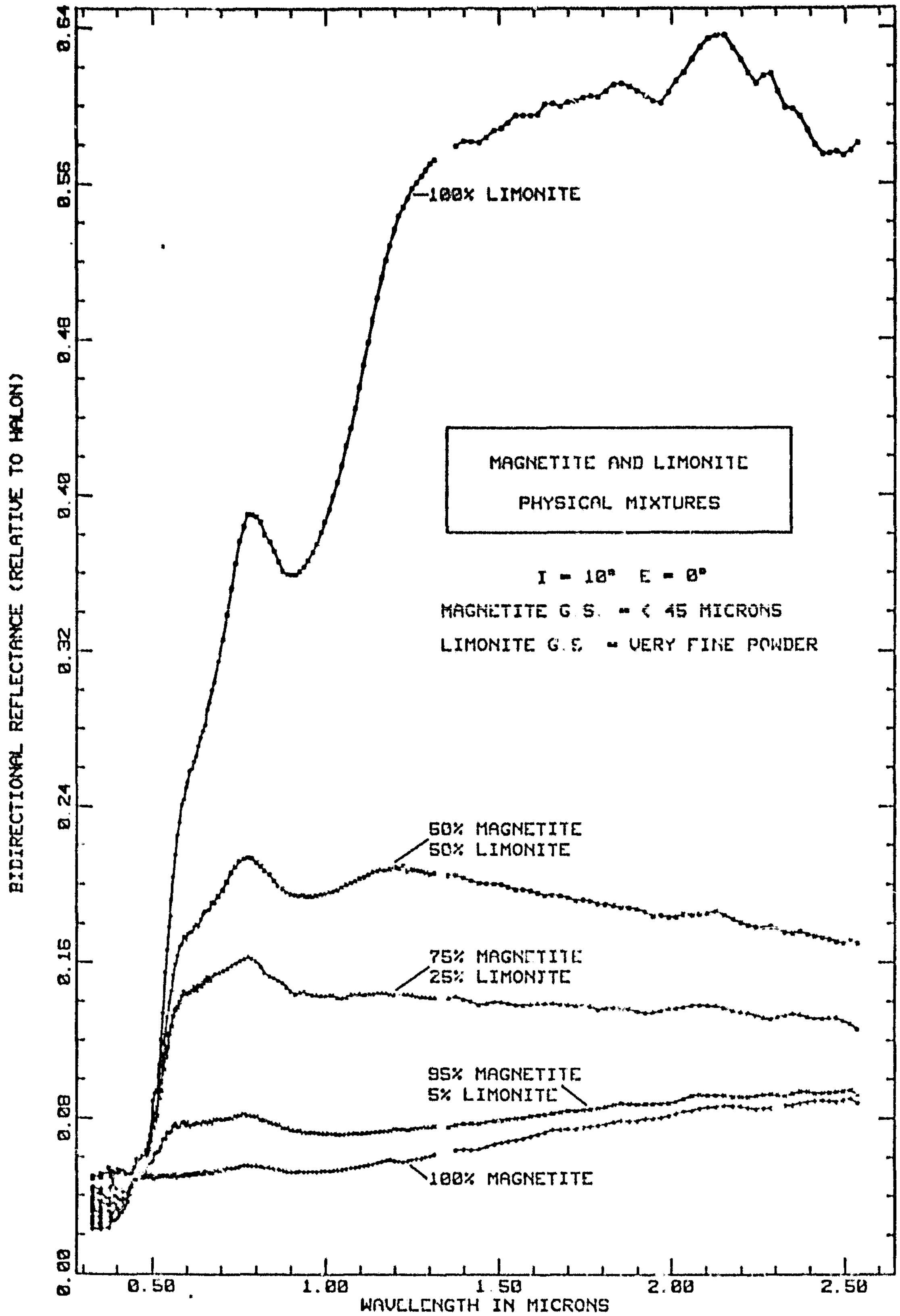

MAGNETITE AND LIMONITE
PHYSICAL MIXTURES
I = 10° E = 0°
MAGNETITE G.S. = < 45 MICRONS
LIMONITE G.S. = VERY FINE POWDER
100% LIMONITE
50% MAGNETITE
50% LIMONITE
75% MAGNETITE
25% LIMONITE
95% MAGNETITE
5% LIMONITE
100% MAGNETITE
BIDIRECTIONAL REFLECTANCE (RELATIVE TO HALON)
WAVELENGTH IN MICRONS
0.00
0.08
0.16
0.24
0.32
0.40
0.48
0.56
0.64
0.50
1.00
1.50
2.00
2.50


Figure 4

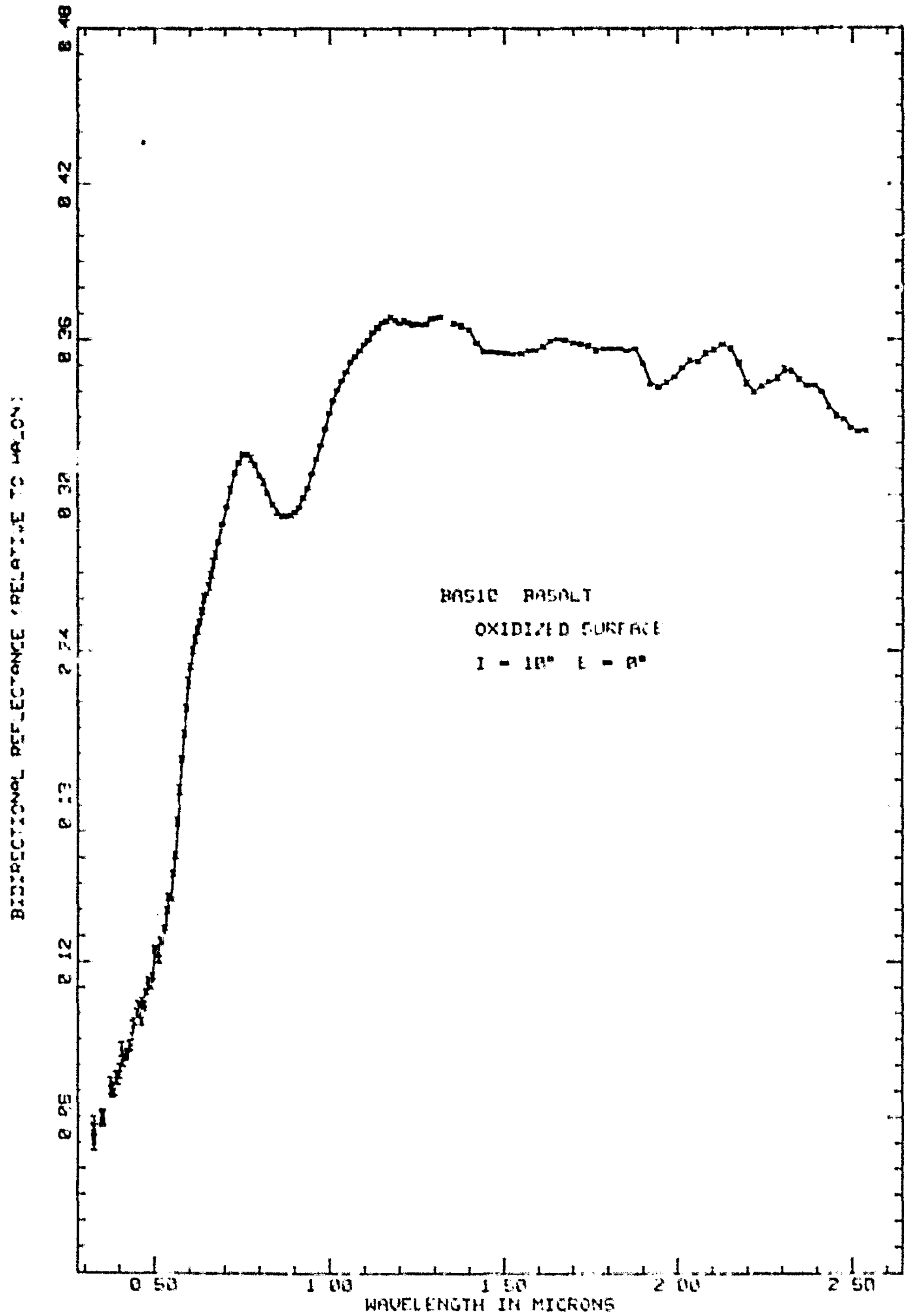
BASIC BASALT
OXIDIZED SURFACE
WAVELENGTH IN MICRONS
0 50
1 00
1 50
2 00
2 50
0 48
0 42
0 36
0 30
0 12

Figure 5a

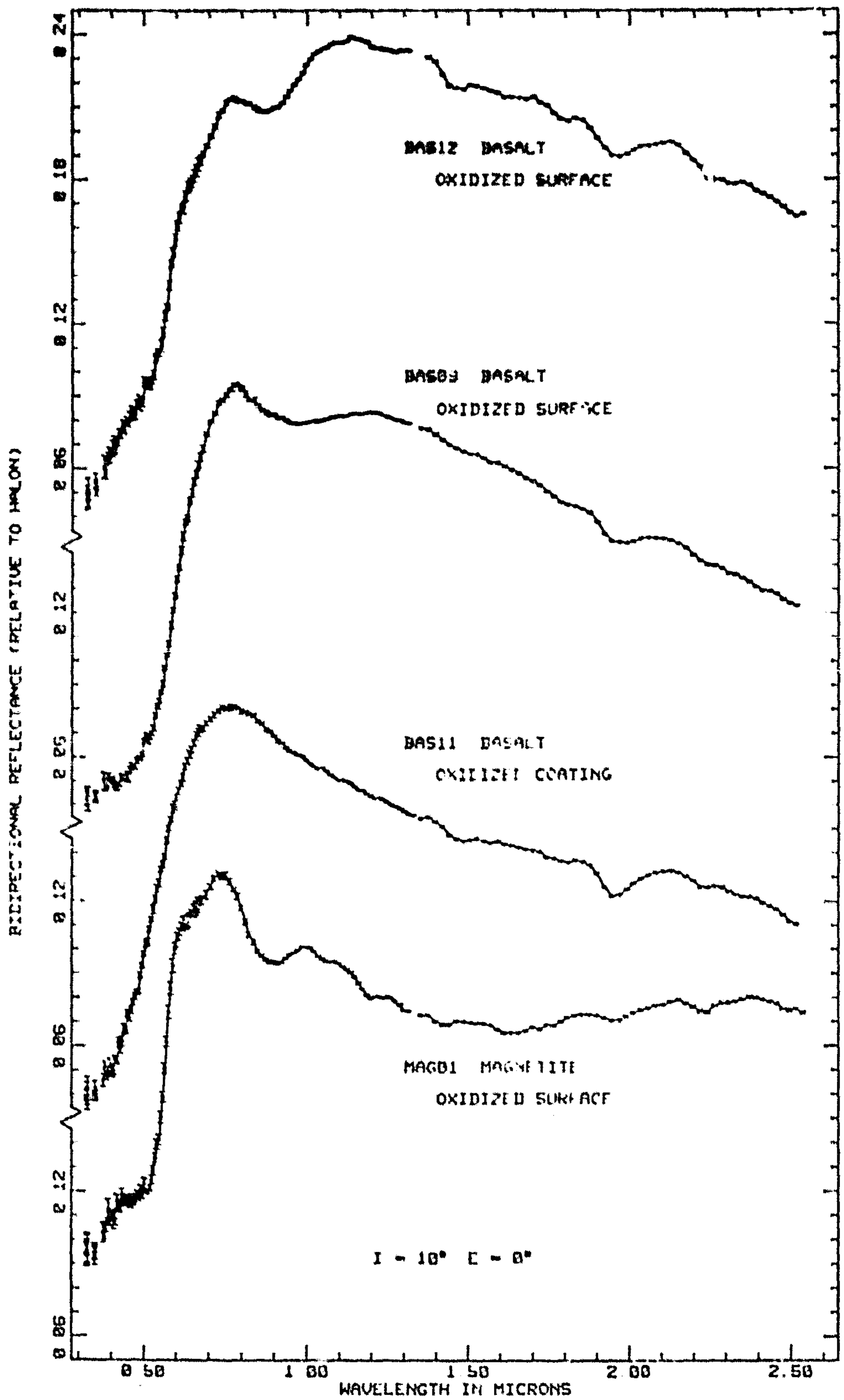
BAS12 BASALT
OXIDIZED SURFACE
BAS03 BASALT
OXIDIZED SURFACE
BAS11 BASALT
OXIDIZED COATING
MAG01 MAGNETITE
OXIDIZED SURFACE
I = 10° E = 0°
BIDIRECTIONAL REFLECTANCE (RELATIVE TO HALON)
WAVELENGTH IN MICRONS
0.50
1.00
1.50
2.00
2.50
0.24
0.18
0.12
0.06

Figure 5b

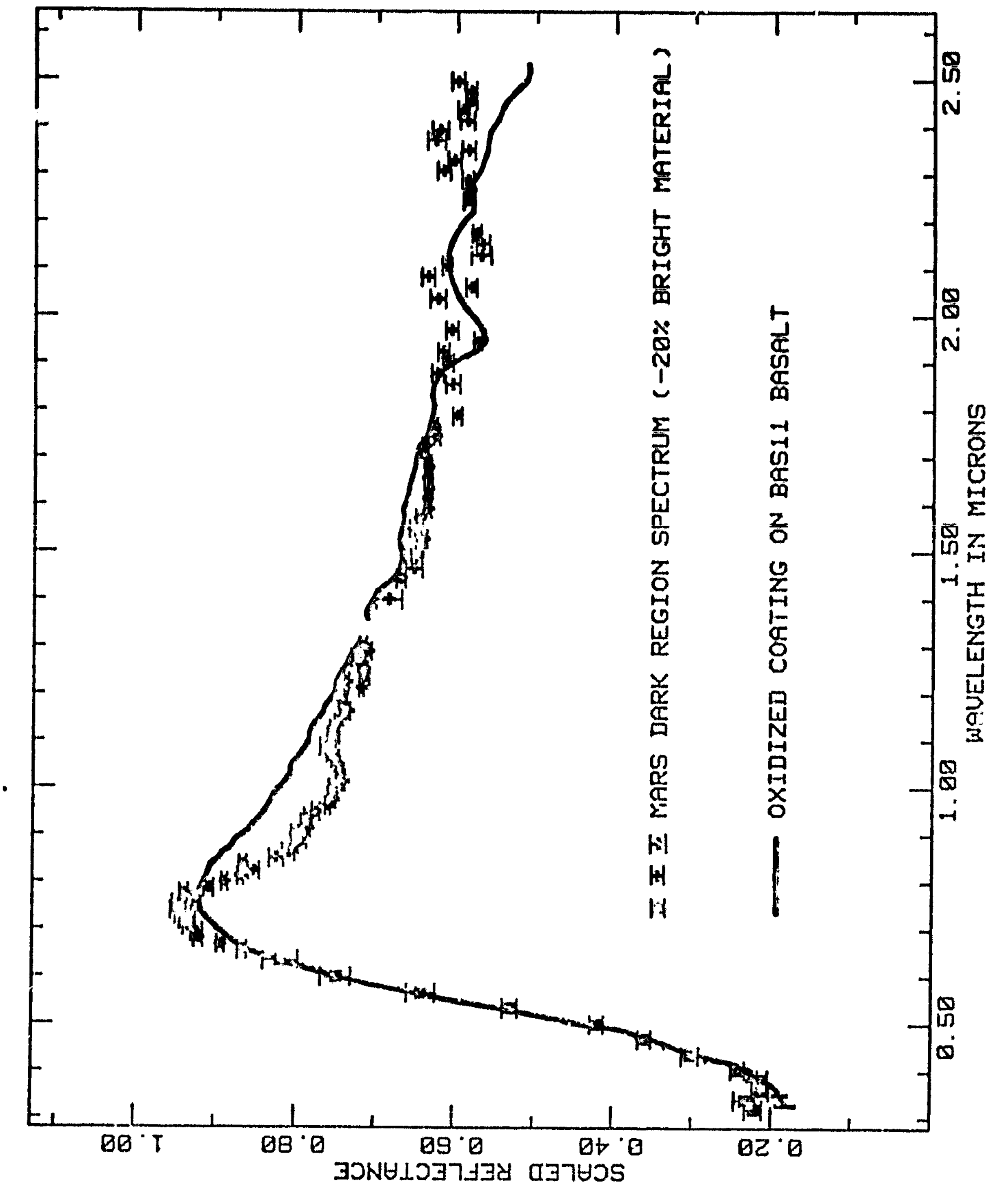
MARS DARK REGION SPECTRUM (~20% BRIGHT MATERIAL)
OXIDIZED COATING ON BAS11 BASALT
WAVELENGTH IN MICRONS
0.50
1.00
1.50
2.00
2.50
SCALED REFLECTANCE
0.20
0.40
0.60
0.80
1.00

Figure 6

# CHAPTER VI

## The Composition of the Martian Dark Regions, II: Analysis of Telescopically Observed Absorptions in Near-Infrared Spectrophotometry

This paper has been submitted to J.Geophys.Res., 1980.
Author: R.B. Singer.

## ABSTRACT

Interpretation of visible and near-infrared spectrophotometry of dark regions on Mars has shown that the dark materials consist of a close physical combination of unweathered dark rock or rock fragments coated by (or possibly mixed with) fine-grained oxidized ($Fe^{3+}$-bearing) material. Specific absorptions in new high quality near-infrared (0.65 to 2.50 μm) spectrophotometry are analyzed here more precisely than possible for previous data to determine the mineralogy and petrology of the dark materials. A spectral continuum, characteristic of a thin oxidized layer on a dark substrate, was removed from the data to isolate specific mineralogic absorptions. Non-linear least-squares fitting with gaussian band shapes defines two overlapping absorptions, centered at 0.88 and 0.99 μm. The 0.88-μm band is due at least primarily to ferric oxide in the fine-grained coating. Possible contributions to this absorption by orthopyroxene in the unweathered substrate cannot be reliably ascertained with existing data. The source of the 0.99-μm absorption is firmly interpreted to be augite clinopyroxene in the unweathered rock. Contrary to previous interpretations of other data no spectral indication of olivine or basaltic glass is found. Re-examination of previously interpreted data, in the light of recent studies of mineral-mixture spectra and dark region

spectral behavior beyond 1.1 μm, yields similar conclusions. Spectral study of terrestrial basalts implies that possibly 5% or at most 10% modal olivine could be present in observed martian dark materials without being apparent in existing reflectance spectra. Ultramafic (high-olivine) lavas such as suggested for Mars by a number of researchers are not consistent with these interpretations. Mafic igneous rock types, similar to many terrestrial basalts, seem likely to predominate in observed dark regions. Since earlier data does indicate compositional variability, obtaining high quality near-infrared observations for additional dark regions around the planet is an important task for the future.

## INTRODUCTION

All reflectance spectra obtained for dark regions on Mars show a broad absorption complex centered near 1μm, at too long a wavelength to be explained entirely by ferric oxides (McCord and Adams, 1969; McCord and Westphal 1971; McCord *et al.*, 1977; McCord *et al.*, 1980). Adams (1968) was the first to associate these features with $Fe^{2+}$ crystal-field absorptions in iron-bearing olivines and/or pyroxenes, common basaltic minerals. The details of observed absorptions vary with location on the planet (McCord *et al.*, 1977; Huguenin *et al.*, 1977, 1978; Singer and McCord, 1979) and indicate some mineralogic variety of dark surface materials. A series of experiments presented by Adams and McCord (1969) demonstrated that the general characteristics of both bright and dark region spectra from 0.35 to 1.15μm could be well reproduced by varying the grain size and degree of surface oxidation of a particular olivine-bearing basalt. This led to the conclusion that the dominant rock types on Mars are probably basaltic. Mariner 9 provided dramatic evidence of volcanism on Mars: ancient volcanic constructs, enormous relatively young shield volcanoes, and extensive lava flows. The morphology of these flows indicates very low viscosity lavas, lending support to low-silica iron-rich compositions (Carr et al., 1977). Independent conclusions supporting the presence of abundant basaltic to ultramafic rocks on Mars come from Maderazzo and Huguenin (1977) based on reflectance spectroscopy and Viking XRF data, Toulmin et al. (1977) based on Viking XRF data, and McGetchin and Smyth (1978) based on petrologic models for the martian mantle.

The most detailed mineralogic interpretations of dark region reflectance spectra previously available are provided by Huguenin et al. (1977, 1978). These are based on filter photometry and multispectral images with average bandpasses of about 300 Å and infrared coverage to wavelengths as long as 1.1μm. New near-infrared spectrophotometry (0.7 to 2.5μm) of Mars dark regions (McCord et al., 1980a) has recently become available. With increased spectral resolution and greater infrared spectral coverage these data substantially improve our knowledge of dark region spectral characteristics.

Certain aspects of the interpretation of these new infrared dark region data have been discussed in a previous paper (Part I: Singer, 1980b). A major conclusion of that work is that the overall shape of the spectrum from 0.3 to 2.5μm can be readily explained only by an intimate physical combination of an $Fe^{3+}$-bearing material which has high infrared reflectance and a darker, less oxidized material. A thin coating (estimated to be 20 to 30 micrometers thick) of the oxidized material bound to a substrate of darker unoxidized rock is the most likely physical situation for the dark materials on Mars.

Presented here are analyses of specific absorptions in the newly obtained near-infrared data and interpretation of the mineralogy of the dark substrate rocks. Previously interpreted dark region spectra are re-examined, using new laboratory reflectance studies of mineral mixtures (Singer, 1980a). Recent results are then synthesized and petrologic implications are discussed.

## DATA USED

Near-infrared (0.7-2.5μm) spectrophotometry of five dark regions on Mars, 1000 to 2000 km in diameter, were obtained during the 1978 apparition ($L_s$ = 48-50°) (McCord et al., 1980a). These spectra and an average of the three brightest region spectra observed at this time are shown in Figure 1. The instrument used was a cooled circularly variable filter (CVF) photometer with an InSb detector, mounted on the Mauna Kea Observatory 2.2m telescope. Data for this instrument are recorded in 120 spectral channels and the effective spectral resolution $(\frac{\Delta\lambda}{\lambda})$ is about 1½%. The size of the regions observed in 1978 is due to the combined effects of an unfavorable opposition and less than ideal observing conditions. These infrared spectra are nevertheless of good quality, with improved spectral resolution and coverage compared to previous observations.

Visible and near-infrared (0.3 - 1.1μm) spectrophotometry of 200 to 500 km diameter regions on the surface of Mars was obtained during the 1969 apparition ($L_s$ = 162-163°) by McCord and Westphal (1971) and during the 1973 apparition ($L_s$ = 301-302°) by McCord et al. (1977). A total of nine dark region spectra from these data sets as well as representative bright region spectra are shown in Figure 2.

Both sets of observations were obtained with double-beam photometers equipped with phototube detectors and up to 25 discrete interference filters with bandpasses on the order of 300 Å.

A composite map showing the surface locations for all data obtained in these 1969, 1973, and 1978 observing programs is given in Figure 3. Individual spectra are referred to by the year of observation and the number assigned in previous publications (McCord _et al_., 1977, 1980a).

For the interpretions which follow much use was made of laboratory reflectance studies performed by Singer (1980a) of iron-bearing mineral mixtures. The observational details for that laboratory data, as well as for the laboratory data presented here, are described in that paper.

## ANALYSIS OF ABSORPTIONS IN 1978 DARK REGION SPECTRA

The overall shape of Mars dark region spectra from 0.3 to 2.5μm has been discussed in detail in a previous paper (Singer, 1980b). The steep rise in reflectance through the visible to a peak near 0.75μm and the more gradual decline in reflectance from this peak to 2.5μm is characteristic of a trans-opaque ferric-oxide-bearing coating overlying a dark substrate. The resultant spectrum is sensitive to the composition and thickness of this oxidized layer; study of terrestrial analogs implies an average thickness of about 20 to 30 micrometers for rock coatings in observed dark regions on Mars. The absorptions at 1.34, 1.45, and 1.62μm as well as the intense absorption complex centered just longward to 2.0μm are caused by $CO_2$ gas in the martian atmosphere. Water ice features occur most strongly for bright regions and appear as broad absorptions centered near 1.6 and 2.0μm (McCord *et al.*, 1980a). The short wavelength edge of the 1.6μm ice band causes at least part of the apparent discontinuity seen in the spectra between 1.3 and 1.4μm. This also tends to be a region of lower quality data and low transmittance of the CVF. Removal of the spectral effects of patches or streaks of bright material from dark region spectra (Singer and McCord, 1979) greatly reduces indications of water ice, implying that for these observations ice was not present in significant amounts on or in the dark materials themselves (McCord et al., 1980a). The rather sharp absorption near 2.3μm is noisy but real and is present for both bright and dark regions on Mars. This feature is most likely due to a combination of OH stretch and Mg-OH bending modes (Hunt, 1977) and implies the presence of magnesian amphibole, serpentine, and or trioctohedral clay minerals (McCord et al., 1980a).

While the five dark regions observed in 1978 have similar spectral characteristics, they do differ somewhat in near-infrared spectral slope. These differences are probably due to variations in rock coating thicknesses and/or amount of bright material included in each region. Because of variations in observing conditions, region 78-10 has the highest quality spectrum and is best suited for detailed analysis. The other spectra show similarity to 78-10 in the 1-μm region but are too noisy for determination of subtle differences.

Of particular importance of interpretation of surface mineralogy and petrology is the spectral region near 1μm, actually extending from the spectrum peak at 0.75μm to beyond 1.3μm. Many diagnostic mineral features occur at these wavelengths, primarily due to $Fe^{2+}$ crystal-field transitions (e.g. Burns, 1970; Adams, 1975). $Fe^{2+}$ absorptions observed for Mars occur in ferromagnesian minerals in the dark substrate rock, visible through the semi-transparent ferric-oxide bearing coating. For spectrum 78-10 there are apparently two slightly resolved bands superimposed on the negatively sloping continuum. Examination of the other dark region spectra in Figure 1 shows similar behavior to the limit of data quality. Filter photometry from 1969 and 1973 (Figure 2) also has similar structure in the 1-μm region but exhibits more variation and will be discussed later.

To allow observed mineral absorptions to be interpretated and compared to unoxidized (uncoated) terrestrial materials it is desirable to remove a spectral continuum or baseline, which isolates and better defines the absorption features of interest (e.g. McCord _et al_., 1980c). In the case of dark regions on Mars the appropriate continuum is the spectral shape produced by a thin $Fe^{3+}$-bearing coating over a featureless dark substrate (c.f. Singer, 1980b, Figure 6).

A continuum such as discussed above was generated for spectrum 78-10 and is displayed in Figure 4a. Certain assumptions must be made in such a procedure about the details of the continuum and its fit to the data; the effects of varying these assumptions are discussed with the results. To remove the continuum shape the observed data were divided by the continuum. The results are given in Figure 4b, showing two overlapping absorptions of similar intensity and width. To better define and quantify these absorptions a non-linear least squares analysis routine was used to find the optimum fit of two gaussian bands to the data (software adapted from Kaper et al., 1966). The generated bands are mathematical gaussians in log-intensity and energy space, which is appropriate for most crystal-field absorptions. Figure 4c shows the individual gaussian components and the combined absorption envelope (converted to wavelength) overlying the data points. Band center positions are at 0.88μm and 0.99μm, with half-height bandwidths of 0.092μm (920 Å) and 0.099μm (990 Å) respectively, and nearly equal depth. Other analyses performed with reasonable variations to the continuum produced some changes in relative band depths, less variation in widths, but virtually no alteration of band center positions.

Subjectively, at least, the double nature of the absorption is based primarily on the four high data points from 0.90 to 0.94μm. The most successful single gaussian fitted to this same data is shown in Figure 4d. It can be seen that, even disregarding the high central data points, the observed feature is too steep-sided and flat-bottomed to be represented by a single gaussian band. Investigations using the gaussian fitting routine on this data set excluding the four high data points confirmed that two gaussians provide a better fit than obtainable with only one. Because data in the 0.90 to 0.94μm region appear relatively high in most of these Mars spectra (within noise limitations), a careful examination was conducted of observations of Saturn's Rings, the Galilean satellites, and Mercury taken with the same instrument (Clark and McCord, 1980a, b; McCord and Clark, 1979). Two different calibration techniques and a number of repeated observations were represented. No conclusive systematic errors were found. As will be shown below, a similar double-band structure was also observed for certain dark regions in 1973 using different instrumentation and calibration techniques. In conclusion, it appears likely that at least part of the increased reflectance observed for Mars around 0.92μm is attributable to the spectral properties of the surface materials.

Bright region spectra obtained in 1978 and 1973 have asymmetric absorptions with band minima located near 0.86 to 0.87μm. These features have been interpreted as $Fe^{3+}$ crystal-field absorptions, characteristic of many ferric-oxide-bearing materials (Huguenin, et al., 1977; McCord et al., 1980a). Because telescopic dark regions are known to contain streaks and splotches of bright material, the possibility exists that the 0.88μm band observed for dark regions is not inherent to the dark material itself. Singer and McCord (1979) have investigated some spectral effects of bright material contamination of dark regions. For spectrum 78-10, as an example, removal of the spectral contribution of up to 30% coverage by bright material leaves a recognizable two-band structure in the resultant dark material spectrum (Singer and McCord, 1979, Figure 4). Continuum removal and gaussian fitting to these "bright-material removed" spectra yields two bands with nearly equal depth and with center positions like those for the unmodified spectrum 78-10. The percentage band depths increase substantially, however, as increased amounts of bright material spectrum are removed. This implies that both the 0.88 and 0.99μm absorptions are intrinsic to the dark materials themselves.

# MINERALOGIC INTERPRETATION
## DARK REGION ABSORPTIONS OBSERVED IN 1978

It has been shown in the previous section that the dark materials observed in 1978 are characterized by two just-resolved absorptions of roughly equal depth, centered near 0.88μm and 0.99μm. Based strictly on band locations, a search of the literature suggests that the shorter wavelength band is caused primarily by a ferric oxide (with some possible contribution from an iron-poor orthopyroxene) and that the longer wavelength band is due primarily to a clinopyroxene (Hunt and Salisbury, 1970, 1971; Hunt et al., 1971, 1972, 1973; Adams, 1974, 1975).

The 0.88μm band

As has been long suspected, ferric oxides (or conceivably $Fe^{3+}$ in some other structure) are ubiquitous on Mars; they need not, however, be a major surface component to produce the observed spectral properties (Adams and McCord, 1969; Huguenin et al., 1977; Singer, 1980b). While pure ferric oxides have a prominent $Fe^{3+}$ crystal field absorption centered between 0.85 and 0.89μm, in a mineral mixture this feature may be suppressed far more rapidly than the stronger UV-visible charge transfer absorptions (Huguenin, 1979, personal communication). In addition some naturally occurring oxidation products of mafic rocks have spectra in which the 0.85-0.89μm feature is absent or reduced to a shoulder on the strong $Fe^{3+}$ charge-transfer absorption wing (Evans and Adams, 1979; Singer, 1980b). Because of these uncertainties the continuum used in the previous section for band fitting did not assume any $Fe^{3+}$ crystal-field absorption in the near-infrared.

Spectra of bright regions observed in 1978 all have asymmetric absorptions with a minimum reflectance near 0.86 to 0.87μm (no continuum removed). By shape and location these are quite certainly caused by $Fe^{3+}$ (McCord _et al._, 1980a). The correspondence between absorptions near this wavelength for 1978 bright and dark regions is very good, leading to the conclusion that the 0.88μm band observed for dark regions is at least primarily due to ferric oxide. The band position implies a somewhat hydroxylated (goethitic) net composition, consistent with previous interpretations and the observed color over most of the planet (Anderson and Huguenin, 1977; Adams, 1975; McCord _et al._, 1980b). Singer (1980b) has demonstrated that for dark materials the ferric oxide occurs as part of a fine-grained component mixed with, or more likely coating relatively unoxidized rocks or rock fragments (also see Adams and McCord, 1969; Huguenin, 1976).

It is possible that some amount of iron-poor orthopyroxene is present in the rocky components of observed martian dark materials, contributing to the ferric-oxide band and shifting the composite band minimum to slightly longer wavelengths. As has been shown by Singer (1980a), however, it is difficult to distinguish the relative spectral contributions near 0.9μm in a mixture of these two phases. The fact that the 0.88-μm band can be fit rather well with a gaussian band shape, despite the known asymmetry of ferric-oxide crystal-field absorptions, might imply some orthopyroxene component; other factors may be more important in this case, though, such as data quality and the details of the fitted continuum. Other strong evidence for ferric oxide indicates that it is the major contributor in this martian case; a definitive conclusion about orthopyroxene content in dark materials on Mars requires even higher quality data for an additional number of regions.

<u>The 0.99μm band</u>

The observed absorption centered near 0.99μm for 78-10 is best explained by clinopyroxene. Using systematics developed by Adams (1974) the composition appears to be that of an augite, with about 30 to 45 mol. % calcium, and greater than or equal to 15 mol. % ir.." Generally a pyroxene with one absorption at 0.99μm would be expected to have a second broader absorption centered between 2.15 and 2.25μm. This feature would overlap the long wavelength side of the 2μm martian atmospheric $CO_2$ absorption and would be difficult to detect with these infrared data. Removal of $CO_2$ absorptions based on a simple model atmosphere (McCord _et al_., 1980a) shows the 2.2-μm region to be fairly flat but with large uncertainties, due to data quality and imperfect removal of terrestrial and martian atmospheric effects. Higher precision data and more exact removal of atmospheric effects are required to determine the presence or absence of a pyroxene feature near 2μ. There is evidence that clinopyroxenes in general have shallower bands near 2μm than near 1μm (Adams, 1974, 1975; Gaffey, 1979 personal communication). Also, when mixed with other minerals, particularly opaques, the long wavelength band of most pyroxenes loses spectral contrast to a greater extent that the short wavelength band (Pieters, 1973; Nash and Conel, 1974). The augite structure can more easily accommodate $Fe^{3+}$ and $Ti^{4+}$ than other pyroxene structure-types (e.g: Deer _et al_., 1966); $Fe^{3+}$ content in an augite tends to increase the spectral slope and mask the 1-μm and particularly the 2-μm bands. An absorption centered between 0.75 and 0.80μm is also introduced, due to $Fe^{2+}$-$Fe^{3+}$ charge transfer (Adams, 1975). Titanium content will suppress this charge-transfer feature without masking the 1-μm band (Adams, 1975). No 0.75 to 0.80μm absorption is apparent in these dark region spectra, although if present it might be difficult to recognize superimposed on the spectrum peak. It is possible that some combination of ferric iron and titanium in this martian augite acts to diminish the 2.2-μm band while leaving the 0.99-μm band well defined. Higher quality spectral data for martian dark regions is required to further investigate these possibilities concerning detailed pyroxene chemistry.

Band widths

An anomaly of the dark region 0.88 and 0.99μm absorptions as analyzed and interpreted here is that they are spectrally resolved, and appear narrower than similar absorptions observed in the laboratory. Adams (1974) showed that for orthopyroxene-clinopyroxene mixtures an unresolved, broadened composite band occurred near 1μm, while the longer wavelength bands were sufficiently separated to be resolved. Singer (1980a) confirmed this, and additionally demonstrated that ferric-oxide/clinopyroxene mixtures also have an unresolved composite absorption centered at some wavelength between the endmember band positions. These discrepancies in apparent band width do not seem so severe as to alter the mineralogic interpretations presented above; nevertheless one or more mechanisms must be invoked to explain the differences. Variation in particle size changes spectral contrast but is not expected to alter the sharpness of sepctral features. This is generally borne out by examination of spectra with differing particle sizes, such as presented by Hunt and Salisbury (1970). In two cases, however, there does appear to be some sharpening of spectral detail with reduced grain size: amphibole S-1C and chlorite S-7B. A perhaps more important mechanism is the reduction of vibrational amplitude with reduced temperature of $Fe^{2+}$ cations about their mean lattice positions. Thermal vibrations contribute to the broadness of crystal field bands by rapidly varying the metal-oxygen distances, and therefore the energy of the $Fe^{2+}$ interelectronic transitions (Burns, 1970). While some very low temperature transmission spectra have been measured for ferrosilicates (e.g. Runciman *et al*., 1973) there is an additional need for laboratory diffuse reflectance measurements of rock forming minerals and their alteration products at realistic temperatures for Mars and the outer solar system.

The olivine question

Olivine has previously been identified from dark region reflectance spectra (Adams and McCord, 1969; Huguenin *et al.*, 1977, 1978) and might reasonably be expected from petrologic arguments (McGetchin and Smyth, 1978). A careful study including new laboratory data for mineral mixtures (Singer, 1980a) and terrestrial basalts has shown, however, that there is no indication of olivine in the 1978 dark region spectra The question of how much olivine can be present but spectrally undetectable in a basalt is also addressed below.

Because olivine is considerably more transparent than equivalently-sized pyroxenes, mixtures of these minerals tend to have spectra dominated by pyroxene characteristics. Olivine content causes some shift of the 1-μm band minimum to longer wavelengths, increases near-infrared spectral slope (reducing 2-μm band contrast), and most importantly broadens the long wavelength side of the pyroxene band near 1μm. This broadening is primarily caused by the 1.3μm component of the three-part olivine absorption envelope (see Singer, 1980a, for details and spectra; also Adams, 1974; Gaffey and McCord, 1979). The absorption envelope for low-iron olivine is very broad compared to pyroxene absorptions near 1μm.

with more fayalitic olivine (higher iron content), as has been proposed for Mars (McGetchin and Smyth, 1978), the 1.3μm olivine absorption becomes stronger, broadening the total feature even further (Hunt and Salisbury, 1970; Adams, 1975).

Plagioclase can also produce a weak band centered near 1.25 to 1.30μm, caused by $Fe^{2+}$ impurities (Hunt and Salisbury, 1970; Adams, 1975). Because of the great transparency of plagioclase relative to olivine and pyroxene this band is generally suppressed in spectra of rocks and mineral mixtures, but can appear as a shoulder or weak depression near 1.3μm in spectra of assemblages with very abundant plagioclase (Nash and Conel, 1974; Adams, 1974).

The spectral effects of olivine in mafic assemblages were also studied by examination of terrestrial basalts, in an effort to determine how much olivine content is necessary in fine-grained igneous rocks to produce an unambiguous olivine spectral signature. The reflectance spectra of three powdered rocks are presented in Figure 5; grain size was 45 to 90 micrometers and phase angle ($\alpha$) was 10°. Thin sections were used to observe the occurrence of olivine and other major minerals.

BAS06 is a Servilleta olivine tholeiite from Taos Plateau, N.M., similar to samples discussed by Dungan et al. (1980). This is a massive basalt with olivine phenocrysts (1mm and less in length) and very abundant plagioclase laths (1/2 to 1mm long) set in a fine-grained (0.05 to 0.20 mm) groundmass of primarily pyroxene and plagioclase. Opaques are abundant (estimated $\geq$ 10%) and occur as 0.1 to 0.2mm grains concentrated in bands. Olivine content is estimated to be as much as 10%, in general agreement with olivine norms given by Dungan et al. (1980) for similar Servilleta basalts.

BAS01 is a tholeiitic basalt from Mauna Loa, Hawaii. It is slightly vesicular, with phenocrysts of olivine (1 to 3mm diameter), very abundant plagioclase (1/2 to 1mm long) and less abundant pyroxene (2 to 3mm diameter) set in a very fine-grained ( 0.05 to 0.10mm) ground mass of plagioclase, pyroxene, and opaques. The abundance of opaques is high (estimated $\geq$ 15%) and they occur as very small, evenly distributed particles. Despite the prominence of olivine crystals in hand samples of this rock, total olivine content is estimated to be somewhat less than the 5% required for definition as an olivine basalt (MacDonald, 1949).

UWE01 is a highly vesicular tholeiite from

Kilauea, Hawaii, similar in some respect to BAS01. The phenocrysts of olivine and pyroxene are smaller than in the previous sample but somewhat more abundant. Plagioclase laths are of quite uniform length (0.2 to 0.3mm long) with larger and smaller crystals nearly absent. The groundmass as a whole is coarser than BAS01, averaging greater than 0.1mm. Opaques are about as plentiful as in BAS01 but are less evenly distributed, tending to occur in aggregates. Olivine content is probably slightly greater than for BAS01, perhaps making UWE01 technically an olivine basalt.

Spectrally, these rocks have certain characteristics in common (Figure 5): they have well-formed absorptions centered near 1μm, and less well-formed shallower absorptions at 2μm and beyond. A closer examination shows that the 2-μm regions include two partially resolved bands, one near 2.2 to 2.3μm (clinopyroxene) and one closer to 2.0μm (orthopyroxene or pigeonite). Additional features, frequently seen in spectra of basalts and basalt powders but not yet well understood, complicate reflectance around 2μm compared to simple mineral mixtures (c.f. Singer, 1980a). As expected from previous laboratory studies (Adams, 1974; Singer, 1980a) the two pyroxene absorptions near 1μm are not resolved and combine to form one composite band, relatively stronger than the bands near 2μm. Because these are tholeiitic basalts it is reasonable that two pyroxenes are present (Deer <u>et</u> <u>al</u>., 1966; Nockolds <u>et</u> <u>al</u>., 1978). Spectral differences among these rocks include near-infrared spectral slope, relative band depths, overall reflectance, and behavior of the long wavelength shoulder of the 1-μm band.

Increased olivine content has the property of increasing the near-infrared spectral slope for many mineral mixtures. Here BAS06, with the highest olivine content, has the steepest slope. UWE01, however, with a slightly greater olivine content than BAS01, has the least slope. Factors controlling <u>apparent</u> mineral abundances in the spectra of natural assemblages include relative actual abundances, compositions, mineral grain sizes, and rock particle size. Apparently factors such as phenocryst size or groundmass crystal size are in this case more significant in controlling spectal slope than is a difference of few percent in olivine content.

To circumvent certain complications which varying slope and reflectance add to spectral comparisons it is desirable to fit and remove a spectral continuum for each curve, similar to the technique used earlier for Mars. The continua shown in Figure 5 consist of a constant slope in the infrared smoothly blended into the visible charge-transfer absorption characteristic of iron-bearing silicates; they were generated using interactive mathematical-operation and cubic-spline-interpolation routines (Clark, 1980). Clearly the exact choice of continuum is somewhat subjective, but it is not arbitrary. Keeping in mind the nature of the uncertainties involved, continuum removal is a valuable tool for interpretation of spectral data (c.f. McCord et al., 1980c).

The three basalt spectra divided by their respective continua are shown in Figure 6. The striking difference is the broad absorption shoulder extending from 1.15μm to beyond 1.5μm for BAS06. This is caused primarily by the 1.3-μm component of the olivine absorption discussed above. A small part of this feature is probably also due to $Fe^{2+}$ in plagioclase, which as discussed above has much weaker absorbance than olivine but which is also more abundant than olivine in this rock. By comparison the spectra of BAS01 and UWE01 have minor absorptions around 1.3μm; this is consistent with their lower spectral slopes and olivine contents. The observed shoulders for the Hawaiian basalts may in fact be largely due to the abundant plagioclase rather than olivine.

These three cases are only a very small sampling of terrestrial basalt types but nevertheless can provide an approximate lower limit for unambiguous olivine determination in fine-grained mafic rocks. BAS01 has the lowest reflectance for this group (Figure 5) but the greatest spectral contrast (Figure 6). The slight infrared continuum slope is probably at least partially controlled by the olivine content of roughly 3%. The shoulder near 1.3μm is, however, not very prominent, and may be primarily due to the abundant ( 40% of greater) plagioclase, as discussed above. By contrast UWE01, with perhaps 5% olivine, is slightly brighter overall but has reduced spectral contrast and a flat infrared continuum. This spectrum also shows little conclusive evidence of olivine. BAS06, with about 10% olivine content and similar plagioclase content to the other basalts, is also somewhat brighter overall and shows a very strong olivine signature. These three examples certainly do not cover all possibilities but do show that up to about 5% olivine content can be spectrally unapparent, while 10% olivine is very apparent spectrally in another rock. Unknown at present is what, for instance, the spectrum of UWE01 would be like if the sample contained 10% olivine rather than 5%. Nevertheless it appears that an olivine content of between 5 and 10% is about the maximum that a mafic igneous rock can have without showing a clear indication of olivine in its reflectance spectrum.

The continuum-removed spectrum for dark region 78-10 (Figure 4) is shown overlaid in Figure 7 by similarly treated spectra of basalts BAS06 and UWE01. The terrestrial basalt spectra have been contrast reduced by adding a constant and then rescaling (dividing by a constant). This method has been shown to yield nearly correct qualitative results for olivine opaque-mixtures in the 1-μm region (Singer, 1980a). The relative weakness of martian absorptions compared to those for terrestrial basalts is presumably due to partial spectral masking by the oxidized surface coatings and perhaps by dark, less spectrally featured components in the rocks. Spectrum 78-10 does not show any indication of a shoulder or broadening on the long wavelength side of the 0.99-μm absorption. From 1.07 to 1.30μm the continuum-removed data show considerable scatter but have a high average relative reflectance (∿1.0). The absorption for BAS06, in contrast, is broader, occurs at a longer wavelength, and has a low relative reflectance out to 1.3μm and beyond. These are all indications of olivine. The spectrum for UWE01 shows little or no sign of olivine and more closely matches 78-10. This basalt absorption is less broad than for BAS06, has its reflectance minimum at a shorter wavelength, and has risen to almost continuum reflectance by 1.2μm.

Modification of the 78-10 continuum in any believable manner does not produce apparent absorption in the 1.2- to 1.3-μm region. With the effects of 20 to 30% bright material removed from spectrum 78-10 (Singer and McCord, 1979) some continua can be fit which define a possible band shoulder between 1.1 and 1.3μm, but confidence in this feature is limited by the noise in the data. These continua are not the ones which provide the most precise fitting of gaussians to the 0.88- and 0.99-μm bands. Improved data are required to further investigate the reality of such subtle features. Nevertheless the amount of olivine that would be indicated by such a weak shoulder is small.

In conclusion, observations for dark region 78-10, and by similarity other dark regions observed in 1978, do not show spectral indications of olivine in the martian surface rocks. As discussed above, olivine in quantities up to 5% or even 10% might exist in these dark materials and still escape detection in existing data. However, the 35 to 40% high-iron olivine contents for martian lavas proposed by Maderazzo and Huguenin (1977) and McGetchin and Smyth (1978) are not consistent with these spectral reflectance observations.

## Volcanic glass

Basaltic glasses have overall reflectances similar to basalts and two generally shallow and very broad $Fe^{2+}$ absorptions, located at or slightly longward of 1 μm and at or slightly shortward of 2 μm (see Adams, 1975, for examples). Because of the width and position of the shorter wavelength band it can be seen that such glasses cannot be providing a significant spectral contribution to the dark regions observed in 1978. Because of the usual weakness of glass bands, however, it is nevertheless possible that some glassy basaltic material is present but not spectrally distinguishable with current data.

## RE-EXAMINATION OF DARK REGION SPECTRA OBTAINED IN 1969 and 1973

Mineralogic interpretations of the 1969 and 1973 dark region spectra (~0.3 to 1.1 μm) have previously been published by Huguenin et al. (1977) describing the spectral features and their probable interpretations. Huguenin et al. (1978) used these data and multispectral imaging to define and characterize compositional units based on the presence and relative abundances of mineral classes. In light of new laboratory studies of mineral mixtures (Singer, 1980a) and the 1978 near-infrared dark region data discussed at length above and by Singer (1980b) it seems appropriate to re-examine the earlier data and their interpretations.

The reflectance spectra obtained in 1969 and 1973 do not lend themselves to band fitting because of their lower spectral resolution and the lack of spectral coverage much beyond 1 μm. Some of the data in particular have rather large formal errors. Despite these limitations these spectra as a whole provide useful information about spatial and temporal variability of martian dark regions.

The question of olivine content must be discussed for these data as well, because of its petrologic importance and because most previous interpretations have concluded that olivine (or glass) is as abundant or more abundant than clinopyroxene. Data which extends to only 1.05 or 1.10 μm cannot fully define the long wavelength side of a band near or longer than 1 μm (such as clinopyroxene). This makes olivine determination, which is largely based on band asymmetry as discussed in the previous section, somewhat uncertain. A common assumption for observations from 0.3 to 1.1 μm of many astronomical objects has been that when the reflectance for the last few filters (1.0 to 1.1 μm) is low, olivine is present, because its absorptions extend to longer wavelengths than pyroxenes (glasses will be discussed below). This assumption is not unreasonable, when used with caution, for objects with flat or positively sloping spectral continua such as many asteroids (e.g. Gaffey and McCord, 1978).

The near-infrared spectral shape for dark regions on Mars, however, has only recently been well determined (McCord _et_ _al_., 1980a) and has a negatively sloping continuum. In defining the mechanism responsible for this shape, Singer (1980b) showed that the details of the negative slope depend on the thickness and composition of the oxidized rock coatings, and therefore might be expected to vary around the planet. A conclusive determination of olivine, then, requires the definition and removal of the appropriate spectral continuum. This is not rigorously possible for data which does not extend beyond the absorption(s) in question, although some estimate may be made based on newer data with full near-infrared coverage. Many aspects of the discussion above also apply to the identification of basaltic glass based on the 1.00 to 1.15 μm band, although as mentioned in the previous section the very broad and shallow nature of glass bands implies that they might be more easily masked than most mineral absorptions.

An absorption between 0.85 and 0.90 μm is present for all 1973 spectra but absent for most of the 1969 spectra, including the bright regions (refer to Figure 2). Huguenin et al. (1977) have suggested that this feature is due to ferric oxide in contaminant dust, on the surface and in the atmosphere, because 1973 observations were made during the initial stages of a global dust storm originating in Solis Planum. The 1969 observations were made during a clear period ($L_s$=162-163$^o$). All 1978 observations have significant absorptions near 0.87 to 0.88 μm, but atmospheric transparency at this time ($L_s$=48-50$^o$) was also high, having fully recovered from the previous dust storms (Viking lander measurements, Pollack et al., 1979). This correlates with evidence discussed previously that $Fe^{3+}$ absorptions not only originate on the surface but are likely to be characteristic of the surface coatings bound to rocks and rock particles. This difference between 1969 and other observations remains unresolved and warrants additional attention in the future. In addition, 1969 bright regions have an absorption centered near 0.95 μm, not apparent for bright regions observed in 1973 and 1978. As discussed by Huguenin et al. (1977) this may indicate incomplete masking of a ferro-silicate surface component in these bright regions. This could be a spatial and/or temporal effect. Repeat coverage of region 69-2 by the larger region 78-5 (Figure 3) does not show identical spectral properties; nevertheless of all the bright regions observed in 1978, 78-5 is the only one which appears to have some dark region characteristics McCord et al., 1980a).

The spectra for regions 73-22, -24, and -26 are quite similar, particularly in the infrared, and have no analog amoung the 1969 spectra. This group is characterized by a drop in reflectance from 0.84 to 0.87 μm, a smooth gradual increase in reflectance to 0.93 μm, a drop in reflectance to 0.97 μm, and another smooth gradual increase in reflectance out to 1.06 μm. The three regions in this group were observed on the same night as was 73-20, which is significantly different spectrally. A comparison of the 73-22, -24, and -26 average to spectrum 78-10 is shown in Figure 8. It can be seen that these 1973 data have a similar double structure to that observed in 1978, adding support to the validity of these resolved absorption bands. The 1973 spectra are consistent enough with spectrum 78-10 to justify a similar mineralogic interpretation. The long wavelength absorption might be centered at a slightly shorter wavelength for these 1973 data, which would indicate a lower calcium clinopyroxene (augite) composition. The 1973 spectra also have flatter slopes in the infrared which could be explained by differences in bright material coverage of the various areas (Singer and McCord, 1979) or by differences in thickness and/or composition of the rock coatings (Singer, 1980b). Calibration differences between the two sets of observations cannot be entirely ruled out, however, as contributing to the differences in slope. Working with criteria discussed at great length above, no convincing evidence is found in these three 1973 spectra for orthopyroxene, olivine, or basaltic glass. This does not eliminate the possibility that they occur in quantities too low to be detected with these data.

Regions 73-21 and 73-25 have considerable overlap on the surface, were observed within 30 minutes of each other (McCord _et al._, 1977), and are spectrally quite similar but not identical. The abruptness of some of these spectral differences implies that the uncertainty in the data is larger than indicated by the formal error bars. Averaging these two observations smooths out some of these discontinuities and shows more clearly a two-band structure. While there appear to be real differences between these two spectra and the ones previously discussed, the data are not felt to be of sufficiently high quality to discuss specific mineralogic differences. As pointed out by Huguenin et al. (1978), spectrum 69-5, despite large formal errors, is similar to 73-21 and 73-25. 69-5 has only a very shallow band near 0.85 μm but a deep, well defined band at 1.0 μm. Again, neither 69-5, 73-21, or 73-25 shows unambiguous spectral indications of olivine.

Spectrum 69-6 has a single shallow depression at wavelengths longer than 0.85 μm. If a typical dark region continuum is sketched in (c.f. Figure 4a) connecting the spectral peak and the longest wavelength data point a broad band with a center wavelength near 0.96 is defined. This could be caused by a single pyroxene (low-calcium augite) or a composite of two pyroxenes in roughly equal quantitites (higher-calcium augite and pigeonite or hypersthene). Without specific knowledge of a continuum more correct than the one assumed above, there is no spectral evidence here for olivine.

Area 73-20 is unique in that its spectrum displays a double structure in the near-infrared (minima at about 0.87 and 0.99 μm) superimposed on a rather flat near-infrared continuum compared to other dark region spectra (Figure 2). The visible slope of spectrum 73-20 clearly identifies it as a dark region, however (McCord et al., 1977). While Huguenin et al. (1978) attribute the suppression of the 0.75 μm peak to titanium content in a clinopyroxene, the work by Adams (1975) indicates that $Fe^{3+}$ in the pyroxene might be a more likely mechanism. An $Fe^{2+}$-$Fe^{3+}$ charge transfer occurs between 0.75 and 0.80 μm which might function to flatten the peak. Laboratory studies of such pyroxenes in dark region simulations would be desirable to test these possibilities. It would be interesting to know the near-infrared (to 2.5 μm) spectral behavior of region 73-20; if the continuum remained level or rose into the infrared, a very different relationship between rocks and oxidized materials would be implied for this region (c.f. Singer, 1980b).

The remaining three spectra, 73-23, 69-7, and 69-4, (Figure 2), differ substantially but have in common relatively featureless negatively slopes near the 1-μm region. Spectrum 73-23 bears a strong resemblance up to 1 μm to 73-21 and 73-25, although it was observed on a separate night and is not for a region located near the other two. Spectral comparisons based primarily on the data for the last filter (73-25) or two filters

(73-21), a somewhat risky proposition, show that spectrum 73-23 appears to have additional absorption beyond 1 μm and therefore may be showing spectral indications of olivine. Once again, however, without further infrared coverage to define the spectral continuum, such an interpretation is not very firm. Spectrum 69-7, although having rather large error bars, has relatively low reflectance from 0.93 to 1.10 μm. The primary cause could be either multiple overlapping ferromagnesian absorptions (clinopyroxene and olivine) in the underlying rock or a steeper negatively-sloping continuum characteristic of a thinner or otherwise more transparent coating on the rock surfaces. The fact that 69-7 also has a relatively low visible spectral slope (McCord _et al._, 1977) lends support to the latter possibility. Spectrum 69-4 is unique in that it has a sharp reflectance peak located at a shorter wavelength than other observed dark regions. This spectrum also has a rather uniform steep negative slope in the near-infrared. The source of these spectral differences are not yet well understood. It would be desirable to obtain additional spectral data for Acidalium Planitia and other dark regions in the northern hemisphere to see whether 69-4 is representative of a different class of dark materials.

In conclusion, the greatest value of 1969 and 1973 spectral data is that they indicate mineralogic diversity in the mafic surface components and perhaps variation in coating/mixing geometries for dark regions around more than half the planet. Because of limitations in spectral resolution and coverage, and in some cases data quality, specific mineralogic interpretations should be made and used cautiously. The discussion here of olivine in particular has been perhaps somewhat conservative, but this seems appropriate for an issue of such petrologic importance.

# SYNTHESIS AND DISCUSSION

The telescopic martian dark regions have been found upon closer inspection to consist of large scale intermixtures of bright soil, much of which is probably aeolian dust deposits, and dark material. Reflectance studies indicate that areal coverage of spectroscopically observed dark regions by bright materials does not exceed 40%, and is probably more generally 20 to 30% maximum (Singer and McCord, 1979). For regions studied the dark materials themselves consist of an intimate physical association of very fine-grained $Fe^{3+}$-bearing material with relatively high near-infrared reflectance and darker relatively unoxidized mafic rock or rock fragments. While these two components could exist finely intermixed in a soil, a number of lines of evidence indicate that the usual occurrence is probably a thin coating (about 20 to 30 micrometers thick) of oxidized material physically bound to the rock surfaces (Singer, 1980b; cf. Huguenin, 1976). With this type of coating geometry the spectral properties of dark materials are largely independent of partical size, from sand ( $\sim \frac{1}{2}$ mm) up to boulders and larger. The oxidized coatings seem likely to be derived by alteration of the underlying rocks, although deposition of genetically unrelated dust has not been ruled out. The oxidized coating material is spectrally similar to bright regions and airborne dust (Singer, 1980b), although Viking orbiter three-color mapping has shown certain dark regions, not yet measured spectroscopically, which are unusually red (Soderblom et al., 1978) and may represent a different weathering process (McCord et al., 1980b).

The rocks underlying the coatings are dark and generally clinopyroxene-bearing. The shallow depth of the pyroxene bands combined with the low overall spectral reflectance indicates that opaque minerals such as magnetite are probably abundant. Regional variation in clinopyroxene band position indicates differing compositions, mainly augites with varying calcium and iron content. Low calcium clinopyroxene (pigeonite) and orthopyroxene may be present in some regions but are not unambiguously detected in existing data. Low- and moderate-iron orthopyroxenes (enstatite, hypersthene) are particularly difficult to detect in current data because of interference from ferric-oxide absorptions. $Fe^{2+}$ absorptions from olivine or basaltic glass are not apparent in new near-infrared dark region spectra and do not seem unambiguously evident in earlier observations either, contrary to previous interpretations (Huguenin et al., 1977, 1978). Nevertheless it seems likely that quantities of olivine as great as 5% or even 10% could be present in observed dark regions without being apparent in these spectral data. Some amount of basaltic glass may also be present, particularly for dark regions which show less spectral detail near 1 μm. Phases which have subtle spectral signatures, such as plagioclase feldspars, are not apparent in existing data but cannot be excluded either. The overall conclusion is that the rocks in observed dark regions on Mars are primarily basaltic, with regional variation in mineralogy but without abundant olivine present. Based on studies of the spectral properties of terrestrial basalts, an ultramafic composition for martian lavas is not required to explain the spectral properties of the regions observed.

The primary discrepancies between these conclusions and results of some other workers in the field concern olivine content and the related question of silica content. The suggestion by Maderazzo and Huguenin (1977) that the average crustal composition is unsaturated picrite basalt (low silica, high olivine) is based in part on the identification of abundant olivine in most 1969 and 1973 dark region spectra. If olivine is in fact not prevalent over much of the surface these conclusions require modification. Low olivine content (5 to 10% or less) would imply lavas which are less mafic and perhaps silica saturated (tholeiitic), although a pyroxenite source rock for martian soils has recently been proposed (B.C. Clark, personal communication, 1979). The Viking XRF analyses at both landing sites show soils high in iron and low in silica, alumina, and potassium (Clark et al., 1977) These characteristics have been interpreted to indicate that the soils are largely alteration products of mafic igneous rocks (Toulmin et al., 1977); an ultramafic parent composition is not required in this case either.

Working from estimates of mantle densities McGetchin and Smyth (1978) calculated mineral assemblages for the martian mantle particularly rich in olivine compared to the earth's mantle. Partial melting of such a martian assemblage was calculated to yield an ultramafic ($SiO_2$=41 to 44%) picritic alkalic basalt lava with 37% normative high-iron olivine, similar to that suggested by Maderazzo and Huguenin. Such a low silica lava is attractive because it has very low viscosity, consistent with the morphology of volcanic features observed on Mars (Carr et al., 1977). If the martian crust were predominantly of this composition the soils sampled by Viking could consist of relatively unweathered material. Weighing against this possibility is strong spectral and albedo evidence that soils such as seen at the landing sites are related to global dust and are heavily weathered (e.g. Adams and McCord, 1969: McCord et al., 1977; Maderazzo and Huguenin, 1977; Evans and Adams, 1979).

The primary martian lavas predicted by McGetchin and Smyth (1978) would contain much more olivine than is apparent spectrally. Two variables are discussed by those authors which could substantially reduce surface olivine content. They state that sulfur reactions with olivine in the interior could produce an olivine depleted mantle assemblage of clinopyroxene, orthopyroxene, oxide, and sulfide. Viking XRF measurements indicate that at least the soils at the landing sites contain abundant sulfur (Clark et al., 1977). McGetchin and Smyth (1978) also state that an assumption of abundant volatiles in the martian interior would cause partial melting to occur at lower temperatures, and low-olivine silica-rich lavas (tholeiitic basalts or even andesites) could be generated as early partial melts. These lavas would also have relatively low viscosity due to their high volatile content. Surface depletion of olivine could have been brought about even with olivine-rich partial me... if crystal settling occurred in either a subsurface cummulate stage or in thick surface flows In either of these cases regional variation in surface olivine content would be expected, since materials from various depths should be exposed by impact and erosional processes. This possibility can be readily explored as additional high-quality near-infrared spectrophometry becomes available for more dark regions on Mars.

Thermodynamic studies of chemical weathering in the present martian environment, such as performed by Gooding (1978), show that mafic igneous assemblages are not stable. The same statement is certainly true for the earth, yet even with its far more active weathering environment there is no lack of exposed igneous rock, some quite ancient. The point, also discussed by Huguenin (1976) and Gooding (1978), is that other factors such as reaction rates and physical geometry can be more significant on a practical level than ultimate thermodynamic stability. Relatively unaltered mafic igneous materials currently exist over much of the martian surface. Many of these regions are ancient, as indicated by cratering density. Reaction rates for weathering of mafic rocks on Mars, then, would appear to have proceeded quite slowly on the average over geologic time. This is consistent with the existance of alteration layers 20 or 30 micrometers thick on martian rocks, which would severly inhibit reaction rates for further gas-solid weathering (Huguenin, 1976; Singer, 1980b).

Visible and near-infrared spectrophotometry of regions on Mars has proven to be an exceedingly useful tool for investigating the martian surface. For a number of years to come it will be our primary source of mineralogic and other compositional information. The field is approaching being data-limited; the further investigation of many specific geologic problems requires new observations. While high spatial resolution, as would be provided by spacecraft observations, is a major goal for the future, the enormous value of earthbased telescopic observations has been proven repeatedly over the past 10 years. Observations of this type should continue as a high priority task in the future.

## ACKNOWLEDGEMENTS

The author is grateful to T. McCord, J. Adams, R. Huguenin, R. Burns, M. Gaffey, R. Clark and R. Hawke for helpful discussions and reviews of the manuscript. Discussions with C. Pieters and L. McFadden were also of great value. Thanks go to C. Pieters for supplying the Servilleta basalt sample. Much of this work was performed while at the Institute for Astronomy, University of Hawaii. This research was funded by NASA grant NSG # 7590

## REFERENCES


Adams, J.B., Lunar and Martian surfaces: Petrologic significance of absorption bands in the near-infrared, Science, 159, 1453-1455, 1968.

Adams, J.B., Visible and near infrared diffuse reflectance spectra of pyroxenes as applied to remote sensing of solid objects in the solar system, J. Geophys. Res., 79, 4329-4336, 1974.

Adams, J.B., Interpretation of visible and near-infrared diffuse reflectance spectra of pyroxenes and other rock forming minerals, in Infrared and Raman Spectroscopy of Lunar Terrestrial Minerals, C. Karr, Jr., ed., Academic Press, 91-116, 1975.

Adams, J.B., and T.B. McCord, Mars: Interpretation of spectral reflectivity of light and dark regions, J. Geophys. Res., 74, 4851-4856, 1969.

Anderson, K.L., and R.L. Huguenin, Photodehydration of martian dust, (abstract) Bull. Am. Astron. Soc., 9, 449, 1977.

Burns, R.G., Mineralogical applications of crystal-field theory, Cambridge University Press, London, 1970.

Carr, M.H., R. Greeley, K.R., Blasius, J.E. Guest, and J.B. Murray, Some martian volcanic features as viewed from the Viking orbiters, _J. Geophys. Res._, _82_, 3985-4015, 1977.

Clark, B.C., III, A.K. Baird, H.J. Rose, Jr., P. Toulmin III, R.P. Christian, W.C. Kelliher, A.J. Castro, C.D. Rowe, K. Keil, and G.H. Huss, The Viking X-ray fluorescence experiment: Analytical methods and early results. _J. Geophys. Res._, 82, 1977.

Clark, R.N., A large scale interactive one dimensional array processing system, _Pub. Astron. Soc. Pacific_, in press, 1980.

Clark, R.N., and T.B. McCord, The Galilean satellites: Near-infrared spectral reflectance measurements (0.65-2.5μm) and a 0.325-5μm summary, _Icarus_, in press, 1980a.

Clark, R.N., and T.B. McCord, The rings of Saturn: New near-infrared reflectance measurements and a 0.326-4.08μm summary, _Icarus_, submitted 1980b.

Deer, W.A., R.A. Howie, J. Zussman, _An introduction to the rock forming minerals_, John Wiley and Sons, New York, 1966.

Dungan, M.A., P.W. Lipman, S. Williams, and V.R. Murthy, Continental rift volcanism, in _Basaltic volcanism on the terrestrial planets_, Lunar and Planetary Institute, Houston, TX, in press, 1980.

Evans, D. L. and J.B. Adams, Comparison of Viking lander multispectral images and laboratory reflectance spectra of terrestrial samples, Proc. Lunar and Planet. Sci. Conf. 10th, 1829-1834, 1979.

Gaffey, M.J. and T.B. McCord, Asteroid surface materials: Mineralogic characterization from reflectance spectra, Space Sci. Rev., 21, 555-628, 1978.

Gaffey, M.J., and T.B. McCord, Mineralogic and petrological characterizations of asteroid surface materials, in Asteroids, T. Gehrels, ed. Univ. of Arizona Press, Tucson, AZ, 1979.

Gooding, J.L., Chemical weathering on Mars: Thermodynamic stabilities of primary igenous minerals (and their alteration products) from mafic igneous rocks, Icarus 33, 483-513, 1978.

Huguenin, R.L, Mars: Chemical weathering as a massive volatile sink, Icarus 28, 203-212, 1976.

Huguenin, R.L., J.B. Adams, and T.B. McCord, Mars: Surface mineralogy from reflectance spectra, in Lunar Science VIII, 478-480, Lunar Science Institute, Houston, 1977.

Huguenin, R.L., J.W. Head, and T.R. McGetchin, Mars: Petrologic units in the Margaritifer Sinus and Coprates Quadrangle, Reports of Planetary Geology Program, 1977-1978, NASA Tech. Memo

79729, 1978.

Hunt, G.R., Spectral signatures of particulate minerals in the visible and near infrared, Geophys. 74, 501-513, 1977.

Hunt, G.R., and J.W. Salisbury, Visible and near infrared spectra of minerals and rocks: I. Silicate minerals, Mod. Geol. 1, 283-300, 1970.

Hunt, G.R., and J.W. Salisbury, Visible and near infrared spectra of minerals and rocks: II. Carbonates, Mod. Geol 2, 23-30, 1971.

Hunt, G.R., J.W. Salisbury, and C.J., Lenhoff, Visible and near infrared spectra of minerals and rocks: III. Oxides and hydroxides, Mod. Geol. 2, 195-205, 1971.

Hunt, G.R., J.W. Salisbury, C.J. Lenhoff, Visible and near infrared spectra of minerals and rocks: III. Sulphides and sulphates, Mod. Geol. 3, 1-14, 1972.

Hunt, G.R., J.W. Salisbury, and C.J. Lenhoff, Visible and near infrared spectra of minerals and rocks: VI. Additional silicates, Mod. Geol. 4, 85-106, 1973.

Kaper, H.G., Smith, D.W., Schwartz, V. Takakubo, K., and Van Woeden, H. Computer analysis of observed distributions into gaussian components, Bull.

Astron. Inst. Neth., 18, 465-487, 1966.

Macdonald, G.A., Petrography of the island of Hawaii. Prof Pap. U.S. Geol. Surv., 214-D, 51-96, 1949.

Maderazzo, M., and R.L. Huguenin, Petrologic implications of Viking XRF analysis based on reflection spectra and the photochemical weathering model, (abstract) Bull. Am. Astron. Soc., 9, 527-528, 1977.

McCord, T.B. and J.B. Adams, Spectral reflectivity of Mars, Science, 163, 1058-1060, 1960.

McCord, T.B., R.L. Huguenin, D. Mink, and C. Pieters, Spectral reflectance of Martian areas during the 1973 opposition: Photoelectric filter photometry 0.33-1.10 μm, Icarus 31, 25-39, 1977.

McCord, T.B., and R.N. Clark, the Mercury soil: Presence of $Fe^{2+}$, J. Geophys. Res., 84, 7664-7668, 1979.

McCord, T.B., R.N. Clark, R.B. Singer, and R.L. Huguenin, Mars: Near infrared reflectance spectra of surface regions and compositional implication, to be submitted to J. Geophys Res., 1980a. Thesis Ch. II

McCord, T.B., R.B. Singer, J.B. Adams, B.R. Hawke, J.W. Head III, R.L. Huguenin, C.M. Pieters, S. Zisk, and P. Mouginis-Mark, Definition and

and characterization of Mars surface units, Icarus, to be submitted, 1980b.

McCord, T.B., R.N. Clark, L.A. McFadden, C.M. Pieters, P.D. Owensby, and J.B. Adams, Moon: Near-infrared spectral reflectance, A first good look, J. Geophys. Res. to be submitted, 1980c.

McCord, T.B., and J.A. Westphal, Mars: Narrowband photometry, from 0.3 to 2.5 microns, of surface regions during the 1969 apparition, Astrophys. J., 168, 141-153, 1971.

McGetchin, T.R., and J.R. Smyth, The mantle of Mars: Some possible geological implications of its high density, Icarus 34, 512-536, 1978.

Nash, D.B., and J.E. Conel, Spectral reflectance systematics for mixtures of powdered hypersthene, labradorite, and ilmenite, J. Geophys. Res., 79, 1615-1621, 1974.

Nockolds, S.R., R.W.O'B Knox, and G.A. Chinner, Petrology for Students, Cambridge University Press, 1978

Pieters, C. Polarization in a mineral absorption band, in Planets, Stars and Negulae Studied with Photopolarimetry, T. Gehrels, ed., 405-418, University of Arizona Press, Tucson, 1973.

Pollack, J.B., D.S. Colburn, F.M. Flaser, R. Kahn, C.E. Carlston, and D. Pidek, Properties and effects of dust particles suspended in the Martian atmosphere, J. Geophys. Res, 84, 2929-2946, 1979.

Runciman, W.A., D. Sengupta, and M. Marshall, The polarized spectra of iron in silicates: I. Enstatite, Am. Min., 58, 444-450, 1973.

Singer, R.B., Near infrared spectral reflectance of mineral mixtures: Systematic combinations of pyroxenes, olivine, and iron oxides, submitted to J. Geophys. Res., 1980a. Thesis Ch. IV

Singer, R.B., The composition of the martian dark regions: I. Visible and near-infrared spectral reflectance of analog materials and interpretation of telescopically observed spectral shape, submitted to J. Geophys. Res., 1980b. Thesis Ch. V

Singer, R.B. and T.B. McCord, Mars: Large scale mixing of bright and dark surface materials and implications for analysis of spectral reflectance, Proc. Lunar and Planet. Sci. Conf. 10th, 1835-1848, 1979. Thesis Ch. III

Soderblom, L.A., K. Edwards, E.M. Eliason, E.M. Sanchez, and M.P. Charette, Global color variations on the Martian surface, Icarus 34, 446-464, 1978

Toulmin, P., III, A.K. Baird, B.C. Clark, K. Kiel, H.J. Rose, Jr., R.P. Christian, P.H. Evans and W.C. Kelliher, Geochemical and mineralogical interpretation of the Viking inorganic chemical results, J. Geophys. Res., 82, 4625-4634, 1977.

## FIGURE CAPTIONS

Figure 1: Near-infrared (0.65 to 2.50 μm) spectrophotometry of regions on Mars observed by McCord et al., (1980a). These curves are scaled to unity at a wavelength of 1.02 μm. At the top is an average for three characteristic bright regions presented for comparison purposes. The other five spectra are for dark regions. Locations on Mars for these observations are shown in Figure 3.

Figure 2: Visible and near-infrared (0.3 to 1.1 μm) spectrophotometry for regions on Mars observed in 1969 (McCord and Westphal, 1971) and 1973 (McCord et al., 1977). These spectra are scaled the same as those in Figure 1 to facilitate comparison. All data are for dark regions except the 1973 bright region average and 69-1. Locations on Mars for these observations are shown in Figure 3.

Figure 3: Locations on Mars for spectrophotometric observations by McCord and others. The first two digits represent the year of observation (e.g. 69-1 was observed in 1969). The 1969 observations (0.3 to 1.1 μm)

are described by McCord and Westphal (1971); the 1973 observations (0.3 to 1.1 μm) are described by McCord *et al.* (1977). The 1978 observations (0.65 to 2.50 μm) are described by McCord *et al.* (1980a). The locations of observations for which the surface was partially or wholly obscured by atmospheric dust are not shown. (Base map: USGS Topographic Map of Mars I-961, 1976.)

Figure 4: Continuum removal and gaussian band-fitting analysis for dark region spectrum 78-10: A) observed data from 0.65 to 1.35 μm fitted with continuum as described in text; B) residual data after removal of continuum (data divided by continuum). The relative depth of the absorption feature is in excess of 4%; C) two gaussian bands fitted to the data by simultaneous least-squares routine discussed in text. Band centers are at 0.88 and 0.99 μm; D) best attempt to fit one gaussian band to the data. Match is poorer than that obtainable with two bands.

Figure 5: Laboratory bidirectional reflectance spectra for three basalt powders (grain size=45 to 90 micrometers). Incidence

angle = $10^{o}$, emission angle = $0^{o}$. Note that the reflectance scale between BAS06 and BAS01 is continuous; between BAS01 and UWE01 it is discontinuous, to prevent overlap. Spectral continua, synthesized as described in text, are shown overlaid on the data.

Figure 6: The three laboratory spectra from Figure 5 are shown here with continua removed (data divided by continuum). This method facilitates comparisons of absorption band strengths, locations, and shapes. Note broad absorption shoulder, centered near 1.3 μm, for BAS06: this is indicative of olivine.

Figure 7: Continuum removed data for Mars dark region 78-10 compared to: Top) continuum removed spectrum for basalt BAS06, and Bottom) continuum removed spectrum for basalt UWE01. Both basalt spectra have calculated reductions in contrast to match the band depth displayed by spectrum 78-10. The strong olivine signature in BAS06 (containing about 10% modal olivine) is seen as a broadening and depression of the long wavelength side of the pyroxene band near 1 μm. UWE01, with about 5% modal

olivine, shows little or no spectral indication of olivine, and is spectrally similar to these Mars data.

Figure 8: A comparison of some 1978 and 1973 martian dark region observations. Observations for regions 73-22, -24, and -26 are similar and have been averaged for this comparison. A similar double structure is apparent near 1 μm for both of these quite independent data sets.

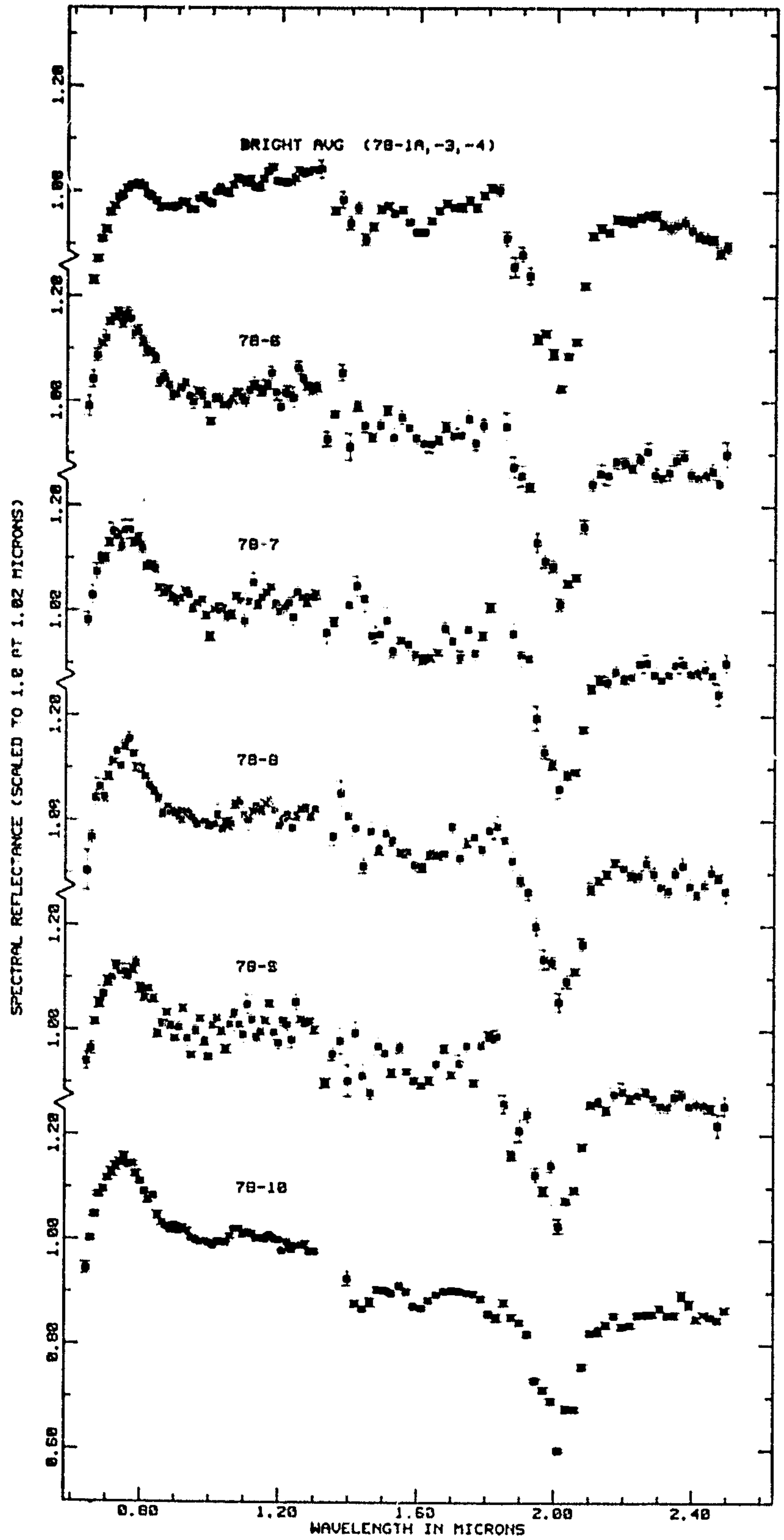
BRIGHT AVG (78-1A,-3,-4)
78-6
78-7
78-8
78-9
78-10
SPECTRAL REFLECTANCE (SCALED TO 1.0 AT 1.02 MICRONS)
WAVELENGTH IN MICRONS
0.80
1.20
1.60
2.00
2.40
1.20
1.00
0.80
0.60

Figure 1

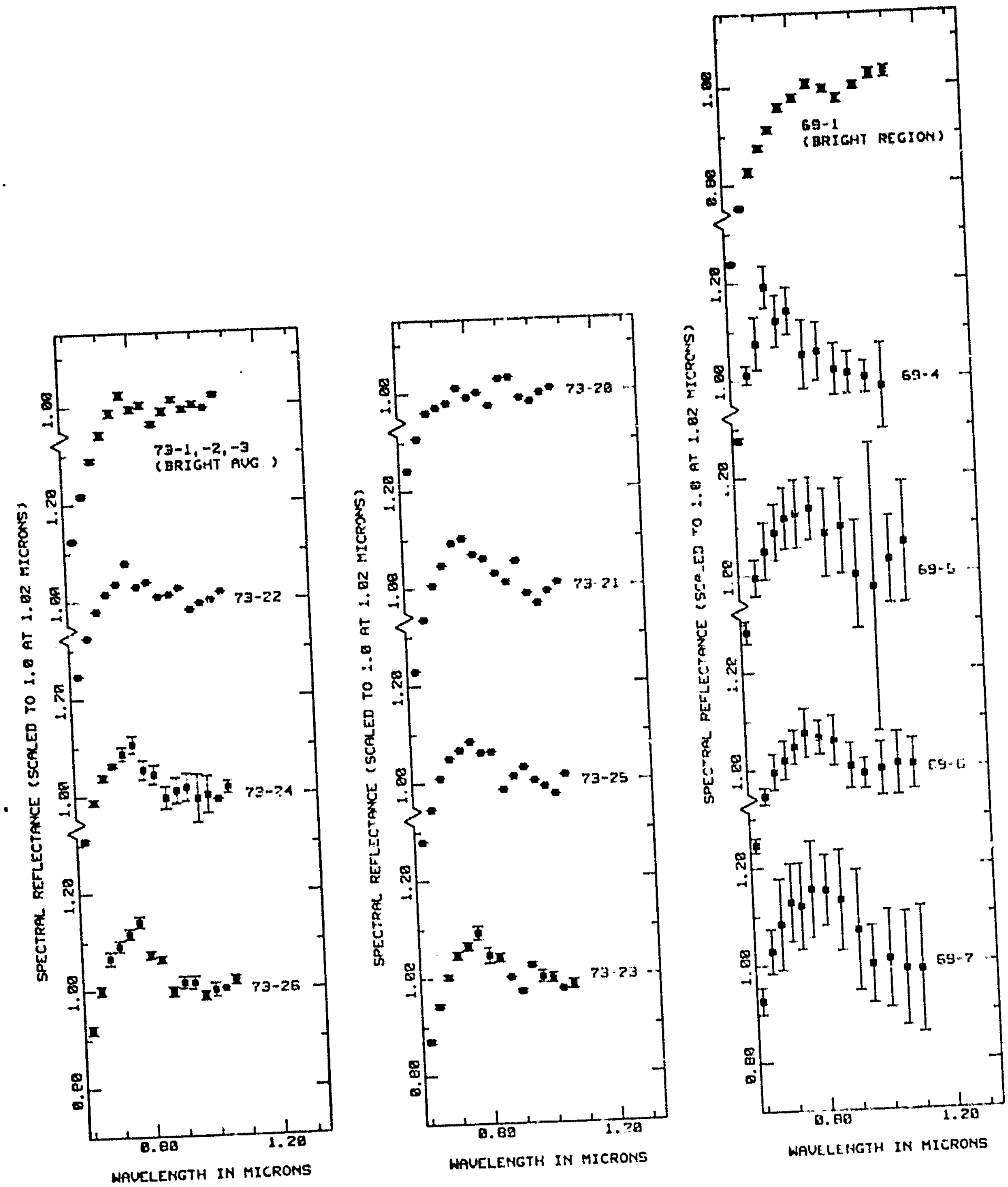
73-1, -2, -3
(BRIGHT AVG. )
73-22
73-24
73-26
73-20
73-21
73-25
73-23
69-1
(BRIGHT REGION)
69-4
69-5
69-6
69-7
SPECTRAL REFLECTANCE (SCALED TO 1.0 AT 1.02 MICRONS)
WAVELENGTH IN MICRONS
0.80
1.20
1.00

Figure 2

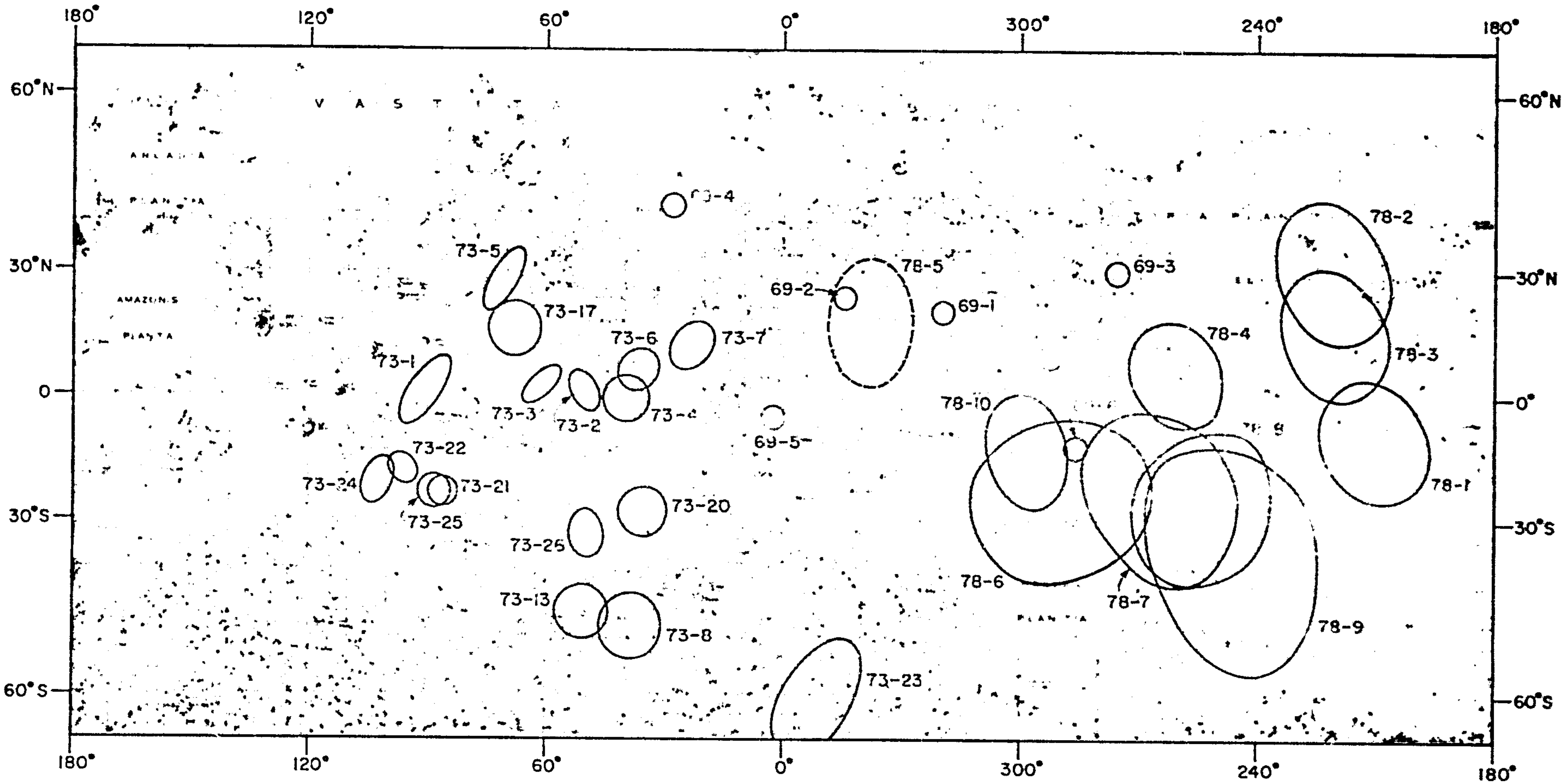
180°
120°
60°
0°
300°
240°
180°
60°N
30°N
0
30°S
60°S
V A S T
AMAZONIS
PLANITA
69-4
69-3
69-2
69-1
69-5
78-1
78-2
78-3
78-4
78-5
78-6
78-7
78-9
78-10
73-1
73-2
73-3
73-4
73-5
73-6
73-7
73-8
73-13
73-17
73-20
73-21
73-22
73-23
73-24
73-25
73-26

Figure 3

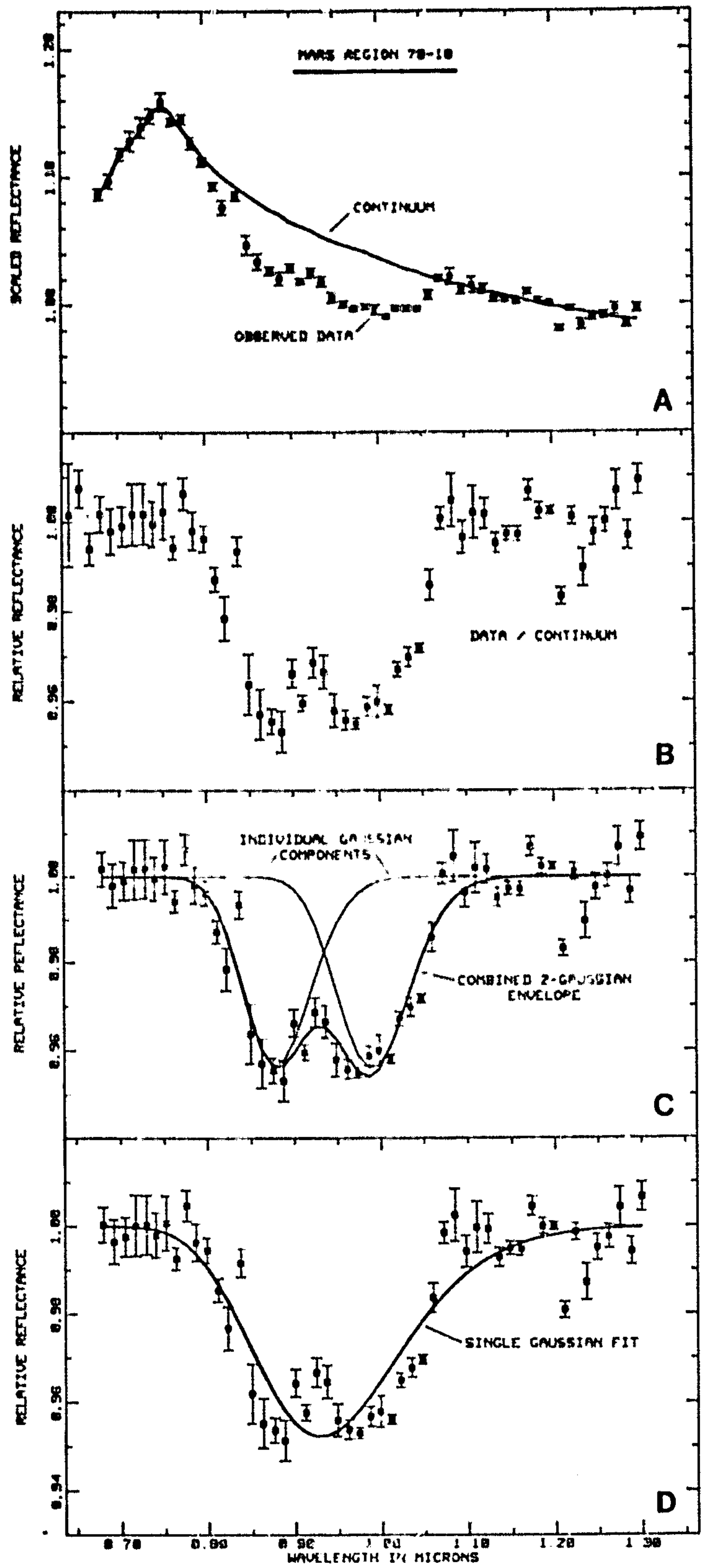
MARS REGION 78-18
CONTINUUM
OBSERVED DATA
SCALED REFLECTANCE
A
DATA / CONTINUUM
RELATIVE REFLECTANCE
B
INDIVIDUAL GAUSSIAN COMPONENTS
COMBINED 2-GAUSSIAN ENVELOPE
C
SINGLE GAUSSIAN FIT
D
WAVELENGTH IN MICRONS

Figure 4

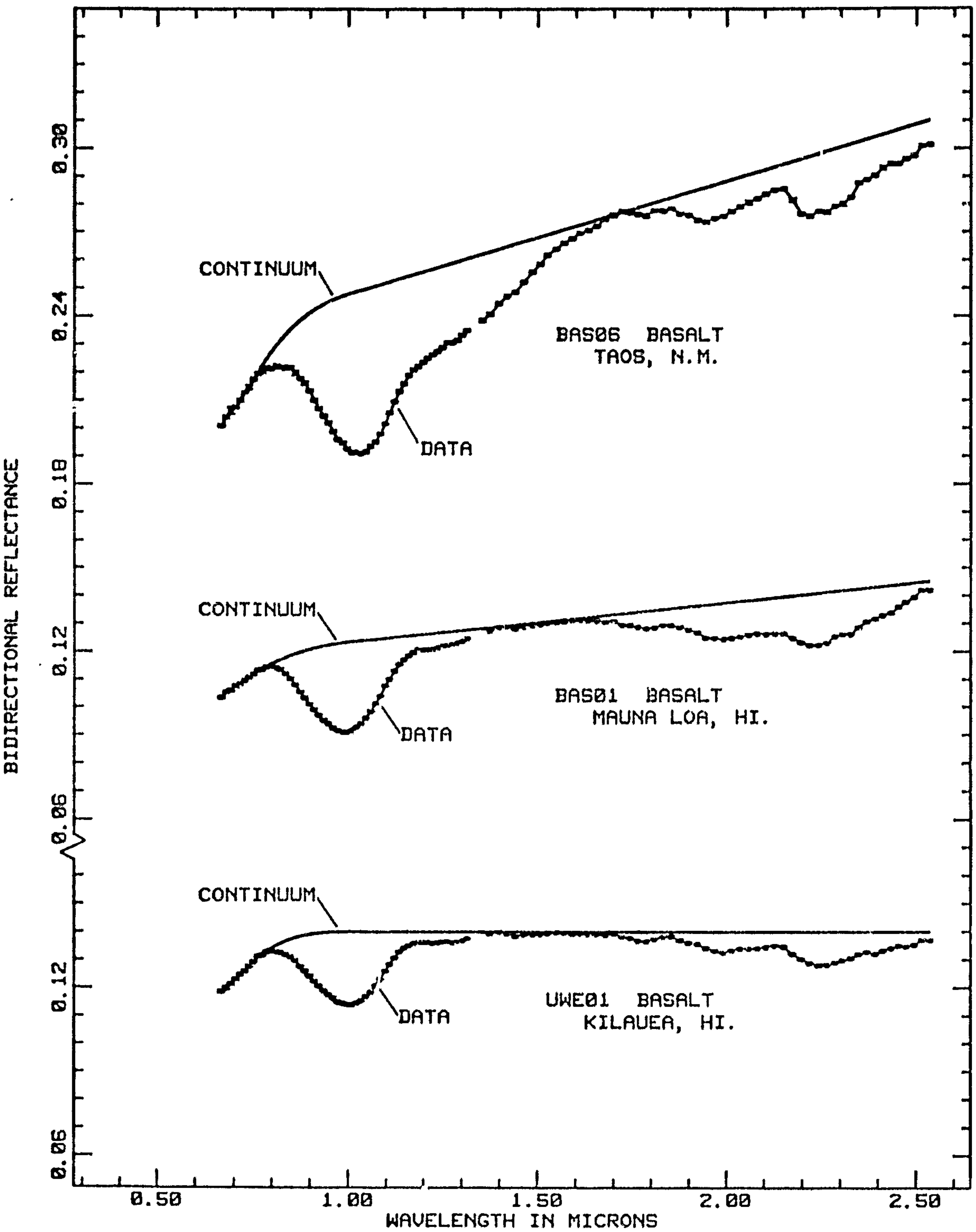

CONTINUUM
DATA
BAS06 BASALT
TAOS, N.M.
CONTINUUM
DATA
BAS01 BASALT
MAUNA LOA, HI.
CONTINUUM
DATA
UWE01 BASALT
KILAUEA, HI.
BIDIRECTIONAL REFLECTANCE
0.30
0.24
0.18
0.12
0.06
0.12
0.06
0.50
1.00
1.50
2.00
2.50
WAVELENGTH IN MICRONS


Figure 5

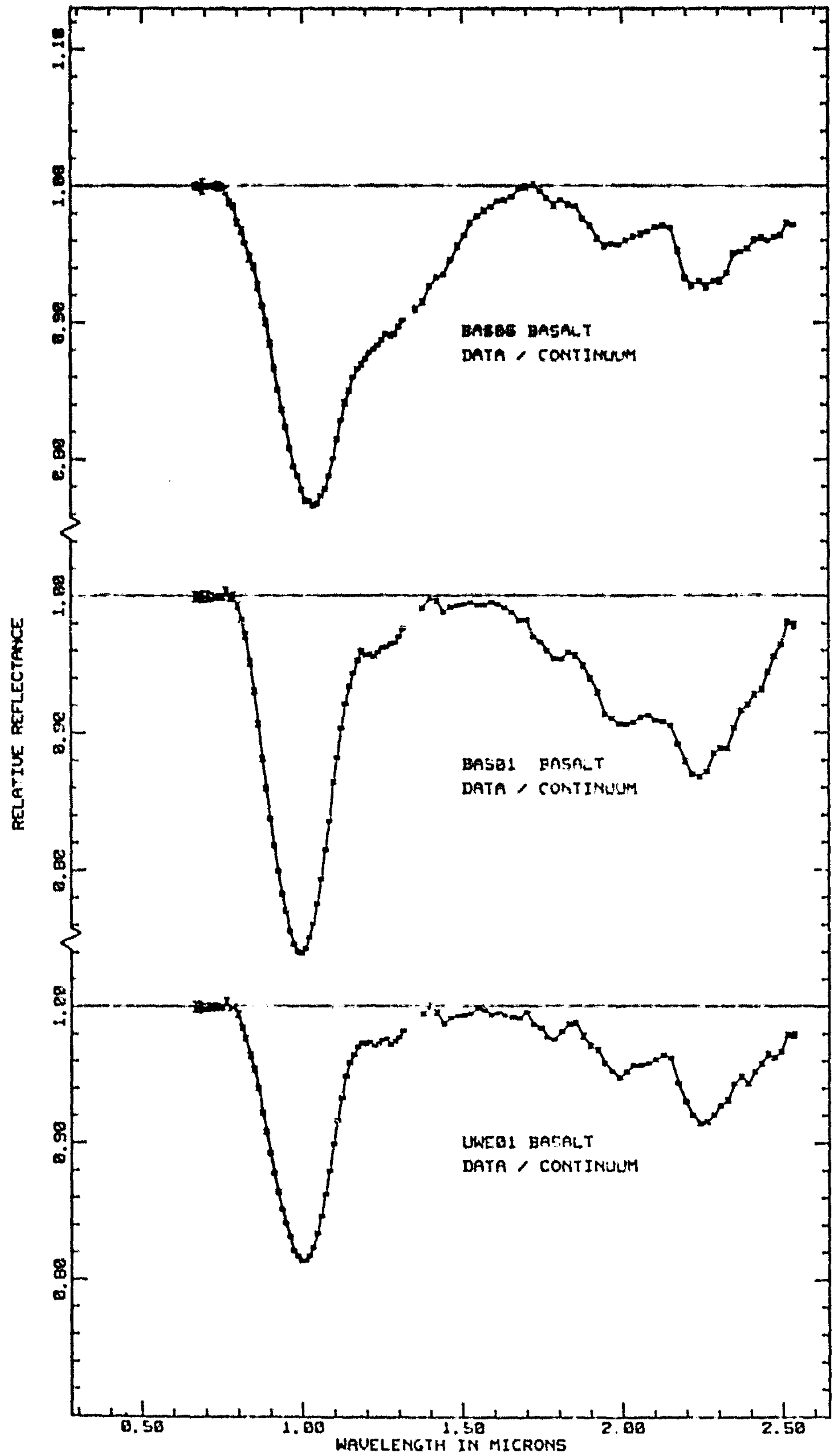
1.10
1.00
0.90
0.80
BAS06 BASALT
DATA / CONTINUUM
BAS01 BASALT
DATA / CONTINUUM
UWE01 BASALT
DATA / CONTINUUM
RELATIVE REFLECTANCE
0.50
1.00
1.50
2.00
2.50
WAVELENGTH IN MICRONS

Figure 6

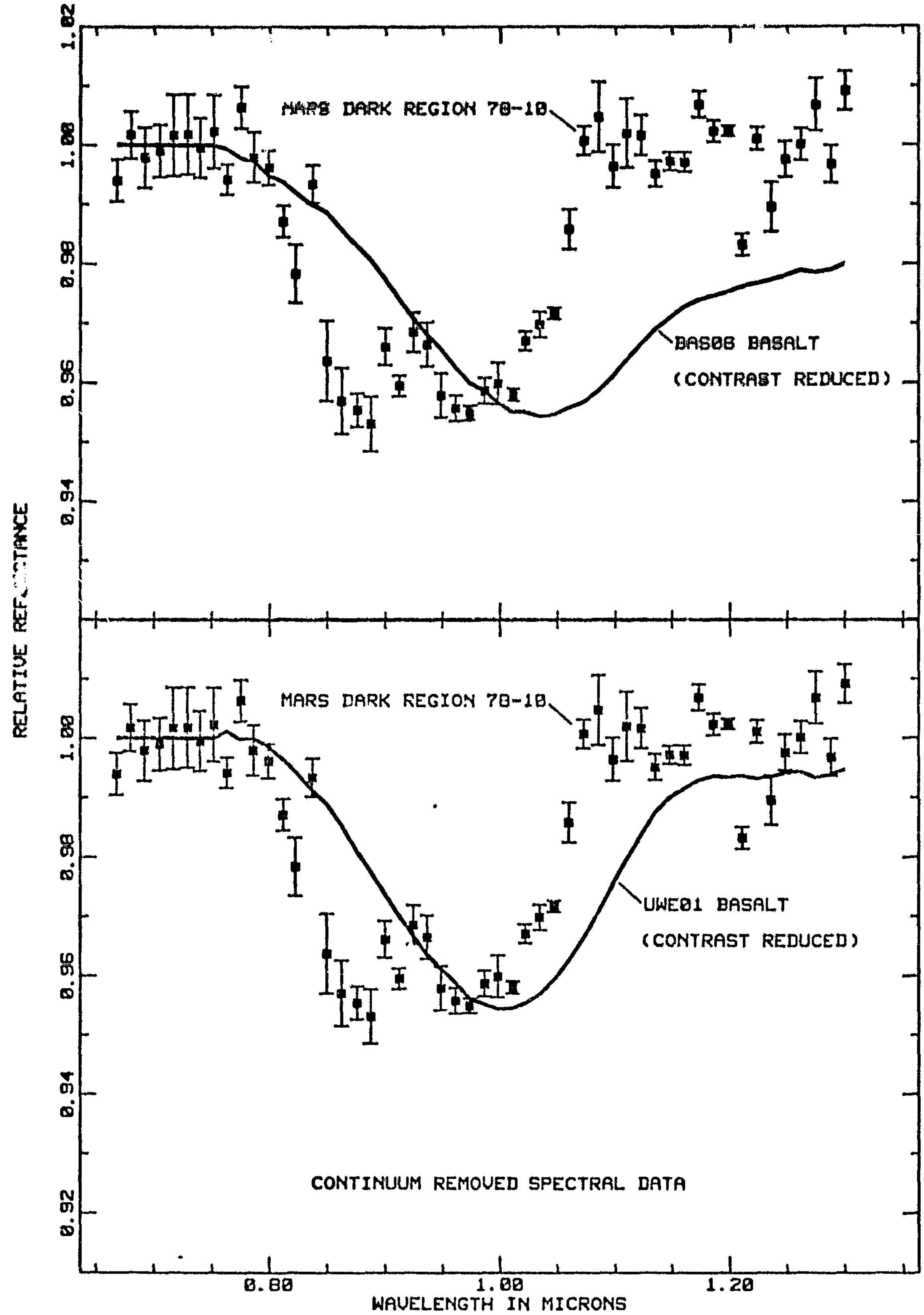

MARS DARK REGION 78-18
BAS08 BASALT
(CONTRAST REDUCED)
MARS DARK REGION 78-18
UWE01 BASALT
(CONTRAST REDUCED)
CONTINUUM REMOVED SPECTRAL DATA
RELATIVE REFLECTANCE
1.02
1.00
0.98
0.96
0.94
0.92
0.80
1.00
1.20
WAVELENGTH IN MICRONS


Figure 7

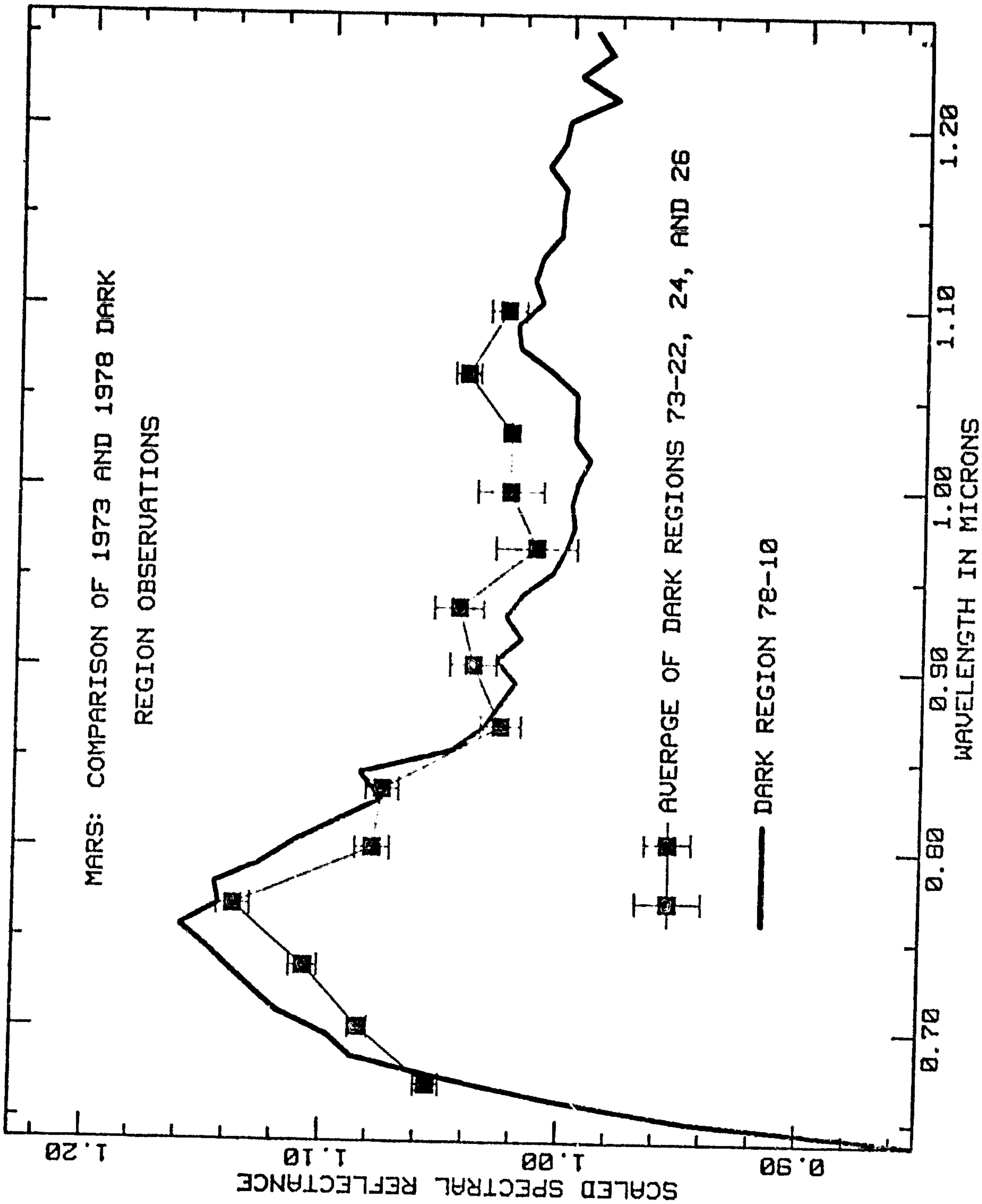
MARS: COMPARISON OF 1973 AND 1978 DARK
REGION OBSERVATIONS
AVERPGE OF DARK REGIONS 73-22, 24, AND 26
DARK REGION 78-10
0.70
0.80
0.90
1.00
1.10
1.20
WAVELENGTH IN MICRONS
0.90
1.00
1.10
1.20
SCALED SPECTRAL REFLECTANCE

Figure 8